



HAL
open science

The design, preparation and performance evaluation of polymetallic complexes based microvesicle capture devices: effect of dendricity

Jian-Qiao Jiang

► **To cite this version:**

Jian-Qiao Jiang. The design, preparation and performance evaluation of polymetallic complexes based microvesicle capture devices: effect of dendricity. Organic chemistry. Université de Bordeaux, 2019. English. NNT : 2019BORD0376 . tel-03904595

HAL Id: tel-03904595

<https://theses.hal.science/tel-03904595>

Submitted on 17 Dec 2022

HAL is a multi-disciplinary open access archive for the deposit and dissemination of scientific research documents, whether they are published or not. The documents may come from teaching and research institutions in France or abroad, or from public or private research centers.

L'archive ouverte pluridisciplinaire **HAL**, est destinée au dépôt et à la diffusion de documents scientifiques de niveau recherche, publiés ou non, émanant des établissements d'enseignement et de recherche français ou étrangers, des laboratoires publics ou privés.

THÈSE PRÉSENTÉE
POUR OBTENIR LE GRADE DE
DOCTEUR DE
L'UNIVERSITÉ DE BORDEAUX

ÉCOLE DOCTORALE DES SCIENCES CHIMIQUES
Chimie Organique

Par Jian-Qiao JIANG

**The design, preparation and performance evaluation of
polymetallic complexes based microvesicle capture
devices: effect of dendricity**

Sous la direction de : Dr. Marie-Christine DURRIEU
et Dr. Sylvain NLATE

Soutenue le 16 Décembre 2019

Membres du jury :

Mme. MIGONNEY, Véronique	Professeur, Université Paris 13	Rapporteur
M. BONTEMPS, Sébastien	Chargé de Recherche CNRS, Université de Toulouse	Rapporteur
M. LEN, Christophe	Professeur, Université de Technologie de Compiègne	Examineur
Mme. ALVES, Isabel D.	Directeur de Recherche CNRS, Université Bordeaux	Présidente
Mme. DURRIEU, Marie-Christine	Directeur de Recherche INSERM, Université de Bordeaux	Directrice de thèse
M. NLATE, Sylvain	Maître de Conférences, Université de Bordeaux	Directeur de thèse

This thesis work was carried out in

UNIVERSITÉ DE BORDEAUX

Institut de Chimie et Biologie des Membranes et des Nanoobjets

(UMR5248 CBMN)

Allée Geoffroy Saint Hilaire, Bât B14, 33600 Pessac, FRANCE

Under the supervision of

Dr. Marie-Christine DURRIEU

And

Dr. Sylvain NLATE

Summary

Microvesicles (MVs) have received a growing research interest at the front line of disease diagnosis. They are used by almost all types of cells in the human body as a tool of intercellular communication, thus can be sampled from most of the extracellular fluids without causing severe damage to the surrounding tissue. They are formed by budding of the cell membrane, thus their membrane proteins are reminiscent to that of their parent cells, allowing them to be traced back to their parent cell types. They contain rich varieties of biomolecules including lipid, protein, and nucleic acids, thus their analysis will provide valuable physiological and pathological information on the cells of origin. They are released under cellular stress, thus they represent the early cellular response to corresponding stimuli. In other words, their analysis is able to provide an approach for the early detection of pathological conditions. A full characterization of the MVs include their population per unit volume of sample liquid, their size distribution, their morphology, their composition of lipid, protein, and nucleic acids. Unfortunately, there isn't a platform developed allowing all the aforementioned tests to be performed at the same time, while existing test protocols are severely limited by the pre-analytical treatments, especially the purification processes. Herein, we present the design and construction of a device on which microvesicles can be captured, accommodating both physical and chemical analysis on the MVs within an extracellular fluid sample.

For the device construction, we first synthesized a series of dendrons with increasing dendricity that are able to specifically bind to phosphatidylserine (PS), a lipid molecule exposing only on the outer leaflet of extracellular vesicles. The dendron peripherals are functionalized with dipicolylamine-Zn²⁺ (DPA-Zn) complexes to provide the dendron-phosphatidylserine interaction. The convergently synthesized dendrons are adopted as the molecular support for the DPA-Zn units, so that the binding ability of dendrons to PS can be controlled and improved through multivalency and synergy of neighboring DPA-Zn units. The core of each dendron is attached to an n-hexylamine spacer, allowing the attachment to material surface.

The interaction mechanisms as well as abilities between synthesized dendrons and PS are studied in solution using the combination of ³¹P NMR and ¹H NMR. The changes in chemical shifts after dendrons binding to PS reveal the binding sites on both dendrons and PS, while the magnitude of the changes determined the relative PS binding strengths of different dendrons.

Upon binding to the dendrons, PS shows largest change in the chemical shift in contact with the dendron of 4 DPA-Zn units, indicating the strongest binding strength. We find that PS interacts with all the synthesized dendrons with the phosphate group, and the dendrons interact with PS using the DPA-Zn units. The ^1H chemical shifts of benzyl ether on dendrons further informed us the conformational change of dendrons when binding to PS. Not surprisingly, the spectrum of the dendron with 8 DPA-Zn units shows the least change, indicating the highest rigidity of the molecule.

Since the binding of MVs to the capture device takes place in an aqueous environment where the dendrons interact with PS containing membranes, the binding ability between dendrons and membranes are determined using a titration experiment based on plasmon waveguide resonance spectroscopy. Before titration, a supported lipid bilayer of PS and phosphatidylcholine was prepared in aqueous environment, and each dendron was titrated incrementally to acquire more realistic dissociation constants (K_{ds}). Due to its dendritic nature, the dendron of 4 DPA-Zn units shows highest apparent binding affinity. Unfortunately, the dendron of 8 DPA-Zn units is insoluble in water and its K_d value can't be determined.

The capture device was then prepared in a series of surface treatment of polyethylene terephthalate (PET), a model material we used to illustrate our idea of surface functionalization. On PET surface, the ester bonds of the polymer chains were hydrolyzed and then oxidized to maximize carboxyl group density. The carboxyls were then activated using the well-established N-(3-Dimethylaminopropyl)-N'-ethylcarbodiimide hydrochloride and N-Hydroxysuccinimide method. With activated carboxyls, the primary amine terminated dendron cores can be easily attached to PET with amide bonds. The process of surface functionalization was monitored by the combination of Toluidine blue-o test and X-ray photoelectron spectroscopy. The surface densities of molecules of different dendricity were found to be on similar order of magnitude.

Finally, the capture of MVs was performed by incubating the functionalized material with a suspension of MVs, and then washed with phosphate-buffered saline. To evaluate the capture performance, the captured vesicles were imaged with both fluorescence microscope and scanning electron cryomicroscope. Surface functionalized with the dendron of 4 DPA-Zn units was the only one being able to capture MVs while maintaining the morphology of MVs, indicating the contents within the captured MVs are also preserved after capture.

In conclusion, using a convergent approach, we have synthesized dendrons with different number of peripheral DPA-Zn units. These molecules are able to bind to PS or PS containing lipid membranes, while the dendron of 4 DPA-Zn units shows the highest binding affinity. Surface functionalized with these molecules are also able to capture MVs, and the capture ability is closely related to the dendricity of the dendrons used. Dendron of 4 DPA-Zn units one again excels at MV capture performance (surfaces that are not functionalized with it are either not able to capture MVs or unable to maintain the contents within MVs), allowing future examination of size distribution, morphology and chemical composition.

Key words: microvesicle, dendron synthesis, phosphatidylserine, phosphatidylserine-dendron interaction, membrane-dendron interaction, surface functionalization, microvesicle capture.

Table of contents

Summary	i
Chapter 1: General Introduction.....	1
Literature review: MV analysis and dendrimer chemistry	1
Microvesicles: Definition, Biogenesis, Characteristics and Biological significance.	1
MV isolation from bodily fluids/ cell culture medium	5
Dendritic molecules: definition, synthesis and the pros and cons for their application in EV capture devices.....	20
A brief introduction of the step-by-step construction of our capture assay.....	40
Characterization for each step: why I decided to use these methods?.....	43
Dendron synthesis.....	43
Dendron-PS interaction.....	44
Dendron-membrane interaction	46
Dendron functionalization of the surface: qualitative & semi-quantitative	48
Characterization of MVs after capture.....	51
Chapter 2: Ligands for capturing microvesicles and Uses thereof.....	53
Field of the invention.....	55
Background of the invention	55
Summary of the invention	56
Figures.....	63
Detailed description of the invention.....	63
- Ligands according to the invention.....	64
- Support and devices comprising the ligands of the invention	80
- Methods and uses according to the invention.....	81
- kits according to the invention.....	85
Examples	87

A. Synthesis of Tert-butyl (6-iodohexyl)carbamate (intermediate)	87
B. Synthesis of complex of formula (III d) (comparative – Cplx1)	88
C. Synthesis of complex of formula (III a) (hereafter Cplx2).....	90
D. Synthesis of 2-(trimethylsilyl)ethyl (6-iodohexyl)carbamate (intermediate).....	92
E. Synthesis of complex of formula (III b) (hereafter Cplx4).....	93
F. Synthesis of complex of formula (III c) (hereafter Cplx8)	95
Example 2: Ligand-PS-enriched microvesicle interaction study by PWR spectroscopy	97
Example 3: Immobilization of ligands on PET film and characterization.....	98
- Immobilization of ligands of the invention.....	98
- TBO characterization.....	99
- X-ray photoelectron spectroscopy (XPS)	100
Example 4: Microvesicle capture and characterization by using cryo-SEM	102
- Microvesicle preparation	102
- Microvesicle staining.....	102
- Microvesicle characterization by fluorescence microscopy	102
- Microvesicle characterization using nanoparticle tracking analysis (NTA):.....	103
- Microvesicle capture.....	103
- Observation of captured microvesicles using FL microscope	103
- Observation of captured microvesicles using Cryo-scanning electron microscopy (Cryo-SEM).....	104
- Results	104
Claims.....	106
Ligands for capturing microvesicles and Uses thereof.....	115
Chapter 3: Dendron-Functionalized Surface: Efficient Strategy for Enhancing the Capture of Microvesicles	116
SUMMARY	117
INTRODUCTION.....	117

RESULTS and DISCUSSION	120
Dendron synthesis	120
NMR investigation of DPA-Zn complex-PS interaction	122
Plasmon waveguide resonance study of DPA-Zn complex-model membrane interaction ..	126
Fabrication and characterization of the MV capture devices	130
The performances of the MV capture devices	134
Limitation of study.....	138
Acknowledgements.....	139
Authur contributions	139
Declaration of interest.....	139
Supplemental Information	141
Conclusions and perspectives	214
Molecule design and synthesis:	214
Complex-PS interaction and complex-membrane interaction studies	215
Surface functionalization and its characterization	215
MV capture device	216
References:.....	218

Chapter 1: General Introduction

Literature review: MV analysis and dendrimer chemistry

Microvesicles: Definition, Biogenesis, Characteristics and Biological significance.

Microvesicles (MVs), also known as microparticles or ectosomes, are defined as the extracellular vesicles (EVs) coming from the budding of cellular membrane into bodily fluids.[1] MVs can be secreted by almost all types of cells in response of stimulations such as infection, activation, transformation, and stress.[2-4] As a means of intercellular communication, MVs transmit bioactive molecules including lipids, proteins, mRNA, miRNA and DNA across human body.[5-11]

As reviewed by Christopher *et. al*, the biogenesis of microvesicles can be three interlinked processes: plasma membrane deformation, vesicle cargo collection towards the deformed plasma membrane, and finally shedding of the vesicle.[2]

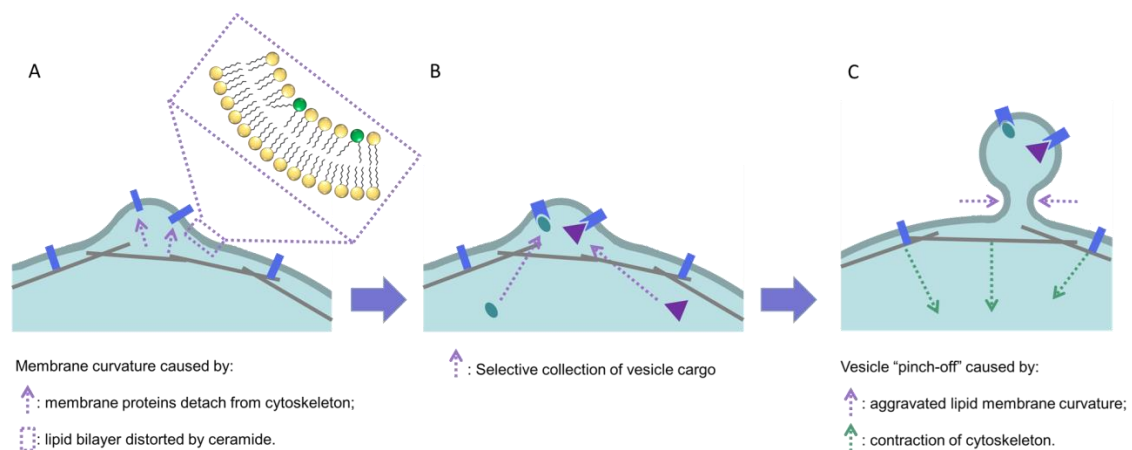


Figure 1: The biogenesis process of MVs. (adapted from [12]).

During the membrane deformation (Figure 1 A), plasma membrane first detaches from cytoskeleton due to corresponding stimulation, for example when red blood cells experience oxidative stress during long term storage, Band3 channels which are responsible for the cellular chloride and bicarbonate anion exchange and supported by Ankyrin, tend to detach from the Ankyrin support and form aggregations, causing the plasma membrane instability.[13] While the membrane-cytoskeleton detachment causes the destabilization of plasma membrane, another pathway of MV genesis includes directly the curvature of local plasma membrane: Sphingomyelin together with cholesterol forms relatively rigid domains on lipid membrane (aka lipid rafts). When sphingomyelin hydrolyses in the presence of acid sphingomyelinase (a SMase), it breaks down into phosphatidylcholine and ceramide. Neither of these two molecules can interact with cholesterol sufficiently to maintain the rigidity, while ceramide with a conical conformation will further induce membrane curvature.[14] As reviewed by Claudia *et. al.*, such curvature process can be observed during MV production from a wide variety of human cells under either physiological or pathological conditions.[9]

The routes of cargo collection to the plasma membrane blebs (Figure 1 B) are highly dependent on the nature of cargo molecules, and most of the transportation of cargo molecules seems to be regulated by proteins: Lipid molecules, for instance the well-known phosphatidylserine is transported to the plasma membrane outer leaflet by scramblase and floppases under an influx of cytosolic Ca^{2+} . [12, 15] Surface protein such as EGFRvIII, an oncogenic receptor found in glioma cells can promote the lipid raft generation related to MV shedding by itself.[16] Cytoplasmic protein on the other hand, for example membrane type 1 matrix metalloproteinases is first bound to vesicle-associated membrane protein 3 (VAMP-3), then transported to plasma membrane by the interaction of VAMP-3 with tetraspanin CD9 in amoeboid LOX cells.[17, 18] The enrichment of nucleic acids to MVs is also a selective process, since multiple publications already suggest that the cellular concentration of multiple nucleic acids is significantly different to that in shedded MVs.[7, 8, 19] A discovery made by Mehmet *et. al.* suggested that in HEK-293T, cells mRNA with a certain “zipcode”-like sequence will bind to miR-1289, while such complex promotes the enrichment of mRNA into microvesicles.[20]

The detachment of blebs from plasma membrane, *i. e.* the shedding of microvesicles, is usually considered as a “pinching off” process (Figure 1 C), and to some extent, the pinching-off

can be considered as either an extreme instance of membrane curvature or cytoskeleton contraction: 1) Proteins regulating membrane curvature are also considered to be involved in the MV fission from the parent cells: a SMase for synthesizing conical ceramides, scramblase for the disruption of lipid distribution asymmetry, all contribute to this process; while other pathways such as the polymerization of endosomal sorting complexes required for transport-III (ESCRT-III) protein is also able to segregate the blebs from plasma membrane.[15, 21, 22] 2) In LOX cells, ARF6 initiates a cascade of reactions that finally leads to the phosphorylation of myosin II light chain, promoting the contraction of cytoskeleton hence provides another pathway for MV detachment from the parent cells.[23, 24]

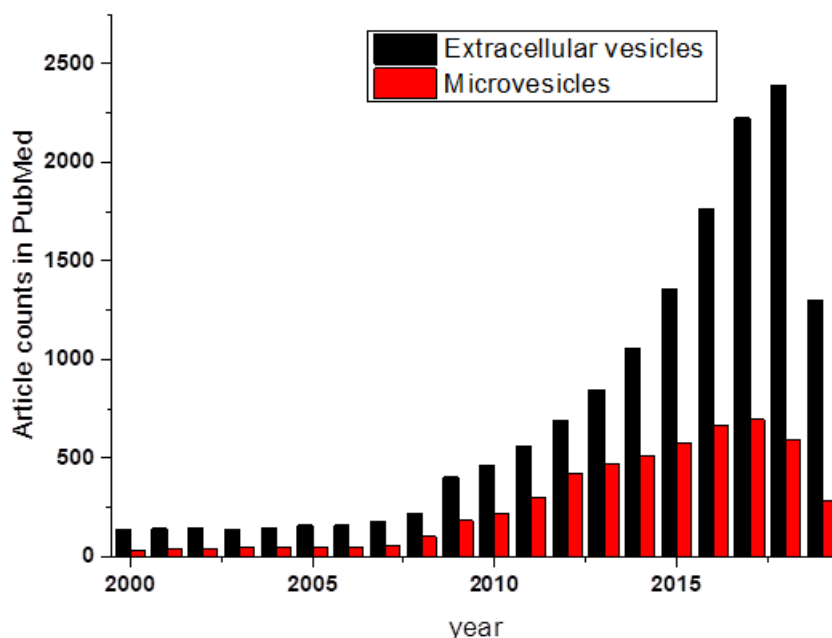


Figure 2. PubMed article counts for keywords: “extracellular vesicles” and “microvesicles” on 22/07/2019.

The above mentioned MV biogenesis pathways are by no means exhaustive, and many crucial intermediate steps in these pathways still remain elusive to our knowledge today. None the less, it is evident that MVs play an important role as a means of transporting biomolecules in extracellular environment.[7, 11, 25] The characteristics of MVs, including the population in a given sample, the size distribution, physical properties and most importantly the molecules they

convey, are determined by the parent cells and stimulation received by the parent cells, resulting in unique features for MVs generated from various pathways.[26] Such diversity of microvesicles is only known for us in the last decade. The number of researches published on the study of MVs as well as other EVs has been growing exponentially since 2008 (Figure 2). And in response to such explosion of interest, Vesiclepedia, a database of EVs, was established in 2011. To date, as many as 5,985 proteins and 12,779 mRNAs have been registered in the “microvesicle” category, most of them correlated to specific biological functions (Figure 3).[27, 28] Many of the recent researches focus on the regulatory functions, exploiting their potential as novel therapeutic reagents or as tool for pathology studies.[29-42] Within such publications, the correlation between MV transmitting bioactive molecules and their biochemical functions are of particular interest. Another important direction for MV research is the identification of MVs as biomarkers for pathology diagnosis: the spontaneous biogenesis of MVs upon stimulation, the abundance of detectable bioinformation on both parent cell types and stimulants, and relatively non-invasive extraction of specimen from bodily fluids can be translated into the early, accurate and pain-free pathology diagnosis.[10, 43-50] In any case, the study of MVs requires the correlation, if not the causal effects of MV characteristics to MV biological functions. For such purpose, MVs should first be isolated from other components of bodily fluids, most importantly other EVs, and thereafter characterized for their population, size distribution, biochemical contents, and in some cases physical properties such as stiffness, etc.

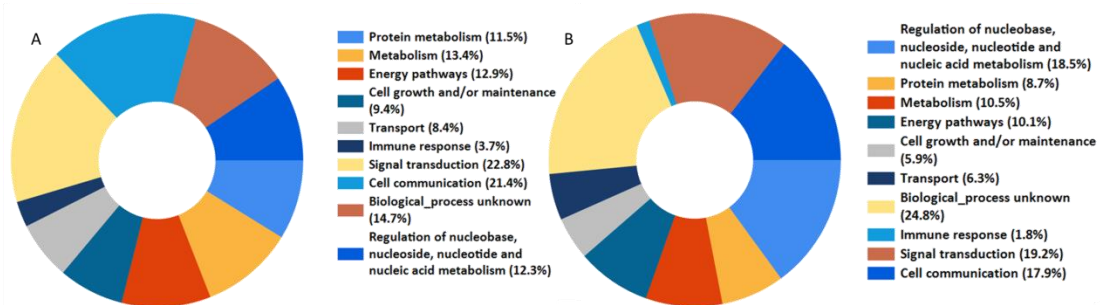


Figure 3. A: 10 of the most frequently reported biological functions of MV proteins; B: 10 of the most frequently reported biological functions of MV mRNAs. Data acquired from Vesiclepedia database (updated 15/08/2018), analyzed with FunRich3.1.3.[27, 28, 51, 52]

MV isolation from bodily fluids/ cell culture medium

A sample of bodily fluid or cell culture medium usually contains cells, cell debris, apoptotic bodies, MVs, exosomes and soluble components (salts, sugars etc.). Hereafter is a brief introduction of the commonly used isolation methods for MVs from such mixture documented in Vesiclepedia including differential centrifugation, density gradient centrifugation, filtration, size exclusion chromatography, and fluorescence activated cell sorting.

Differential centrifugation and density gradient centrifugation

In centrifugation processes, sedimentation of different components within a bodily fluid sample is dependent on two major factors: density and size (and for sufficiently small components such as exosomes, electrokinetic potential is also an important factor). Only components with density higher than that of the medium can be sediment out as pellet. Larger and/or denser components will pellet out at lower centrifugation speed within minutes, while smaller and/or less dense components can only be pelleted after high velocity centrifugation for a much longer period of time.

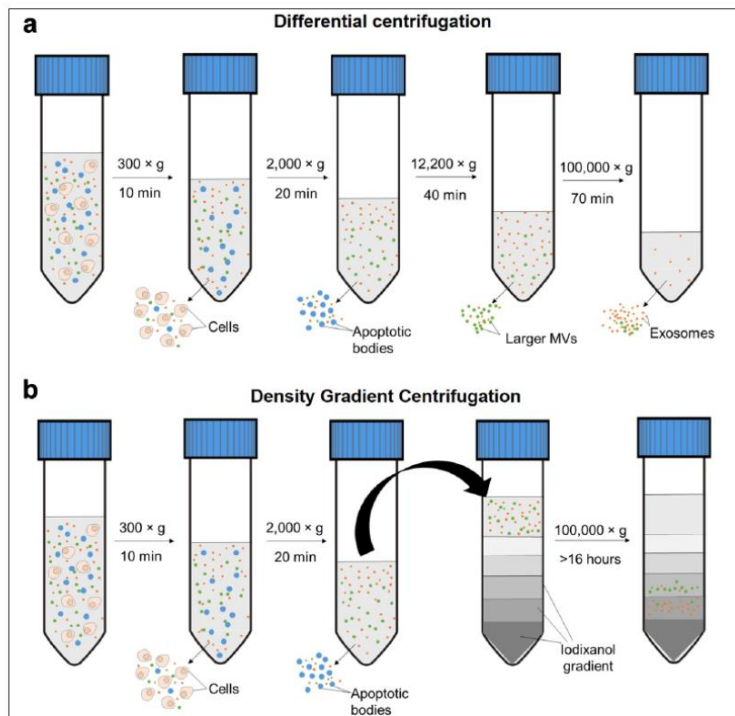


Figure 4. Centrifugation methods used for MV isolation. Image is taken from Ref. [53].

The theory of differential centrifugation is that low centrifugation speed is applied for just enough time for the sedimentation of heaviest/largest particles, so that this component can be removed as pellet. Supernatant of the first centrifugation will go through another centrifugation of higher velocity and /or longer centrifugation time to sediment the second heaviest/largest particles. With the propagation of centrifugation velocity/time, multiple components can be acquired. In the case of cells and EVs, differential centrifugation is considered as a size selective/sensitive process. Figure 4 A shows a series of centrifugation to acquire multiple components from bodily fluid, in which MVs can be collected after 3 cycles of centrifugation. Differential centrifugation can process large quantities of samples, and has been adopted as the gold standard for MV purification.[54, 55] It is also noteworthy that differential centrifugation doesn't yield pure samples of MVs.[53, 56] MVs usually have a wide window of size distribution, the upper limit often overlaps with apoptotic bodies, while the lower limit of size distribution overlaps with that of exosomes.[1] Besides, cellular debris, protein aggregates and viruses are also reported as contaminants found in MV samples acquired by differential centrifugation.[57] In real life, viscosity and density of a bodily fluid sample with or without pathological conditions can also

vary significantly, thus centrifugation protocol should also adapt accordingly. Apart from the purity concerns, differential centrifugation is also a notoriously time consuming process, the isolation and purification of MVs could take as long as several hours.[58] The high g force experienced by MVs during centrifugation has also been reported to be destructive for MV integrity, the redispersed pellet won't present the same size distribution, morphology and molecular contents as the original sample.[59]

To address the issue of contamination from particles of similar sizes but different in densities, a complementary centrifugation method, density gradient centrifugation, is adopted as another method for MV purification. As illustrated in Figure 4 B, The principle of separation is that the mixture to be purified is layered on top of a separation medium of discontinuous density gradient that the density increases from top to bottom. After centrifuging for sufficient amount of time, a particle of a certain density will reside in a gradient layer where the next layer has higher density than the particle itself. Unlike differential centrifugation, density gradient centrifugation won't pellet the vesicles, giving less mechanical stress for vesicle destruction. Unfortunately, such advantage doesn't necessarily translate into better vesicle preservation. Density gradients are created by layering lower concentration solutions of, for example, sucrose on top of solutions of higher concentrations. Sucrose can generate osmotic pressure difference at vesicle membrane, causing an increase in surface tension for vesicle species that could also lead to vesicle destruction. Isosmotic mediums prepared with iodixanol (commercially known as OptiPrep™) in contrast can overcome such disadvantage, as iodixanol is of low osmolality and can be dissolved in isosmotic solutions such as PBS or HEPES.[60] In comparison to differential centrifugation, density gradient centrifugation has higher resolution in density differences, but contaminants of similar density (for instance high-density lipoproteins) is still hard to remove.[61]

Filtration and size exclusion chromatography (SEC)

As reviewed above, centrifugation methods can isolate MVs from a bodily fluid sample or a cell culture sample according to the densities of suspending particles. The time required for sufficient separation is also related to the size of particles, making such process time consuming and incompetent for isolating contaminants of similar density.

As a complementary method applied after centrifugation, a simple filtration of MV samples can exclude any contaminants that don't correspond to the size of MVs (Figure 5 A). For small particles such as proteins, ultrafiltration can provide molecular weight cut-offs allowing small molecules passing through the filtering membrane.[62] Larger contaminants can also be removed by filtering the sample through submicron pore sized filters.[63, 64] Simple filtration of a sample is usually not enough for isolation of MVs, as components of similar size will also be collected.

SEC is a size sensitive chromatographic method for MV purification (Figure 5 B). In a chromatography column is loaded with Sepharose (cross-linked agarose) or Sephacryl (cross-linked copolymer of allyl dextran and N,Nmethylenebisacrylamide) beads.[65-68] Such beads possess porous structures allowing the adsorption and desorption of particles of smaller sizes, leading to the differences in elution speed for particles of different sizes: smaller particles go through more cycles of adsorption/desorption than larger particles that can't fit into the pores of polymer beads thus coming out of the column later. MVs can therefore be achieved by collecting corresponding fraction of eluate. Such method is proven to yield more vesicles as compared to differential centrifugation, however contamination from lipoproteins can't be removed by the chromatography itself.[65, 67, 69]

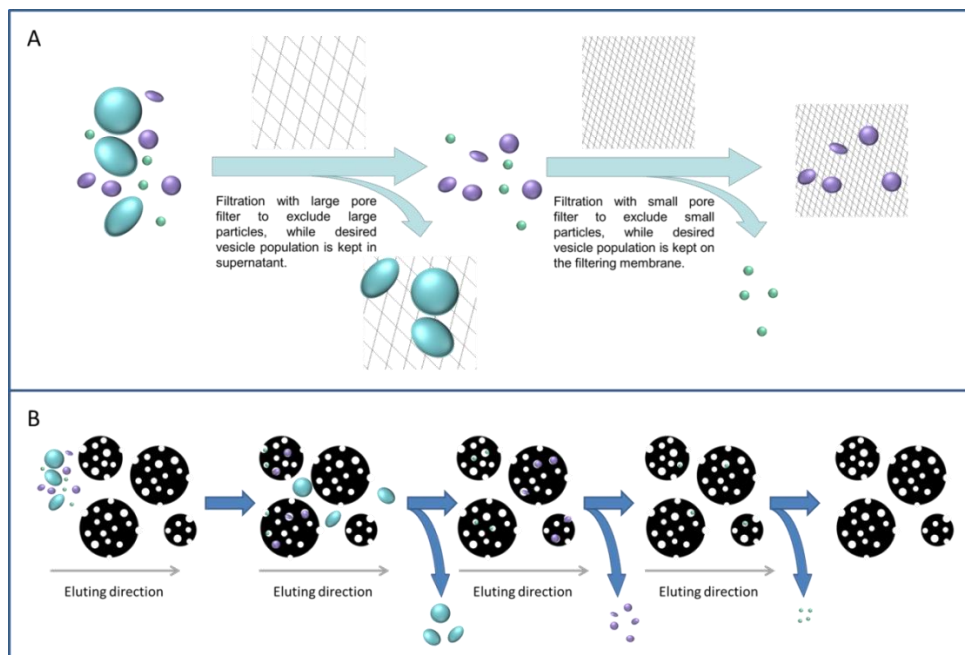


Figure 5. Size selective methods for MV isolation. A: principles of filtration methods; B: principles of SEC.

In recent years, other size-selective isolation methods for MVs, especially novel filtration methods such as tangential flow filtration, field-flow fractionation, etc. have been developed.[70-72] Similar to the traditional filtration processes, these methods also use filtering membranes for the separation of different sized particles. Flowing methods often result in higher yields than conventional filtration methods due to reduced aggregation, but contaminants of similar size are still present in the filtrate. It is suggested therefore to combine the density selective methods such as centrifugation to acquire pure samples of MVs.[55]

Fluorescence activated cell sorting (FACS)

Flow cytometry is a well-developed method for particle counting, while FACS can also be integrated to detect the presence of specific protein containing particles. A sample is first incubated with fluorescent antibodies targeting MV-related proteins so that only MVs can express the specific fluorescence signal.[73] During flow cytometry experiment, scatter events are used to quantify the total number of particles within a sample while only fluorescence positive (at the emission wavelength of fluorescent antibodies) events are counted as MVs and corresponding particles are collected as pure samples of MVs (Figure 6).

In many cases, the MV quantification by side/front scattering signal detection on different flow cytometers often yields different results when testing the same sample. Such variation of results usually comes from the testing parameters of individual cytometers. Cointe et al. conducted a study in the hope that MV enumeration could be standardized on most of the flow cytometers, therefore they have prepared specialized polystyrene microbeads for calibration and tested the such protocol on 52 flow cytometers in 44 labs.[74] Using the same calibration beads, the variation of results is indeed less prominent than before, however, the detection of MVs below a certain size is still unachievable, since the majority of the beads they used are over 200 nm in diameter, well above the diameter of most of the MVs reported in literature.[10]

Compared with abovementioned density/size dependent isolation methods, FACS should be the most selective MV recruiting approach as it is able to collect particles with specific proteins

while exclude the particles without the desired fluorescence signals. However, reports indicate that compared to cells, MVs generate significantly less intensive fluorescence signals due to reduced surface area, making the fluorescence detection even less sensitive compared to the scatter signals.[74, 75] Such high specificity is also highly dependent on the antigen chosen for the isolation studies, for example during the biogenesis of HIV-1 particles, it is difficult to discriminate HIV-1, exosomes and MVs as HIV-1 hijacks the biogenesis exosomes in macrophages and dendritic cells and MV biogenesis of T cells.[61, 76] And of course, such visible light detection dependent method always face the problem of small particle resolution, leading to the omission of exosome existence during MV collection.[55]

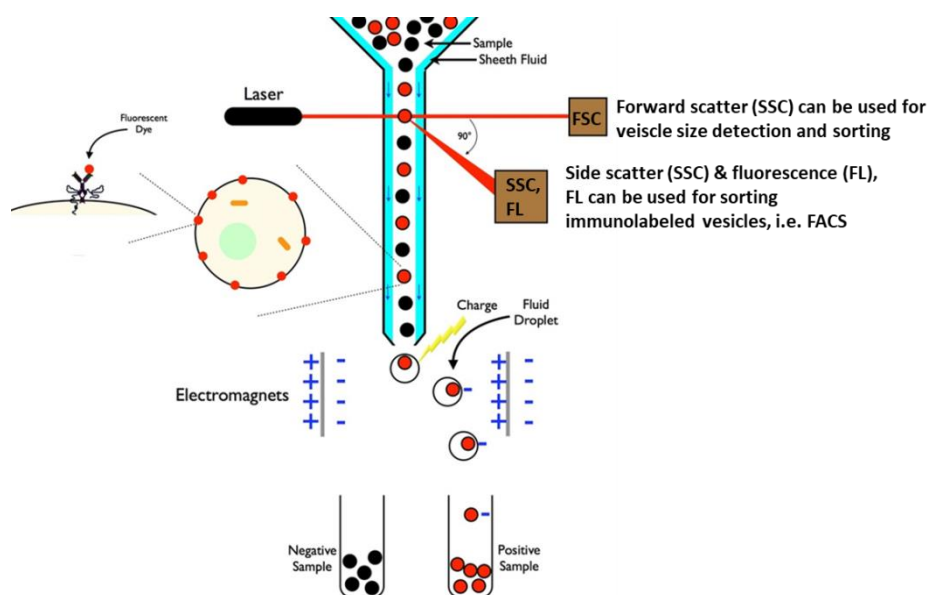


Figure 6. Schematic presentation of FACS for EVs. Image taken from [77] and modified.

Capture assays: a novel pre-analytical processing method for the study of MVs.

In the FACS selection of MVs, one crucial part of the design is the highly selective fluorescent dyes. Such molecules are able to bind to specific proteins that reside on MV surface through selective intermolecular interactions. Selectivity is usually realized through antibody-

antigen interactions that are well studied in immunology to be strong and selective, hence adopted in fluorescence labeling and capture assays for MVs.

A widely adopted model for MV isolation is antibody coupled magnetic microbeads. For example, Taylor and coworkers has reported beads coated with anti-EpCAM(epithelial cell adhesion molecule) antibodies, targeting the exosomes exposing EpCAMs on their surface.[65] The microbeads are cultured within ascites of ovary cancer patients, so that EpCAM exposing vesicles will adhere to the microbeads. The beads can be isolated from the ascites using magnets (Figure 7). Takao et. al. also reported anti-EpCAM coupled magnetic microbeads for EV isolation, however the reported study wasn't able to identify exosomes from MVs since EpCAM is over-expressed by epithelial cancer cells and it's not surprising to find them on epithelial MVs.[75] Cointe et. al. reported leukocyte derived MV isolation from platelet free plasma using CD15 exposing magnetic microbeads adopting a similar isolation procedure. Such procedure is selective so long as the target molecules are correctly chosen, i. e. such molecules can only be found on target MVs, and all the MV population to be detected also expose the target molecules with no exception. In this sense, such method is quite useful to exclude non-vesicular contaminants, however it could still be difficult to distinguish exosomes from MVs.

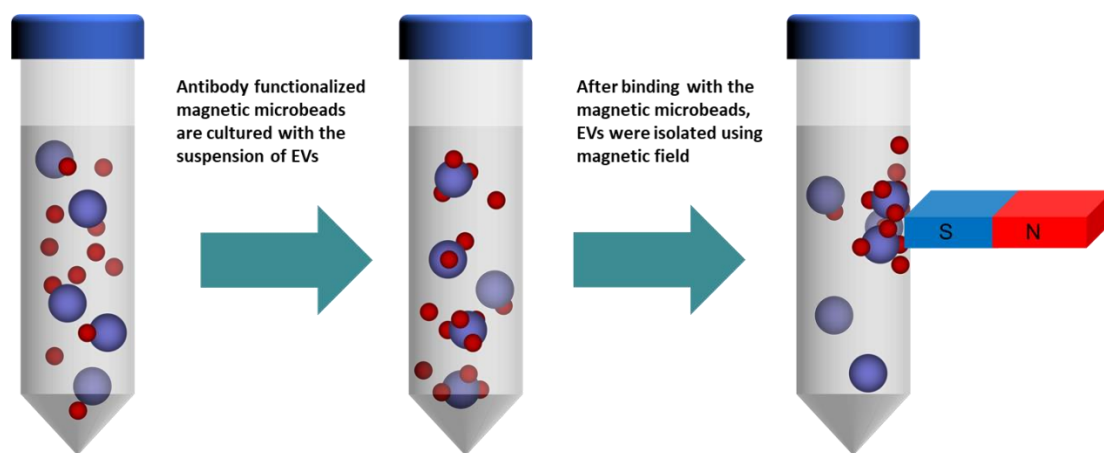


Figure 7. A schematic presentation of magnetic microbeads based EV isolation. The illustration of magnetic microbeads (red spheres) and EVs (purple spheres) are not to scale.

The abovementioned antibody-antigen interaction based isolation methods are beyond doubt the most selective vesicle isolation methods to exclude the non-vesicular components, yet

they face the problem that such isolation protocols are very dependent on the MV parentage, for instance EpCAM targeted isolation can only collect vesicles from epithelial cells with EpCAM overexpression. Other vesicle population within the same sample will be excluded, encumbering the complete extraction of bioinformation from a given sample. What's more, MVs from different cellular parentage can only be isolated with specialized antibody/antigen, meaning that in theory for different diagnostic targets, different isolation media should be specifically developed, provided that surface protein exposures are well studied for different cell types.

A more generalized target molecule is required therefore for the isolation of MVs while excluding non-vesicular contaminants. For different MVs surface proteomics may vary significantly, while in contrast lipid molecule varieties of vesicle membrane are limited. Amongst which, phosphatidylserine (PS), is quickly noticed by the scientific community. PS is best known as a "eat me" signal during early apoptosis, and related engulfment mechanisms were reviewed by Segawa and Nagata.[78] It is noteworthy that such engulfment processes are not only executed by specialized cells like macrophages. Non-specific clearing of PS exposing cells can also be attributed to immature dendritic cells, epithelial and mesenchymal cells, meaning that PS is a widely accepted "eat me" signal for many cell types.[79]

Before further delve into how the PS can be exploited in MV capture, let's first establish the rationality of such design and understand why PS is exposed in the MVs. As shown in Figure 8 PS is synthesized at the cytoplasmic leaflet of endoplasmic reticulum, and then quickly transferred to the luminal leaflet by an ATP dependent manner. PS is then transferred to Golgi apparatus by vesicles. Until the trans-Golgi network (TGN), PS remains at the inner luminal leaflet, while at TGN PS is flipped to the cytoplasmic leaflet. Through budding of TGN, PS is transferred to plasma membrane and also remains at the cytoplasmic leaflet. PS of plasma membrane can travel back into cytoplasm in early endosomes on cytoplasmic leaflets. Early endosomes go through fission process to recycle PS via vesicles either to Golgi apparatus or directly back to plasma membrane, leaving little amount of PS residue in those late endosomes to be fused with lysosomes. Multi-vesicular bodies (MVBs) are usually considered as a subpopulation of late endosomes. Through inward budding using ESCRT machinery, endosomes collect biomolecules from cytosol and generate intraluminal vesicles (ILVs) during MVB formation.[22] To facilitate the engulfment by recipient cells, exosomes from various cell types

are found to be PS enriched, so much so that many exosome populations have even higher PS content than the plasma membrane of their parent cells.[80] The mechanism of PS enrichment of exosomes can be considered similar as the PS enrichment process of PS-recycling vesicles segregated from the early endosomes, however the machinery for such processes remain unknown today. The PS enrichment on certain leaflet of Golgi apparatus, early endosomes, and plasma membrane on the other hand is well known to be predominantly maintained by the function of flippases (a.k.a. P4-ATPases, therefore ATP dependent).[81] After the formation of MVs or ILVs, such distribution asymmetry is promptly stopped due the depletion of ATP within such vesicles. PS distribution on the double leaflet thereby quickly reaches symmetry, causing PS exposure to the extracellular environment for MVs and exosomes, facilitating the recognition and engulfment by recipient cells.

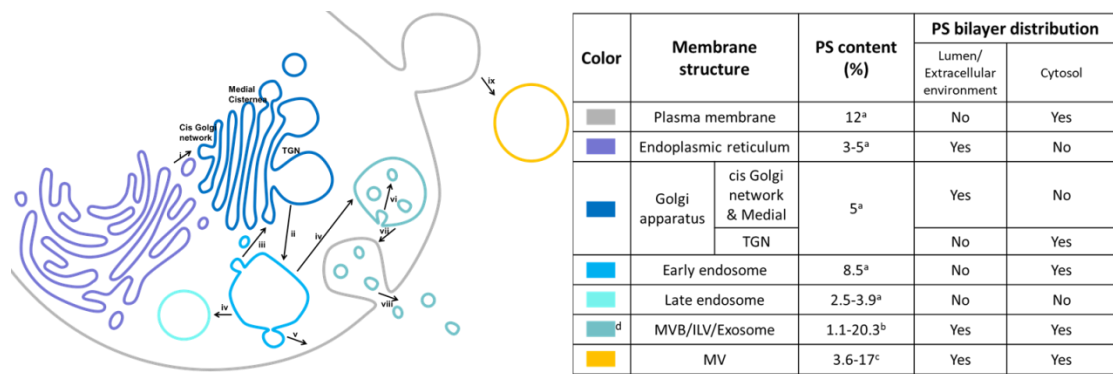


Figure 8. Cellular/Extracellular membrane structures involved in the biogenesis & transport of PS. i: vesicle transfer from endoplasmic reticulum to cis Golgi network; ii: Fission of TGN, a pathway for early endosome biogenesis; iii: fission of early endosome, generating vesicle transportation back to TGN; iv: fission of early endosome, generating late endosomes including MVBs; v: fission of early endosomes, generating vesicles to fuse with plasma membrane; vi: inward budding of late endosomes, forming MVBs with ILV inclusion; viii: release of exosomes into extracellular environment upon MVB fusion with plasma membrane; ix: outward budding of plasma membrane, generating MVs. PS contents acquired from references: a [82], b [80], c [83]. d: MVB should be categorized as late endosomes, however its lipid composition is closer to that of exosomes, while its PS distribution at lipid bilayer resembles that of early endosome.[84]

As discussed above, it seems that a universal expressing molecule on surfaces of MVs from all cellular origins is PS; however PS is also widely expressed in exosomes. If PS is used for MV capture, exosomes will also be recruited inevitably. For the isolation of these components, specific binding is no longer an option since both resembles each other greatly on their surface

molecule compositions while the variation in many cases only lies in the abundance.[6, 85, 86] For a truly MV specific surface biomarker to be used for MV isolation, such marker should 1st be omnipresent on all MV subtypes to rule out discrimination, 2nd be abundant enough for the intermolecular binding take place for sufficient capture strength, 3rd be exclusively expressed on MVs so that exosomes won't be captured at the same time. Unfortunately to date, no such molecule is reported. The size and density distribution of MVs also overlaps to that of exosomes, thus isolation exploiting these parameters will also inevitably exclude certain MV populations and retain certain exosome populations. Since MVs will only be produced in mass by cells under stimulation, in the context of disease detection, the size distribution and cargo contents of the captured vesicles in a sample will change drastically compared to a healthy control.[4, 87-90] In this sense, even the exclusive collection of MVs is impossible, the capture of the entire EV population will still play an important role in the future of diagnosis.

The presence of PS in both exosomes and MVs is well acknowledged, thus the next quest for PS's application in EV isolation is to find biomolecules that bind to PS with high specificity. The immediate answer to this question is annexin V, a molecule first discovered in human umbilical cord and studied for its anticoagulant properties.[91, 92] The anticoagulation was found to be effective through binding to plasma membrane phospholipid in a Ca²⁺ dependent manner, and the binding was soon afterwards recognized specifically targeting PS with high affinity (Kd=1.17nM).[93, 94] Among the first applications of annexin V, it is coupled to fluorescent molecules for FACS and imaging of cells undergoing apoptosis.[95, 96] Thereafter similar idea is adopted for the isolation of PS exposing EVs using FACS and got improved over the years.[97, 98] Annexin V based capture assays on the other hand, has emerged even earlier: Freyssinet et. al. reported in 1997 that streptavidin-coated microtitration plates can be functionalized with biotinylated annexin V for MV capture, while such device has similar, if not better performance compared to microtitration plates functionalized with CD4 or CD11a (quantification was achieved by quantifying PS content of microtitration plate wells after MV capture).[99] Besides annexin V, other biomolecules are also discovered to bind to PS with high specificity: Nagata's group has reported T-cell immunoglobulin- and mucin-domain-containing molecule (Tim-4) as a PS receptor with affinity comparable to that of annexin V (Kd≈2nM) in 2007, and the molecule is used in commercially available magnetic beads based EV capture device.[100, 101] In 2008, C2 domain of lactadherin (Lact-C2) was reported as a biomolecule that exclusively bind to phosphatidyl-L-

serine ($K_d=190\text{nM}$) in the presence of other phospholipids at physiological concentrations.[102] Such high specificity is indeed attractive for MV isolation applications, however to date no such application is reported.

At the moment, capture devices are considered to be a highly specific MV isolation method. In particular, annexin V functionalized surface can be used as a universal isolation method for EVs from other components of various biological fluids. In 2018, International Society of EVs updated the “Minimal Information for Studies of Extracellular Vesicles” since the first proposal in 2014, in which they summarized the major analysis directions of EVs: particle number, total protein amount, quantification of total lipids, quantification of total RNA, quantifications of specific molecules, single and multiple measures and implications for purity.[55] Capture devices seem to meet all the requirements provided that a device is able to capture the majority of EVs within a sample. Yet in an evaluation of Tim-4 magnetic beads capture device reported this year, such device is still facing the problem of low yield and small processing quantity.[103] A possible reason to the problem is that all the above mentioned biomolecules are binding to PS in a Ca^{2+} dependent manner, where Ca^{2+} is often required at concentrations as high as mM.[100, 102] As a matter of fact, most of the protein-PS interactions in biological environments are mediated by Ca^{2+} , for instance the binding of PS to prothrombin ($K_d = 1.8 \text{ nM}$).[104] Thus in the test conditions of annexin V, Tim-4 or Lact-C2, PS binding is in competition with many other potential interactions. Ca^{2+} is also a well-known regulator in myriads other biochemical processes, and such high concentration will cause potential chemical changes in vesicles of interest.[105, 106] In addition, these biomolecules also face the difficulty of biosynthesis and extraction, limiting the mass production and the price of these capture devices. Considering the protein nature of these molecules, storage temperature has to be sufficiently low to avoid degradation while test temperature has to be controlled carefully at 37°C , and incubation time of capture devices in vesicle-rich samples are usually as long as hours.

Zinc-dipicolylamine complex (DPAZn), an alternative option for PS targeting capture devices

In 2002, Hamachi's group first reported a series of chemically synthesized complexes with the ability to sense phosphorylated peptides in aqueous medium by fluorescence change.[107] These molecules are constituted by 3 segments: anthracene (fluorophore), DPA-Zn, the phosphate binding group and a methylene group connecting the two parts (molecule 1 in Figure 9). The year next, Smith's group reported the same molecules binding specifically to PS rather than phosphatidylcholine (PC), thereby labeling PS exposing apoptotic cells.[108] In both publications results also suggest two DPA-Zn units in close proximity are required for the efficient binding to PS, whereas fluorophores with only 1 DPA-Zn attached hardly respond to the phosphate rich environment. A later study from Smith's group showed that such binding is not limited to PS.[109] Anionic phospholipids such as phosphatidic acid (PA) and phosphatidylglycerol (PG) also caused intensified fluorescence responses of 1. The binding mechanism is therefore assumed to be the electrostatic interaction of negatively charged phosphate groups and Zn^{2+} cations, despite the lack of other evidences supporting this hypothesis. Hamachi's group on the hand explored the binding of DPAZn to various phosphate containing compounds, and they succeeded in acquiring crystal structure of molecule 2 binding to phenyl phosphate, shedding light on the mechanism of DPAZn binding to phospholipids: each Zn^{2+} cation binds to two phosphates, and each phosphate also bind with two Zn^{2+} cations.[110] Hamachi's study also suggests that such binding highly favors phosphate compounds with more net negative charge: 1) pyrophosphates (such as ATP or ADP) are generally preferred than monophosphate species; 2) phosphorylated peptides with more negative charge are preferred than less negative species.

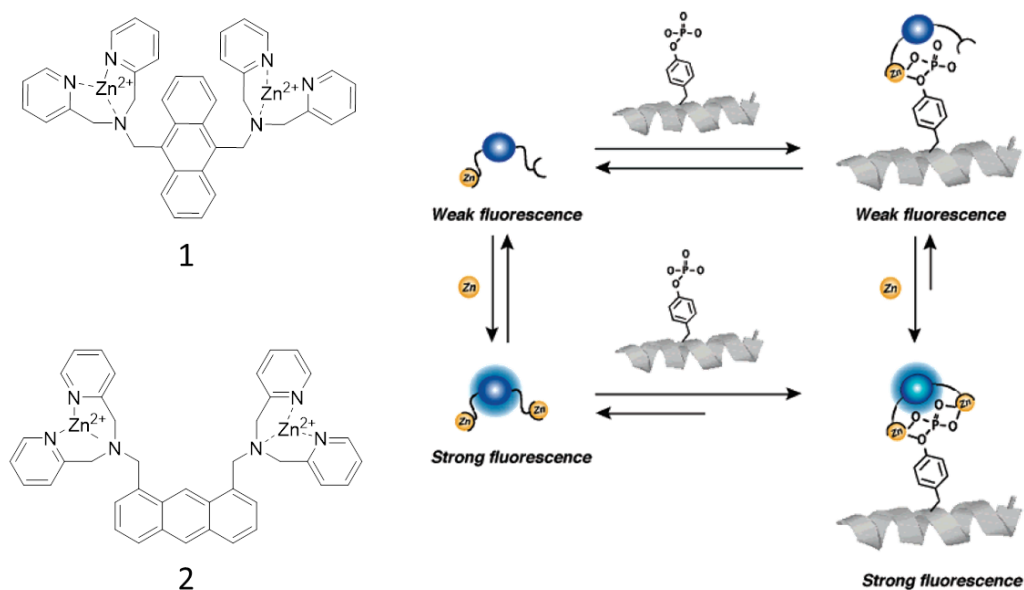
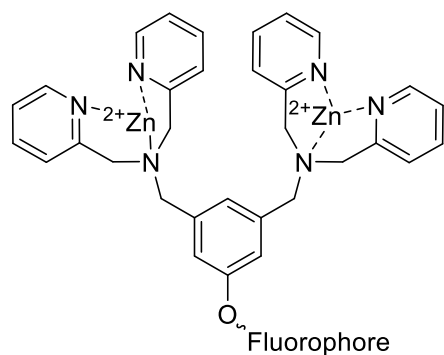


Figure 9. Phosphate binding molecules and their mechanism for fluorescence enhancement.

In later years, Smith's group extensively exploited the molecular design of bi-DPAZn group conjugating various fluorophores (Scheme 1). While bi-DPAZn group targeted anionic phospholipids, the fluorophores illuminated the targeted regions, thereby: 1) acting as imaging reagents for bacteria and dying cells; 2) acting as sensitizers in photodynamic therapy.[111-115] Similar targeting-spacer-functioning conjugates of bi-DPA-Zn are also reported in other applications: a conjugation with topoisomerase-1 inhibitor using an enzyme cleavable spacer was proven effective for the treatment of colorectal cancer in mouse.[116] Another conjugation with magnetic nanoparticles leads to the nanoparticles attaching to negatively charged *E. coli* membrane, allowing the removal of bacteria from blood in a microfluidic device.[117]



Scheme 1. Smith's design of bi-DPAZn conjugated fluorophores.

The conjugation with magnetic nanoparticles is reminiscent of the magnetic beads based vesicle capture device mentioned above. Such "capture" is also realized through bi-DPAZn and anionic phospholipid (lipopolysaccharide, to be precise) interactions. Are they applicable in the EV capture devices?

For anionic phospholipid binding strength, bi-DPAZn compounds are usually reported with K_{ds} at $10^{-5}M$ to $10^{-6}M$. [118] Such value is several orders lower than that of Annexin V, but according to ref. [117], such binding strength is adequate for the capture *E. coli*, whose particle size is much larger than that of exosomes or MVs. Binding strength is also determined by the number of interaction sites between vesicle and capture devices: annexin V is as large as 35kDa in terms of molecular mass, while the stoichiometry of PS-annexin V binding is only 8. [119, 120] In comparison, bi-DPAZn reported in most references has a molecular mass of 465Da, almost 100 times smaller than annexin V. Considering the limited surface area of all the capture devices, bi-DPAZn will have much higher molecular density. According to ref. [109], when fluorescently labeled Annexin V and molecule 1 (of Figure 9) adsorb onto anionic PS-PC membrane until saturation, 1 adhered lipid membrane emits more intense fluorescence, indicating its higher molecular density on membrane surface. By their estimation, 1 is at least 10 times more concentrated than Annexin V.

In terms of functionalization efficiency to capture device surfaces, smaller molecules are also favored for the less steric hindrance. As to the PS binding kinetics, annexin requires thousands of seconds before reaching binding equilibrium, while bi-DPA molecules only require less than a minute, making MV capture much more time efficient than any other existing methods. [121, 122]

From the perspective of binding selectivity, while PS is mostly reported for annexin V binding, there are also publications showing annexin V binding to other anionic phospholipids. [123, 124] The K_{ds} of these interactions are not documented, but the interaction principle is similar to that of DPAZn-anionic lipid membrane interactions: bivalent metal cation mediated electrostatic interaction. There are indeed concerns about the interference of PS binding in the presence of other anionic phospholipids, however Smith's results in fluorescence imaging

can still discriminate apoptotic cells from healthy ones. In a lipodimic study of EVs from various parent cells, results indicate that interfering phospholipid (such as PA and PG) concentration in MVs and exosomes either remains the same or decreases compared with parent cells, giving higher hopes for DPAZn's selective binding to PS in the context of EV capture devices.[125]

None the less, further modification of bi-DPAZn towards higher selectivity is desired in future applications. For the increased binding ability towards anionic phospholipids, Smith's group has come up with two strategies: 1) multivalent binding, i.e. a single fluorophore is bound to multiple bi-DPAZn units to increase its affinity towards anionic lipid membrane;[111] 2) amide attachment onto the pyridine rings of the dipicolylamine, creating further interaction of NH-COO⁻ hydrogen bonding.[126] Another issue for DPAZn's application in vesicle capture lies in the biophysical effect of bi-DPAZn when it binds to small PS rich vesicular structures: Zn²⁺ can induce membrane phase separation, causing leakage (therefore loss of biomolecule contents) of vesicular structures.[127] Such leakage promotion is only effective when bi-DPAZn is in contact with liposomes of ternary mixture of cholesterol, saturated DPPC, and unsaturated POPS at specific ratios, however they have only explored the leakage inducing effect on liposomes of 262 nm in size, which only represent a tiny population of actual EV population. As a matter of fact, most MVs and entire population of exosomes are much smaller than the liposomes they synthesized, therefore in a realistic situation EVs usually experience larger surface tension even without the presence of bi-DPAZn. It is conceivable that the majority of EVs will be even more sensitive to the presence of bi-DPAZn, therefore EVs with lipid compositions differs from that reported trio could also experience leakage or burst when in contact with bi-DPAZn molecules.

In 2012, Belle et al. published a patent in which they presented the possibility of using bi-DPAZn as the PS binding molecule in MV capture devices.[128] Using primary amine as the active group for attaching bi-DPAZn units to material surfaces, they discussed the possibility of imine bond formation with aldehyde exposing surfaces. To date this is still the only record to our knowledge that applied the chemical sensor molecule in the realm of MV capture devices. Unfortunately this patent elaborated only on the synthesis of possible PS binding molecules, the actual fabrication of a capture device and the performance evaluation of such device are not followed by any later published results.

To summarize the points discussed above, DPAZn could be a more attractive candidate for the PS binding capture devices for EV isolation in comparison with biosynthesized molecules: As a chemically synthesized molecule, the cost of production and storage is lower than that of biologically synthesized proteins; it is not Ca^{2+} dependent, reducing the possibility of initiating Ca^{2+} dependent biochemical/biophysical reactions of EVs; it's a much smaller molecule with faster PS binding kinetics, which could reduce the capture time and efficiency. On the other hand, technical difficulties for its EV capture application are also obvious: Higher anionic surface binding strength is desired; the possible destruction of EVs upon contact with DPAZn should also be taken into consideration.

Dendritic molecules: definition, synthesis and the pros and cons for their application in EV capture devices

In the pioneering work of turn-on fluorescence sensing phosphorylated peptides using DPAZn attached anthracenes, Ojida and coworkers reported 3 candidate molecules: 1-DPAZn anthracene, 1,8-bi-DPAZn anthracene, and 9,10-bi-DPAZn anthracene.[107] They reported that upon binding to phosphorylated peptides, 9,10-bi-DPAZn anthracene experiences a more significant fluorescence turn-on compared to 1,8-bi-DPAZn anthracene, while 1-DPAZn anthracene hardly shows any difference at all. In a later publication, they explored the reason behind such different behaviors.[110] As shown in Figure 9, the fluorescence of anthracene can be quenched by the lone pair electron from DPA units through photo-induced electron transfer (PET). When DPA is bound to Zn^{2+} , the lone pair will no longer be available for such quenching process, hence the enhanced fluorescence emission. In the case of bi-DPAZn anthracenes, only one of the DPA is able to bind to Zn^{2+} with sufficient strength to suppress the PET phenomena, while the other DPA showed little ability binding to Zn^{2+} , resulting weakened fluorescence of anthracene. In the presence of phosphorylated peptides, both DPA units can bind to Zn^{2+} sufficiently when both Zn^{2+} cations are bound to the same phosphate group, resulting the fluorescence turn-on. 1-DPAZn anthracene on the other hand is able to sense Zn^{2+} without intramolecular interference, so no change in fluorescence can be observed. As to phosphate binding strength, the bi-DPA anthracenes are determined with fluorescence titration while 1-DPAZn anthracene is determined using a competition experiment: the bi-DPA anthracenes have

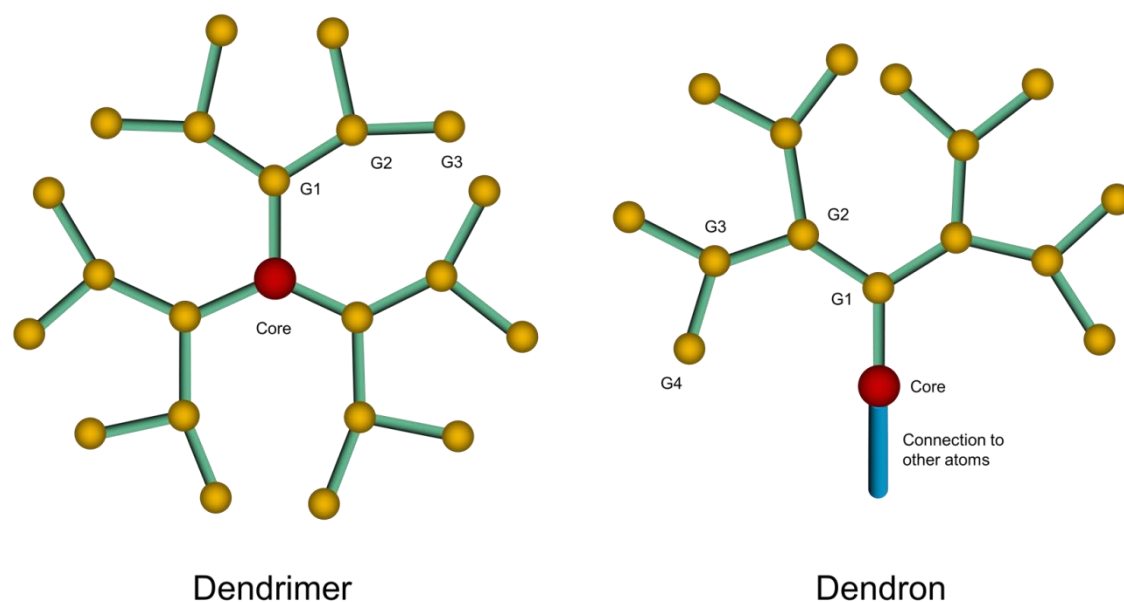
similar Kds, and 1-DPAZn anthracene has a Kd two orders of magnitude higher, indicating the much weaker binding strength. In 2003, Smith's group discovered similar fluorescence enhancement of 9,10-bi-DPAZn anthracene in the presence of PS containing lipid bilayer, and in 2005 they published the enhancement mechanism similar to that of phosphorylated peptides sensing.[108, 109]

The aforementioned reports illustrated two important principles for designing DPAZn containing molecules for PS binding: 1) more DPAZn units can result in higher binding affinity; 2) closely packed DPAZn units can work cooperatively when binding to phosphate. The further demonstration of the first principle is ref. [111], in which molecules of multiple bi-DPAZn can increase their affinity to PS rich membranes; however the second principle hasn't been explored in greater depth to this date. A design that meets both requirements should be a molecule with multiple closely packed DPAZn at its peripheral, while at the same time provides a reactive site to bind to supporting materials. An immediate molecular design to satisfy both principles is a dendritic molecule with DPAZn units attached to its periphery: At dendron periphery, the number of DPAZn attaching sites grows exponentially as generation of dendron increases; and due to the reducing space for each branch/terminus to occupy with the increase of dendron generations, the close packing requirement for DPAZn synergy can also be achieved. The detailed dendritic structure design and the rationality of such design are discussed as follows.

Dendrimers and dendrons: Definition and synthetic approaches

Dendrimers are a group of monodispersed molecules defined by their unique structures. [129, 130] A dendrimer develops from a center moiety (known as core or generation 0) of multiple branching sites. From each site, a first layer of identical units offering two or more branching sites are attached, which is defined as the first generation. On each branching site of 1st generation, another layer of the same units are attached, yielding the 2nd generation. With the repetitions of such layered development, a dendrimer is formed. Ideally a dendrimer has a defined number of generations, while with each growth of generation, the number of repeating units grow exponentially (Scheme 2). Since the first day dendrimers are reported, they are considered to be a specific kind of polymer.[131] As a matter of fact, the physical and chemical properties of dendrimers are quite different from that of traditional polymers. Dendrimers are different with

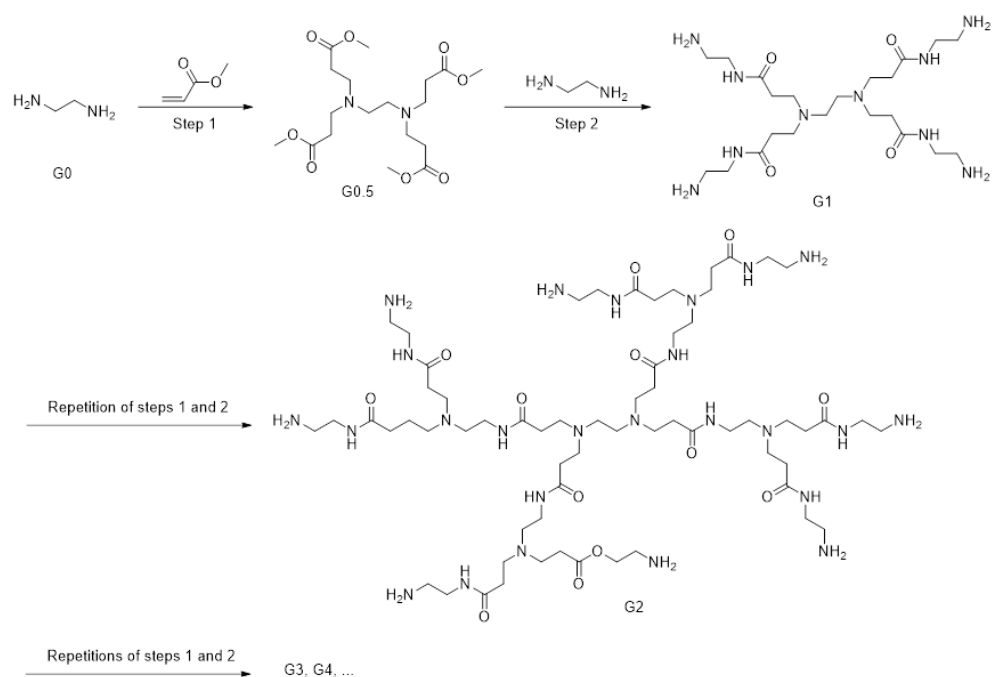
hyperbranched polymers in two ways: 1) Dendrimers have specifically designed repetitions, therefore in theory monodispersed molecular weight. Dendrimer of former generation needs to be activated to react with monomers at designed stoichiometry to form designed generation. After the development of this generation, the reactions sites are closed for further attachment of next monomers. 2) Due to the steric hindrance, there is an upper limit for the molecular weight or generations of a dendrimer with a specific repeating unit.[132]



Scheme 2. Schematic presentation of dendrimer and dendron (dendron has a focal point used to attach it onto something) structures.

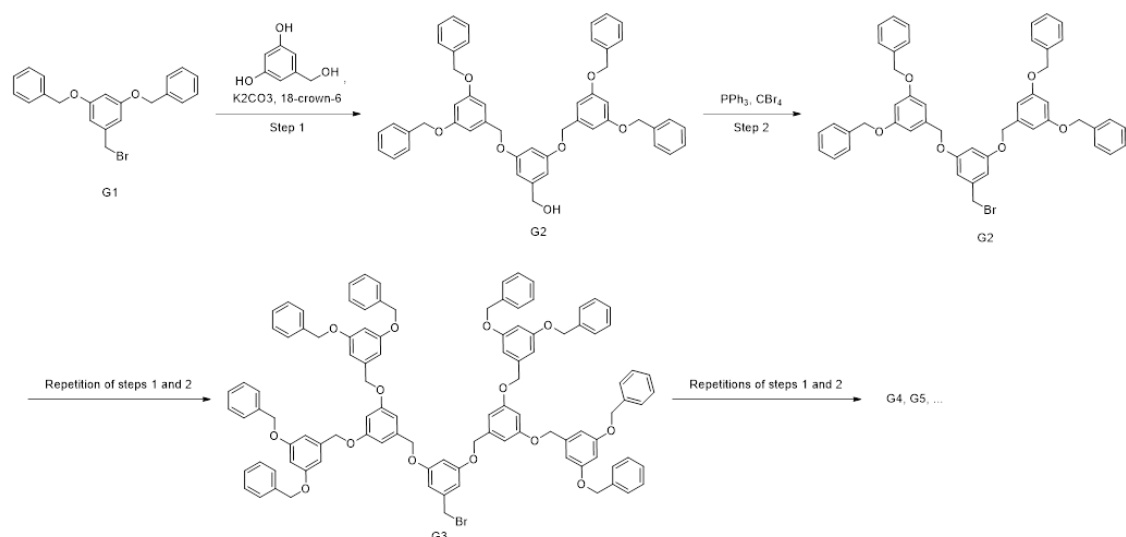
The huge varieties of the dendritic structures are well documented in a number of review articles each with its own focus.[130, 133-136] The principles for dendrimer synthesis on the contrary are strictly limited in two approaches: the divergent synthesis (the synthesis starts from the core and develop with each reaction step into designed generation) and convergent synthesis (the synthesis start by combining peripherals with the repeating unit and develop inwards with each step until the designed generation).[130] Dendrimer core with a single branch developed from it is defined as a dendron, therefore one may argue that each step of the convergent synthesis is only about dendron development instead of dendrimer synthesis. For both approaches, a most well-known example is provided below.

Divergent synthesis of polyamidoamine (PAMAM) dendrimers (Scheme 3) [131]: The synthesis usually starts from a primary amine. Using Michael addition, two molecules of methyl acrylate are attached to each primary amine forming two branches. For the next generation to be developed, the resulting ester then goes through amidation with a large excess of ethylenediamine, so that more primary amines are exposed for the next round of Michael addition.



Scheme 3. The divergent synthesis of PAMAM dendrimers.

Convergent synthesis of poly(benzyl ether) dendrons (Scheme 4) [137]: The synthesis starts with a molecule of 3,5-dihydroxybenzyl alcohol nucleophilically attacks two benzylic halide, leaving behind a benzyl alcohol. For the next generation to be developed, the benzyl alcohol was transformed into another halide through various halogenation reactions (in this case Appel reaction using PPh_3 and CBr_4), ready for the next nucleophilic substitution.



Scheme 4. The convergent synthesis of poly(benzyl ether) dendrons.

In the divergent approach, the number of reactive sites grows exponentially with the increase of dendrimer generation. If we presume that the structure of dendrimers always allow the last generation exposed to the outside environment (that is to say every branch are radiating outwards from the dendritic core without folding back), peripheral sites will remain high reactive even at high generations, giving better chance for the formation of the next dendrimer generation. For instance, Tomalia et al. synthesized PAMAM of G10, and Caminade et al. reported phosphorus-containing dendrimers of even G12.[138, 139] On the other hand, even if the reactivity of peripheral groups keeps the same between generations, statistically there will still be more defected branches for dendritic structures of high generations. Besides, since the structural difference is minimal within the same generation, the isolation of defected dendrimers from the perfect ones is difficult, and the defection found in this generation will be carried into the next, and thus resulting in the accumulation of imperfections in the high generation dendrimers.

At each step of convergent synthesis, the reactive site is usually located at the core (focal point) of the dendritic structure, and when the dendritic structure goes to higher generation, the reactive site is unavoidably shielded by the branches attached from the new core molecule to be attached; therefore convergent dendrimers of high generations are rarely reported.[130] On the other hand, the convergent synthesis is known to produce pure and perfect dendrimers. After reaction, usually there will only be unreacted former generation, core molecule, partially reacted

of this generation and perfect molecules of this generation. The difference in molecular weight between the perfect molecules and other components of this generation are quite significant, making the purification process much easier, and of course the defects in this generation won't be carried on to the next.

In our case, the MV capture device multivalent binding can be achieved without using dendritic molecules, since the material surface will be sufficient to accommodate billions of simple DPAZn molecules. The important factor is therefore to explore the synergetic effect of closely packed DPAZn units. To make comparison between the monometallic DPAZn complex and a dendritic molecule counterpart bearing multiple DPAZn units, one of the crucial information is to know exactly how many DPAZn units appear in a single dendron. In this sense, even though both approaches are able to produce dendrimers of high generations that will satisfy our requirement of multiple closely packed DPAZn at peripheral, convergent synthesis is obviously a better choice because of its structural perfection. Besides, dendrons have a functional group at the focal point used to attach them to a variety of functional molecules and nanoscale materials. Thus, dendrons are convenient for our project, as this function will help to connect them onto the material surface.

The physical and chemical properties of dendrimers/dendrons

Solubility, monodispersity and solvent residue

To construct multivalent molecule with DPAZn located adjacent to each other, dendritic structure is not the only choice. For example, when DPAZn is attached to a monomer that can be used in polymer synthesis, a synthesized polymer is also able to realize out molecular design. As reviewed by Zheng et al., in most cases the synthesis and purification of polymers is relatively easier than that of dendrimers.[140] Polymerization usually requires one step of reaction and relatively facile purification, thus much less intensive effort than dendrons syntheses. A question to ask before the synthesis of dendrons therefore, is why use the globular structured dendrimer instead of a linear polymer or hyperbranched polymer?

Kampf and coworkers synthesized a series of linear counterparts to poly(benzyl ether) dendrons up to G6, and compared the molecular size, solubility and crystallinity of the two families of the hyperbranched dendritic systems.[141] They find that at lower generations when there isn't enough inter-branch steric repulsion for the dendrons to assume a globular shape, linear counterparts have similar solubility and crystallinity compared with the dendrons. From G5, dendron molecular size is significantly smaller, glass transition temperature is lower, while solubility in solvents such as THF, acetone, or chloroform is higher compared to that of the linear counterparts. The highly crystalline nature of the linear molecules clearly indicates a stronger intermolecular interaction. When at high generations, the highly compact dendrimer molecular conformation won't allow branches of neighbor molecules to be inserted to promote intermolecular interactions, while none of the branch from the compact molecule itself is able to reach out to interact with adjacent dendrimer.

To functionalize material surface with our synthesized molecule, good solubility in both organic solvents and aqueous buffers is highly desirable for functionalization and washing, making the linear polymer a less attractive candidate compared to dendrimer. Besides, the strong intermolecular interaction between linear molecules also hinders the exposure of DPAZn units in the context of MV capture devices. Thus due to solubility and functional group exposure issues, peripheral functionalized dendritic structures are preferred than linear polymers.

For hyperbranched polymer, indeed solubility is less of a problem, while the molecular size can also be controlled to be comparable to that of dendrimers. However it is still less than ideal for similar reasons as we prefer convergent synthesized dendrimers over divergent ones as discussed above.

Dendrimer conformation: extended or back folded

As suggested by Genne and Herve in their theoretical study, with the growth of dendrimer generations, the branches attached should be increasing exponentially, leading to the exponential growth of molecular weight.[132] Meanwhile, the growth of dendrimer molecule size grows cubically due to the limitation of interatomic bond length. Because of this, space available for each atom shrinks drastically with the growth of dendrimer generation to the point when such

growth is no longer possible. In their studies, they have presumed that every single branch of the polymer is radiating away from the dendrimer core, making the space close to dendrimer center relatively vacant while the peripheral highly crowded. Tomalia has performed computer simulation of the molecular dynamic conformations of PAMAMs at different generations.[139] In contrary to the assumption made by Genne and Hervet, the dendrimers of high generation has higher atomic density inside the molecule globe than on its periphery, which indicated at least some of the dendrimer branches are folded back into the molecular cavity (Figure 10). Such information is crucial to our molecular design first because after we synthesized dendritic structures with dipicolylamine attached to the molecular peripheral, might be hindered by such back folding can prevents the complexation of Zn^{2+} ; second, when the DPAZn functionalized dendron is used to bind to PS, back folding may also interfere with the binding. If some of the branches are folded inwards, the desired synergetic PS binding effect may also be disrupted due to longer distance between the DPAZn units.

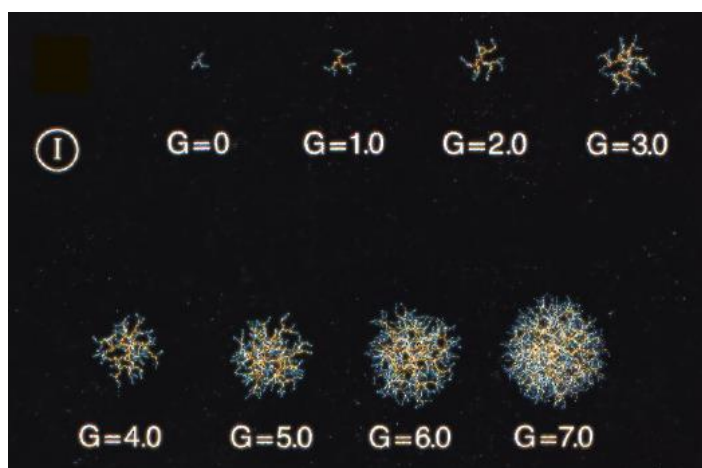


Figure 10. The Conformations of G0 to G7 PAMAM dendrimers by computer simulation. Picture taken from ref. [139]

Back-fold or not, in later research was found to be controllable for some dendrimers. Welch and Muthukumar studied the conformational change of poly(propylene imine) using Metropolis Monte Carlo simulations, in which they consider every amine group positively charged.[142] As shown in Figure 11, in a solution of high salt concentration or high pH, the molecule would assume a highly back folded, contracted conformation due to the neutralization of

the positive charge; while when the salt concentration or pH is low, the dendrimer would be stretched due to the repelling force between the ammonium cation. Beside such polyelectrolyte dendrimers (in which ammonium cations are dispersed throughout the entire molecule), another type of dendrimer or rather functionalized dendrimer that only have ions at its periphery, display even more intriguing properties as they are highly reminiscent of micelles, and therefore named as “unimolecular micelles”. Hawker et al. reported poly(benzyl ether) dendrimers with methyl benzoate functionalized peripheral.[143] Under basic conditions, the ester bond was hydrolyzed, exposing cationic benzoate. Such dendrimer is soluble in water, as the poly(benzyl ether) scaffold is completely shielded by the hydrophilic benzoates. What’s more, the poly(benzyl ether) scaffold can be used to dissolve other hydrophobic molecules while peripheral benzoates provide water solubility, making each dendrimer molecule behaves like a micelle. In fact, the increase of ionic strength in the aqueous solution can further increase the loading ability of this unimolecular micelle, making similar dendrimers highly useful in drug delivery systems.[144-146]

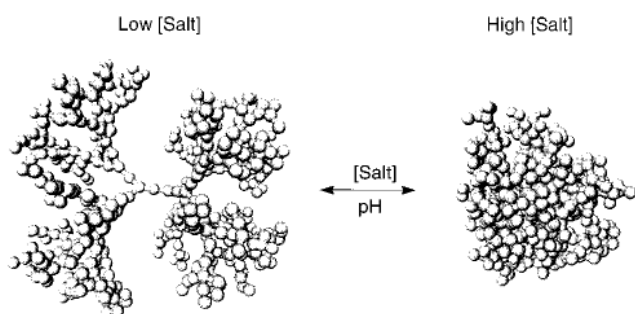


Figure 11. Computer simulated conformational change of G6 poly(propylene imine) dendrimer, picture taken from ref. [142]

In our case, to fully expose the DPAZn units to the aqueous environment, the obvious strategy is to construct the dendritic scaffold using hydrophobic molecules. At dendron periphery, DPAZn units will fully expose to the aqueous environment, while the material surface will further restrict the free space for dendron conformational change, promoting the “close pack” of the DPAZn units.

Periphery functionalization of dendrimers

The solubility of dendrimers is highly tunable by the modification of their end groups.[147] Such controllability is exceptionally prominent when dendrimers are at high generations, when the internal scaffold is shielded by the dendrimer peripheral groups.[148] At higher generations, not only the solubility of dendrimer itself can be tuned, small molecules adsorbed into its scaffold will also present similar solubility, making dendrimers useful candidates for drug delivery.[149] For example, in a recent publication Erturk and coworkers discussed the solubility of candesartan cilexetil (a drug against hypertension[150]) in the presence of PAMAM dendrimers.[151] As shown in Figure 12, the solubility is highly dependent on both generation and the peripheral groups of the dendrimers. While higher generation dendrimers provide more adsorption area for the drug to adsorb onto the polymer, the acidic carboxyl end groups can provide stronger drug-dendrimer interaction by hydrogen bonding with the tetrazole and benzimidazole moieties of the drug molecule, increasing the drug loading per dendrimer.

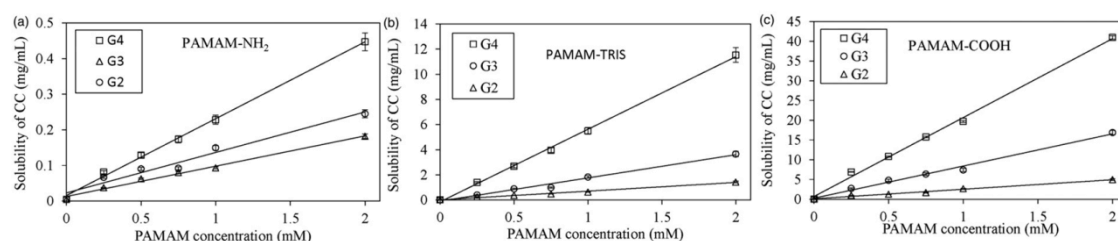


Figure 12. The impacts of surface functionalization and generation of co-dissolved PAMAM dendrimers on the solubilities of candesartan cilexetil. Picture taken from ref. [151].

A step further from drug loading systems would be the controlled drug release, which requires more elaborate peripheral modification of the unimolecular micelles as well as the combination with other materials. Chen and coworkers have reported a drug release system that is able to continuously release rapamycin (an anti-intimal hyperplasia medicine [152]) over a time of more than four months.[145] They synthesized a tri-layer unimolecular micelle (Figure 13 A): G4 PAMAM polymer (with hydroxyl ending groups) was used as the molecular scaffold, while valerolacetone was attached to the polymer onto PAMAM as hydrophobic drug loading layer. Afterwards, another layer of PEG (with one carboxyl ending groups and one methoxyl ending group) is attached to valerolacetone as hydrophilic reagent. Suspended in a triblock copolymer,

this drug loading system can release its content in dialysis experiment continuously over 140 days (Figure 13 B). In the releasing kinetics, the dendrimer construction was found to be the major contributor to this prolonged release due to its chemical stability.

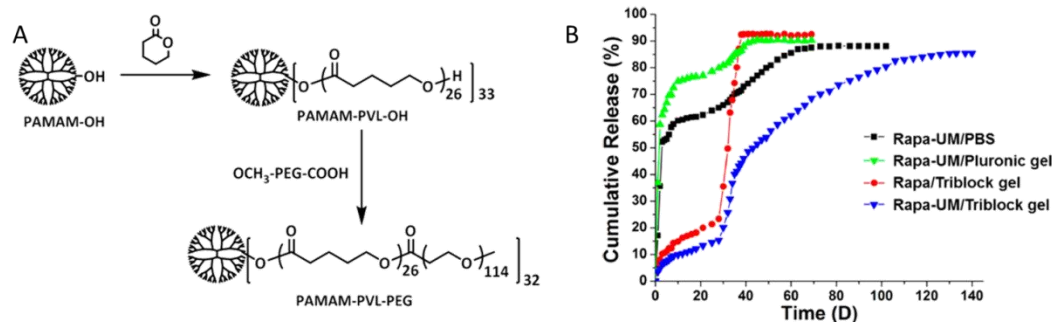


Figure 13. A, The synthesis of tri-layer unimolecular micelle based on G4 PAMAM; B, the cumulative release of rapamycin (Rapa) from different drug loading systems: UM/PBS: unimolecular micelles dispersed in PBS; UM/Pluronic gel: unimolecular micelles suspended in pluronic gel; Triblock gel: triblock copolymer gel; UM/Triblock gel: unimolecular micelles suspended in triblock copolymer gel. Picture taken from Ref. [145].

The application of dendrimer peripheral modification is not limited to solubility manipulation. By grafting certain molecules onto the dendrimer peripheral, functions such as fluorescence imaging, specific site targeting can also be achieved. In an earlier publication from the same group of people who developed the controlled drug releasing system described in Ref. [145], they made further modification on the three-layer slow release unimolecular micelle (Figure 14) [153]: instead of finishing the last layer with only PEG-OMe, they used a mixture of PEG finishing with methoxy groups (for increasing solubility), Cy5.5 (a fluorescent dye molecule for tracing the unimolecular micelle), and maleimide (for thiol group attachment). The maleimide was then substituted by thiol substituted non-toxic cholera toxin B for its retinal ganglion cell targeting ability. In this construction, a peripheral functionalized unimolecular micelle was able to achieve drug loading/slow releasing, specific targeting and fluorescence tracing at the same time. Similar designs of surface modification is widely adopted over the years of using dendrimers as drug delivering systems, since the dendrimer provides a robust platform for achieving targeting, drug delivering and imaging at the same time.[154-157]

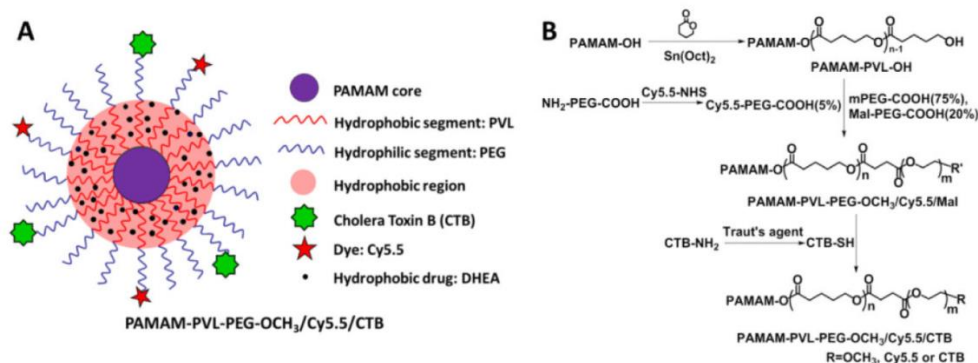


Figure 14. A, a schematic presentation of multifunctionalized PAMAM unimolecular micelle; B, the synthesis of multifunctionalized PAMAM unimolecular micelle. Picture taken from Ref. [153]

The benefits of ending group functionalization didn't end here: Hrushikesh et al. reported surface modification of G5 poly(propylene imine) dendrimer using the method developed by Stoddart's group (Ref. [158]) with 4 kinds of groups: Boc protected glycine, Boc protected phenylalanine, lactose and mannose.[159] They found that functionalized dendrimers drastically reduced both toxicity and hematological response by masking the ammonium peripheral groups of dendrimer. Similar peripheral "masking effect" was also summarized in a book published by Boas et al., in which they discussed the biocompatibility of cationic, anionic, lipid functionalized and PEG functionalized dendrimers (Figure).[160]

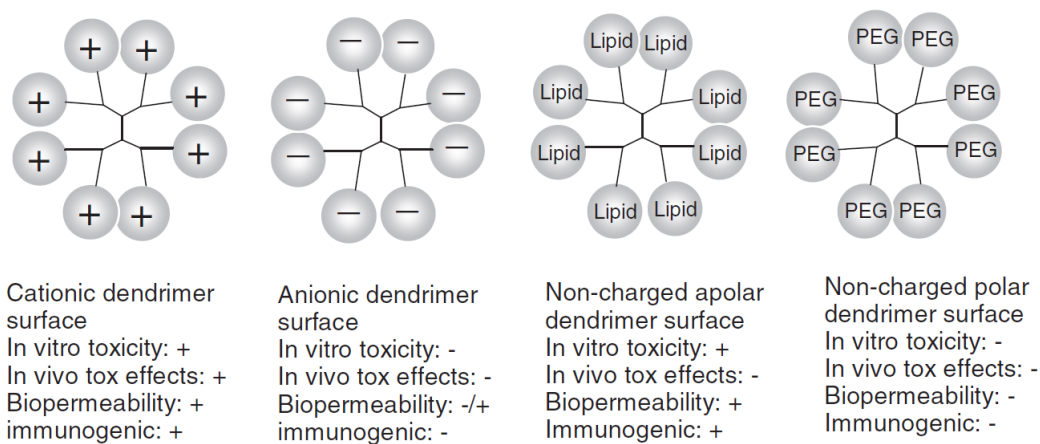


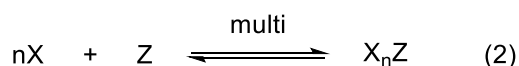
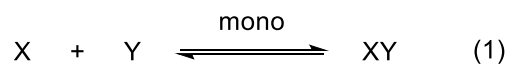
Figure 15 Biocompatibilities of surface functionalized dendrimers. Picture taken from ref. [160]

The nature of multivalency and the common misconception of synergetic binding

As reviewed above, in recent drug delivery system designs, the dendrimers are extensively exploited as the molecular scaffold due to 1) the ease of surface functionalization; 2) the high stability of scaffold compared to liposomes; and 3) the improved delivery targeting ability. The specificity is usually achieved by attaching specifically binding molecules such as antibodies, peptides, folic acid and other small molecules to the dendrimer peripheral.[146, 153, 155, 161, 162] In all the cases, there are multiple binding sites on a single dendrimer molecule. From the reaction kinetics perspective, such design significantly increased the chance of binding when the dendrimer is in contact with a targeting site. However as explained by Mammen et al. in their review article about biological multivalent binding, from a thermodynamics perspective, the multiplicity design tells a more complex story[163].

In a monovalent binding reaction, for example reaction (1) of Scheme 5, the association constant is defined as $K_{a1} = \frac{[XY]}{[X][Y]}$ with a unit of M^{-1} . The Gibbs free energy change during this reaction is defined as ΔG_1 , therefore we have $\Delta G_1 = -RT \ln K_{a1}$ (to be precise, ΔG_1 is independent from the solution concentration, therefore K_a used henceforth should divide by $C_0^{-1} = 1 M^{-1}$ to get rid of the concentration unit, but since the values of ΔG won't change, I haven't deliberately discriminate this two constants). And in parallel, we assume there is a multivalent X binding molecule constructed by attaching n Ys onto a single molecule (all binding sites are equivalent), i.e. the molecule Z, the reaction of X with Z would be as shown in reaction (2) of Scheme 5. The total association constant in this case would be: $K_{at} = \frac{[XY]}{[X]^n[Y]}$ with a unit of M^{-n} , with the total change in Gibbs free energy: $\Delta G_t = -RT \ln K_{at}$. In this binding process, if we define the average change in Gibbs free energy for each binding site is ΔG_{av} with corresponding association constant of K_{aav} , then we have: $\Delta G_{av} = -RT \ln K_{aav}$. Considering $\Delta G_t = n\Delta G_{av}$, we should also have $\ln K_{at} = n \ln K_{aav}$, therefore $K_{aav}^n = K_{at}$, and the cooperative factor of this multivalent binding can be defined as: $F_c = \frac{\Delta G_{av}}{\Delta G_1} = \frac{\Delta G_t}{n\Delta G_1}$. Since association constants or dissociation constants are more often reported in literatures, F_c is translated: $F_c = \frac{\ln K_{at}}{n \ln K_{a1}}$

$\frac{\log K_{at}}{n \log K_{a1}}$. By definition, only when $F_c > 1$, the binding is synergetic, when $F_c = 1$ or $F_c < 1$, the binding is additive or interfering, respectively. [163]



Scheme 5. monovalent and multivalent binding reactions.

Unfortunately, in most literatures the strength measurement of the multivalent binding process is confused with that of monovalent binding, with the most obvious evidence that the total association constants are always recorded in unit M instead of M^n . In Table 1 of the review article [164], the authors listed over fifty cases of “binding enhancement” using the multivalent strategy claiming the enhancement is calibrated by binding ligand valency, yet such calibration is done by dividing the apparent strength (association constant or free analyte concentration $[X]$) with the valence of the ligand. The proper approach would be using the cooperative factor F_c , comparing the thermodynamics instead of concentration.[160, 163]

Why K_a or concentration $[X]$ is not the parameter to be used in such analysis? For K_a (or dissociation constant, K_d), the answer is quite simple: monovalent K_{a1} has the unit M^{-1} while multivalent K_{an} has the unit M^{-n} , making them incomparable to each other. In the case of $[X]$, let's investigate an example ref. [165]. They have made competition experiments for a series of mannose functionalized molecules to compete with ^{125}I marked Man₂₁-ALK-HAS for E.coli binding, and recorded the IC_{50} (the concentration of inhibitor that causes 50% reduction in the binding of the labeled reference ligand. [166]), as shown in Figure 16. Afterwards, they came up with the term “ IC_{50} per monosaccharide” by multiplying the observed IC_{50} with the number of mannose in each molecule. While in monovalent binding IC_{50} is linearly dependent to K_a , again, such mistake came from the misconception that K_a is comparable between monovalent binding and multivalent binding.

Inhibitors	IC ₅₀ [nM]	IC ₅₀ per mono-saccharide [nM]
TFA-ah- α -Man	74	74
Man ₂₉ -Al-BSA	175	5075
Man ₃₅ -AD-BSA	87	3045
Man ₁₉ -SQA-HSA	5.7	108
Man ₃₂ -SQA-HSA	1.0	32
Man _{7,3} -ALK-HSA	29	212
Man ₁₁ -ALK-HSA	21 \pm 0.7	231
Man ₁₈ -ALK-HSA	12	216
Man ₂₁ -ALK-HSA	5.0 \pm 1.5	105
Man ₂₅ -ASA-BSA	0.88 \pm 0.2	22
Man ₃₄ -ASA-BSA	0.2 \pm 0.01	6.8

Figure 16 The IC₅₀s of various multivalent mannose functionalized neoglycoproteins against ¹²⁵I-Man₂₁-ALK-HAS when binding to E. coli. Table taken from ref. [165].

But does this mistake matter? As illustrated in Figure 16, such mistake doesn't stop people come up with "highly efficient multivalent binding molecules", since even in the parameter IC₅₀ itself, molecules with more mannose performs better than the ones with less mannose. The **multivalent molecular design** must be useful. The response to this argument, unfortunately, is no. What this strategy actually have achieved is deceiving us into synthesizing more and more complex molecules without thinking what we actually can do instead, is **simply prepare a more concentrated solution of the monovalent ligand**. In other words, an n-valent molecule of 1 M is a less effective and labor intensive way to prepare a solution of n M monovalent molecule.

As an example, let's study the acidities of a series of linear saturated dicarboxylic acids (CH₂)_n(COOH)₂ in comparison with H(CH₂)_nCOOH. Every dicarboxylate (A in short) can be considered as a bivalent proton binding ligand, while the acidities pK_{a1} and pK_{a2} (to avoid confusion with association constants, pK_{a1} and pK_{a2} are henceforth referred to as p₁ and p₂) give us the values of the binding association constants. Similarly, the corresponding monocarboxylic acid's acidity is referred to as p₀. In each step of protonation of dicarboxylate, there is: $K_a' = \frac{[HA][H]}{[A][H]^2}$, $K_a'' = \frac{[H_2A]}{[HA][H]}$, therefore $K_{at} = K_a'K_a''$ Considering $p_1 = \log K_a''$, $p_2 = \log K_a'$, $p_0 = \log K_{a1}$, the cooperative factor is $F_c = \frac{\log K_{at}}{n \log K_{a1}} = \frac{p_1+p_2}{2p_0}$. As shown in the inset table in Figure 17, the F_cs of short chain dicarboxylates have values significantly lower than 1, while the long chained ones have F_cs only slightly higher than 1. In view of this, when the purpose of a research

is only achieving more efficient bindings, a simpler and more practical way of realizing this goal is simply using a more concentrated solution of monomers whenever possible. If we go back to Figure 16 (or table in ref. [164]), indeed we don't observe 34 orders of magnitude's binding efficiency growth when they use a molecule of 34 mannose, the F_c in this circumstance, is extremely close to 0.

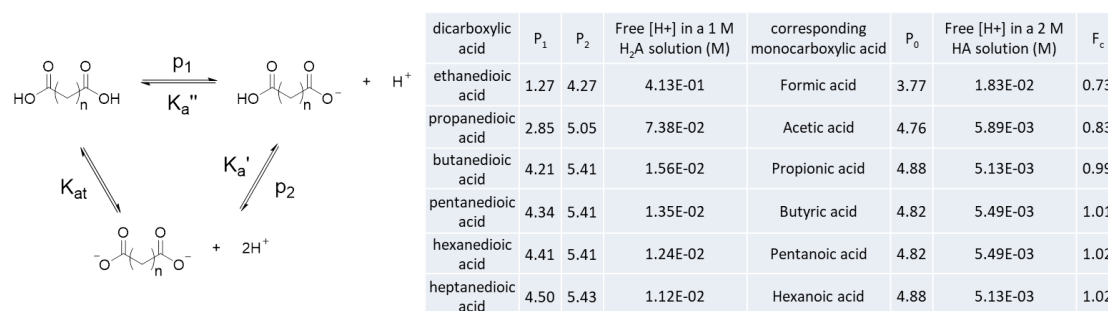


Figure 17. left: schematic representation of dicarboxylic acid hydrolysis; right: comparison of hydrolysing abilities of dicarboxylic acids and monocarboxylic acids. Note that acid hydrolysis is the reverse reaction of carboxylates binding to protons.

But our research of multivalent binding systems, especially dendrimer systems shouldn't be completely discouraged due to the discussion above. Peripheral functionalized dendrimers provide a platform for the binding sites to dissolve or localize in a highly concentrated form. Specific binding in essence is the interaction of an electron donating moiety with an electron accepting moiety. When we construct a multivalent binding system, we have increased the local electron negativity/positivity to some extent, while the firstly bound sites will have negative effects on the other binding sites, the first binding(s) could achieve higher binding strength itself (themselves). For instance, in the inset table of Figure 17, the P_2 values of dicarboxylic acids are higher than corresponding monocarboxylic acids' P_0 s, indicating at low concentration, protons will bind to dicarboxylates more readily than to monocarboxylates. Such enhancement could be an interesting topic of study, unfortunately to the best of my knowledge, no stepwise K_a values are determined in any currently published literatures for dendrimer bindings.

In the case of DPAZn-PS binding, although there is no direct evidence reported, but people believe such binding has the same mechanism as when DPAZn binds to other phosphates.[118, 126, 167] As reviewed in section "Zinc-dipicolylamine complex (DPAZn), an

alternative option for PS targeting capture devices”, when DPAZn moieties increase from one to two, the two units still binds to one phosphate synergistically, therefore the change in K_d values is beyond the realm of multivalency.[110] As to Further increase in the number of DPAZn units in a dendritic system, first, there is possibility that further synergic binding could take place; and second, at material surface, when the beneficial factor of local concentration outweighs the detrimental factor of inter-ligand interference, better binding performance can also be achieved. As to the other important factors in dendrimer-vesicle interaction, they are discussed in the section below.

Dendrimer interaction with lipid bilayers

As reviewed above, dendrimers are widely adopted for binding applications in biological context. Since most biological systems are encapsulated in vesicles made of lipid bilayers, the question of how the dendrimer molecules interact with lipid membrane is raised for concerns of cytotoxicity, cell membrane penetration and other biocompatibilities.[136, 168] One dendrimer family of particular interest is the PAMAM, since its surface charge can be switched from negative (on half generation, carboxyl group exposing structures) to positive (on full generation, amine exposing structures), and it is believed that biocompatibility issues mainly come from the surface charge.[160, 169]

Parimi et al. studied the influence of PAMAM solution on substrate supported DMPC (1,2-dimyristoyl-sn-glycero-3-phosphocholine) lipid bilayer membrane with the combination of optical waveguide lightmode spectroscopy and AFM.[170] They found that regardless of dendrimer generation, at 1 nM and 10 nM concentrations, all the dendrimers were able to influence the amount of adsorbed lipid by aggravating the already existing defects (irregular in shape) on the supported lipid layer (Figure 18 A); while at 100 nM all the dendrimers were able to remove materials from the adsorbed membrane by generating holes spontaneously (Figure 18 B). To study the mechanism of mass removal from the lipid bilayers, Mecke et al. also carried out similar experiments with AFM.[171, 172] They proposed that PAMAM can interact with lipid membrane so strongly that it can rip part of the adsorbed lipid membrane from the substrate. The smallest holes observed on lipid membrane has roughly the same surface area with a lipid coated dendrimer particle (if this kind of nanospheres i.e. “dendrimersomes” are formed, as shown in

Figure 19 A).[173] They further examined this hypothesis by adding PAMAM into a small unilamellar vesicle (SUV) suspension (Figure 19 B), and found in the dynamic light scattering (DLS) results a new population of particles of 12-16 nm in diameter (the calculated membrane coated PAMAM particle should have diameter of around 17 nm). ^{31}P NMR spectrum of this suspension after PAMAM addition also reveals a new peak (Figure 19 C), indicating the formation of a novel phosphate component, which could be the hypothesized PAMAM-membrane complex.

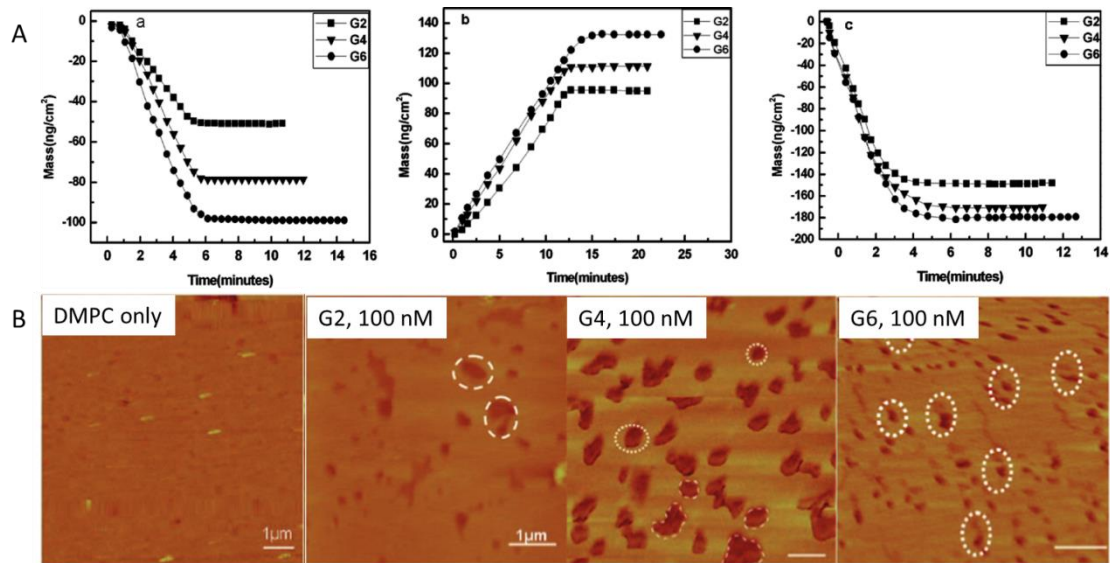


Figure 18 A Mass changes of DMPC supported lipid bilayers monitored with optical waveguide lightmode spectroscopy: a, in the presence of 1 nM PAMAMs; b, in the presence of 10 nM PAMAMs; c, in the presence of 100 nM PAMAMs. B Morphological change of DMPC supported lipid bilayers in the presence of 100 nM PAMAMs monitored with AFM.

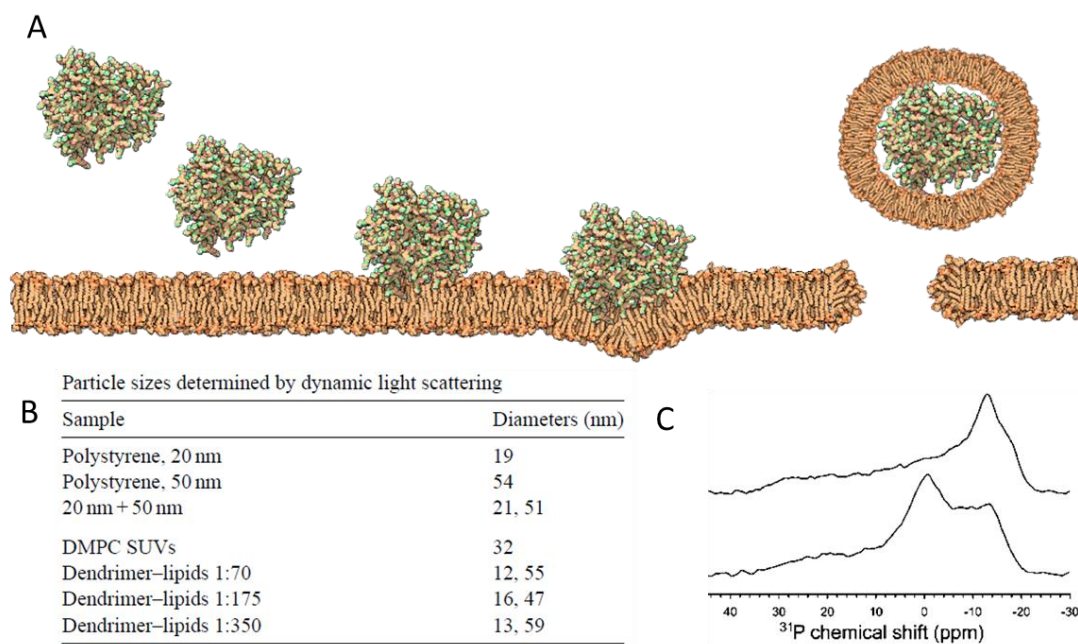


Figure 19 A Proposed hole-generation mechanism on DMPC supported lipid bilayers by formation of dendrisomes; B DLS detected particle sizes in DMPC SUV suspension before and after adding PAMAM; C ^{31}P NMR of DMPC SUV suspension before (upper spectrum) and after (lower spectrum) adding PAMAM. Picture A is taken from ref. [173], Picture B and C are taken from ref. [172]

The experiment results above are further explained with computer simulations. Wang et al. studied the interaction of single PAMAM molecules (full generations) with DMPC (1,2-dimyristoyl-sn-glycero-3-phosphocholine) membrane with computer simulation using coarse grain method.[174] As shown in Figure 20, from G3 to G9, all the dendrimers bind to the hydrophilic head groups of the top layer membrane. With the increase of dendrimer generation, while G3 and G5 molecules only disrupts the molecular assembly of the top layer, G7 and G9 dendrimers are able to cause deformation of the bottom lipid layer. As we can see from the top view, from G3 to G9, despite the large difference in molecular mass, the volume occupied by each dendrimer haven't changed accordingly, indicating that dendrimers of smaller generations prefer to take more flattened conformation and distribute unit amount surface charge to more lipid molecules, causing less surface tension. On the side view, while all the dendrimers try to integrate into the lipid bilayer and form smooth transition from dendrimer-bound to dendrimer free areas, dendrimers of higher generations are simply too bulky and conformationally restricted to allow such smooth morphology. Using similar method, Lee and Larson found the deformation of DMPC

membrane is a concentration dependent process: at the surface of lipid bilayer they have deposited 1, 4, and 16 G5 PAMAMs or 1 and 4 G7 PAMAMs. At higher surface concentrations, both G5 and G7 dendrimers are able to induce membrane destruction by pore formation.[175]

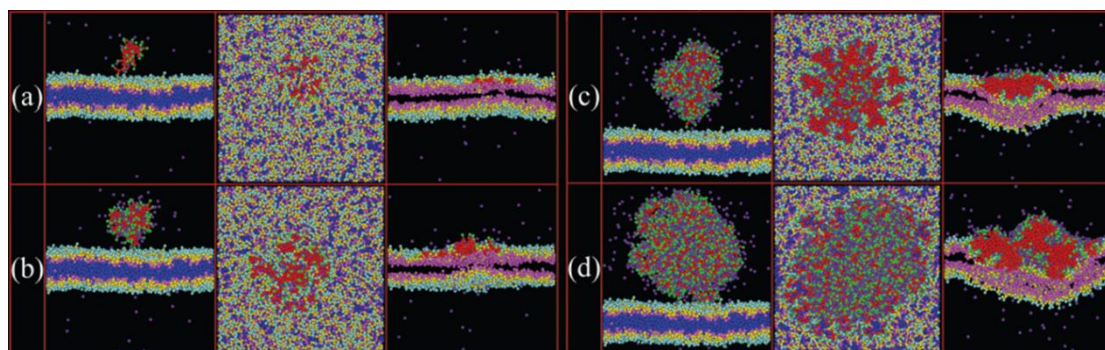


Figure 20 Snapshots of complexes formed by charged PAMAM dendrimers on DMPC membranes at the beginning (left images, side view) and the end (middle images, top view; right images, cross-sectional view) of computer simulations. (a) G3, (b) G5, (c) G7, and (d) G9. Picture taken from Ref. [174].

Berényi et al. further characterized the DMPC multilamellar vesicles-PAMAM interaction with an integration of characterization approaches[176]: In differential scanning calorimetry, they find the enthalpy change related to polar headgroups change drastically when lipid vesicles are in contact with PAMAM, while the enthalpy change related to hydrophobic tails is less sensitive. In small angle X-ray scattering spectra, clear widening distances between Bragg reflection peaks indicated the detachment of multilamellar from one another (possibly due to dendrimer insertion, [177]), while wide angle X-ray scattering spectra that correlate to the packing of aliphatic chains again showed minimal changes. The layer detachment is verified with freeze-fracture electron microscope, while small quantities of small vesicles/micelles are also observed (possibly the dendrimersomes hypothesized above [172]). This small population of spherical structures was assumed to be responsible for the appearance of a new peak in ^{31}P spectra. Fourier-transform infrared spectroscopy was also applied to study the molecular level changes of both DMPC and PAMAM, which also indicated the amine-polar head interaction.

In summary, regardless of dendrimer generations, positively charged PAMAM is always able to interact with lipid bilayer (to be precise, the polar head group of phospholipids). In many cases, higher generation dendrimers will cause damage to the integrity of the membrane

structures, which is informative for the design of our microvesicle binding dendrimers: while higher generation dendrimers are able to bind with vesicles strongly due to higher local concentration, such interaction could also be destructive by damaging the vesicle membrane and causing leakage of vesicle content.

A brief introduction of the step-by-step construction of our capture assay.

MVs due to the diversity of their cellular origins are unique in its molecular contents. While such diversity gives us rich information on their parent cells, a design of universally applicable MV isolation method is challenging. Many readily adopted size or density dependent methods require expensive apparatus with time consuming processes, yet contaminations such as protein aggregations are still unavoidable. In view of this, isolation methods based on specific recognition is now considered the only approach to collect MVs of high purity.

By attaching the recognition molecules onto a substrate, the specific recognition is now exploited not only for its selectivity but also their strengths of binding, allowing the capture of MVs onto the substrate to realize isolation. The commonly used antibody-antigen recognition is highly specific to MVs from cells of certain origins. Capture devices based on these recognitions are unavoidably biased since only a certain population in a sample can be recognized, while the rest of vesicles are neglected. What's more, for MVs from different cellular origins, corresponding devices have to be tailored accordingly, making the devices impractical for laboratory or clinical applications. Thus phospholipid recognition came into sight for new MV capture device designs because of the omnipresence of phospholipid in these vesicle-bound structures. In particular, PS is a universal "eat me" signal throughout human body, and its presence on MVs' membrane outer leaflet is well characterized. PS binding biomolecules, for instance annexin V, were grafted onto material surface for MV capture, yet the Ca^{2+} dependence of these molecules give rise to concerns that the capture itself might alter the biochemical properties of the MVs. In addition, such biosynthetic molecules face the problem of low stability, high cost, and difficult mass production.

DPAZn as a synthetic PS binding molecule has only come into sight in the 21st century. Its conjugation with fluorophores is now commercially available as a marker of apoptosis, yet hardly any report can be found for its use in MV recognition, let alone capture. Besides, DPAZn units are still used today with very limited optimization, thus it has great potential in MV capture, preferably improved with higher PS affinity.

Our design of MV detection system is therefore a capture device utilizing the interaction between PS and DPAZn. When model material surface is functionalized with DPAZn, the material will be able to capture MVs through interaction with PS. To further enhance the capture performance, a series of dendrons with DPAZns attached on peripheral are synthesized for material functionalization, while dendron core is free to connect to substrates with covalent bonding. Multivalent dendritic structures can promote the PS-DPAZn interaction through increased local concentration. Meanwhile the synergetic binding of two closely attached DPAZn units to a single phosphate was proven to be beyond the definition of multivalency, therefore the attachment of DPAZns onto peripheral of a dendron also has the potential of achieving similar synergetic effects and acquire better PS binding performance.

On the other hand, many published literatures have reported cationic dendrimers of high generations are able to destroy lipid bilayers by removing lipid molecules from the membrane assembly. Such results hinted that there could be a ceiling of dendricity for our dendron molecule designs: while higher generation dendrons could interact with PS containing membranes stronger, the loss of dendron conformation flexibility could also backfire on dendron design and result in membrane destruction.

Based on the above information, we have come up with a design as follows:

1) *Device design*: As shown in Figure 21, to realize capture, DPAZn complexes are grafted onto the device. The capture device will incubate with samples of extracellular fluids containing MVs, and the interactions between PS and DPAZn will allow the capture of MVs onto the device. After a while, the device will be removed from the incubation fluids and washed with buffer solution, leaving only the MVs captured above for further examination.

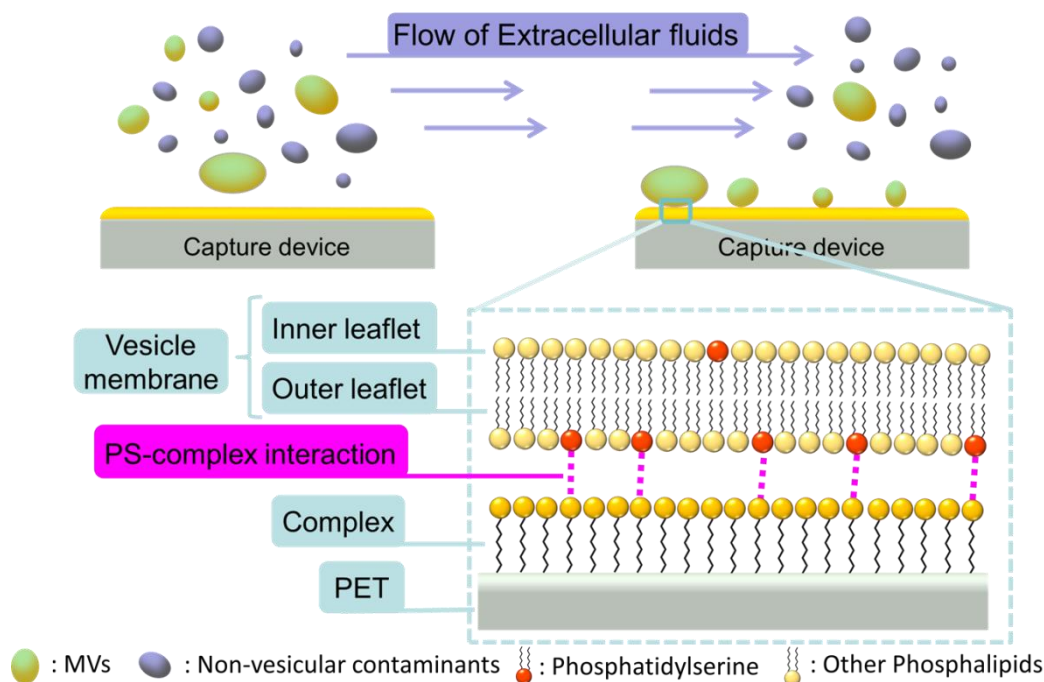
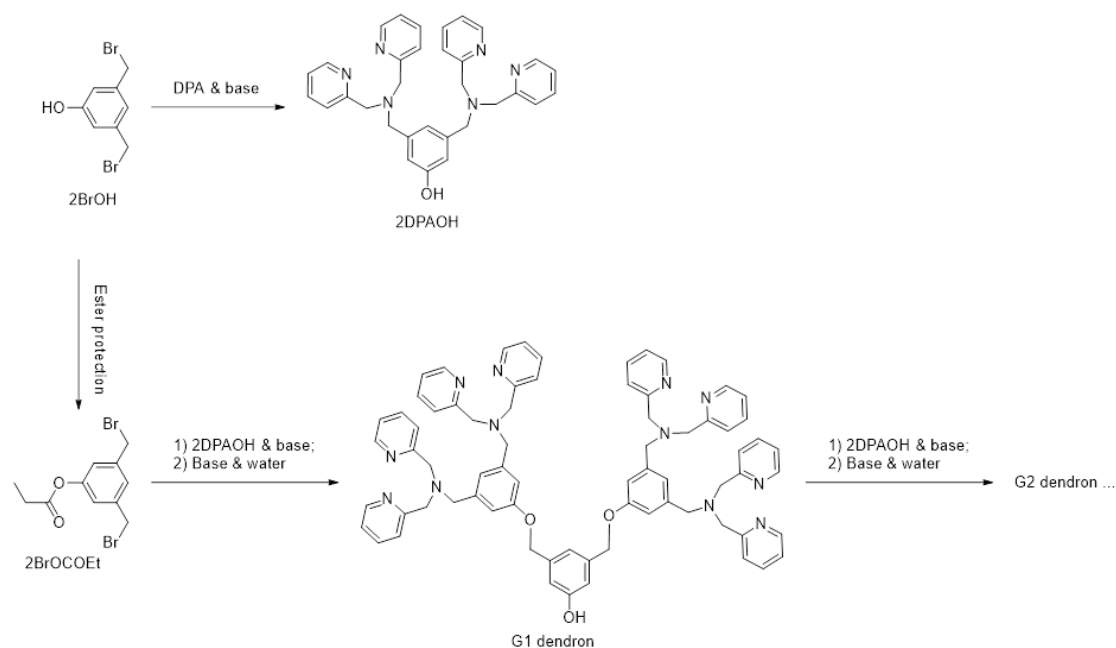


Figure 21. A schematic presentation of our capture device design and the conceptual capture mechanism.

2) *Molecular design*: As discussed above in the “Dendrimers and dendrons: Definition and synthetic approaches” section, the syntheses of dendrons by convergent method are preferred for our purpose. The widely adopted bi-DPAZn unit was synthesized using the strategy shown in Scheme 6, in which two DPA units react with 3,5-dibromomethylphenol by nucleophilic substitution to give the corresponding phenol with two DPA groups. The phenol group will be used for the synthesis of higher generation dendrons. The synthesis of dendrons starts conveniently from the protected phenol (2BrOCOEt) as shown in figure 6, using similar strategy to that mentioned in Scheme 4. Nucleophilic substitution by 2DPAOH will result in the G1 dendron with 4 peripheral DPA units. The ester protection is removed under basic conditions, and the G1 dendron can be used for the synthesis of the G2 dendron..



Scheme 6 Synthesis strategy for DPA terminated dendrons.

The concept of “multivalency” is already achieved in the capture device design, since material surface will be covered with DPAZn containing molecules. Despite this, dendritic structure is still useful to accelerate the binding kinetics and hopefully achieving further PS binding synergy. Meanwhile, the membrane destruction of high generation cationic dendrimers should also be taken into consideration. Thus to determine the ideal dendritic generation for MV capture, we have considered dendrons with increasing peripheral DPAZn units, in order to evaluate their PS binding ability and MV capture performance on polyethylene terephthalate (PET) substrate.

Characterization for each step: why I decided to use these methods?

Dendron synthesis

NMR is the most widely adopted method for characterization of organic compounds. For our dendrimer designs, from monomer to dendrimer, the most significant change in ^1H NMR would be the peaks of methylene groups. From halide to ether, it is expected a significant change

in chemical shift. The integration of each of these methylene groups is also informative on the defects at lower generations: From G0 to G1, the change should be 0 to 4 protons, while from G1 to G2, the increase is from 8 to 12 protons, etc. However, such increase becomes less prominent in higher generations, for instance from G2 to G3, the proton integration increase from 24 to 28, making it difficult to distinguish G3 dendron from G2. Thus in this case it is difficult to confirm the completion of the reaction. In the case of ^{13}C NMR, the shift of the carbon of the methylene is not significant from one generation of dendron to another, thus we have used another method for the identification of these dendrons.

Mass spectrometry to date still remains the most reliable method for the determination of molecular weight. In the synthesis of dendrons, since the molecular weight grows exponentially from one generation to the next in each step of convergent synthesis, the molecular peaks are the most direct proof of successful reaction. Matrix Assisted Laser Desorption Ionization (MALDI) and Electron Spray Ionization (ESI) are currently the most used ionization methods in dendrimer characterization, since both are considered to be relatively “soft” ionization methods and are able to preserve the molecular peaks.[178, 179] However, Felder et al. reported that MALDI process could result in the reaction of acidic matrix with the sample, yielding “false negative” results for dendrimer defects.[180] Although not reported yet, similar reactions could happen to the DPA units as well, since the reaction that proceed for the synthesis of dendrons is in general nucleophilic substitution on tertiary amines, leading to possible elimination of molecular peaks. For this reason, we adopted ESI for all mass experiments performed with our dendrons.

Dendron-PS interaction

Binding events between two organic molecules can be considered as a special kind of chemical reaction; therefore the chemical environment near binding sites will change drastically after the reaction. Such change in chemical environment can translate into chemical shift changes in NMR spectra. In the case of dendron-PS interaction, ^1H NMR for the identification of DPAZn units in dendrons and ^{31}P NMR for the identification of PS are of particular interest, because phosphorus from PS and methylene protons from DPAZn should be affected during the complexation, as they are directly bind to the Zinc atom of or to the nitrogen bind to Zinc (i.e. Zn^{2+} to phosphate).

The most significant difference between binding and conventional organic reactions is that binding is a reversible event. Such difference is reflected in the NMR spectra, by the positions and shapes of the corresponding peaks. As shown in Figure 22, in organic reaction, when reactant A is in excess, there will be two individual peaks for the reacted and unreacted compounds. In contrary, during binding, there is a fast exchange between the bounded and the unbounded molecules, resulting in a single broad peak between the chemical shift of bounded and unbounded molecules. The position of the broad peak is determined by the binding equilibrium, since it is at the center of weight of the bounded and free molecules: $\delta = \delta_X \frac{[X]}{[X]+[XY]} + \delta_{XY} \frac{[XY]}{[X]+[XY]}$. [181] Due to the involvement of K_d , the NMR has also been used to determine the binding affinity by linearization or fitting of a titration curve. Unfortunately such titration is only sensitive enough to K_d s as high as 10^5 M, while the binding of bi-DPAZn containing molecules to PS containing membranes have one or two orders of magnitude for higher affinity. [126, 182] In spite of this, NMR remains a powerful tool for the determination of binding stoichiometry using job plot method. As discussed in section “The nature of multivalency and the common misconception of synergetic binding”, such information could be essential for the evaluation of multivalency design and also informative to the binding mechanism when structural information is limited.

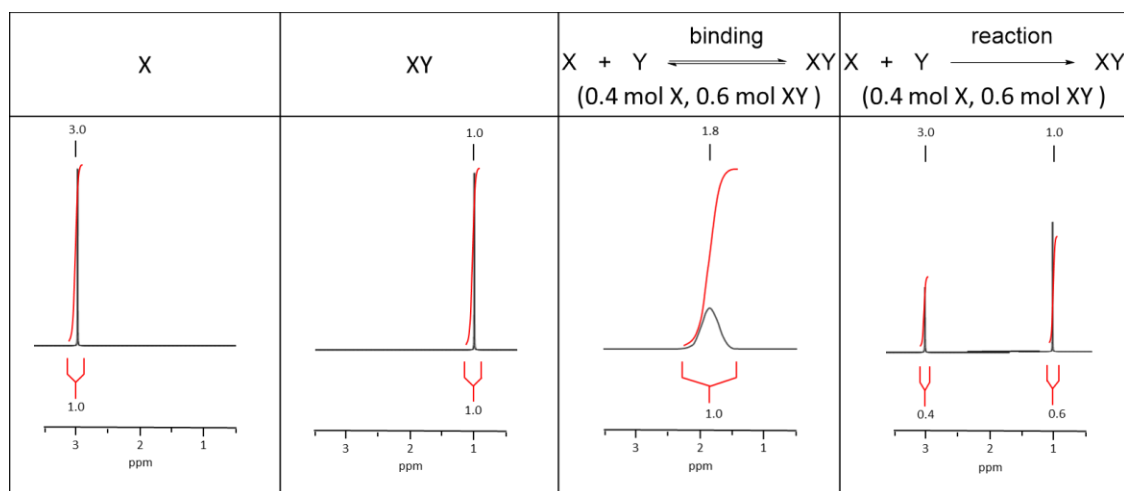


Figure 22: Simulated ^1H NMR spectra of X, XY, mixture of X and XY when X and Y are binding to each other, mixture of X and XY when X and Y react with each other, respectively.

Dendron-membrane interaction

The desired membrane-complex interaction would be simply Zn^{2+} in complexes are binding to the outmost lipid layer's hydrophilic groups without disrupting the self-assembly of the lipid molecules, as illustrated in Figure 21. It is therefore desirable to monitor physical changes of a lipid bilayer while the complexes are binding to it. While imaging methods, for example AFM, are able to provide pictorial information of the interaction, the quantification of binding strength and physical changes of the lipid membrane during this binding event is beyond the capability of such approaches.[170-172] Our choice of technique to meet these requirements is therefore plasmon waveguide resonance (PWR) spectroscopy, a homemade modification of commonly known surface plasmon resonance (SPR) spectroscopy that specializes in lipid-molecule interaction analysis.

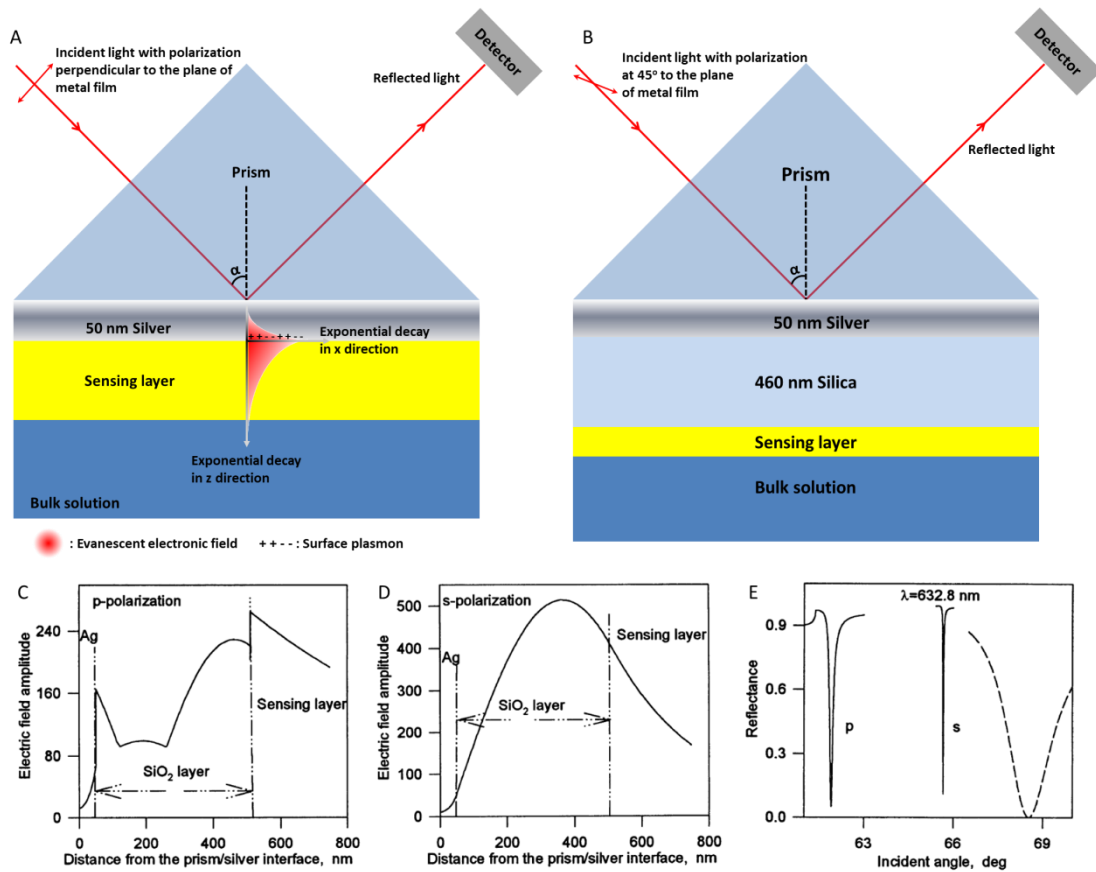


Figure 23. A: The setup of SPR spectrometer; B: The setup of PWR spectrometer; C: The evanescent field intensity of p-polarized light; D: the evanescent field intensity of s-polarized light; E: Calculated reflectance

spectra of: dashed line: SPR presented in A; p: p-polarized light of PWR presented in B; s: s-polarized light of PWR presented in B. In all 5 figures, the light source is a continuous wave He-Ne laser at 632.8 nm. Figures C, D, E were taken from ref. [183].

In a typical setup of SPR shown in Figure 23 A, under total internal reflection (TIR) conditions, the incident light (with electric vector perpendicular to the silver film, in other words p-polarized) is able to generate an evanescent wave at the prism-silver interface, which in turn can propagate to the other side of the silver film, inducing the generation of an evanescent electronic wave, i.e. surface plasmon (“plasmon” is defined as collective oscillation of free electrons in metal, where the free electrons are considered as plasma).[184, 185] This electronic wave can further penetrate into the dielectric material on the other side (sensing layer and a small part of bulk solution) and form electromagnetic interaction with it. Due to the evanescent nature of both waves, there is no energy loss in these processes. Therefore reflected light intensity doesn’t decrease after TIR, and the reflected light intensity recorded by the detector remains constant as the incident angle α changes. However, at a certain position where the evanescent wave meets the surface plasmon resonance conditions, energy from the incident light is able to transfer to the silver film, resulting the decrease in light intensity recorded by the detector.[186] If the reflected light intensity is plotted against α , a SPR spectrum can be acquired. Due to the interaction between surface plasmon and the dielectric material in contact with the silver film, the chemical/physical change happens at the interface can be reflected in the changes in the SPR spectra (dashed line in Figure 23 E). Furthermore, since the surface plasmon electronic field dies down exponentially as it propagates away from the silver film, the sensing layer at the interface is also limited to a thickness of hundreds of nanometers.[186]

Salamon et al. has developed a variant of the conventional SPR setup which was named as PWR.[183] Similar with SPR, PWR acquired its high sensitivity to surface changes by exploiting the characteristics of surface plasmon. On top of the silver layer, another coating of 460 nm silica is applied. Acting as a waveguide, this coating has broken the limitation of p-polarized excitation light, allowing the absorption of light with electric vector parallel to the silver coating (s-polarized). For this reason, the light source has a polarization usually placed at 45° angle to the silver surface, introducing plasmon resonance signals of both p- and s- polarizations (Figure 23 B). As shown in Figure C and D, the two evanescent electric fields have completely different behaviors when passing through the silica coating. As a result, although the same light source is

used, the resonance angles are different for the two polarizations as shown in Figure E. The difference in s- and p- polarization can be translated into the difference of molecular deposition onto the silica coating, meaning the analysis of material anisotropy can also be achieved by analyzing the PWR spectra. Another interesting phenomenon is that for both polarizations the electric field strengths increase significantly after passing through the silica layer, resulting the sensing layer thickness decreased to only 5 nm, comparable to the thickness of a lipid bilayer adsorbed on silica.[183] As mentioned in the section “Dendrimer interaction with lipid bilayers”, such adsorbed lipid bilayer is widely used as a lipid model for lipid-molecule interaction studies and is known as supported lipid bilayers. From the aspects of both sensing layer thickness and anisotropy, PWR is an ideal technique for the study of supported lipid bilayers.[187-189] Besides, since the silver layer is protected by silica, the silica layer is less prone to the chemical erosion caused by exposure, allowing the washing of PWR prisms, making such tests more economical than SPR.

Dendron functionalization of the surface: qualitative & semi-quantitative

Before discussing the ideal characterization technique(s) for the functionalized PET surface, it is necessary to describe the functionalization process itself, since the characterization is used to evaluate the material change before and after the chemical treatments.

The surface treatment of the PET sheets was conducted using a protocol developed in our lab with modifications suited for functionalization of DPAZn complexes. The original protocol are described in detail in ref. [190, 191], and the modified protocol was described in later chapters. The description herein focuses on the aspects important for surface characterization, while the technical details are omitted. As shown in Figure 24, PET sheets go through first hydrolysis and oxidation, transforming the material surface into a carboxyl groups exposing state. These two steps are conducted in aqueous environment, and reagents used in these two steps are unable to penetrate deep into PET sheets. The reactions happened in these steps are therefore superficial, causing no change in the chemistry or physics on the material bulk. The activation of carboxyl groups is also conducted in aqueous solution using EDC/NHS chemistry. Again, the reagents used

are unable to penetrate into the matrix of PET polymer, besides, the carboxyl groups are almost exclusively exposed at material surface, it is reasonable to consider surface activation also happens exclusively superficially on PET. In the step of DPAZn functionalization, although DMSO was used as solvent, the amide bond formation is only possible at places with NHS activated carboxyl groups, while the non-covalently linked molecules will be washed away during the sonication-shaking washing cycles. Again, the molecules of interest only localize at the surface of PET sheets as a single layer of molecule covalently attached. Thus, the analysis techniques required is a method detects only the chemical property changes of the material surface, ideally the single layer of molecule on top of the PET substrate. Especially for the purpose of comparing the performance of complexes with different dendricity (including first, how many molecules of different complexes are able to attach to the PET surface under the same experiment conditions and second, what are the MV capture abilities of different complexes when similar amounts of molecules are fixed onto PET surface), the knowledge of molecule per square nanometer material would be most desirable to exclude the effects of surface concentration.

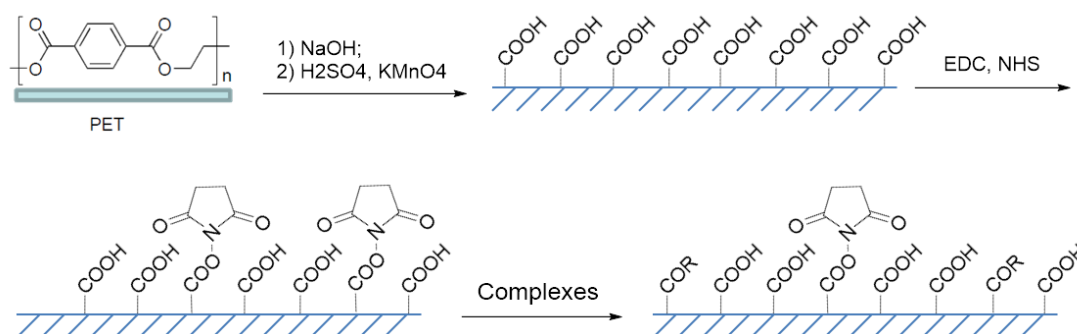


Figure 24: Chemistry on PET surface for the grafting of complexes. R represents the complexes of various dendricity.

The most ideal characterization of complex functionalized PET surface would be the quantification of the absolute amount of Zn^{2+} , since only Zn^{2+} chelated DPA units are active during MV binding while some of the Zn^{2+} in surface complexes will be inevitably washed away during the intensive sonication-shaking cycles. Unfortunately, to the best of our knowledge, to date there isn't a technique able to achieve Zn^{2+} quantification at material surface with sensitivity high enough to detect a single molecular layer. Our solution is therefore to overcome this technical

problem with a combination of Toluidine blue-O (TBO) test and X-ray photoelectron spectroscopy (XPS).

TBO is a method widely adopted for the analysis of surface carboxyl group density as reported previously.[190, 192, 193] The test mechanism in brief, is that under basic conditions the COOH groups are transformed to COO⁻, which is able to bind with cationic TBO⁺ ions with a 1 to 1 stoichiometry. The bound TBO⁺ can be washed off with acid and since it's a molecule with high molar extinction coefficient, its amount can be easily measured with a UV-vis absorption spectrometer, and then translate into surface carboxyl group density by calculation. After activation step, many of the COOH groups are substituted by NHS, thus a decrease in the TBO adsorption amount is expected. The substitution of NHS by synthesized DPAZn complexes are able to further decrease the TBO adsorption by the integration of at least three mechanisms: 1) the cationic Zn²⁺ repels the adjacent TBO⁺ ions; 2) The complexes are on top of the COOH layer, shielding it from the TBO molecules; 3) Despite low reactivity, amine terminated complexes are still able to react with COOH without the help of NHS activation, further decrease the COOH group counts. This method undoubtedly is able to qualitatively characterize the complex functionalization process since its reaction with PET surface only occurs on the PET surface as a single molecular layer. However due to the three complications discussed above, the quantification of complex surface concentrations is unable to achieve. Besides, it only monitors the counts of carboxyl groups, yielding no information of the deposited molecule layer.

XPS on the other hand, is a method able to analyze the atomic composition of functionalized PET.[191] However, its measurement is not limited to the top layer of molecule. As described in the later chapters, under our test conditions its penetration into the PET bulk is around 5-10 nm. Because of this, although it gives information on atomic percentage of various atoms in the detected depth, such percentage is not equivalent to elemental analysis of surface grafted molecules. None the less, molecular density on PET can be reflected in specific atomic percentages, for instance Zn, and parallel comparison of Zn percentage is equivalent to the comparison of grafted amount of complexes, making XPS a useful semi-quantitative method for complex functionalization on PET.

For the qualitative analysis of material surface, i.e., despite the challenge that only the very top layer of molecules on functionalized PET should be analyzed, there are other characterization techniques available other than XPS. For instance, with the control of primary ion species and ionization parameters, time-of-flight secondary ion mass spectrometry (ToF-SIMS) has been reported to have nanometer resolution on the depth profile when studying polymer materials.[194] In this case, fragments coming off the polymer surface as secondary ions could be analyzed with mass spectrometer to yield information on the chemical composition. Attenuated total reflectance Fourier transform infrared (ATR-FTIR) spectroscopy is also able to provide information on functional groups appearing on material surfaces. On common ATR-FTIR spectrometers, the internal reflection elements usually only allow micrometer scale penetration depth (a depth of 0.65 μm can be achieved using a Ge prism), far deeper than the desired several nanometers.[195, 196] However in a recent publication, it is already reported that on a polymer film as thin as 10 nm, ATR-FTIR has comparable depth resolution as XPS when a specific substrate and linearly polarized IR light (electric field polarized parallel to the plane of incidence) are adopted.[197]

Characterization of MVs after capture

As discussed above, the MVs are prone to destruction when in contact with cationic dendrimers of higher generations. Vesicle destruction can also be observed in the cases of liposomes in contact with highly hydrophilic surfaces like silica, forming planar membranes such as “supported lipid bilayers”.[198-200] Such destruction is only limited to the membrane structure, leading to leakage of vesicle content into the aqueous medium. In this context, immunological fluorescence imaging and ELISA tests focusing on the binding of cell membrane proteins is quite limited for such purpose. Destroyed or not, the captured vesicle membrane will always give positive results regardless of the morphology of the vesicles captured. We believe that a proper characterization of MV content composition (both inside the vesicle and within its membrane bilayer) should only be conducted after confirming the vesicle integrity, otherwise the analysis will become incomplete and biased. What we need first is the characterization of vesicle morphology. The vesicle size as we characterized is around 100 nm, and to reach such high resolution conventional fluorescence imaging is out of the question. Scanning electron microscope

(SEM) on the other hand, is able to reach such high resolution while giving us information on material surface, however the high vacuum test environment in the SEM setup will surely destroy the MVs because of water evaporation. For the preservation of morphology for SEM tests, the captured MVs are first frozen in slush of nitrogen and then dried by sublimation. Such technique was widely adopted for the imaging of cells and tissues.[201, 202] In the study of extracellular vesicles, electron cryomicroscopy is also considered to be the best to study vesicle morphology.[55]

The content of the next two chapters

The content in chapter 2 is a patent submitted to European patent office under the number EP19185572.5, describing the application directed part of the work. The content of chapter 3 is a research article published in iScience, in which the scientifically important topics such as the molecule-molecule interaction, possible explanations of different capture performances of different capture devices, are discussed.

Chapter 2: Ligands for capturing microvesicles and Uses thereof (patent EP19185572.5)

Patent submitted to European patent office: EP19185572.5

Inventors: Marie-Christine Durrieu, Sylvain Nlate, Jian-Qiao Jiang and Christel Chanseau

Field of the invention

The invention relates to synthetic ligands for capturing microvesicles and their use in the diagnostic and prognostic of diseases in a subject.

Background of the invention

Microvesicles (also known as cellular microparticles) are submicron extracellular vesicles that are found both in the interstitial space between cells and in body fluids. Microvesicles are released from the surface or plasma membrane of cells by the outward budding and fission of the plasma membrane. The budding process involves multiple signaling pathways including the elevation of intracellular calcium and reorganization of the cell's structural scaffolding. The budding takes place at unique locations on the cell membrane that are enriched with specific lipids and proteins reflecting their cellular origin. At these locations, proteins, lipids, and nucleic acids are selectively incorporated into microvesicles and released into the surrounding environment. Microvesicles play a role in intercellular communication and can transport molecules such as mRNA, miRNA, mitochondrial DNA and proteins between cells.

Microvesicles are released during cell activation or during apoptosis, in the course of various pathological conditions, including cancer, inflammation or and a variety of diseases such as diabetes, Parkinson disease, cardiovascular disease with increased risk of thrombosis or even neurovascular ischemic conditions.

Microvesicles have a high density of phosphatidylserines exposed on the outer leaflet. They also expose a variety of cell surface proteins according to their cell origin and the type of pathology or physiological event inducing their release. Moreover, it was shown that an increase in microvesicles can be correlated with the onset and presence of diseases in patients. For instance, increased leukocyte-derived microvesicles levels have been reported in the blood of patients with sepsis or with high atherothrombotic risk. It is also believed that microvesicles play an important role in the regulation of intercellular communication, inflammatory response and vascular function.

Thus, it was proposed to detect, quantify and/or analyze microvesicles present in body fluids so as to diagnose and assess the risk of developing various diseases and associated disorders, in particular thrombotic, inflammatory and/or metabolic disorders in patients.

Methods for detecting and quantifying microparticles have been described in the prior art. Flow cytometry is the most widely used. This technique allows the measurement and the identification of the phenotype of the microvesicles by using (CD)-specific antibodies. It is also possible to use Annexin A5 as a probe to mark microvesicles due to the high affinity of A5 for phosphatidylserine molecules present in the out layer of microvesicles.

Methods for capturing/quantifying microparticles have been also proposed and are based on the use of solid supports such as microplates or magnetic beads having thereon a ligand able to specifically capture microvesicles. These ligands include Annexin 5, antibodies as well as synthetic ligands.

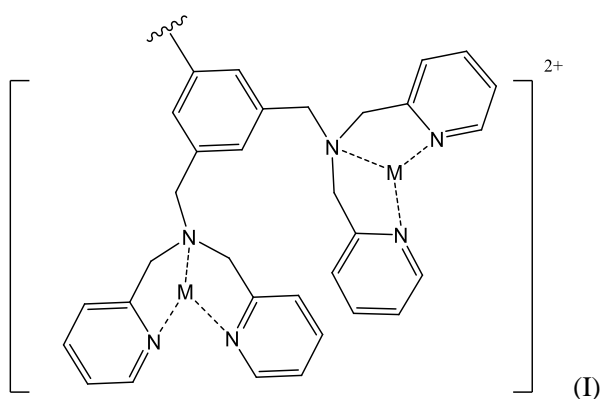
For instance, Cointe et al. (J Extracell vesicles, 2018, 7(1):1494482) describe a bio-assay for capturing leukocyte-derived microvesicles and the measurement of their plasmin generation capacity, for instance for the prognostic of the outcome of sepsis in patients.

The International patent application WO 2012/127175 describes dinuclear metal complexes which can be used as ligands to specifically capture microvesicles and their uses in the diagnosis of diseases.

However, there is still a need for alternative methods for capturing microvesicles from biological samples, in particular in the context of diagnosis of diseases.

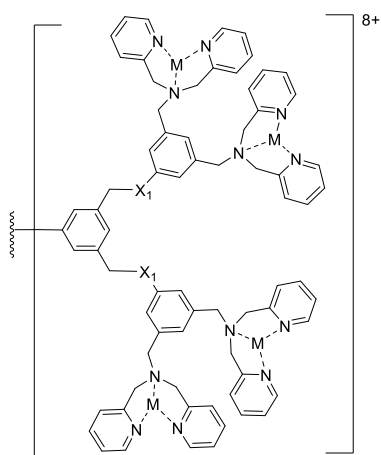
Summary of the invention

The invention relates to a molecule able to bind to microvesicles which comprises at least one, preferably two moieties of formula (I):

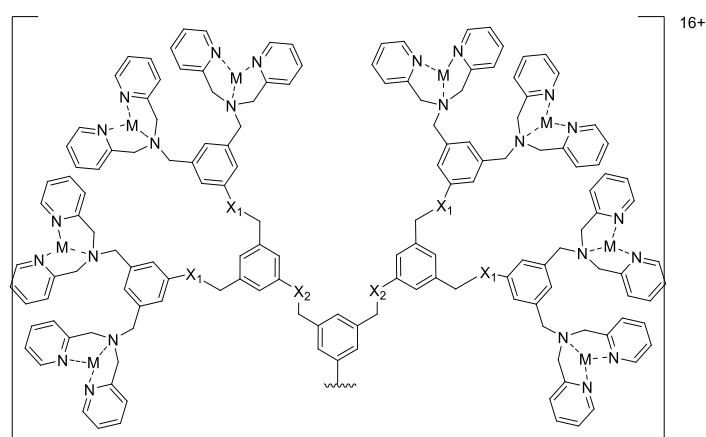


Wherein M is a metal cation preferably selected from the group consisting of Zn^{2+} , Mn^{2+} , Co^{2+} , Ni^{2+} , Cu^{2+} and Fe^{2+} .

In some embodiments, the molecule of the invention may comprise a moiety of formula (Ia) or (Ib) as follows:



(1a) or



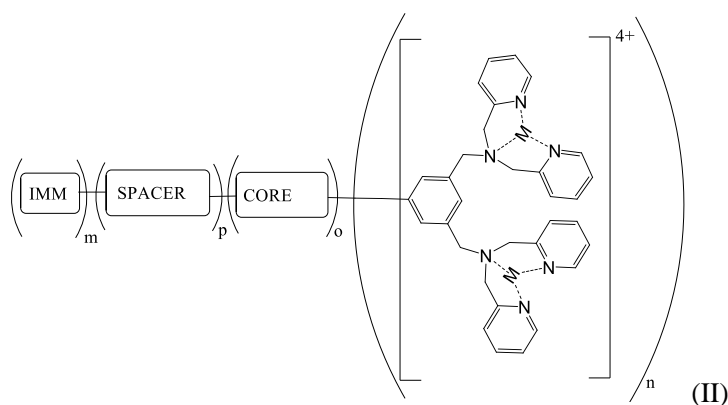
(1b)

Wherein:

- each X_1 is independently O, S, or NH,
- each X_2 , when present, is independently O, S or NH,
- M is selected from Zn^{2+} , Co^{2+} , Cu^{2+} and Fe^{2+} , preferably Zn^{2+} .

In some embodiments, the molecule of the invention is a dendrimer comprising a branched core bearing a plurality of moieties of formula (I), said branched core preferably comprising a group selected from 3,5-di(hydroxymethyl) phenol, 3,5-di(thiomethyl)phenol, 3,5-di(thiomethyl) thiophenol, 3,5-dialkylphenol, 3,5-di(aminomethyl)phenol, - and 3,5-di(aminomethyl) phenylamine as building block, more preferably comprising 3,5-di(hydroxymethyl) phenol as building block. In some alternative or additional embodiments, the molecule of the invention may further comprise a mean for immobilization on a support attached at the extremity of a spacer chain.

For instance, the molecule of the invention may be of formula (II)



Wherein:

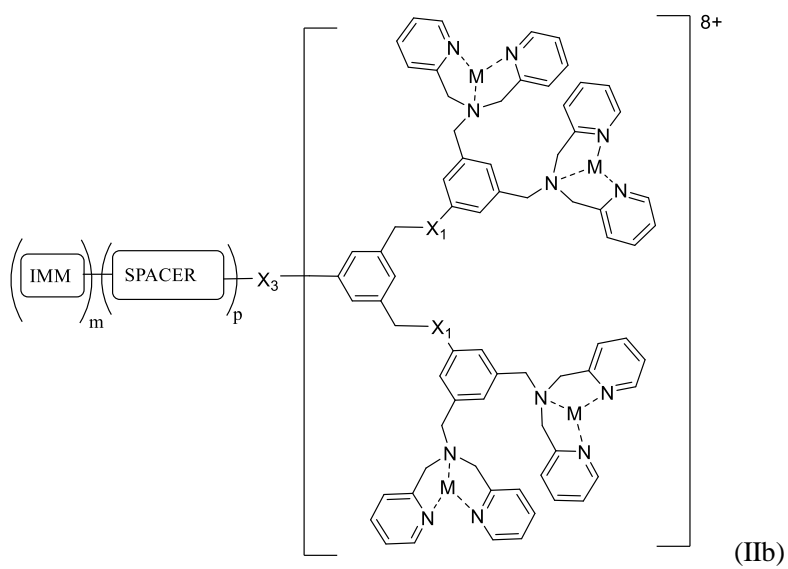
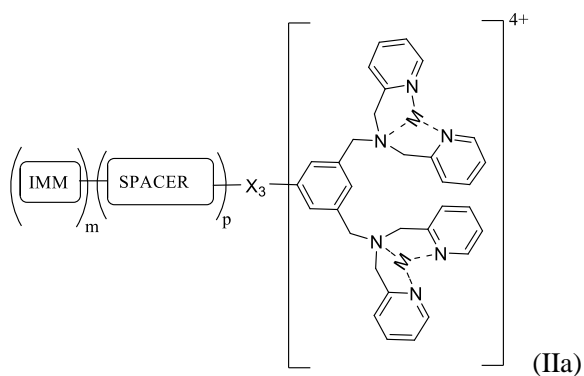
- n is an integer from 1 to 10, preferably from 2 to 6,
- m, p and o are independently 0 or 1,
- M is a divalent metal cation,
- [CORE] is a chemical entity bearing the at least one moiety of formula (I) and having a molecular weight of at most $10\,000\text{ g}\cdot\text{mol}^{-1}$, preferably of at most $5000\text{ g}\cdot\text{mol}^{-1}$
- [IMM] is a mean for covalently or non-covalently immobilization on a support, and
- [SPACER] is selected from the group consisting of a peptide, a polypeptide, an oligo- or polysaccharide, a saturated or unsaturated hydrocarbon chain optionally interrupted by one or several heteroatoms (e.g. S, O or NH), optionally having an heteroatom such as S, O and NH on at least one of its ends, and optionally substituted by one or several substituents such as hydroxyl, halogens, $\text{C}_1\text{-C}_3$ alkoxy, $-\text{CN}$, $-\text{CF}_3$, or $\text{C}_1\text{-C}_3$ alkyl, polymers including homopolymers, copolymers and block polymers, and combinations thereof.

Said molecule may further be characterized by one, several or all of the following features:

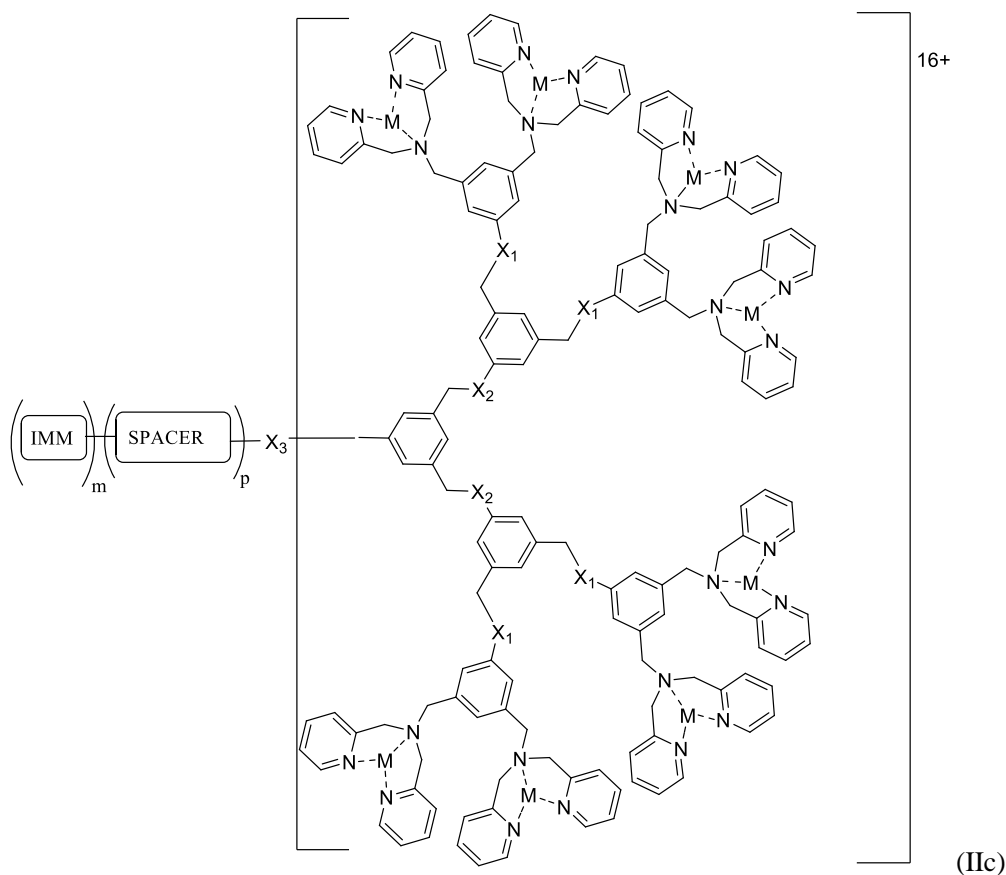
- m, p and o are 1,
- M is selected from Zn^{2+} , Co^{2+} , Cu^{2+} and Fe^{2+} , preferably Zn^{2+} ,
- [SPACER] is selected from $\text{C}_2\text{-C}_{20}$ saturated or unsaturated hydrocarbon chains optionally substituted, polyamide chains, polyester chains and polyether chains, such as polyethylene, comprising from 2 to 20 monomers and combinations thereof.
- [IMM] comprises, or consists of, a moiety selected from the group consisting of an amino group, preferably $-\text{NH}_2$, OH, $-\text{COOH}$, an activated carboxylic acid, $-\text{SH}$, iodoacetyl group, a carbonyl, a hydrazide group, an azido, and a strained alkyne.

- [CORE] is a chemical moiety made of at least one 3,5-di(hydroxymethyl) phenol.

In particular, the molecule of the invention may be a compound of formula (IIa), (IIb) or (IIc):



- and



Wherein

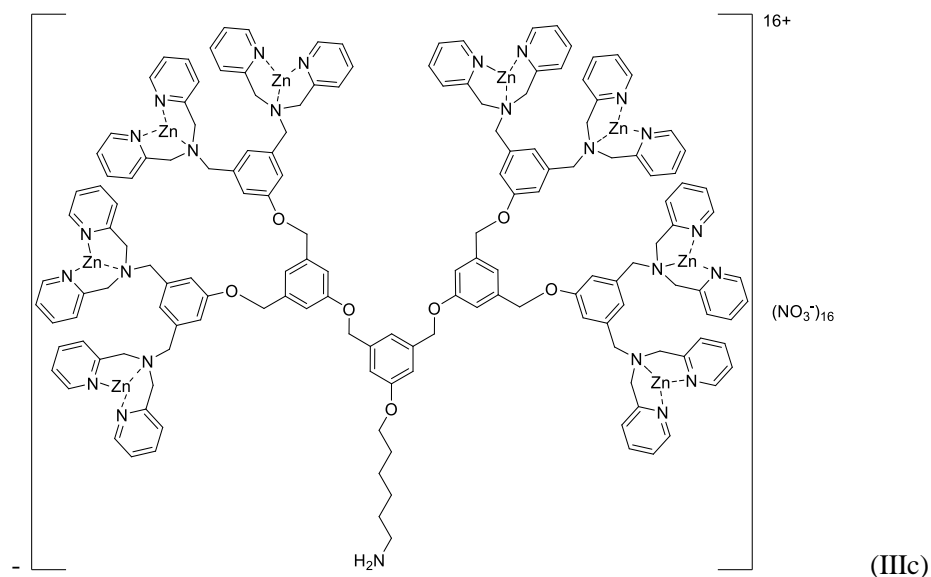
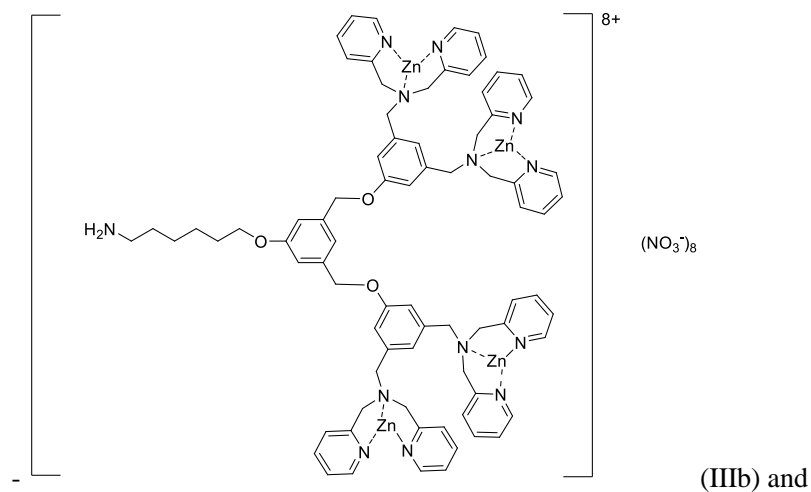
- M, m, p, [IMM] and [SPACER] are as defined above for formula (II),
- each X_1 and X_2 , when present, are selected from the group consisting of O, NH, and S,
- X_3 is selected from -O-, C(=O)-OC(O)-, -C(O)O-, -OC(O)O-, -S-, -SS-, -SC(O)-, -OC(S)-, NR_1 -, $-NR_1C(O)$ -, $-C(O)NR_1$ -, $NR_1C(S)$ -, $C(S)NR_1$ -, $-OC(O)S$ -, $-OC(S)O$ -, $-SC(O)O$ -, $-OC(S)S$ -, $-SC(O)S$ -, $-SC(S)O$ -, $-SC(S)S$ -, $OC(O)NR_1$ -, $-OC(S)NR_1$ -, $-NR_1C(S)O$ -, $-NR_1C(O)S$ -, $NR_1C(O)NR_2$ -, $-NR_1C(S)NR_2$ -, $-SC(O)S$ -, $-SC(S)O$ -, $-S(O)$ -, $-S(O)_2$ -, $-P(O)(R_1)$ -, $-P(O)(OR_1)$ -, $P(O)(R_1)O$ -, $OP(O)(OR_1)$ -, $OP(O)(R_1)O$ -, $NR_1P(O)(R_2)$ -, $-NR_1P(O)(OR_2)$ -, $NR_1P(O)(R_2)O$ -, $OP(O)(OR_1)$ -, and $OP(O)(R_1)O$ - wherein R_1 and R_2 are independently H or CH_3 .

For instance said molecule of formula (IIa), (IIb) or (IIc) may be characterized by:

- m and p are 1,
- M is Zn^{2+} , Co^{2+} , Cu^{2+} or Fe^{2+} , preferably Zn^{2+} ,
- X_1 and X_2 , when present, are O,
- X_3 is O, NH, NHCO, CONH, O(C=O), (O=C)O, O(C=O)O, or NHCONH,

- [IMM]-[SPACER] is $\text{NH}_2-(\text{CH}_2)_r-$ with r an integer from 2 to 10, and
- Said molecule comprises one or several counter-anions selected from the group consisting of perchlorate, tosylate, nitrate, sulphate, sulphonate, thiosulfate, halide, hexafluorophosphate, tetraphenylborate, carbonate, and tetrafluoroborate.

Examples of molecules of the invention are ligands of formula (IIIb) and (IIIc):



The invention also relates to a support for capturing microvesicles, which comprises a molecule as defined above on its surface, and a support comprising such a surface.

The invention also relates to an *in vitro* method for capturing microvesicles from a sample, which comprises contacting the sample with a molecule or a support as defined above. Said *in vitro* method of may further comprise at least one step selecting from:

- a step of providing a sample susceptible to contain the microvesicles of interest from a body fluid of a subject, and/or
- a step of washing the support after the step of contacting the support with the sample, and/or
- a step of detecting the formation of the complex between the microvesicles of interest and said support or molecule of the invention and/or
- a step of recovering the complex formed between the microvesicles and the molecules of the invention, and/or
- a step of quantification of said microvesicles of interest, and/or
- a step of characterization of the captured microvesicles, e.g. by detecting and/or quantifying a biomarker present on the surface or within the microvesicles, and/or
- a step of releasing the microvesicles from the complex, and/or
- a step of recovering the microvesicles of interest.

The invention also relates to an *in vitro* method for the diagnosis, the differential diagnosis, the prognosis, the assessment of the risk of, and/or the monitoring a disorder in a subject which comprises:

- (a) providing a support or a molecule of the invention,
- (a) contacting said support or said molecule with a sample obtained from the subject, in conditions suitable for the formation of a complex between the molecules of the invention and the microvesicles possibly present in the sample, and
- (b) detecting, quantifying and/or characterizing the microvesicles captured in step (b) by complexation.

Typically, the disorder may be selected from the group consisting of cancer, parasitic diseases, diabetes and related disorders such as diabetic nephropathy, diabetic neuropathy, diabetic retinopathy, and diabetic foot syndrome, multiple sclerosis, cancer, Alzheimer's disease, Parkinson's disease, aneurysm, cerebral vasospasm, stroke, and coronary artery disease, and/or

the sample may be or derive from, blood, blood plasma and urine.

A further object of the invention is the use of a molecule, or a support as defined above as means for capturing microvesicles from a sample of a subject, preferably for the diagnosis, the prognostic or the monitoring of a disease in a subject such cancers, parasitic diseases, as diabetes and related disorders including diabetic nephropathy, diabetic neuropathy, diabetic retinopathy, and diabetic foot syndrome, multiple sclerosis, cancer, Alzheimer's disease, Parkinson's disease, aneurysm, cerebral vasospasm, stroke, and coronary artery disease.

Figures

Figure 1 PWR titration of different complex solutions to PSPC membrane. A, B: Fitting of Cplx1-PSPC membrane titration in s and p polarization, respectively; C, D: Fitting of Cplx2-PSPC membrane titration in s and p polarization, respectively; E, F: Fitting of Cplx4-PSPC membrane titration in s and p polarization, respectively. PSPC membrane composition: PS 1 equivalent, PC 5 equivalent. The fitting curves were acquired using GraphPad Prism 7.

Figure 2: TBO calibration curve of carboxyl group density plotted against solution absorbance at 633 nm.

Figure 3: Carboxyl group density on treated PET surfaces (unit: pmol/mm²) determined by TBO experiment.

Figure 4: Cplx1 grafted PET surface incubated with microvesicles. A: fluorescence micrograph, B: cryo-SEM micrograph. Scale bars are provided within the images.

Figure 5: Cplx2 grafted PET surface incubated with microvesicles. A: fluorescence micrograph, B: cryo-SEM micrograph. Scale bars are provided within the images.

Figure 6: Cplx4 grafted PET surface incubated with microvesicles. A: fluorescence micrograph, B: cryo-SEM micrograph. Scale bars are provided within the images.

Figure 7: PET surface grafted with cplx8 incubated with microvesicles. A: fluorescence micrograph, B: cryo-SEM micrograph. Scale bars are provided within the images.

Detailed description of the invention

The Inventors conceived new synthetic ligands able to selectively bind to microvesicles with high affinity. These ligands are metal complex comprising a plurality of metal(II)-bis(dipicolylamine) (M-BDPA) moieties able to interact with phosphatidylserine present in the outer leaflet of the microvesicles. Without to be bound by any theory, the Inventors are of the opinion that the number of M-BDPA and their

proximity in the ligands of the invention enable to optimize the binding to phospholipid-enriched microvesicles with high specificity.

As illustrated in the examples, the ligands of formula (IIIa), (IIIb) and (IIIc) have dissociation constant (K_d) for enriched-phosphatidylserine microvesicles in the 10^{-6} M range. When immobilized on a support, these ligands were able to capture microvesicles. In contrast, support grafted with the ligand of formula (IIIId), which comprises one dipicolylamine moiety only, was shown to have very limited ability to capture microvesicles.

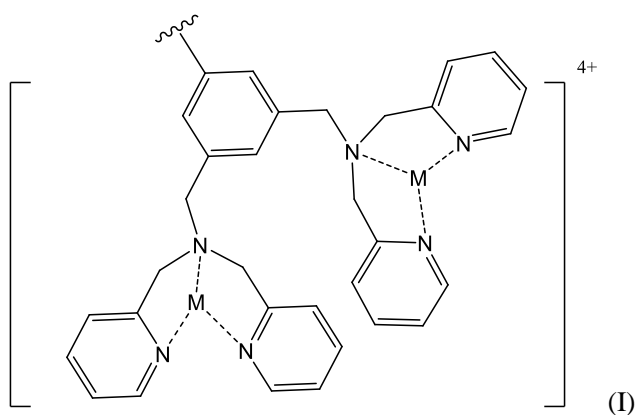
The ligands of the invention were shown to be effective ligands to capture microvesicles on a support, enabling the subsequent detection, quantification and characterization of microvesicles. Noteworthy, the multivalent ligand of formula (IIIb) (also called Cplx4 in the Example section) was able to capture the microvesicles while maintaining their shape, making it possible to detect and quantify biomarkers of interest present within the membrane of the microvesicles but also present inside the microvesicles. The possibility to detect biomarkers in the membrane and/or inside the microvesicles is of high interest in the conception of diagnostic methods, because it was shown that the microvesicle proteome reflect the pathological status of the origin cells.

Thus, the ligands of the invention find applications in *in vitro* diagnosis and prognostic of various disorders.

- Ligands according to the invention

In a first aspect, the Invention relates to a ligand binding to microvesicles, preferably phosphatidylserine-enriched microvesicles, comprising a plurality of metal(II)-bis(dipicolylamine) (M-BDPA) moieties.

More precisely, the Invention relates to a molecule able to bind to microvesicles comprising at least one moiety of formula (I):



Wherein M is a metal cation, preferably a divalent metal cation.

In some embodiments, M is selected from the group consisting of Zn^{2+} , Mn^{2+} , Co^{2+} , Ni^{2+} , Cu^{2+} and Fe^{2+} , preferably Zn^{2+} , Fe^{2+} , Co^{2+} and Cu^{2+} , more preferably Zn^{2+} .

In a preferred embodiment, the molecule of the invention comprises at least two moieties of formula (I), e.g. 2, 3, or 4 moieties of formula (I).

Typically, the molecule of the invention has a molecular weight of at most 25000 $g \cdot mol^{-1}$, preferably of at most 20000, e.g. of at most 15000, 10000, 7000, 5000 or 3000 $g \cdot mol^{-1}$.

As explained in the background of the invention, “*Microvesicles*” (also known as cellular microparticles) refer to submicron extracellular vesicles that are found both in the interstitial space between cells and in body fluids. Microvesicles are released from the surface or plasma membrane of cells by the outward budding and fission of the plasma membrane. Microvesicles play a role in intercellular communication and can transport molecules such as mRNA, miRNA, and proteins between cells.

Phosphatidylserine (PS) roughly accounts for 2-10% of total cellular phospholipids in a typical mammalian cell plasma membrane. In healthy cells, PS is almost exclusively sequestered to the inner leaflet of the cell. Under certain conditions, in particular in cell death pathway, PS appears in the outer leaflet of the plasma membrane, due to the attenuation of the active transport mechanisms that maintains the asymmetric transmembrane distribution of PS. It was shown that microvesicles exhibit phosphatidylserine in the outer leaflet of their membrane.

As used herein, “*phosphatidylserine-enriched microvesicles or phosphatidylserine-rich microvesicles*” refer to microvesicles in which PS can be found in the outer leaflet of the membrane of the vesicles. In other words, “*phosphatidylserine-enriched microvesicles*” refer to microvesicles having PS present in the outer leaflet of the bilayer lipid membrane. For example, such microvesicles may derive from cells in which a cell death pathway is activated. Synthetic vesicles made of POPC (1-palmitoyl-2-oleoyl-sn-glycero-3phosphocholine) and POPS (1-palmitoyl-2-oleoyl-sn-glycero-3phosphoserine) with a weight ratio of 5:1 (w/w) can be used as a model of “*PS-enriched microvesicles*” in order to assess the ability of molecules to bind to microvesicles in vitro

As used herein, “*a molecule binds to a microvesicle*” means that the molecule is able to bind to a microvesicle, preferably a phosphatidylserine-enriched microvesicle. Such a molecule herein also refers to “*ligand of microvesicles*” or “*ligand*”.

Preferably “*a molecule binds to a microvesicle*” refers to a molecule able to bind a microvesicle with high affinity e.g. with a dissociation constant (Kd) of at most 10^{-3} M such as at most 10^{-4} or 10^{-5} M.

The K_d is preferably determined by plasmon waveguide resonance spectroscopy, as illustrated in Example 2. Such assay is performed by using vesicles prepared by mixing POPC with POPS with a weight ratio of 5:1 (w/w) and 1x Dulbecco's Phosphate Buffered Saline (pH 7.1-7.5) as medium.

Alternatively, it is possible to identify whether a molecule is able to bind to microvesicles by a capture assay using e.g. cryo-scanning electron microscopy (Cryo-SEM) as illustrated in Example 4. Typically, the molecule to assess is immobilized on a support and then incubated with a solution comprising microvesicles in phosphate saline buffer. After washing and cryofixation, the surface of support is analyzed by Cryo-SEM so as to determine whether microvesicles are immobilized thereon.

In some embodiments, the molecule of the invention binds to microvesicles with specificity, which means that their affinity for microvesicles (i.e. phosphatidylserine-enriched microvesicles) is higher than that for other cellular particles such as exosomes and more generally for cellular particles which do not exhibit PS in the outleaflet of their membrane. For instance, the molecule of the invention may have a K_d for a microvesicle which is at least 5-fold, preferably, at least 10, 20, 30, 40, 50, 100, 200, 500, or 1000-fold lower than its K_d for another cellular microparticles such as exosomes. In some embodiments, the molecule of the invention do not cross-react with cellular particles other than microvesicles, i.e. has relatively little detectable reactivity with other molecules which may be present in the sample.

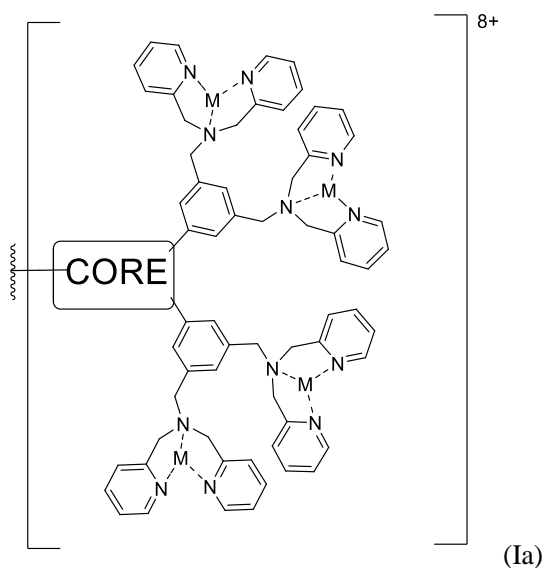
The ligand of the invention can comprise one or several counter-anions to counterbalance the positive charge of the moieties of formula (I). The counter-anion may be selected from the group consisting of perchlorate, tosylate, nitrate, sulphate, sulphonate, thiosulfate, halide, hexafluorophosphate, tetraphenylborate, carbonate, and tetrafluoroborate, more particularly from perchlorate, nitrate, sulphate, halide and carbonate anions. In some preferred embodiments, the counter-anion(s) is/are selected from nitrate and perchlorate.

As shown in Example 3, the ligand of formula (IIIb) (called Cplx4 in the Example section) is particularly effective to capture microvesicles while maintaining their integrity. Indeed, Figure 6 shows that the captured microvesicles uniformly covered the surface functionalized with Cplx4 without any significant fusion or aggregates between them, whereby the integrity of microvesicles is maintained.

Noteworthy, the ligand of formula (IIIb) bears two moieties of formula (I).

Thus, in a preferred embodiment, the molecule of the invention comprises at least two moieties of formula (I).

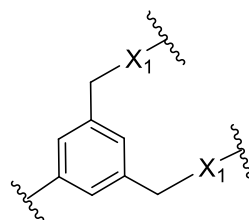
For instance, the ligand of the invention comprises at least one moiety of formula (Ia) (e.g. 1, 2, 3 or 4 moieties):

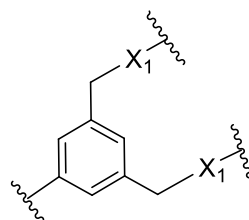


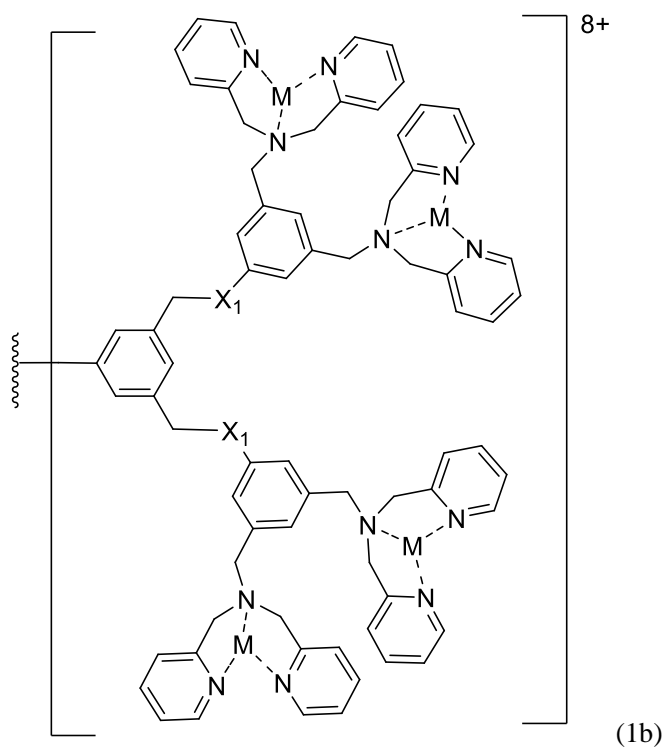
Wherein:

- M is a divalent metal cation. M may be selected from the group consisting of Zn^{2+} , Mn^{2+} , Co^{2+} , Ni^{2+} , Cu^{2+} and Fe^{2+} , preferably Zn^{2+} , Fe^{2+} , Co^{2+} and Cu^{2+} , more preferably Zn^{2+} , and
- [CORE] is a chemical entity bearing at least one metal-bis(dipicolylamine) group.

[CORE] is typically a chemical moiety having a molecular weight of at most 20000 g.mol^{-1} , preferably of at most 10000, 7000, 5000, 3000 or 2000 g.mol^{-1} . [CORE] may comprise acyclic and/or cyclic moieties. For instance, [CORE] may be selected among bifunctional, trifunctional and tetrafunctional linkers having a backbone of 1 to 60 carbon atoms and at least two heteroatoms independently selected from N, S and O. Alternatively or additionally, [CORE] may comprise one or several cyclic groups (e.g. at least 2, 3, 4, 5, or 6) preferably selected from pyrrole, furan, thiophene, pyrazole, imidazole, oxazole, triazole, triazine, phenyl, naphthalene, pyridine, piperidine, pyridazine, pyrimidine, pyrazine, oxazine, dioxine, piperazine, morpholine, and thiazine.



In some embodiments, "CORE" may be of formula: . In such a case, the ligand of the invention comprises at least one moiety of formula (Ib):

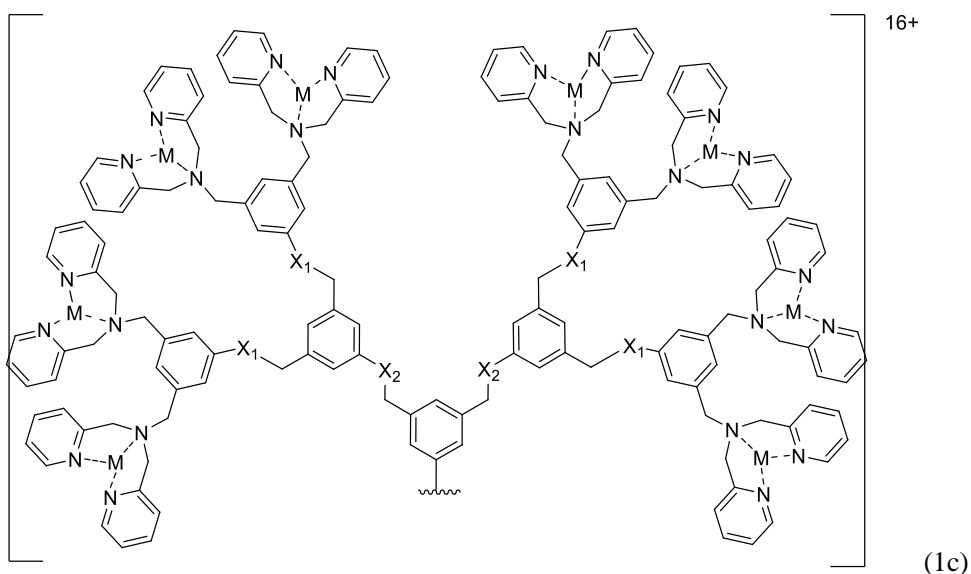


Wherein:

- each X_1 is independently selected from S, O and NH. Preferably, all the X_1 are identical, preferably O, and
- M is as defined above, preferably Zn^{2+} .

In another or additional embodiment, the ligand of the invention comprises two moieties of formula (1b).

For instance, the ligand of the invention comprises the moiety of formula (1c):



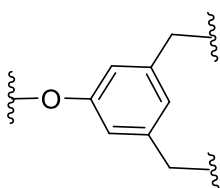
Wherein

- M is as defined above
- X_1 are as defined above, and
- each X_2 is independently O, NH, or S,

In some embodiments, all X_1 and X_2 are the same, e.g. S, O or NH, preferably O.

In a particular embodiment, the ligand of the invention is a dendrimer comprising a branched core bearing a plurality of moieties of formula (I), preferably at least 2, 4, 6 or 8 moieties of formula (I). Said dendrimer comprises from 1 to 8, preferably from 1 to 4, e.g. 1, 2 or 3 layers of molecules that emanate radially from a central core. The outermost layer is the layer bearing the moieties of formula (I). The building block of the dendrimer may be selected from the group consisting of 3,5-di(hydroxymethyl) phenol, 3,5-di(thiomethyl)phenol, 3,5-di(thiomethyl) thiophenol, 3,5-dialkylphenol, 3,5-di(aminomethyl)phenol, 3,5-dialkylphenol and 3,5-di(aminomethyl) phenylamine.

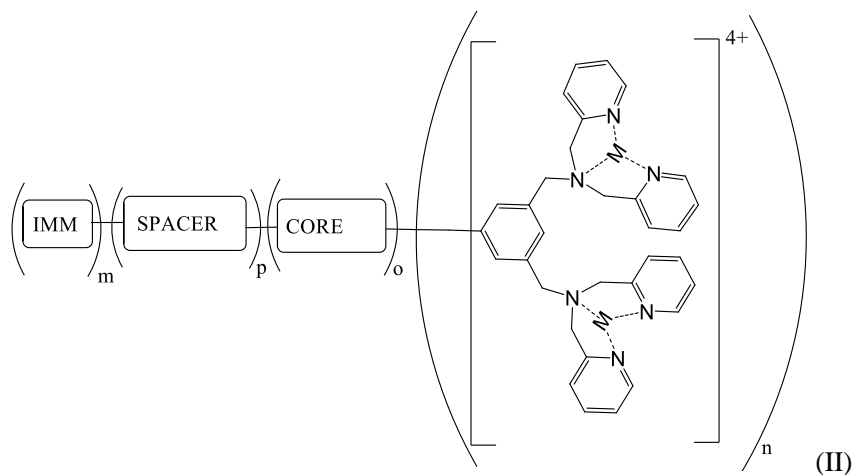
In some embodiments, the building block of said dendrimer is 3,5-di(hydroxymethyl) phenol. Accordingly, the ligand of the invention may comprise a branched core based on the following repeated unit:



As mentioned above, the molecule of the invention finds applications in the detection, the quantification and the analysis of microvesicles. Consequently, the molecule of the invention may comprise one or several additional moieties enabling to retrieve and/or to detect the complex formed between the molecules of the invention and microvesicles. For instance, the molecule of the invention may comprise one or several moieties selected from the group consisting of a reporter moiety and/or a mean for immobilization on a support.

A mean for immobilization on a support is described further below (*see the definition given for [IMM]*). On the other hand, the report moiety may be selected from the group consisting of a fluorescent molecule, a dye, a biotin, a radioactive agent, a quantum dot, an enzyme such as horseradish peroxidase and the like.

In a particular embodiment, the molecule of the invention is to be immobilized on a support. In that case, the molecule of the invention may further comprise a mean for immobilization attached on a spacer chain. More precisely, the molecule of the invention may comprise or may be of formula (II):



Wherein:

- n is an integer from 1 to 10, preferably from 2 to 6,
- m, p and o are independently 0 or 1,
- M is a divalent metal cation as defined above,
- [CORE] is a chemical entity bearing at least one moiety of formula (I), e.g. as defined above,

- [IMM] is a mean for covalently or non-covalently immobilization on a support.

- [SPACER] is selected from the group consisting of a peptide, a polypeptide, an oligo- or polysaccharide, a saturated or unsaturated hydrocarbon chain optionally interrupted by one or several heteroatoms (e.g. S, O or NH), optionally having at least one of its extremity an heteroatom such as S, O and NH, and optionally substituted by one or several substituents such as hydroxyl, halogens, C₁-C₃ alkoxy, -CN, -CF₃, or C₁-C₃ alkyl, polymers including homopolymers, copolymers and block polymers, and combinations thereof.

The molecule of the invention may have a molecular weight of at most 25000 g.mol⁻¹, preferably of at most 20000, e.g. of at most 15000, 10000, 7000, 5000 or 3000 g.mol⁻¹.

As mentioned above, said molecule may comprise one or several counter-anions to counterbalance the positive charges of the metallic complexes. Said counter-anions are as defined above and are preferably selected from the group consisting perchlorate, tosylate, nitrate, sulphate, sulphonate, thiosulfate, halide, hexafluorophosphate, tetraphenylborate, carbonate, and tetrafluoroborate, more particularly from perchlorate, nitrate, sulphate, halide and carbonate anions. In some preferred embodiments, the counter-anion(s) is/are selected from nitrate and perchlorate..

[CORE] is typically a chemical moiety having a molecular weight of at most 20000 g.mol⁻¹, preferably of at most 10000, 7000, 5000, 3000 or 2000 g.mol⁻¹. [CORE] may comprise acyclic and/or cyclic moieties. For instance, [CORE] may be selected among bifunctional, trifunctional and tetrafunctional linkers having a backbone of 1 to 60 carbon atoms and at least two heteroatoms independently selected from N, S and O. Alternatively or additionally, [CORE] may comprise one or several cyclic groups (e.g. at least 2, 3, 4, 5, or 6) preferably selected from pyrrole, furan, thiophene, pyrazole, imidazole, oxazole, triazole, triazine, phenyl, naphthalene, pyridine, piperidine, pyridazine, pyrimidine, pyrazine, oxazine, dioxine, piperazine, morpholine, and thiazine.

In some embodiments, [CORE] is composed of one or several 3,5-dimethoxyphenol moieties. In other embodiments [CORE] is a branched core, preferably a dendritic core, made of 3,5-di(hydroxymethyl) phenol 3,5-di(thiomethyl)phenol, 3,5-di(thiomethyl) thiophenol, 3,5-dialkylphenol, 3,5-di(aminomethyl)phenol, 3,5-dialkylphenol and 3,5-di(aminomethyl) phenylamine and all related oxo, thio and amino derivatives as building block.

As used herein, “combinations” means that [SPACER] (hereafter “the spacer”) may comprise several hydrocarbon chains, oligomer chains or polymeric chains (e.g. 2, 3, 4, 5 or 6) linked by any appropriate group, such as -O-, -S-, -NHC(O)-, -OC(O)-, -NH-, -NH-CO-NH-, -O-CO-NH-, phosphodiester or phosphorothioate groups.

Typically, the spacer may comprise from 2 to 200 carbon atoms, preferably from 2 to 40, such as 2 to 20 carbon atoms. The length and the chemical nature of the spacer may be optimized depending on the support on which the molecule is to be immobilized and/or in order to optimize the interaction between the molecule and the microvesicles.

In some embodiments, the spacer may be selected from the group consisting of polyethers such as polyethylene glycol (PEG) or polypropylene glycol, polyvinyl alcohol, polyesters such as polylactate, polyacrylate polymethacrylate, polysilicone, polyamide such as polycaprolactone, unsaturated or saturated, branched or unbranched, hydrocarbon chains optionally having a heteroatom such as O, NH and N on at least one end, and combinations thereof.

In some preferred embodiments, [SPACER] is selected from C₂-C₂₀ saturated or unsaturated hydrocarbon chains optionally having a heteroatom such as O, NH and N on at least one extremity, polyether chains comprising from 2 to 20 monomers and combinations thereof.

For instance, the spacer comprises at least one polyethylene glycol moiety comprising from 2 to 20 monomers. For illustration only, the spacer may comprise from 2 to 10 triethyleneglycol blocks linked together by linkers. As another example, the spacer may be a C₁₂ hydrophilic triethylene glycol ethylamine derivative. Alternatively, the spacer may be a C₂-C₄₀ hydrocarbon chain, in particular a C₁₀-C₂₀ alkyl chain or a C₂-C₁₀ alkyl chain such as a C₆ alkyl chain. The alkyl chain may have a group such as NH, S or O on at least one end.

In a particular embodiment, [SPACER] is selected from linear or branched C₂-C₂₀ alkyl chains and a polymer such as a polyethyleneglycol, a polyester, or a polyamide comprising from 2 to 10 monomers. In a particular embodiment, the spacer is selected from C₂-C₂₀ alkyl chains and a polyethyleneglycols having from 2 to 10 monomers. The alkyl chain may have a group such as NH, S or O on at least one of its ends.

[IMM] (hereunder “mean for immobilization”) is to be selected depending on the support for immobilization and the type of binding (covalent or non-covalent binding) which is sought.

For instance, [IMM] may comprise a moiety enabling non-covalent binding with a support.

For instance, [IMM] may comprise a biotin while the support may comprise streptavidin or avidin thereon or *vice versa*. [IMM] may comprise a ligand moiety such as a short oligosaccharides, e.g. comprising from 1 to 6 saccharides, a peptide, protein fragments in particular an antigenic fragment while the support has a binding moiety able to specifically binds to said ligand such as antibodies, antibodies fragments or constructs e.g. as Fab, Fc fragment, or ScFv, aptamers, and the like, or *vice versa*.

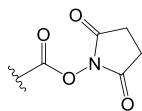
Preferably [IMM] comprises a chemical reactive group for immobilizing the molecule of the invention by a covalent bound on the support. Said chemical reactive is typically selected so as to react with a chemical entity present on the support of interest in conditions which would not alter the binding specificity of the molecule of the invention, in particular the ability of the molecule to specifically bind to

the microvesicles of interest. In other words, [IMM] and the chemical entity present on the support may be selected so as to react together in conditions which are not likely to alter the structure and/or the conformation of the ligand of the invention.

For instance, [IMM] may comprise an amino group, preferably a primary amino group (-NH₂), or a primary hydroxyl group and the support may comprise a chemical reactive group able to form a covalent bond with said amino or hydroxyl group or *vice versa*. Chemical reactive groups able to form a covalent bond with an amino or hydroxyl group encompasses, without being limited to, a carboxylic acid group, an activated carboxylic acid group, a lactone group, and an imidazole carbamate.

The term “*activated carboxylic acid group*” is intended to mean a chemical function derived from the “*carboxylic acid*” group capable of reacting with a nucleophile such as a primary amino group. “*Activated carboxylic acid*” groups are well known to those skilled in the art and encompass acyl chlorides, mixed anhydrides and esters.

In some embodiments, the activated carboxylic acid group is in the form of an ester. This ester may result from the reaction of a carboxylic acid group with a compound selected from 1-hydroxybenzotriazole (HOBt), 1-Hydroxy-7-azabenzotriazole (HOAt) and N-hydroxysuccinimide, or a derivative thereof, preferably N-hydroxysuccinimide, or a derivative thereof such as sulfo-NHS or N-bromosuccinimide. In a particular embodiment, the activated carboxylic acid group is a N-hydroxysuccinimidyl ester of the



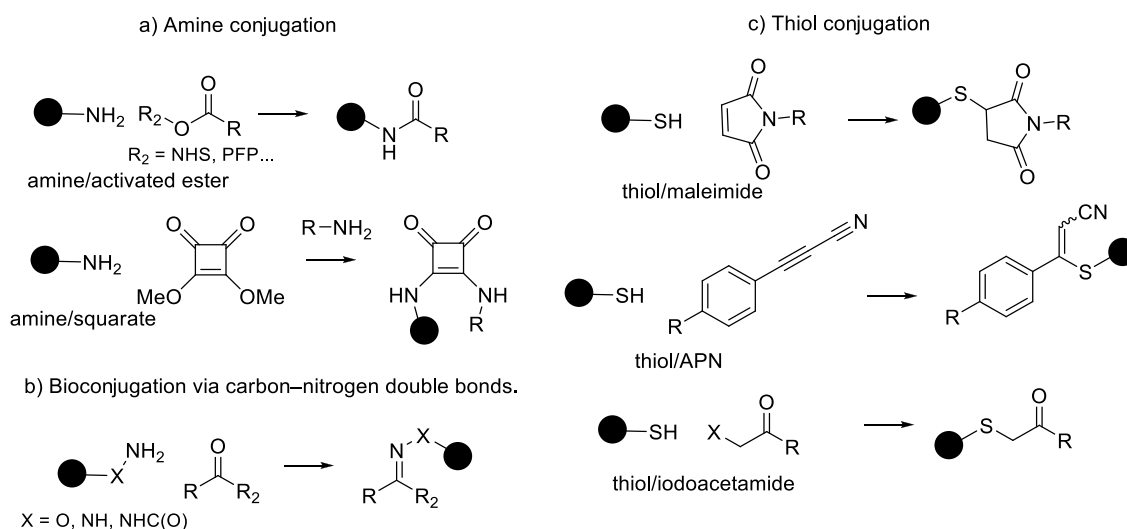
following formula

In some other embodiments, [IMM] comprises a sulfhydryl group (-SH) and the chemical entity of the support comprises a chemical reactive group able to form a covalent bond with said sulfhydryl group such as an iodoacetyl group, or *vice versa*. The resulting bond is a thioether bond.

In other embodiments, [IMM] comprises a carbonyl group (-C(=O)-H) and the chemical entity of the support comprises a chemical reactive group able to form a covalent bond with said carbonyl group such as a hydrazide group, or *vice versa*. The resulting bond formed is a hydrazine bond.

In some embodiments, [IMM] may comprise a chemical reactive moiety suitable to create a covalent bond by click-chemistry or by bioconjugation reaction.

Bioconjugation reactions encompass reactions between amino acids such as lysine, cysteine or tyrosine with reactive groups as detailed in Koniev, O., Wagner, A, Chem. Soc. Rev., 44, 5495 (2015). For instance, the functional moiety may comprise a maleimide group or a squarane moiety, which can react with cysteine or tyrosine residues, respectively. The maleimide or the squarane moiety may be present in [IMM] while the amino acid residue may be present on the support and *vice versa*. Bioconjugation reactions encompass, without being limited to:

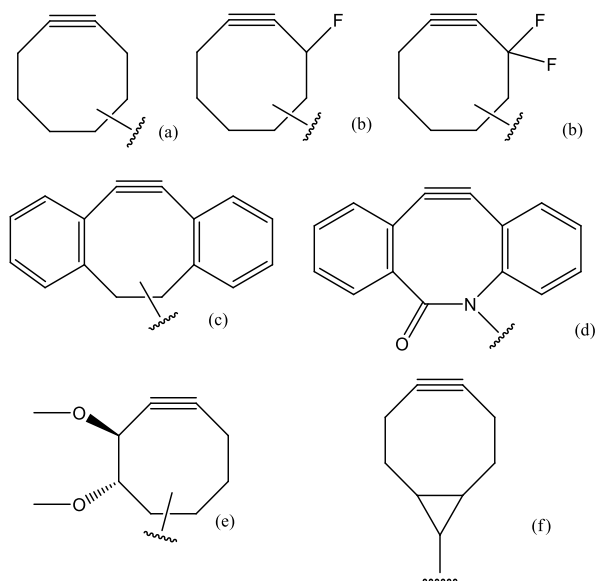


On the other hand, “Click-reaction” or “Click-chemistry” refers to chemical reactions characterized by high yields, high chemoselectivity, which are simple to conduct and which generate inoffensive by-products. Click reactions are typically used to create covalent heteroatom links (C-X-C) between two entities of interest. For review about click chemistry, one can refer to Kolb et al., *Angew. Chem. Int. Ed.* 2001, 40, 2004-2021 and to Rudolf et al., *Current opinion in Chemical Biology*, 2013, 17:110-117.

Examples of click reactions encompass, without being limited to, copper-catalyzed azide-alkyne dipolar cycloadditions (CuAAC), strain-promoted alkyne-azide cycloaddition (SPAAC), Diels-Alder reactions with tetrazines and strained alkyne or alkenes, tetrazine-isonitrile cycloadditions, thiol-alkene click reactions such as maleimide-cysteine cycloadditions, Staudinger azide-triarylphosphine conjugation, and sydnone-alkyne cycloadditions.

In some embodiments, the chemical reactive group of [IMM] and the chemical entity of the support may be selected so as to promote a free-metal click reaction. Preferred free-metal click reaction is strain-promoted alkyne-azide 1,3-dipolar cycloaddition (SPAAC). This reaction refers to the reaction between an azido group and a strained alkyne moiety which leads to the formation of a triazole moiety. The azido group may be present in [IMM] and the strained alkyne moiety may be present on the support, and *vice versa*.

Preferred strained alkynes are C₆-C₃₀ alkynes, preferably C₈-C₂₀ alkynes, wherein the triple bond is sterically strained, in particular in a cyclooctyne scaffold. The strained alkyne may comprise a cyclooctyne scaffold which may be optionally substituted by one or several substituents such as halogens and/or fused to one or several cycles, including heterocycles. For instance, the strained alkyne may comprise one of the following cyclooctyne scaffolds (a)-(f):



In some other embodiments, [IMM] may comprise a photoreactive group. A photoreactive group, also called photoreactive crosslinker, refers to a chemically inert compound that becomes reactive when exposed to ultraviolet or visible light. Photoreactive groups encompass, without being limited to, aryl azides, azido-methyl-coumarins, benzophenones, anthraquinones, diazo compounds, diazirines, and psoralen derivatives. One can cite as examples of photoreactive groups phenyl azide, ortho-hydroxyphenyl azide, meta-hydroxyphenyl azide, tetrafluorophenyl azide, diazirine, azido-methylcoumarin, benzophenone, and psoralen. A photoreactive group can react with many amino acids. Accordingly, when [IMM] comprises a photoreactive group, the chemical moiety on the support may be an amino acid and *vice versa*.

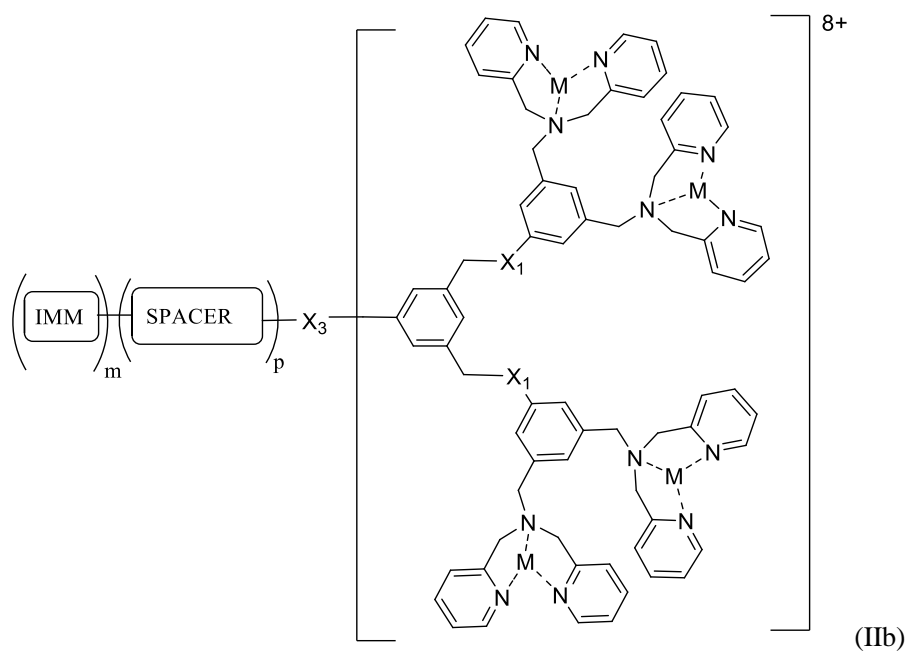
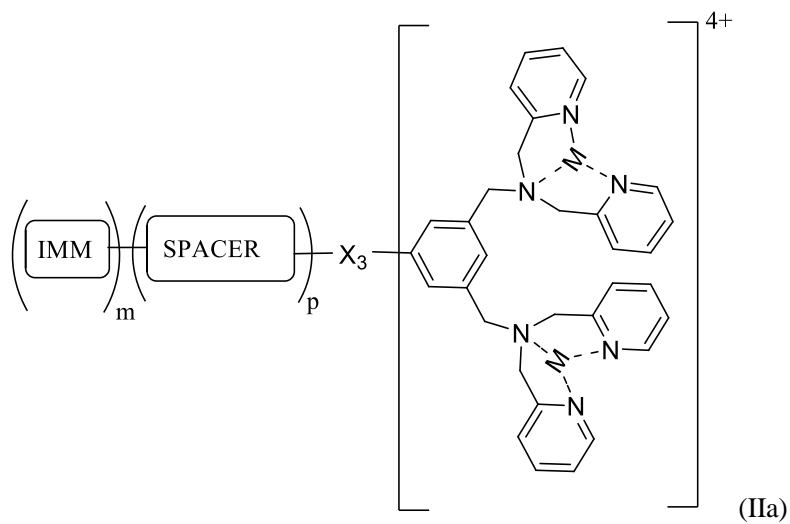
In a particular embodiment, [IMM] comprises, or consists of, a moiety selected from an amino group, preferably $-NH_2$, $-COOH$, OH , an activated carboxylic acid, $-SH$, iodoacetyl group, a carbonyl, a hydrazide group, an azido, and a strained alkyne. For instance, [IMM] comprises, or consists of, a moiety selected from $-NH_2-COOH$ and activated carboxylic acid groups for instance hydroxy-succinimidyl ester.

In a further embodiment, the molecule of the invention is of formula (II) wherein:

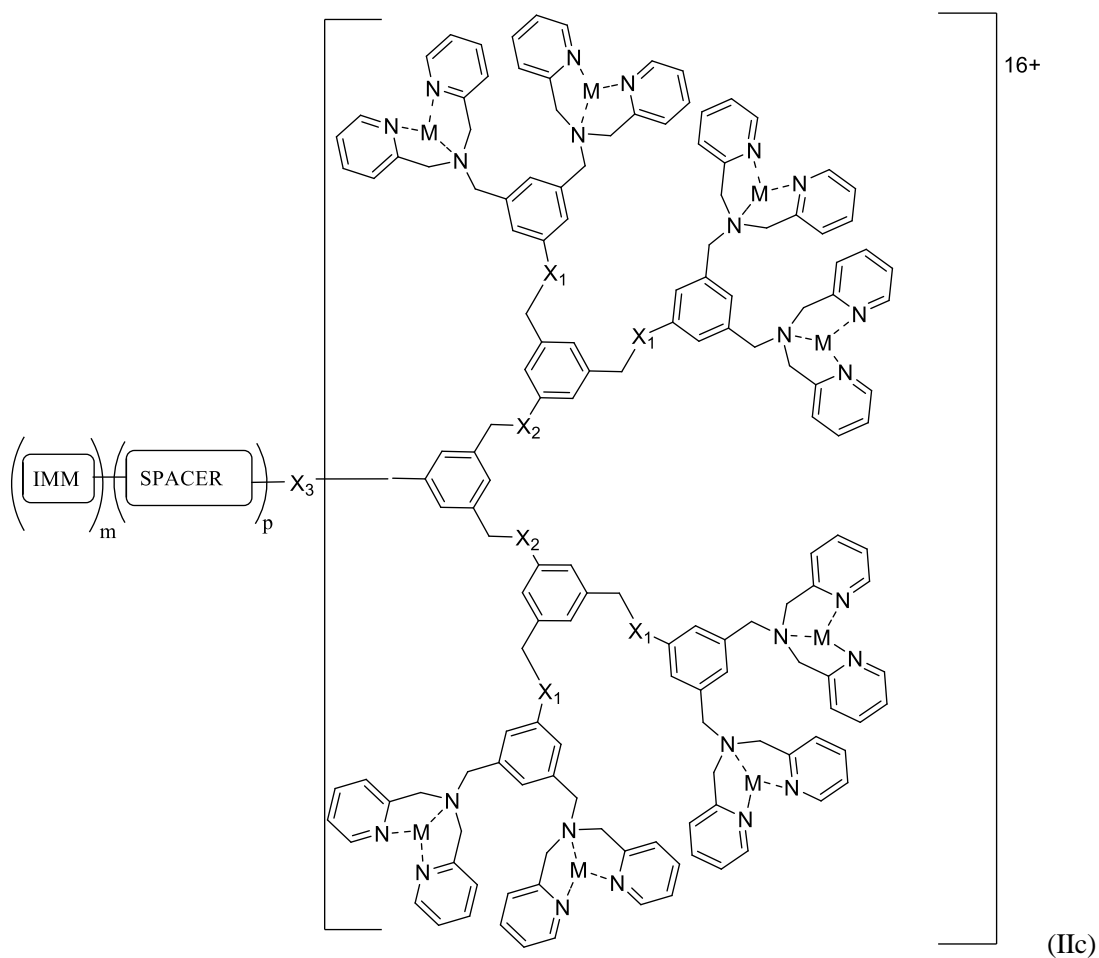
- n is an integer from 1 to 6, preferably from 2 to 4,
- m and p are 1,
- [SPACER] and [IMM] are as described above, and

- [CORE] is a chemical moiety made of at least one (e.g. at least 2, 3, 4, 5, or 6) 3,5-di(hydroxymethyl) phenol moiety.

In a particular embodiment, the molecule of the invention is selected from the group consisting of:



- and



Wherein

- M, m, p, [IMM] and [SPACER] are as defined above for formula (II),
- each X_1 and X_2 , when present, are independently selected from the group consisting of O, NH, or S. Preferably, all X_1 and X_2 are identical, e.g. O,
- X_3 is selected from -O-, C(=O)-OC(O)-, -C(O)O-, -OC(O)O-, -S-, -SS-, -SC(O)-, -OC(S)-, NR_1 -, $-NR_1C(O)$ -, $-C(O)NR_1$ -, $NR_1C(S)$ -, $C(S)NR_1$ -, $-OC(O)S$ -, $-OC(S)O$ -, $-SC(O)O$ -, $-OC(S)S$ -, $-SC(O)S$ -, $-SC(S)O$ -, $-SC(S)S$ -, $OC(O)NR_1$ -, $-OC(S)NR_1$ -, $-NR_1C(S)O$ -, $-NR_1C(O)S$ -, $NR_1C(O)NR_2$ -, $-NR_1C(S)NR_2$ -, $-SC(O)S$ -, $-SC(S)O$ -, -S(O)-, -S(O)₂-, -P(O)(R₁)-, -P(O)(OR₁)-, P(O)(R₁)O-, OP(O)(OR₁)-, OP(O)(R₁)O-, $NR_1P(O)(R_2)$ -, $-NR_1P(O)(OR_2)$ -, $NR_1P(O)(R_2)O$ -, OP(O)(OR₁) and OP(O)(R₁)O- wherein R₁ and R₂ are independently H or CH₃, preferably H. Preferably, X_3 is O, NH, NHCO, CONH, O(C=O), (O=C)O, O(C=O)O, or NHCONH

In some embodiments, the molecule of the invention is a molecule of formula (IIa), (IIb) or (IIc), wherein:

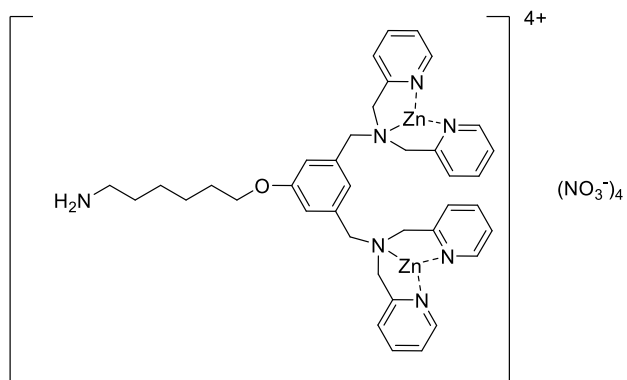
- m and p are 1,
- M is Fe²⁺, Cu²⁺ or Zn²⁺, preferably Zn²⁺,
- X₁ and X₂ are O,
- X₃ is O, NH, NHCO, CONH, O(C=O), (O=C)O, O(C=O)O, or NHCONH,
- -[SPACER] is selected from the group consisting of unsaturated or saturated C₂-C₂₀ hydrocarbon chains, optionally substituted, polyamides, polyesters, polyethers such as polyethylene glycol (PEG) or polypropylene glycol, polyvinyl alcohol, polyacrylate, polymethacrylate, polysilicone, unsaturated or saturated, branched or unbranched, hydrocarbon chains and combinations thereof. In some preferred embodiments, [SPACER] is selected from C₂-C₂₀ saturated or unsaturated hydrocarbon chains optionally having an heteroatom such as O, NH or S on at least one of its extremities, polyether chains comprising from 2 to 20 monomers and combinations thereof, and
- [IMM] comprises, or consists of, a moiety selected from an amino group, preferably -NH₂, -SH, -OH, an activated carboxylic acid, preferably N-hydroxysuccinimidyl ester, -SH, an azido, and a strained alkyne.

In an additional embodiment, the molecule of the invention is a molecule of formula (IIa), (IIb) or (IIc), wherein:

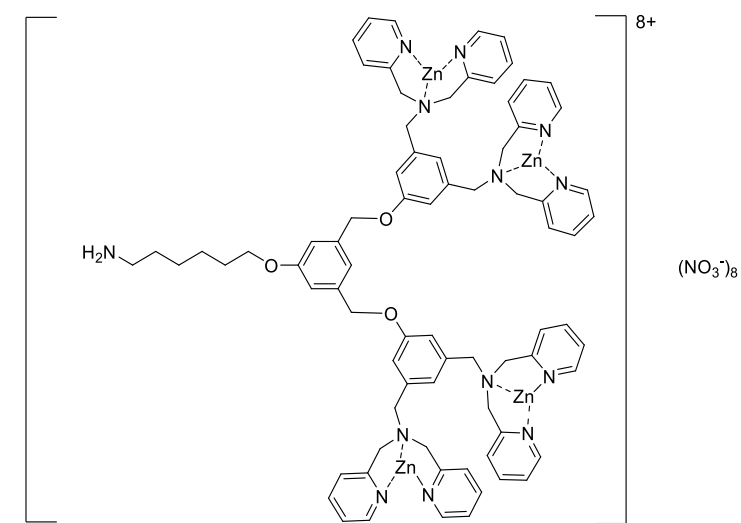
- m and p are 1,
- M is Fe²⁺, Cu²⁺ or Zn²⁺, preferably Zn²⁺,
- X₁ and X₂ are O,
- X₃ is O, NH, NHCO, CONH, O(C=O), (O=C)O, O(C=O)O, or NHCONH, and
- [IMM]-[SPACER] is NH₂-(CH₂)_r- with r an integer from 2 to 10.

The counter-anions present in the molecules of formula (IIa), (IIb) and (IIc) are preferably selected from perchlorate, nitrate, sulphate, halide and carbonate.

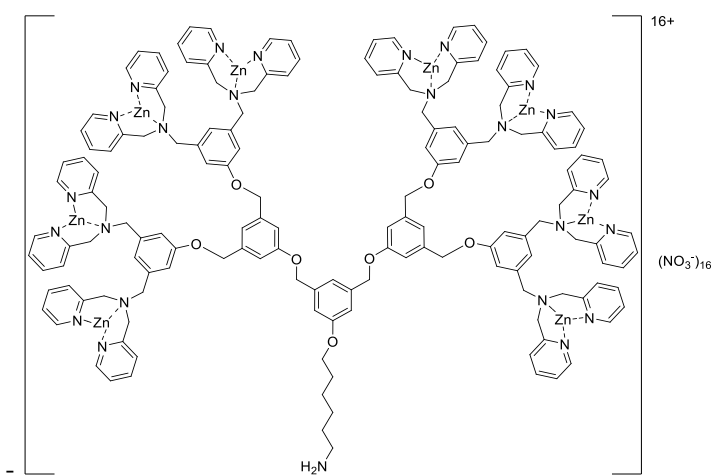
In a particular embodiment, the molecule of the invention is selected from:



(IIIa) – also called herein Cplx2



(IIIb) – also called herein Cplx4



(IIIc) – also called herein Cplx8.

It goes without saying that the counteranions shown in formula (IIIa), (IIIb), and (IIIc) can be replaced by any other anions, in particular biological compatible anions such as perchlorate, tosylate, nitrate, sulphate, sulphonate, thiosulfate, halide, hexafluorophosphate, tetraphenylborate, carbonate, and tetrafluoroborate, more particularly from perchlorate, nitrate, sulphate, halide and carbonate anions. In some preferred embodiments, the counter-anion(s) is/are selected from nitrate and perchlorate.

The molecules of the invention can be synthesized by conventional chemical reactions and can be adapted from the synthesis of molecules of formula (IIIa), (IIIb) and (IIIc) as shown in Example 1.

- Support and devices comprising the ligands of the invention

As mentioned above, the molecule of the invention may be immobilized on a support. Accordingly, the invention also relates to a support having thereon a ligand as defined above as well as devices comprising such a support.

In other words, the invention relates to supports functionalized, e.g. grafted, with a ligand as defined above. Preferred ligands are those shown in formula (II), (IIa), (IIb), (IIc), (IIIa), (IIIb) and (IIIc). In some embodiments, the support of the invention comprises at least one ligand of formula (IIb) or (IIIb).

The ligand of the invention may be covalently or non-covalently bound to the support.

The support may be of any type with proviso that the ligand can be covalently or non-covalently immobilized on it. The support may be pre-functionalized, e.g. chemically pre-treated or functionalized with a specific binding entity to allow the immobilization of the ligand of the invention.

The constituent of the solid support may be of any type and encompasses glass, metals for instance steel, gold, silver, aluminum, or copper, ceramic, hydroxyapatite, silica, bentonite, polysaccharide such as cellulose, carboxy methylcellulose, hydroxypropyl methylcellulose, diethylaminocellulose (DEAE), dextran, cross-linked dextran agarose, cross-linked agarose, starches, alginate, chitosan and derivatives thereof, plastics and polymers such as polyethylene, polypropylene, polyamide, polyvinylidene fluoride, polyacrylamide, polyesters such as polyethylene terephthalate (PET), polyglycolic acid (PLA), polycaprolactone (PCL), polyethylene adipate (PEA), polybutylene terephthalate (PBT), or Poly(3-hydroxybutyrate-co-3-hydroxyvalerate), commonly known as PHBV, polymers and copolymers based on acrylic acid and derivatives thereof, polyamide, polystyrene (PS), organopolysiloxane, polyacrylate, polyvinyl polyacrilin, derivatives or combinations thereof. Such supports are commercially available.

In some embodiments, the support is a polymeric support, preferably a support made of polyvinyl chloride (PVC), polystyrene (PS) or polyethylene terephthalate (PET).

For illustration only, when the ligand of the invention comprises a primary amine group as mean for immobilization, the support can be, for instance, a polystyrene support pre-functionalized with N-oxysuccinimide (NOS) or a pre-functionalized PET. The PET can be pre-functionalized by a treatment comprising the hydrolysis of the ester groups present at the surface of the support, the increase of COOH surface density by oxidation (e.g. with potassium permanganate) and activation of COOH groups e.g. with N-hydroxysuccinimide as shown in Example 3.

The device comprising such a support may be of any type and any form. For instance, the device may be a film, a strip, a sheet, a chip, a microchip, a sensor, a reactor, for instance a microreactor a microfluidic chamber or channel, a cartridge, a plate or a microplate, a chromatography column resin or gel, a support for lateral flow immunochromatography assay, a support for ELISA-type assay, a filtration membrane, a filter, a bead such as a polymeric bead or a magnetic bead

- Methods and uses according to the invention

Typically, the molecule, the support and the device of the invention can be used to capture, immobilize, detect, quantify and/or analyze microvesicles present in a sample. More generally, the Invention relates to the use of the molecule, support and device as described above for capturing microvesicles present in a sample for the *in vitro* diagnosis of the pathological status of a subject.

In a particular aspect, the Invention relates to a method for capturing microvesicles from a sample, said method comprising:

- providing a support or a molecule of the invention,
- contacting said support or said molecule with a sample susceptible to contain the microvesicles of interest, in conditions suitable for the formation of a complex between the molecules of the invention and the microvesicles, whereby the microvesicles are captured.

The sample may be any composition which potentially comprises the microvesicles of interest. Typically, the sample may be, or may derive from, a body fluid. The body fluid is typically retrieved from a human being, preferably a human being suffering from, or at risk of developing a disease as described further below.

As used herein, the term “*biological fluid*” refers to any extractable or retrievable body fluid, including for example, blood, blood plasma, cerebrospinal fluid, bronchoalveolar fluid, urine, synovial fluid, breast milk, saliva, tears, seminal fluid, ascitic fluids, amniotic fluid and effusions (pleural or other). In the context of the invention, preferred biological fluids are blood, blood plasma and urine.

As used herein, “a *sample derives from a body fluid*” means that the sample is obtained from said body fluid by subjecting the body fluid to one or several treatment steps, e.g. in order to remove contaminants and/or separate the microvesicles from certain constituents of the body fluid. For instance, the body fluid may be subjected to one or several treatments such as a precipitation step e.g. salt precipitation, cryo-precipitation or flocculation, a filtration step such as depth filtration or ultrafiltration, centrifugation, clarification, chromatography, an extraction step such as a liquid-liquid or a solid-liquid extraction, viral inactivation, pasteurization, concentration, dialysis, freezing/thawing steps and the like.

The sample typically comprises contaminants from which microvesicles of interest is to be separated. The contaminants may be of any type and depend on the nature of the starting composition. The contaminants encompass proteins, salts, hormones, vitamins, nutriment, lipids, cells, cell debris such as cell membrane fragments and the like.

In some embodiments, the methods of the invention are performed on a non-treated body fluid, preferably on non-treated urine or plasma blood.

In some embodiments, the method may further comprise one or several steps selected from:

- a step of providing a sample susceptible to contain the microvesicles of interest from a body fluid of a subject, and/or
- a step of washing the support after contacting the support with the sample, e.g. so as to remove contaminants, and/or
- a step of detecting the formation of the complex between the microvesicles of interest and said support or molecule of the invention and/or
- a step of recovering the complex formed between the microvesicles and the molecules of the invention, and/or
- a step of quantification of said microvesicles of interest, and/or
- a step of detection of said microvesicles, and/or
- a step of characterization of the captured microvesicles, e.g. by detecting and/or quantifying a biomarker present on the surface or within the microvesicles, and/or
- a step of releasing the microvesicles from the complex, and/or
- a step of recovering the microvesicles of interest.

As mentioned above, the molecules, supports and devices of the invention find applications in the *in vitro* diagnosis.

Indeed, the detection, the quantification and/or the characterization of microvesicles in a sample may be useful in the context of the diagnosis and prognostic of diseases in a patient. The level of microvesicles in the body fluid as well as their compositions in terms of lipids, proteins and genetic materials such as mRNA and mitochondrial RNA is indicative of the pathological status of the subject.

Besides, the determination of microvesicle proteome may enable to determine the physiological and/or pathological status of the cell from which they originate, and can therefore represent a tool of choice for the early detection of a pathological state.

Accordingly, the detection, quantification and/or characterization of the captured microvesicles may allow the diagnosis of a pathology, the evaluation of the risk of developing a pathology, the prognosis of a pathology, the differential diagnosis of a pathology, the follow-up of the evolution of a pathology, and/or the monitoring of the therapy effectiveness in the patient.

Thus, in an additional aspect, the invention relates to the use of a molecule, support or device of the invention in an *in vitro* method for the diagnosis, the differential diagnosis, the prognosis, the assessment of the risk of, and/or the monitoring of the evolution of a disorder in a subject. The Invention also relates to the use of a molecule, support or device of the invention in an *in vitro* method for monitoring the efficacy of therapeutic treatment in a patient.

The disease or disorder of interest may be of any type and includes thrombotic, inflammatory and/or metabolic disorders, as well as cardiovascular or neurovascular diseases. For instance, disorders of interest include diabetes and related disorders such as diabetic nephropathy, diabetic neuropathy, diabetic retinopathy, and diabetic foot syndrome, multiple sclerosis, cancer, Alzheimer's disease, Parkinson's disease, aneurysm, cerebral vasospasm, stroke, coronary artery disease, parasitic diseases, cancers and other related pathologies.

In a particular embodiment, the invention relates to an *in vitro* method for the diagnosis, the differential diagnosis, the prognosis, the assessment of the risk of, and/or the monitoring a disorder in a subject which comprises:

- (a) providing a support or a molecule of the invention,
- (b) contacting said support or said molecule with a sample obtained from the subject, in conditions suitable for the formation of a complex between the molecules of the invention and the microvesicles possibly present in the sample,
- (c) detecting, quantifying and/or characterizing the microvesicles captured in step (b) by complexation.

As mentioned above, preferred disorders include thrombotic, inflammatory and/or metabolic disorders, as well as cardiovascular or neurovascular diseases. In a preferred embodiment, the disorder is selected from the group consisting of diabetes and related disorders such as diabetic nephropathy, diabetic neuropathy, diabetic retinopathy, and diabetic foot syndrome, multiple sclerosis, cancer, Alzheimer's disease, Parkinson's disease, aneurysm, cerebral vasospasm, stroke, coronary artery disease, parasitic diseases, cancers and other related pathologies.

Said method may further comprise a step of comparing the result obtained in step (c) with that obtained from one or several control samples in similar conditions.

The control sample(s) may be obtained from a healthy subject or from a subject suffering from the disorder to diagnose. Alternatively, the sample is from the same subject, but obtained earlier. Comparison with earlier samples from the same subject may enable to monitor the evolution of the disease and/or the efficacy of the treatment and/or to predict the outcome of the disease or treatment in the subject.

The detection, quantification and/or characterization of the microvesicles can be carried by standard methods known by the skilled artisan.

As used herein “*the characterization*” of microvesicles refer to the detection, the determination of the presence or the absence and/or the quantification of at least one biomarker susceptible to be present in the microvesicles and correlated with the disorder to diagnose.

The biomarker may be any molecule of interest such as proteins, lipids, hormones, mitochondrial DNA, miRNA or mRNA. Such biomarkers can be detected and/or quantified by methods well-known by the skilled artisan.

For instance, proteins can be detected and quantified by standard immunological assays, e.g. by ELISA or Western blot techniques. Detection and characterization of nucleic acids may include specific nucleic acid detection methods such as PCR /qPCR, RT-PCR / RT-qPCR and sequencing.

In some embodiments, the method comprises a step of normalization of the result obtained in step (c). For instance, said normalization can be carried out on the basis of the quantification of a marker present on or in the microvesicles such as annexin-A5 and beta-actin.

Thus, in certain embodiments, step (c) of the method may comprise:

- a step of quantifying a biomarker of interest in the captured microvesicles,
- a step of quantifying a normalization biomarker in the captured microvesicles,

- a step of normalizing the amount detected for the biomarker by the amount obtained for the normalization biomarker (e.g. by calculating the ratio of the amount of biomarker to that of the normalization biomarker), and
- optionally comparing the resulting normalized amount of the biomarker of interest with that obtained for a control sample in similar conditions.

The comparison with a normalized amount obtained for a control sample, e.g. a sample obtained from a healthy subject, or a sample obtained from a subject suffering from the disorder to diagnose, may enable to determine the diagnosis or prognostic of the disease in the subject.

In the method of the invention, it goes without saying that the biomarker(s) to detect or quantify the microvesicles is selected depending on the disorder of interest.

For illustration only:

- For the diagnosis, in particular of early diagnosis, of nephropathy in a subject, the biomarker may be podocalyxin.
- For the diagnosis, in particular of early diagnosis, of Parkinson's disease, the biomarker may be alpha-synuclein.
- For the diagnosing, in particular early diagnosis, of diabetic nephropathy, the biomarker may be CD41.

- kits according to the invention

The invention also relates to a kit comprising a molecule, a support or a device according to the invention. Such a kit is typically dedicated for implementing, at least in part, a method of the invention, e.g. the method for capturing microvesicles from a sample, and/or the *in vitro* method for the diagnosis, the differential diagnosis, the prognosis, the assessment of the risk of, and/or the monitoring a disorder in a subject.

Typically, the kit comprises a molecule of the invention, for instance as shown in any one of formula II, (IIa), (IIb), (IIc), (IIIa), (IIIb) or (IIIc) or a support or device having thereon said molecules as described above and at least one additional mean useful to implement a method of the invention.

For instance, the at least one additional mean may be selected from:

- means for providing the sample to analyze, for instance mean for pre-treating the body fluid obtained from the subject,
- buffers for implementing the methods of the invention, e.g. suspension buffers, washing buffers, elution buffers (e.g. for the dissociation of the complex form between microvesicles and the molecules of the invention)
- a mean for the detection of the captured microvesicles,
- a mean for the characterization of the captured microvesicles, for instance a mean for detecting, and/or quantifying at least one biomarker possibly present in the microvesicles
- a mean for detecting and/or quantifying at least one normalization biomarker in the captured microvesicles such as annexin V or beta-actin
- a control sample for the normalization of the biomarker quantified in the microvesicles
- a control sample, such as a positive or negative control sample, for validation

As used herein, "*a mean for the detection or quantification of a biomarker*" refers to any mean known by the skilled artisan for detecting or quantifying said biomarker. Said mean depends on the nature of the biomarker. For instance, a protein biomarker may be detected/quantified by immunological techniques (in particular ELISA and Western-blot) while nucleic acid biomarkers can be detected by specific amplification techniques, which can be qualitative or quantitative.

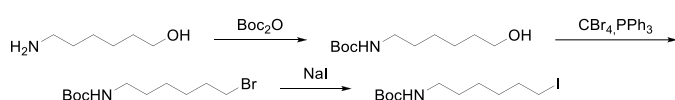
Moreover, the kit according to the invention may comprise a notice providing its user with instructions for implementing the method according to the invention by means of the kit.

Further aspects and advantages of the present invention are disclosed in the following experimental section, which should be regarded as illustrative and not limiting the scope of the present application.

Examples

Example 1: Synthesis of ligands according to the invention

A. Synthesis of Tert-butyl (6-iodohexyl)carbamate (intermediate)

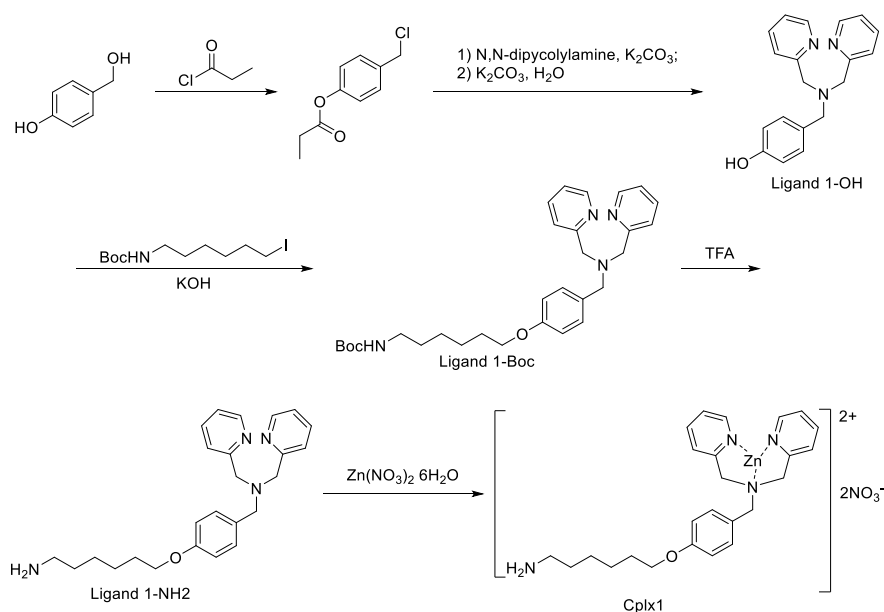


Tert-butyl (6-hydroxyhexyl)carbamate: 3.72 g (17 mmol) of Di-tert-butyl-dicarbonate was added into a solution of 2 g (17mmol) 6-amino-1-hexanol in 40 mL tetrahydrofuran at 0 °C under stirring. The reacting mixture was allowed to slowly warm up to room temperature. After 24 h, the solvent was evaporated. The residue was dissolved in dichloromethane 50 mL and was washed with 50 mL of water for 3 times. The organic phase was gathered and dried over sodium sulfate, and then the solvent was removed with a rotary evaporator. The product is colorless oil, and the yield was 91 %. ¹H NMR (CDCl₃, 300 MHz, 25 °C): δ(ppm) 3.60 (t, 2H), 3.08 (t, 2H), 1.59-1.28 (m, 17H).

Tert-butyl (6-bromohexyl)carbamate: To a solution of 1 g (4.6 mmol) tert-butyl (6-hydroxyhexyl)carbamate and 2.1 g (8.1 mmol) of triphenylphosphine in 12 mL tetrahydrofuran, a solution of 2.7 g (8.1 mmol) of tetrabromomethane in 8 mL tetrahydrofuran was added dropwise at 0 °C under stirring. The reacting mixture was allowed to slowly warm up to room temperature. After 24 h of reaction, the solvent was removed. The residue was added into a solvent mixture of 50 mL petroleum ether and 10 mL ethyl acetate. A precipitate formed instantly and then was filtered off while the filtrate was collected and evaporated to leave colorless oil behind. The oil went through a flash column of silica using an eluent of petroleum ether: ethyl acetate= 10:1. The solvent was removed with a rotary evaporator. The product is colorless oil, and the yield was 93 %. ¹H NMR (CDCl₃, 300 MHz, 25 °C): δ(ppm) 3.44 (t, 2H), 3.14 (t, 2H), 1.91-1.86 (m, 2H), 1.52-1.33 (m, 15H).

Tert-butyl (6-iodohexyl)carbamate: 1.5 g (5.4 mmol) of tert-butyl (6-bromohexyl)carbamate was dissolved in 15 mL acetonitrile. 4.02 g (26.8 mmol) of sodium iodide was added into the solution. The mixture was stirred under room temperature and kept in darkness for 48 h. The solvent was removed under vacuum, and the residue was extracted with 50 mL of dichloromethane and 50 mL water. The organic phase was washed with a saturated solution of sodium thiosulfate and then dried over sodium sulfate. The solvent was removed with rotary evaporator. The product is colorless oil, and the yield was 96 %. ¹H NMR (CDCl₃, 300 MHz, 25 °C): δ(ppm) 3.21 (t, 2H), 1.90-1.80(m, 2H), 1.56-1.30 (m, 15H).

B. Synthesis of complex of formula (IIIId) (comparative – Cplx1)



4-(chloromethyl)phenyl propionate: Under stirring, 30 mL propionyl chloride was cooled to 0 °C. 5.1 g (41 mmol) of 4-(hydroxymethyl)phenol was added slowly into the flask so as to control the generation of hydrogen chloride at a moderate rate. After the addition, the mixture was allowed to slowly warm up to room temperature. After 12h, the mixture was poured into 500 mL ice-cold water, and then neutralized with sodium bicarbonate. The mixture was then extracted with 50 mL diethyl ether for 3 times. The organic phase was combined and washed with 30 mL water for 3 times. The solution was then dried over sodium sulfate, and the solvent was removed using a rotary evaporator. The product is pale yellow oil, and the yield was 97%. ¹H NMR (CDCl₃, 300 MHz, 25 °C): δ(ppm) 7.42 (d, 2H), 7.12 (d, 2H), 4.60 (s, 2H), 2.62 (q, 2H), 1.30 (t, 3H).

Ligand 1-OH: 199 mg (1 mmol) of 4-(chloromethyl)phenyl propionate and 199 mg (1 mmol) of di-(2-picolyl)amine was dissolved in 10 mL dimethyl sulfoxide under stirring. After adding 414.6 mg (3 mmol) of potassium carbonate, the mixture was then heated to 60 °C. 24 h later, the reaction was cooled to room temperature, and then a solution of 0.6 g potassium carbonate in 3 mL water was added at room temperature. Another 24 h later, the reaction mixture was dissolved in 30 mL dichloromethane, then washed with water (30 mL, 3 times), dried over sodium sulfate. The solvent was removed under vacuum to give the product as white solid. The yield was 74%. ¹H NMR (DMSO, 300 MHz, 25 °C): δ(ppm) 9.31 (s, 1H), 8.51-8.49 (m, 2H), 7.83-7.77 (m, 2H), 7.58 (d, 2H), 7.28-7.24 (m, 2H), 7.20 (d, 2H), 6.73 (d, 2H), 3.68 (s, 4H), 3.51 (s, 2H); ¹³C NMR (DMSO, 75MHz, 25°C): δ(ppm) 159.80, 156.87, 149.26, 137.08, 130.38, 128.98, 122.87, 122.59, 115.48, 59.33, 57.35.

Ligand 1-Boc: 305 mg (1 mmol) of ligand 1-OH was dissolved in 4 mL dimethylformamide under stirring. 112 mg (2 mmol) of potassium hydroxide was added to the solution at room temperature. 1 h later,

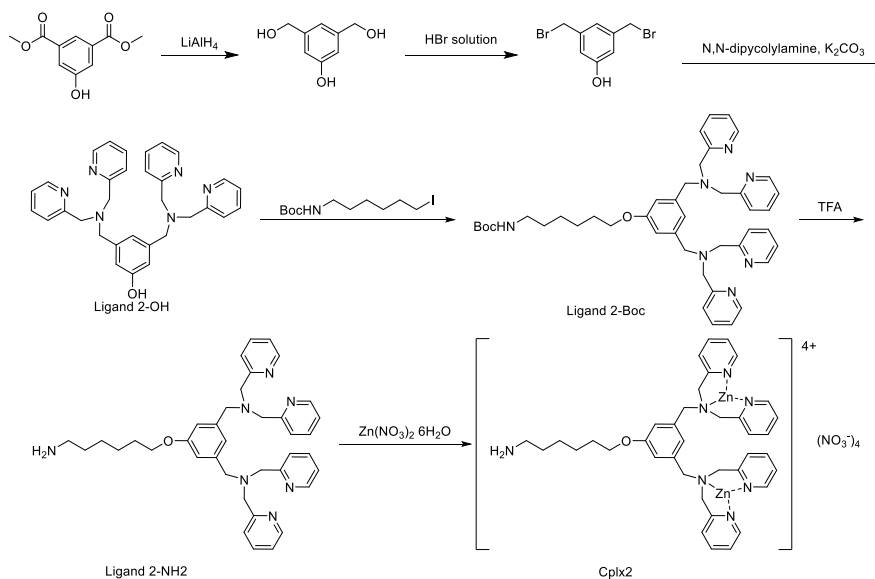
the mixture was cooled to -20 °C, then 392 mg (1.2 mmol) of tert-butyl (6-iodohexyl)carbamate was added into the mixture. The reaction was allowed to slowly warm up to room temperature. 3 h later, the reaction was quenched with water. The mixture was extracted three times with 20 mL dichloromethane, then the combined organic phase was washed two times with 20 mL brine, and dried over sodium sulfate. The solvent was removed under vacuum to afford a brown oil. The crude product was then purified by silica gel column chromatography with an eluent of ethyl acetate: acetonitrile (5:1). The product is obtained as a pale yellow solid in 75% yield. ¹H NMR (MeOD, 300 MHz, 25 °C): δ(ppm) 8.43 (m, 2H), 7.86-7.71 (m, 2H), 7.70 (d, 2H), 7.32-7.28 (m, 4H), 6.89 (d, 2H), 3.99 (t, 2H), 3.77 (s, 4H), 3.61 (s, 2H), 3.06 (t, 2H), 1.81-1.76 (m, 2H), 1.54-1.44 (m, 15H); ¹³C NMR (MeOD, 75MHz, 25°C): δ(ppm) 159.34, 154.18, 147.94, 137.34, 129.86, 123.88, 123.32, 122.39, 113.99, 67.45, 66.43, 59.12, 57.81, 28.94, 27.39, 25.48;

Ligand 1-NH₂: 802.2 mg (1.6 mmol) of ligand 1-Boc was dissolved in 15 mL tetrahydrofuran. Trifluoroacetic acid was then added into the solution slowly at room temperature. 5 min after the addition of trifluoroacetic acid, the solution was heated to 60 °C. 30 h later, the solution was cooled to room temperature and then poured into an ice-cold sodium bicarbonate solution. The product was extracted with dichloromethane (30 mL, under vacuum and the compound was obtained with 85% yield. ¹H NMR (MeOD, 300 MHz, 25 °C): δ(ppm) 8.54 (d, 2H), 7.71-7.66 (m, 2H), 7.60 (d, 2H), 7.19-7.14 (m, 2H), 6.87 (d, 2H), 3.96 (t, 2H), 3.82 (s, 4H), 3.64 (s, 2H), 2.73 (t, 2H), 1.83-1.77 (m, 2H), 1.53-1.41 (m, 6H); ¹³C NMR (MeOD, 75MHz, 25°C): δ(ppm) 159.94, 158.25, 148.96, 136.44, 130.69, 130.06, 122.81, 121.94, 114.31, 67.86, 59.84, 57.88, 41.88, 33.24, 29.27, 26.66, 25.94;

Complex of formula (IIIId) – comparative – also referred as Cplx1 herein

108 mg (0.27 mmol) of ligand 1-NH₂ was dissolved in 10 mL methanol at room temperature under stirring. 79.4 mg (0.27 mmol) of zinc nitrate hexahydrate was dissolved in 5 mL methanol and was added in to the solution of ligand dropwise. 12 h later, the solvent was removed under vacuum to give quantitatively the final product as pale yellow powder (yield 100%). ¹H NMR (DMSO, 300 MHz, 25 °C): δ(ppm) 8.69 (d, 2H), 8.12 (t, 2H), 7.66 (m, 4H), 7.30 (d, 2H), 7.02 (d, 2H), 4.25 (d, 2H), 4.02 (t, 2H), 3.71 (t, 4H), 2.80 (t, 2H), 1.78-1.73 (m, 2H), 1.60-1.56 (m, 2H), 1.48-1.39 (m, 6H); ¹³C NMR (MeOD, 75MHz, 25°C): δ(ppm) 159.34, 154.81, 148.40, 141.26, 133.32, 125.33, 125.19, 123.98, 114.90, 67.88, 56.40, 55.68, 29.22, 29.01, 28.09, 26.10;

C. Synthesis of complex of formula (IIIa) (hereafter Cplx2)



5-hydroxyphenyl-1,3-dimethanol: To a dispersion of 1.3 g (34.3 mmol) of lithium aluminum hydride in 40 mL anhydrous tetrahydrofuran at 0 °C, a solution of 3 g (14.3 mmol) of dimethyl 5-hydroxyisophthalate in 60 mL anhydrous tetrahydrofuran was added dropwise. The reaction was allowed to warm up to room temperature during 3 hours. After 12 h, the mixture was cooled to 0 °C again and quenched with 10% hydrochloric acid. The solvent was removed under reduced pressure. The residue was diluted in 50 mL brine and ethyl acetate was used to extract the product from the aqueous solution (6x50 mL). The organic layers were combined, dried over sodium sulfate and the solvent was removed under vacuum. The product is obtained as a white solid in 94% yield. $^1\text{H NMR}$ (CDCl_3 , 300 MHz, 25 °C): δ (ppm) 6.69 (s, 1H), 6.61 (s, 2H), 4.41 (s, 4H). 3,5-bis(bromomethyl)phenol

3,5-bis(bromomethyl)phenol: 8.2 mL of 33% hydrogen bromide solution was added dropwise at 0 °C to a solution of 2 g (13 mmol) of 5-hydroxyphenyl-1,3-dimethanol in 20 mL acetic acid. The mixture was extracted with 3 x 70 mL dichloromethane. The combined organic phases were washed with 2x100 mL water, then 2x100 mL saturated sodium bicarbonate solution and again 100 mL water. The organic phase was dried with sodium sulfate, filtered and concentrated. The crude product was purified with a flash column silica chromatography, with a mixture of petroleum ether: ethyl acetate (9:1) to afford white solids (yield 90%). $^1\text{H NMR}$ (CDCl_3 , 300 MHz, 25 °C): δ (ppm) 3.21 (t, 2H), 1.90-1.80(m, 2H), 1.56-1.30 (m, 15H).

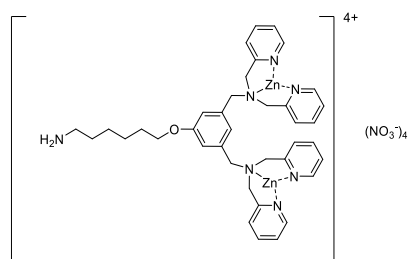
Ligand 2-OH: 672 mg (2.4 mmol) of 3,5-bis(bromomethyl)phenol, 1196 mg (6 mmol) of $\text{N,N-dipicolylamine}$ and 398 mg (2.88 mmol) of potassium carbonate was added into 10 mL dimethylformamide under nitrogen protection. The mixture was stirred under room temperature. After 3 hours, 50 mL water was added into the mixture, and was extracted with 2x50 mL of dichloromethane. The organic layers were combined and washed with 2x50 mL of water, dried over sodium sulfate, filtered and evaporated using rotary evaporator. The remainder was purified using silica gel column chromatography to

give the final product as white solid (yield 80%). ^1H NMR (CDCl_3 , 300 MHz, 25 °C): δ (ppm) 8.48-8.46 (m, 4H), 7.60-7.58 (m, 8H), 7.11 (q, 4H), 6.96 (s, 1H), 6.86 (s, 2H), 3.79 (s, 8H), 3.57 (s, 4H);

Ligand 2-Boc: 520 mg (1 mmol) of ligand 2-OH was dissolved in 4 mL dimethylformamide under stirring. 120 mg (2 mmol) of potassium hydroxide was added to the solution at room temperature. 1 h later, the mixture was cooled to -20 °C, then 400 mg (1.2 mmol) of tert-butyl (6-iodohexyl)carbamate was added into the mixture. The reaction was allowed to slowly warmup to room temperature. 3 h later, the reaction was quenched with water. The mixture was extracted with 20 mL dichloromethane for three times, then the combined organic phase was washed with 20 mL brine twice, and dried with sodium sulfate. The solvent was removed under vacuum to afford brown oil. The crude product was then purified by silica gel column chromatography with an eluent of ethyl acetate: acetonitrile (5:1). The product is pale yellow solid with 75% yield. ^1H NMR (DMSO, 300 MHz, 25 °C): δ (ppm) 8.43 (d, 4H), 7.79 (ddd, 4H), 7.28 (tt, 4H), 7.04 (s, 1H), 3.97 (t, 2H), 3.80 (s, 8H), 3.65 (s, 4H), 3.07 (t, 2H), 1.79 (t, 2H), 1.58-1.48 (m, 15H);

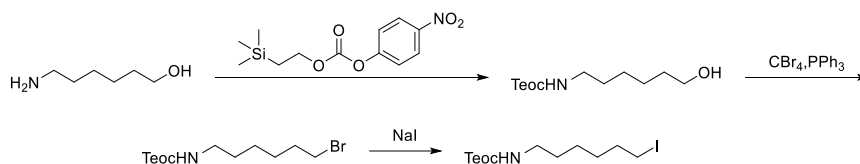
Ligand 2-NH₂: 1350 mg (1.89 mmol) of ligand 2-Boc was dissolved in 15 mL tetrahydrofuran. 7.2 mL (94.3 mmol) of trifluoroacetic acid was then added into the solution slowly at room temperature. 5 min after the addition of trifluoroacetic acid, the solution was heated to 60 °C. 30 h later, the solution was cooled to room temperature and then poured into an ice-cold sodium bicarbonate solution. The product was extracted with dichloromethane (3x30 mL). The organic phase was then dried over sodium sulfate and the solvent was removed using rotary evaporator. The yield was 85%. ^1H NMR (DMSO, 300 MHz, 25 °C): δ (ppm) 8.49 (d, 4H), 7.74 (ddd, 4H), 7.57 (d, 4H), 7.25 (dd, 4H), 7.07 (s, 1H), 6.82 (s, 2H), 3.93 (t, 2H), 3.71 (s, 8H), 3.60 (s, 4H), 3.32 (b, 4H), 1.69 (t, 2H), 1.42-1.34 (m, 6H); ^{13}C NMR (MeOD, 75MHz, 25°C): δ (ppm) 159.79, 159.20, 148.97, 140.49, 136.42, 122.76, 121.95, 121.48, 113.56, 67.85, 60.09, 58.63, 41.31, 29.07, 26.81, 26.58, 26.13.

Complex of formula (IIIa) – (hereunder Cplx2)



1110 mg (1.8 mmol) of ligand 2-NH₂ was dissolved in 10 mL methanol at room temperature under stirring. 1072 mg (3.6 mmol) of zinc nitrate hexahydrate was dissolved in 5 mL methanol and was added in to the solution of ligand dropwise. 12 h later, the solvent in the mixture was removed under vacuum to give the final product as pale yellow powder (yield 100%). ^1H NMR (DMSO, 300 MHz, 25 °C): δ (ppm) 8.71 (b, 4H), 8.11 (t, 4H), 7.67 (t, 4H), 7.60 (d, 4H), 7.01 (b, 2H), 6.89 (s, 1H), 4.35 (d, 2H), 4.07 (b, 2H), 3.81 (d, 8H), 2.84 (t, 2H), 1.79 (b, 2H), 1.65-1.46 (m, 6H); ^{13}C NMR (MeOD, 75MHz, 25°C): δ (ppm) 162.85, 159.27, 155.04, 148.50, 141.37, 134.32, 127.12, 125.32, 117.96, 68.03, 57.51, 56.15, 39.86, 36.26, 31.24, 29.05, 27.79, 26.11, 25.62.

D. Synthesis of 2-(trimethylsilyl)ethyl (6-iodohexyl)carbamate (intermediate)

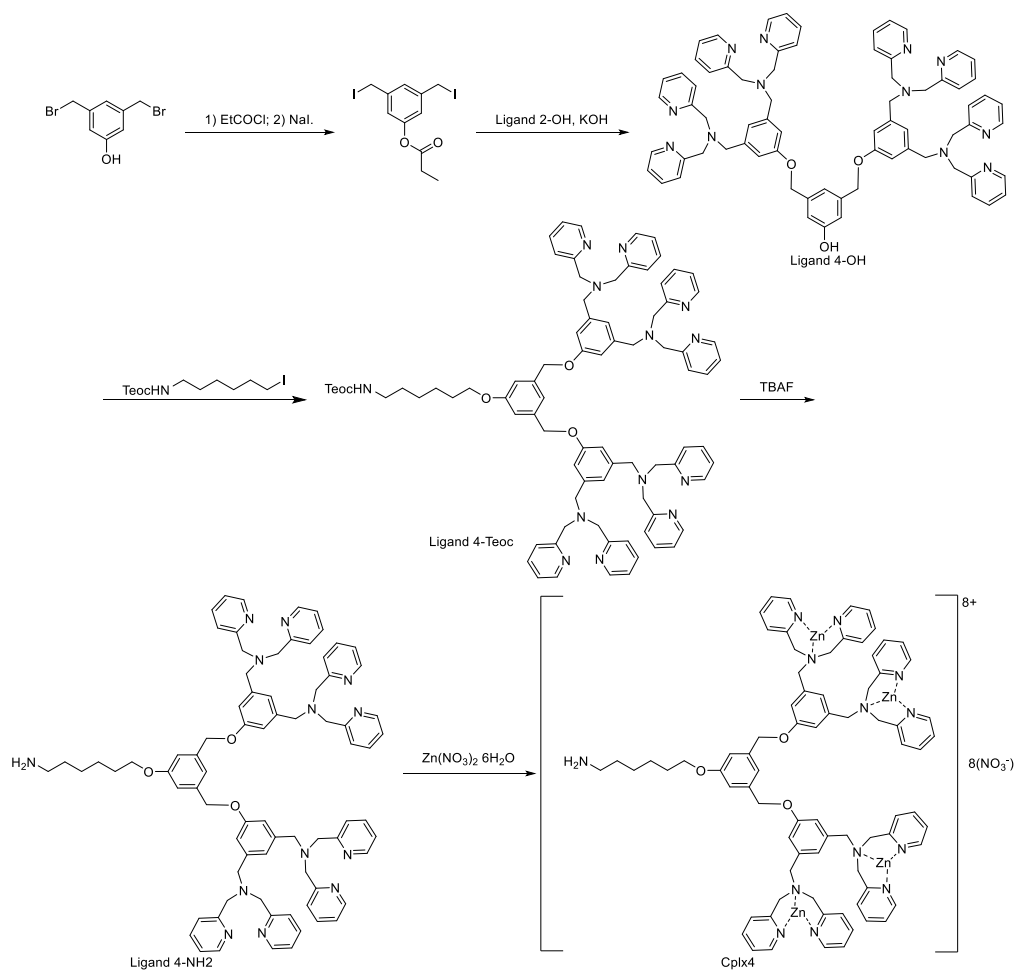


2-(trimethylsilyl)ethyl (6-hydroxyhexyl)carbamate : 352 mg (3 mmol) of 6-amino-1-hexanol was dissolved in 5 mL dichloromethane. 0.9 mL (6 mmol) triethylamine was added into the solution and then 850 mg (3 mmol) of 4-Nitrophenyl 2-(trimethylsilyl)ethyl carbonate in 1.4 mL dichloromethane was also added into the mixture at room temperature under stirring. After 24 h, the solvent was evaporated. The residue was dissolved in dichloromethane 50 mL and washed with 3x50 mL of saturated NaHCO₃ solution and then 3x50 mL of NaOH (2M) solution. The organic phase was gathered and dried over sodium sulfate, and the solvent was removed with a rotary evaporator. The product is obtained as a colorless oil in 98 % yield. ¹H NMR (CDCl₃, 300 MHz, 25 °C): δ(ppm) 4.64 (b, 1H), 4.17 (t, 2H), 3.67 (t, 2H), 3.20 (q, 2H), 1.68-1.34 (m, 8H), 1.00 (t, 2H), 0.07 (s, 9H);

2-(trimethylsilyl)ethyl (6-bromohexyl)carbamate : To a solution of 748 mg (2.86 mmol) of 2-(trimethylsilyl)ethyl (6-hydroxyhexyl)carbamate and 1311 mg (5 mmol) of triphenylphosphine in 12 mL tetrahydrofuran, a solution of 1.66 g (5 mmol) of tetrabromomethane in 8 mL tetrahydrofuran was added dropwise at 0 °C under stirring. The reacting mixture was allowed to slowly warm up to room temperature. After 24 h of reaction, the solvent was removed. The residue was added into a solvent mixture of 50 mL petroleum ether and 10 mL ethyl acetate. A precipitate formed instantly and filtered off. The filtrate was collected and evaporated to give a colorless oil. The oil went through a flash chromatography column of silica gel using an eluent of petroleum ether: ethyl acetate (10:1). The solvent was removed under vacuum and a colorless oil was obtained in 84 % yield. ¹H NMR (CDCl₃, 300 MHz, 25 °C): δ(ppm) 4.61 (b, 1H), 4.18 (t, 2H), 3.43 (t, 2H), 3.19 (q, 2H), 1.94-1.84 (m, 2H), 1.62-1.34 (m, 6H), 1.00 (t, 2H), 0.07 (s, 9H);

2-(trimethylsilyl)ethyl (6-iodohexyl)carbamate : 846 mg (2.61 mmol) of 2-(trimethylsilyl)ethyl (6-bromohexyl)carbamate was dissolved in 15 mL acetonitrile. 2 g (13 mmol) of sodium iodide was added into the solution. The mixture was stirred under room temperature and kept in darkness for 48 h. The solvent was removed under vacuum, and the residue was extracted with 50 mL of dichloromethane and 50 mL water. The organic phase was washed with a saturated solution of sodium thiosulfate and then dried over sodium sulfate. The solvent was removed under vacuum and the product was obtained as a colorless oil in 96 % yield. ¹H NMR (CDCl₃, 300 MHz, 25 °C): δ(ppm) 4.61 (b, 1H), 4.18 (t, 2H), 3.24-3.16 (m, 4H), 1.89-1.80 (m, 2H), 1.58-1.33 (m, 6H), 1.00 (t, 2H), 0.07 (s, 9H);

E. Synthesis of complex of formula (IIIb) (hereafter Cplx4)



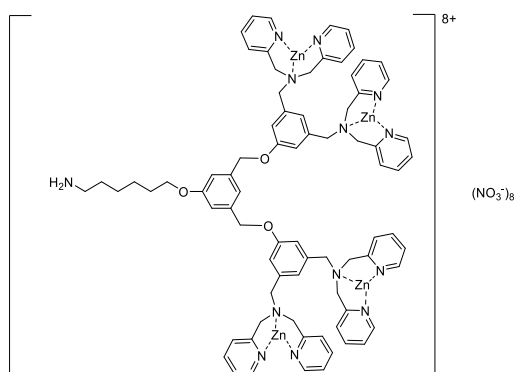
3,5-bis(iodomethyl)phenylpropionate : 1.15 mL (13 mmol) of propionyl chloride was dissolved in 30 mL of dichloromethane. At 0°C, 2.8 g (10 mmol) of 3,5-bis(bromomethyl)phenol dissolved in 10 mL dichloromethane was added into the solution under stirring. 5 min later, 3 mL (13 mmol) of triethylamine in 10 mL dichloromethane was also added into the solution and the cold bath was removed. 2h after the addition of triethylamine, the reaction was quenched with 10 mL water. The mixture was extracted with 50 mL dichloromethane twice, and the organic phase was combined and washed first with 15 mL saturated sodium bicarbonate solution, then with 15 mL brine. The organic phase was dried with sodium sulfate before the solvent was removed under vacuum. The product was dissolved in 15 mL acetonitrile. 7.5 g (50 mmol) sodium iodide was added into the solution. The mixture was stirred under room temperature and kept in darkness for 48 h. The solvent was removed under vacuum, and the residue was extracted between 50 mL of dichloromethane and 50 mL water. The organic phase was washed with a saturated solution of sodium thiosulfate before the organic phase was collected and dried over sodium sulfate. The solvent was removed with a rotary evaporator. The product is a colorless solid (96 %). ¹H NMR (CDCl₃, 300 MHz, 25 °C): δ(ppm) 7.27 (t, 1H), 7.04 (d, 2H), 4.41 (s, 4H), 2.62 (q, 2H), 1.30 (t, 3H);

Ligand 4-OH: 1284 mg (2.5 mmol) of ligand 2-OH was dissolved in 4 mL dimethylformamide under stirring. 126 mg (2.5 mmol) of potassium hydroxide was added to the solution at room temperature. 1 h later, the mixture was cooled to -20 °C, then 520 mg (1.2 mmol) of 3,5-bis(iodomethyl)phenyl propionate was added into the mixture. The reaction was allowed to slowly warm up to room temperature. 3 h later, the reaction was quenched with water. The mixture was extracted with 20 mL dichloromethane for three times, then the combined organic phase was washed with 2x20 mL brine, and dried with sodium sulfate. The solvent was removed with rotary evaporator to afford brown oil. The crude product was then purified by silica gel column chromatography with an eluent of ethyl acetate: acetonitrile= (5:1). The product is pale yellow solid. The yield was 75%. ¹H NMR (DMSO, 300 MHz, 25 °C): δ(ppm) 8.47 (tt, 8H), 7.71 (ddd, 8H), 7.54-7.51 (m, 8H), 7.20 (qq, 8H), 7.06 (s, 2H), 6.96 (s, 1H), 6.90 (s, 4H), 6.83 (s, 2H), 5.01(s, 4H), 3.70 (s, 16H), 3.57 (s, 8H); ¹³C NMR (CDCl₃, 75MHz, 25°C): δ(ppm) 159.68, 158.63, 157.79, 148.87, 140.61, 139.88, 138.99, 136.64, 122.84, 122.49, 122.05, 117.89, 114.94, 115.18, 69.96, 59.87, 58.33.

Ligand 4-Teoc: 930 mg (0.8 mmol) of ligand 4-OH was dissolved in 10 mL dimethylformamide under stirring. 90.5 mg (1.6 mmol) of potassium hydroxide was added to the solution at room temperature. 1 h later, the mixture was cooled to -20 °C, then 360 mg (0.97 mmol) of 2-(trimethylsilyl)ethyl (6-iodohexyl)carbamate was added into the mixture. The reaction was allowed to slowly warm up to room temperature. 3 h later, the reaction was quenched with water. The mixture was extracted with 3x20 mL dichloromethane, then the combined organic phase was washed with 2x20 mL brine, and dried with sodium sulfate. The solvent was removed with rotary evaporator to afford brown oil. The crude product was then purified by silica gel column chromatography with an eluent of ethyl acetate: acetonitrile (5:1). The product is pale yellow solid. The yield was 75%. ¹H NMR (CDCl₃, 300 MHz, 25 °C): δ(ppm) 8.54-8.51 (m, 8H), 7.65-7.55 (m, 16H), 7.16-7.11 (m, 11H), 7.00-6.98 (m, 6H), 5.05 (s, 4H), 4.17 (t, 2H), 3.97 (t, 2H), 3.82 (s, 16H), 3.68(s, 8H), 3.18 (q, 2H), 1.83-1.72 (m, 2H), 1.54-1.34 (m, 6H), 0.99 (t, 2H), 0.06 (s, 9H); ¹³C NMR (CDCl₃, 75MHz, 25°C): δ(ppm) 162.55, 159.75, 159.67, 159.02, 148.99, 140.73, 139.09, 136.42, 122.73, 121.96, 121.88, 118.52, 113.82, 113.11, 69.91, 67.92, 60.10, 58.57, 40.86, 36.49, 30.94, 30.05, 29.19, 26.54, 25.79, 17.80, -1.44;

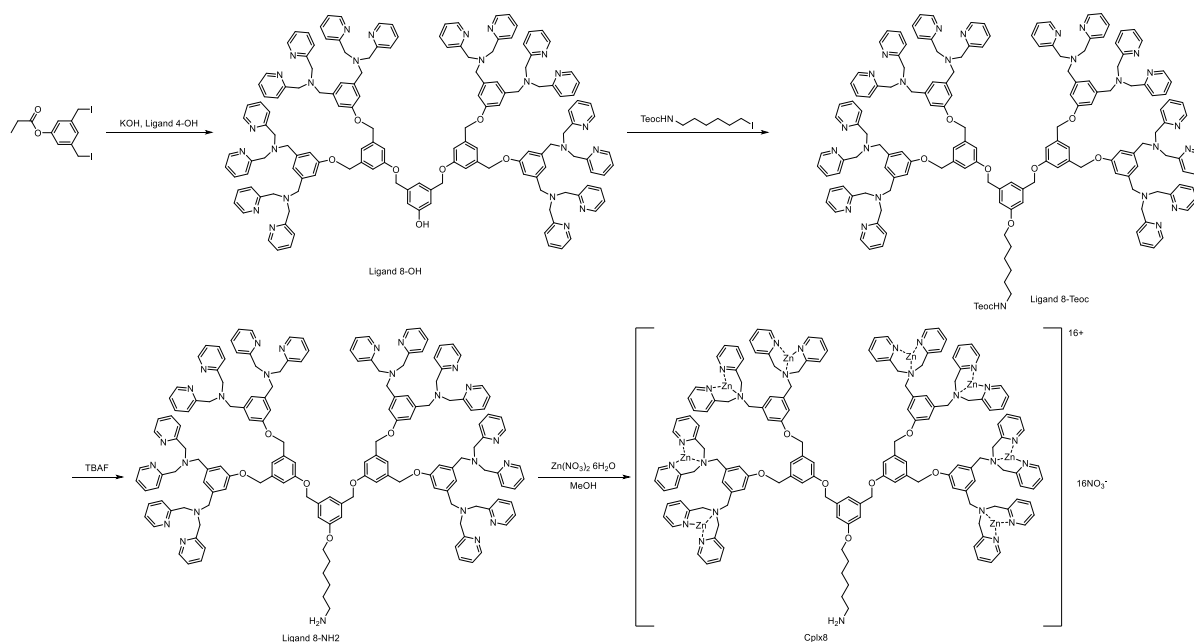
Ligand 4-NH₂: 900 mg (0.65 mmol) of ligand 4-Teoc was dissolved in 10 mL tetrahydrofuran under stirring. 6.5 mL (6.5 mmol) of 1 M tetrabutylammonium fluoride solution was then added at room temperature. The reaction mixture was then kept at 60 °C overnight. After cooled to room temperature, the solvent was removed in vacuo. The residue was dissolved in dichloromethane, and then washed with 50 mL 0.5 M NaOH solution once and 50 mL saturated NaHCO₃ solution twice. The organic phase was dried with sodium sulfate. The solvent was removed with rotary evaporator to afford brown solid in 90% yield. ¹H NMR (DMSO, 300 MHz, 25 °C): δ(ppm) 8.48-8.45 (t, 8H), 7.70 (ddd, 8H), 7.51 (d, 8H), 7.22 (ddd, 8H), 7.11 (s, 1H), 7.06 (s, 2H), 6.97 (s, 2H), 6.92 (s, 4H), 5.07 (s, 4H), 3.89 (t, 2H), 3.69 (s, 16H), 3.57 (s, 8H), 1.61 (t, 2H), 1.37-1.19 (m, 6H); ¹³C NMR (DMSO, 75MHz, 25°C): δ(ppm) 159.61, 159.29, 158.79, 149.79, 149.26, 140.72, 139.49, 136.95, 122.81, 122.57, 121.69, 114.10, 113.30, 69.48, 59.66, 57.94, 55.39, 41.52, 32.60, 29.05, 26.48, 25.80.

1) Complex of formula IIIb – (hereafter Cplx4)



125 mg (0.1 mmol) of ligand 4-NH₂ was dissolved in 10 mL methanol at room temperature under stirring. 119 mg (0.4 mmol) of zinc nitrate hexahydrate was dissolved in 5 mL methanol and was added in to the solution of ligand dropwise. 12 h later, the solvent in the mixture was removed under vacuum to give quantitatively the final product as brown powder (yield 100%). ¹H NMR (DMSO, 300 MHz, 25 °C): δ(ppm) 8.70 (d, 8H), 8.10 (t, 8H), 7.67 (t, 8H), 7.58 (d, 8H), 7.27 (s, 1H), 7.17 (s, 4H), 7.06 (s, 1H), 6.96 (s, 2H), 5.27 (s, 4H), 4.38 (d, 8H), 4.10 (q, 2H), 3.83 (t, 16H), 2.81 (t, 2H), 2.22 (t, 2H), 1.55 (t, 2H), 1.44-1.32 (m, 4H); ¹³C NMR (DMSO, 75MHz, 25°C): δ(ppm) 159.44, 159.08, 154.85, 148.45, 141.27, 139.20, 134.29, 127.73, 125.32, 125.13, 118.35, 114.09, 69.86, 68.05, 57.42, 56.14, 49.09, 29.27, 26.05, 25.55, 20.34, 19.72;

F. Synthesis of complex of formula (IIIc) (hereafter Cplx8)



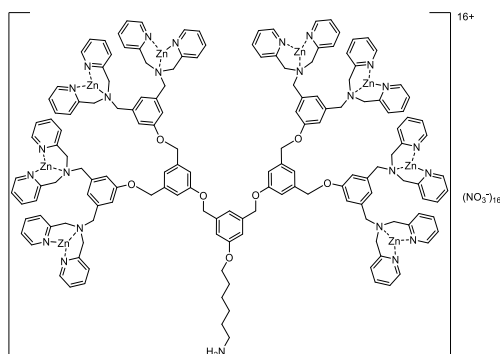
Ligand 8-OH: 1151 mg (1 mmol) ligand 4-OH was dissolved in 4 mL dimethylformamide under stirring. 126 mg (2.25 mmol) potassium hydroxide was added to the solution at room temperature. 1 h later, the mixture was cooled to -20 °C, then 220 mg (0.51 mmol) 3,5-bis(iodomethyl)phenyl propionate was added

into the mixture. The reaction was allowed to slowly warm up to room temperature. 3 h later, the reaction was quenched with water. The mixture was extracted with 3x20 mL dichloromethane, the combined organic phase was washed with 2x20 mL brine, and dried with sodium sulfate. The solvent was removed with rotary evaporator to afford brown oil. The crude product was then purified by silica column chromatography with an eluent of ethyl acetate: acetonitrile= 5:1. The product is obtained as a pale yellow solid in 75% yield. ¹H NMR (DMSO, 300 MHz, 25 °C): δ(ppm) 8.48-8.44 (m, 16H), 7.74-7.64 (m, 16H), 7.54-7.51 (m, 16H), 7.22-7.14 (m, 16H), 7.07 (d, 6H), 6.96 (s, 1H), 6.90 (d, 8H), 6.83 (s, 2H), 6.79 (s, 1H), 6.75 (s, 1H), 6.71 (s, 1H), 6.66 (s, 1H), 5.05-4.97(m, 12H), 3.69 (d, 32H), 3.57 (d, 16H); ¹³C NMR (CDCl₃, 75MHz, 25°C): δ(ppm) 159.68, 158.63, 157.79, 148.87, 140.61, 139.88, 138.99, 136.64, 122.84, 122.49, 122.05, 117.89, 114.94, 115.18, 69.96, 59.87, 58.33.

Ligand 8-Teoc : 605 mg (0.25 mmol) ligand 8-OH was dissolved in 10 mL dimethylformamide under stirring. 30 mg (0.54 mmol) potassium hydroxide was added to the solution at room temperature. 1 h later, the mixture was cooled to -20 °C, then 95 mg (0.256 mmol) 2-(trimethylsilyl)ethyl (6-iodohexyl)carbamate was added into the mixture. The reaction was allowed to slowly warm up to room temperature. After 3 h, the reaction was quenched with water. The mixture was extracted with 3x20 mL dichloromethane, and the combined organic phase was washed with 2x20 mL brine, and dried with sodium sulfate. The solvent was removed with rotary evaporator to afford brown oil. The crude product was then purified by silica gel column chromatography with an eluent of ethyl acetate: acetonitrile (5:1). The product is pale yellow solid obtained in 73% yield. ¹H NMR (DMSO, 300 MHz, 25 °C): δ(ppm) 8.47-8.43 (m, 16H), 7.72-7.63 (m, 16H), 7.53-7.47 (m, 16H), 7.23-7.13 (m, 16H), 7.00 (b, 2H), 6.93-6.88 (m, 9H), 6.81 (s, 1H), 6.78 (s, 1H), 5.13-4.99 (m, 12H), 4.05-3.98 (m, 2H), 3.67 (d, 32H), 3.55 (d, 16H), 1.71-1.58 (m, 2H), 1.43-1.20 (m, 8H), 0.94-0.84 (m, 2H), 0.00(s, 9H); ¹³C NMR (CDCl₃, 75MHz, 25°C): δ(ppm) 162.55, 159.75, 159.67, 159.02, 148.99, 140.73, 139.09, 136.42, 122.73, 121.96, 121.88, 118.52, 113.82, 113.11, 69.91, 67.92, 60.10, 58.57, 40.86, 36.49, 30.94, 30.05, 29.19, 26.54, 25.79, 17.80, -1.44;

Ligand 8-NH₂ : 400 mg (0.15 mmol) ligand 8-Teoc was dissolved in 10 mL tetrahydrofuran under stirring. 1.5 mL of 1 M tetrabutylammonium fluoride solution was then added at room temperature. The reaction mixture was then kept at 60 °C overnight. After cooled to room temperature, the solvent was removed in vacuo. The residue was dissolved in dichloromethane, and then washed with 50 mL 0.5 M NaOH solution once and 50 mL saturated NaHCO₃ solution twice. The organic phase was dried with sodium sulfate. The solvent was removed with rotary evaporator to afford brown solid. The yield was 90%. ¹H NMR (DMSO, 300 MHz, 25 °C): δ(ppm) 8.45-8.43 (m, 16H), 7.73-7.58 (m, 16H), 7.56-7.45 (m, 16H), 7.24-7.11 (m, 18H), 7.10-6.97 (m, 10H), 6.93-6.88 (m, 9H), 5.05-4.99 (m, 12H), 3.91-3.84 (m, 2H), 3.67 (b, 32H), 3.55 (b, 16H), 1.64-1.56 (m, 2H), 1.37-1.23 (m, 8H); ¹³C NMR (DMSO, 75MHz, 25°C): δ(ppm) 159.61, 159.29, 158.79, 149.79, 149.26, 140.72, 139.49, 136.95, 122.81, 122.57, 121.69, 114.10, 113.30, 69.48, 59.66, 57.94, 55.39, 41.52, 32.60, 29.05, 26.48, 25.80;

Complex 8-NH₂ (molecule of formula IIIc – hereafter Cplx8):



250 mg (0.1 mmol) ligand 8-NH₂ was dissolved in 10 mL methanol at room temperature under stirring. 30 mg (1 mmol) zinc nitrate hexahydrate was dissolved in 5 mL methanol and was added in to the solution of ligand dropwise. 12 h later, the solvent was removed under vacuum to give the final product as brown powder (yield 100%). ¹H NMR (DMSO, 300 MHz, 25 °C): δ(ppm) 8.45 (b, 16H), 7.67 (b, 16H), 7.51 (b, 16H), 7.20 (b, 18H), 7.07 (b, 9H), 6.90 (b, 10H), 5.05 (b, 12H), 3.90 (b, 2H), 3.67 (b, 32H), 3.56 (b, 16H), 1.58 (b, 2H), 1.25 (b, 8H); ¹³C NMR (DMSO, 75MHz, 25°C): δ(ppm) 159.44, 159.08, 154.85, 148.45, 141.27, 139.20, 134.29, 127.73, 125.32, 125.13, 118.35, 114.09, 69.86, 68.05, 57.42, 56.14, 49.09, 29.27, 26.05, 25.55, 20.34, 19.72.

Example 2: Ligand-PS-enriched microvesicle interaction study by PWR spectroscopy

The detailed setup of PWR and lipid bilayer constitution used herein is described in Calmet, et al., (Sci Rep, 2016. 6: p. 36181).

After the formation of POPC:POPS = 5:1 (w/w) bilayer on the prism surface, a titration experiment is performed for each complex. Briefly, each complex was dissolved in PBS buffer, and then titrated into the Teflon sample chamber. As equilibrium is reached in each addition, the complex concentration and the spectral shifts of s-polarized light (parallel to the membrane surface) was recorded. The titration stopped when addition of complex solution doesn't induce further change in spectral positions. The complex concentration was then plotted against the resonance angle, and the plot was fitted using GraphPad Prism 5. The acquired K_d values are shown in Table 1 hereunder. Figure 1 shows the titration curves for each tested ligand.

Ligand	Cplx1	Cplx2	Cplx4
	1.25×10^{-7}	2.092×10^{-7}	1.771×10^{-7}
K_d (M)	$4 \pm 3.163 \times 10^{-5}$	$5 \pm 9.509 \times 10^{-6}$	$7 \pm 9.617 \times 10^{-8}$; 8.622×10^{-7}

			${}^7 \pm 1.496 \times 10^{-7}$;
			9.346×10^{-7}
			${}^6 \pm 2.565 \times 10^{-6}$;
			1.217×10^{-7}
			${}^6 \pm 3.904 \times 10^{-7}$.
			1.42×10^{-7}
			${}^7 \pm 2.811 \times 10^{-8}$;
			2.282×10^{-7}
			${}^7 \pm 2.811 \times 10^{-8}$;
1.498×10^{-7}	7.232×10^{-7}		3.489×10^{-7}
${}^4 \pm 5.054 \times 10^{-5}$	${}^6 \pm 2.178 \times 10^{-6}$		${}^6 \pm 1.849 \times 10^{-7}$;
			6.056×10^{-7}
			${}^6 \pm 1.208 \times 10^{-6}$.

Table 1 Complex-POPS-POPC membrane interaction dissociation constants

Example 3: Immobilization of ligands on PET film and characterization

- Immobilization of ligands of the invention

10 cm² PET films were first cleaned with ethanol, and then immersed in a hydrolysis solution (20 mL water, 20 mL acetonitrile and 0.2 g NaOH). The hydrolysis was kept at 60 °C for 18 h. The films were cleaned with water, and then immersed in an oxidation solution (38.4 ml fresh milliQ water, 1.6 ml H₂SO₄, 2 g KMnO₄). The oxidation was kept at 60 °C for 1 h. The oxidized film was washed first with 50% HCl once and then water 3 times. The oxidized films were immersed in the activation solution (MES hydrate 390.5 mg/2 mmol, ethylcarbodiimide hydrochloride(EDC) 766.8 mg/4 mmol, N-hydroxysuccinimide(NHS) 230.18 mg/2 mmol), then kept at room temperature for 1h. The films were washed with water. The activated films were subsequently immersed in 20 mL 1 mM solution of complexes in DMSO under room temperature. 24 h later, the films were removed from the solution and washed intensively with water.

- TBO characterization

The functionalization of the PET surface is constantly accompanied by the change of carboxyl group density on the material surface: the hydrolysis of ester bonds and the oxidation of alcohol groups increase the carboxyl density, while EDC/NHS activation and the immobilization of complexes successively decrease the carboxyl density. The absolute amount of the complexes immobilized onto PET surface is difficult to determine using established analytical methods; meanwhile the change of carboxyl group density can be easily determined by toluidine blue-o (TBO) adsorption test. Therefore, the TBO test can provide indirect evaluation of the complex density on PET surface. Briefly, a carboxyl group on material surface was first deprotonated in a basic medium, followed by the adsorption of a TBO cation. Provided that TBO reacts with carboxyl groups with the stoichiometry of 1:1, The surface density of carboxyl groups can be determined by measuring the amount of adsorbed TBO molecules.[192] The adsorbed TBO molecules can be easily washed off with acid, and its concentration in acid can be determined by UV-Vis absorption.

The TBO test is done following reported procedures (Chollet, C., et al., *Biomol Eng*, 2007. 24(5): p. 477-82.):

First, a linear correlation between TBO concentration in 50% AcOH and the solution's absorbance at 633nm (200 μ L solution in each well of a transparent 96 well plate) was established using a series of TBO solutions shown in Tab. 3. In future TBO tests, 5 mL 50% acetic acid would be used to remove the TBO dye adsorbed on 1 cm² squares, and 200 μ L of each solution would also be added into each individual well of a transparent 96 well plate for absorbance test. Thus TBO concentrations in Table 2 can then be further converted into molecule density on PET surface. The plot was then linearly fitted, as shown in Figure 2.

Table 2: TBO solutions used in absorbance calibration

Desired TBO concentration (mM)	TBO solution used for dilution	50% (V/V) acetic acid (μ L)	Total amount
0.5	100 μ L of TBO 5mM	900	1mL
0.1	200 μ L of TBO 5mM	800	1mL
0.05	100 μ L of TBO 0.5mM	900	1mL
0.01	200 μ L of TBO 0.5mM	800	1mL
0.005	100 μ L of TBO 0.05mM	900	1mL
0.001	200 μ L of TBO 0.05mM	800	1mL
0.0005	100 μ L of TBO 0.005mM	900	1mL
0.0001	200 μ L of TBO 0.005mM	800	1mL
0.00005	100 μ L of TBO 0.0005mM	900	1mL
0.00001	200 μ L of TBO 0.0005mM	800	1mL

After acquiring the calibration curve, the TBO test was performed:

A 5×10^{-4} M solution of toluidine blue-o solution was prepared by first dissolving NaOH into milli-Q water until pH 10, then dissolving toluidine blue-o to reach desired concentration. 1 cm by 1 cm PET squares were immersed in 10 mL of the TBO solution and then were kept under shaking in darkness at room temperature. 6 hours later, the supernatant was removed from tube and the stained PET surface was washed with 10 mL NaOH solution (pH 10) once and 2x10 mL pure water. The stained films were then immersed in 5 mL 50% acetic acid to remove the adsorbed TBO dye during 10 min. 200 μ L of the washed solution from each sample was loaded into 96 well plate and the absorption at 633 nm is measured with a 96 well plate reader. The absorbance was then translated to the surface density of carboxyl groups and summarized in Figure 3 using the calibration curve shown in Figure 4. After the activation step, there is a drop of 43.06 pmol/mm² in COOH density, resulting from the substitution of hydrogen in COOH by NHS. A further drop in the COOH density can be observed after the grafting of the complexes onto the surface. This drop can result from 2 events: firstly, there is a reaction of amine and COOH in the presence of complexes, further eliminating the carboxyl groups on PET surface; secondly, when they are grafted on to PET surface, positively charged complexes repel the TBO⁺ ions, preventing them from adsorbing onto PET.

- X-ray photoelectron spectroscopy (XPS)

A VG Scientific ESCALAB photoelectron spectrometer was used for the surface analysis with a non-monochromatized MgK 1253.6 eV source of 100 W. The area of the analytical X-ray spot on the sample surface is about 250 microns. We used a 45 degree insert angle that corresponds to 3-5 nm of analyzed depth. A flood gun was used for charge compensation. Acquisition of high resolution spectra was done at constant pass energy of 20 eV. Fitting was then realized with software provided by VG Scientific, each spectrum being referenced to carbon pollution at 284.8 eV. Binding energies values are given with a precision of ± 0.2 eV.

Table 3: The peak areas after fittings of the high resolution spectra (unit: atomic %)

Name	Oxy.	Act.	Cplx1	Cplx2	Cplx4	Cplx8
Si2p	0.33	0.38	0.53	0.39	0.49	0.63
S2p	0.33	0.33	0.27	0.23	0.23	0.29
Cl2p	0.15	0.11	0	0	0	0
C-C	32.20	26.62	34.18	28.02	31.97	28.25
C-CO	12.36	14.64	15.46	18.06	15.08	23.28

C-O	12.39	14.44	13.73	13.55	14.15	13.69
N-C=O	0.24	1.55	2.29	2.19	1.38	2.85
COO	12.09	11.65	7.33	9.40	8.38	5.32
291.6	1.77	1.34	0.80	0.96	1.31	1.02
N1s 398.0	0	0.27	0.13	0.09	0.23	0.01
N1s 399.9	0	1.77	3.05	2.85	3.42	5.30
N1s 401.9	0	1.05	0.28	0.29	0.28	0.40
O1s 530.7	0	0	1.32	0.33	1.22	0.75
O1s O=C	13.41	14.02	11.63	11.81	11.32	10.37
O1s O-C	14.72	11.84	8.49	11.32	10.06	7.56
Zn2p3	0	0	0.51	0.50	0.50	0.27

The peak areas after fittings of the high resolution spectra were summarized in Tab. 4. The XPS results well correspond to each treatment of PET surface: After hydrolysis and oxidation steps, the ester bonds were hydrolyzed and then oxidized into carboxyl groups; therefore the highest value of COO signal among all the samples is observed. In the activation step, NHS molecules substituted the hydrogen of carboxyl groups. In the process, number of surface carboxyl groups remains the same, while the NHS brings nitrogen onto the surface, leading to a significant increase in the N1s and N-C=O signals and no change in the -COO signal intensity. After the functionalization with complexes, multiple changes in the XPS spectra can be observed. 1st, the emergence of Zn indicates the successful attachment of complexes onto material surface. 2nd, the significant increase in C1s N-C=O/ C1s COO and N1s 399.9/ O1s O=C can be interpreted as the successful replacement of NHS by complexes, further confirming the covalent attachment of the complexes to PET surface. 3rd, comparing the Zn content among the complex grated surfaces, Cplx1 has the most abundance on the surface while the other complexes became more and more difficult to attach to the material surface; meanwhile a comparison of N1s 399.9 signals indicate that Cplx1, Cplx2 and Cplx4 should have almost the same amount on the material surface and Cplx8 had the highest content on material surface. The two conclusions seem to be controversial with each other, but they can be explained if solubility and stability are taken into consideration: Cplx1, Cplx2 and Cplx4 are water soluble therefore the non-covalently attached molecules can be easily washed away in the washing process; Cplx8 on the other hand is insoluble in water, the adsorbed molecules will be much more difficult to remove by water. During the washing, water behaved as a complexing agent and remove the Zn(II) ion from the complex, leaving only the ligand on the surface. This effect can become more prominent with the increase of dendricity, when Zn(II) cations come closer to each other in space and experience more repelling force from each other.

For impurities appear in the XPS spectra, Si is most likely coming from the glass containers where we processed all the PET sheets; S is from the manufacturing of the material as it's concentration is relatively stable throughout the grafting procedures; lastly, Cl in oxidized and activated surface comes from the hydrochloric acid used in surface washing of PET.

Example 4: Microvesicle capture and characterization by using cryo-SEM

- Microvesicle preparation

Microvesicles were collected from mesenchymal stem cells. After 6 passages, TNF α was introduced into the incubation medium at a concentration of 100 ng/ml. After 36 h, the supernatant was collected, and then purified in 3 steps: 1) Removal of cellular debris: Centrifuge the incubation supernatant at 4 °C 1500 g for 15 min, take the supernatant and centrifuge at 4 °C 13000 g for another 2 min. 2) Concentrating microvesicles: Take the supernatant again, centrifuge at 4 °C 20000 g for 90 min and then take the pellet. 3) Wash the microvesicles: Re-disperse the pellet in 500 μ L 1x PBS of 4 °C, centrifuge at 4 °C 20000 g for 90 min. Remove 400 μ L of the supernatant without disturbing the pellet, then add another 400 μ L fresh 1x PBS of 4 °C, re-disperse again, and centrifuge at 4 °C 20000 g for 90 min. Remove 450 μ L of the supernatant without disturbing the pellet, then add 50 μ L 1x PBS of 4 °C to redisperse the pellet. When not being used, the microvesicles were stored at – 80 °C.

- Microvesicle staining

Stock of microvesicles was allowed to warm up to room temperature, and then 950 μ L 1x PBS was used to dilute the suspension. 1 μ L CellMask™ Deep Red Plasma membrane Stain was added into the diluted suspension to stain the microvesicles under room temperature. 15 min later, the stained suspension was centrifuged at 4 °C 20000 g for 90 min. 950 μ L of the supernatant was then removed without disturbing the pellet, and another 950 μ L of fresh PBS was added to redisperse the pellet. The centrifugation-redispersion step was repeated twice so as to remove the free CellMask™ Deep Red molecules from the PBS buffer.

- Microvesicle characterization by fluorescence microscopy

Stained microvesicles were visible under fluorescence microscope (Leica microsystem DM5500B, microscope with a motorized, programmable stage using a CoolSnap HQ camera controlled by Metamorph 7.6). Fluorescent dots of different sizes were observed. Smaller ones should be monodispersed microvesicles, while the dots with larger diameter were suspected to be aggregations of microvesicles. Obviously, morphological studies of microvesicles were impossible to perform as their diameters are usually below the resolution of such instrument.

- Microvesicle characterization using nanoparticle tracking analysis (NTA):

NTA experiment of prepared microvesicles was performed using NanoSight NS300 instrument. The analysis was performed under 22 °C, using 532nm laser beam as light source. The instrument was calibrated using the standard nanoparticle dispersions provided by the manufacturer before test.

For the test, stock of microvesicles was allowed to warm up to room temperature, and then 1x PBS was used to dilute the suspension to 1 mL. The suspension was then vortexed to reach an even distribution of microvesicles inside the dilution.

The NTA experiment was performed by 5 video recordings of 30s of the microvesicle dispersion flowing through the sample chamber at the syringe pump speed of 70 (AU).

The videos were simultaneously analyzed by software NTA 3.2 Dev Build 3.2.16, where the microvesicle concentration and size distribution per frame of picture were recorded.

The concentration of the microvesicles in 5 videos was determined to be $1.87 \times 10^8 \pm 4.69 \times 10^6 \text{ mL}^{-1}$. The uniformity of the microvesicle suspension was proved by small standard deviation in the 5 videos. Multiple subpopulations of particles of different sizes were found in the microvesicle suspension. The mean diameter of the total particles was $139.9 \pm 1.1 \text{ nm}$, which is in good agreement with former published results, while only a small population of 2.45×10^5 was found with the size below 50 nm, which were suspected to be exosomes.

- Microvesicle capture

For all materials, the same procedure was used to capture the microvesicles: The stock microvesicle (stained with CellMask™ Deep Red for FL microscopy and nonstained for Cryo-scanning electron microscopy) dispersion was diluted to 2 mL with 1 × PBS. 250 μL of the dispersion was added onto a functionalized 1 cm² PET square and was incubated under room temperature for 15 min. The PET squares were then washed with milli-Q water to remove any free vesicles adhered to the surface.

- Observation of captured microvesicles using FL microscope

After the capturing process, fluorescence microscopy (Leica microsystem DM5500B, microscope with a motorized, programmable stage using a CoolSnap HQ camera controlled by Metamorph 7.6) of PET sheets was used to evaluate the capture ability of PET functionalized with different complexes.

- Observation of captured microvesicles using Cryo-scanning electron microscopy (Cryo-SEM)

After the capturing process, PET sheets were mounted on freezing stub for the preparation chamber Quorum PP3000T specimen shuttle. The whole was plunged in slush nitrogen paste for cryo-fixation. After quick transfer under vacuum in the preparation chamber the samples were sublimed at -95 °C during 30 min and then coated by platinum sputtering. They were at last transferred in the cryo-SEM Quanta 250 FEG chamber and kept at -140 °C for observation at an accelerating voltage of 10kV.

- Results

Figure 4 – Cplx1

Figure 4 shows how the microvesicles responded to the Cplx1 grafted surface. In FL micrograph (A), a small amount of donut shaped red fluorescent spots can be observed. These structures were of sizes around 1 µm, much larger than the diameter of microvesicles. On the cryo-SEM image (B), the PET surface was blank and of a smooth morphology. No vesicle structures can be observed. Both experiments indicate the PET surfaces functionalized with Cplx1 have very limited ability to capture microvesicles.

Figure 5 – Cplx2

Microvesicle capture using Cplx2 functionalized PET is shown in Figure 5A. The whole material surface was covered with membrane structures, although inhomogeneity was observed throughout the surface. While large areas of the surface were covered with fluorescent membranes, there were also bright dots of microvesicle size in the less fluorescent areas. Very bright membrane aggregations with size over 1 µm and of irregular shapes can also be observed. Figure 5B and C illustrates the surface of the same material observed using cryo-SEM. The majority of the PET surface was found as shown in Fig. 8B. PET was covered by coalesced membrane structures, while at the boundaries of the aggregations, holes in membrane structures and little amount of vesicle attached to PET surface can be observed.

Cplx2 functionalized surface was able to capture microvesicles. When in contact with the functionalized surface, vesicles are prone to fuse with each other into membranes. The fused membranes form web-like structures in less concentrated areas and form large aggregations at highly concentrated places. The interaction between PS and Cplx2 was strong enough to capture the vesicles, but the morphology of the microvesicles was destroyed. Contents within the vesicles were suspected to be lost during the capture process.

Figure 6 – Cplx4

As shown in Figure 6A and B, both FL micrograph and cryo-SEM show the microvesicles uniformly cover the whole surface functionalized with cplx4. After zooming in (Fig. 9C), microvesicles were found individually attached to the material surface, while no obvious fusion of membranes was observed. Cplx4 functionalized surface is also able to capture microvesicles. Due to the minimal intervesicular interactions, both the vesicle morphology and the contents within the microvesicles should be well preserved.

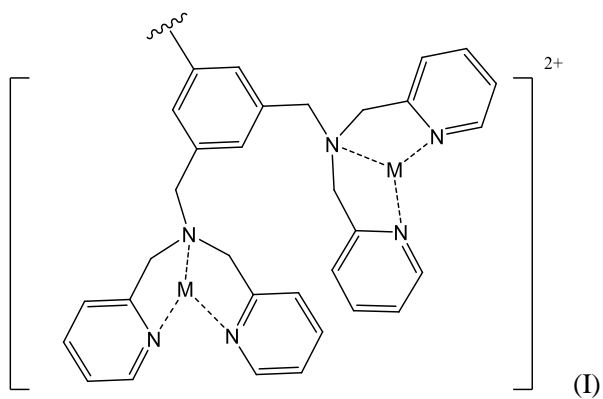
Figure 7 – Cplx8

FL micrograph and cryo-SEM in Fig. 7A and B both show the particles uniformly cover the whole surface functionalized with Cplx8. On the zoomed in cryo-SEM image (C), the particles were found to be of the same size as microvesicles, however irregular in shape.

Both FL micrograph and cryo-SEM confirmed that the cplx8 functionalized surface was able to capture particles in the microvesicle suspension, and the fluorescence clearly indicates that the particles consisted of phospholipids. The zoomed in cryo-SEM also show that the particles were of the same size as microvesicles without the vesicle structure as expected from microvesicles. Individual microvesicles were captured by the surface; however the vesicle membranes were destructed by the capture, leaving only the membrane on the surface, while the vesicle contents were lost.

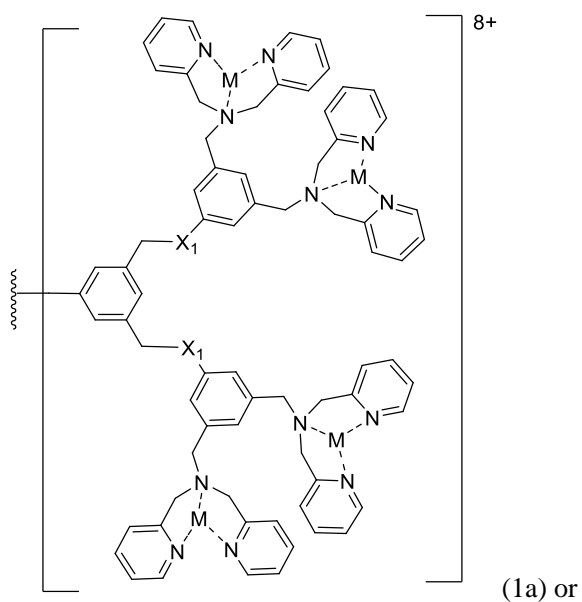
Claims

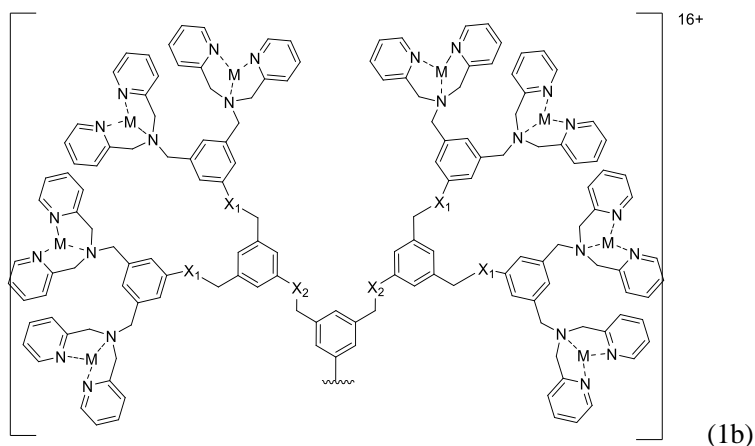
1. A molecule able to bind to microvesicles which comprises at least one, preferably two moieties of formula (I):



Wherein M is a metal cation preferably selected from the group consisting of Zn^{2+} , Mn^{2+} , Co^{2+} , Ni^{2+} , Cu^{2+} and Fe^{2+} .

2. The molecule of claim 1, which comprises a moiety of formula (Ia) and (Ib) as follows:





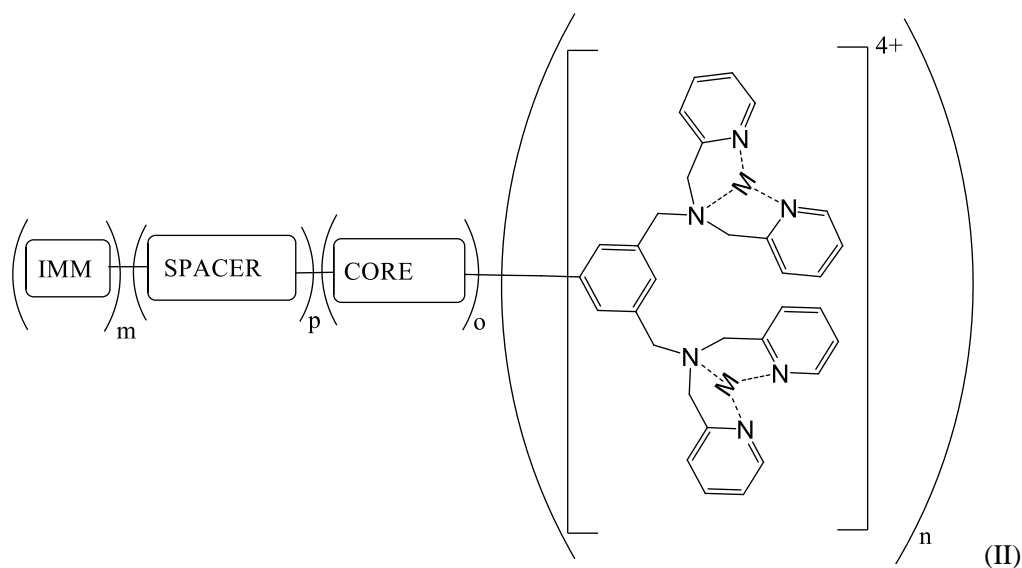
Wherein:

- each X_1 is independently O, S, or NH,
- each X_2 , when present, is independently O, S or NH,
- M is selected from Zn^{2+} , Co^{2+} , Cu^{2+} and Fe^{2+} ., preferably Zn^{2+} .

3. The molecule of any one of claim 1 or 2 which is a dendrimer comprising a branched core bearing a plurality of moieties of formula (I), said branched core preferably comprising a group selected from 3,5-di(hydroxymethyl) phenol, 3,5-di(thiomethyl)phenol, 3,5-di(thiomethyl) thiophenol, 3,5-dialkylphenol, 3,5-di(aminomethyl)phenol, 3,5-dialkylphenol and 3,5-di(aminomethyl) phenylamine as building block, more preferably comprising 3,5-di(hydroxymethyl) phenol as building block.

4. The molecule of any one of claims 1 to 3, which further comprises a mean for immobilization on a support attached at the extremity of a spacer chain.

5. The molecule of claim 1, which is of formula (II).



Wherein:

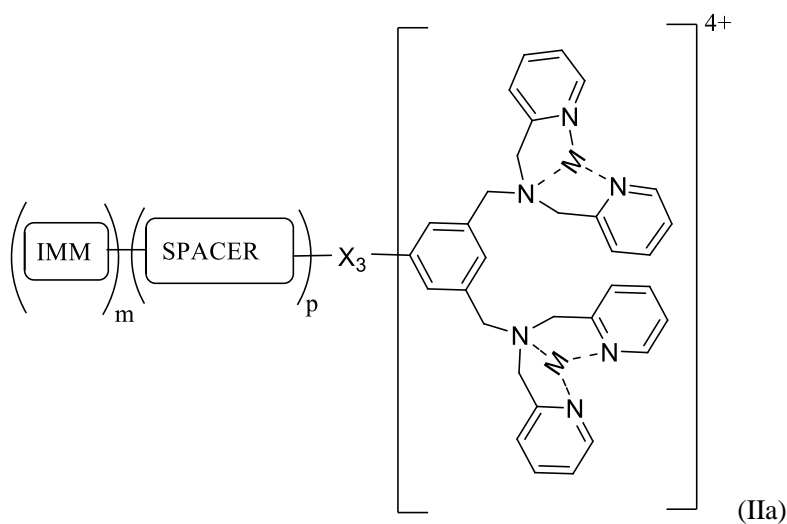
- n is an integer from 1 to 10, preferably from 2 to 6,
- m, p and o are independently 0 or 1,
- M is a divalent metal cation,
- [CORE] is a chemical entity bearing the at least one moiety of formula (I) and having a molecular weight of at most $10\,000\text{ g}\cdot\text{mol}^{-1}$, preferably of at most $5000\text{ g}\cdot\text{mol}^{-1}$
- [IMM] is a mean for covalently or non-covalently immobilization on a support, and
- [SPACER] is selected from the group consisting of a peptide, a polypeptide, an oligo- or polysaccharide, a saturated or unsaturated hydrocarbon chain optionally interrupted by one or several heteroatoms (e.g. S, O or NH), optionally having a heteroatom such as S, O and NH on at least one of its ends, and optionally substituted by one or several substituents such as hydroxyl, halogens, $\text{C}_1\text{-C}_3$ alkoxy, $-\text{CN}$, $-\text{CF}_3$, or $\text{C}_1\text{-C}_3$ alkyl, polymers including homopolymers, copolymers and block polymers, and combinations thereof.

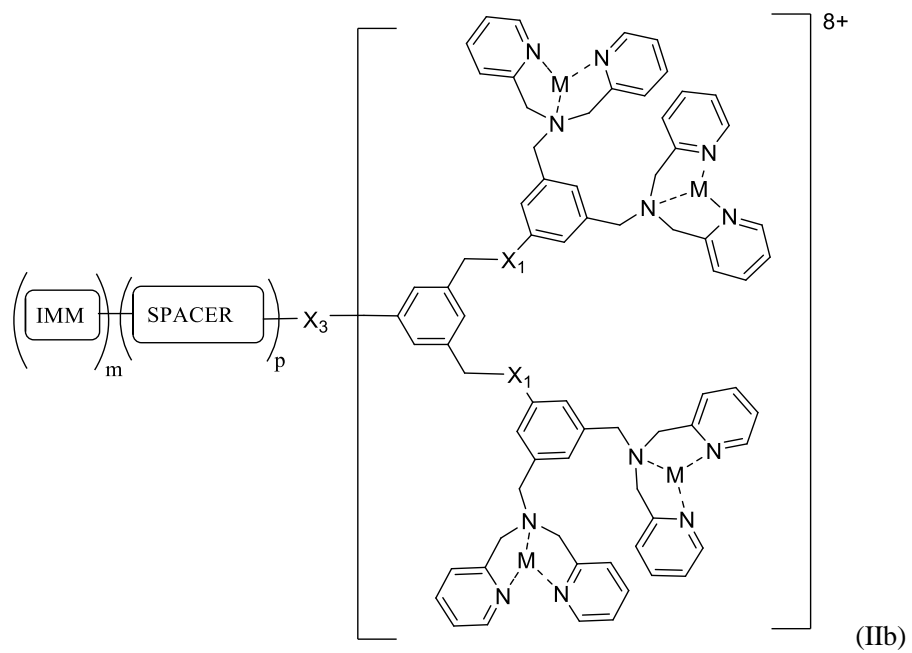
6. The molecule of claim 5, which is further characterized by one, several or all of the following features:

- m, p and o are 1,
- M is selected from Zn^{2+} , Co^{2+} , Cu^{2+} and Fe^{2+} , preferably Zn^{2+} ,
- [SPACER] is selected from :

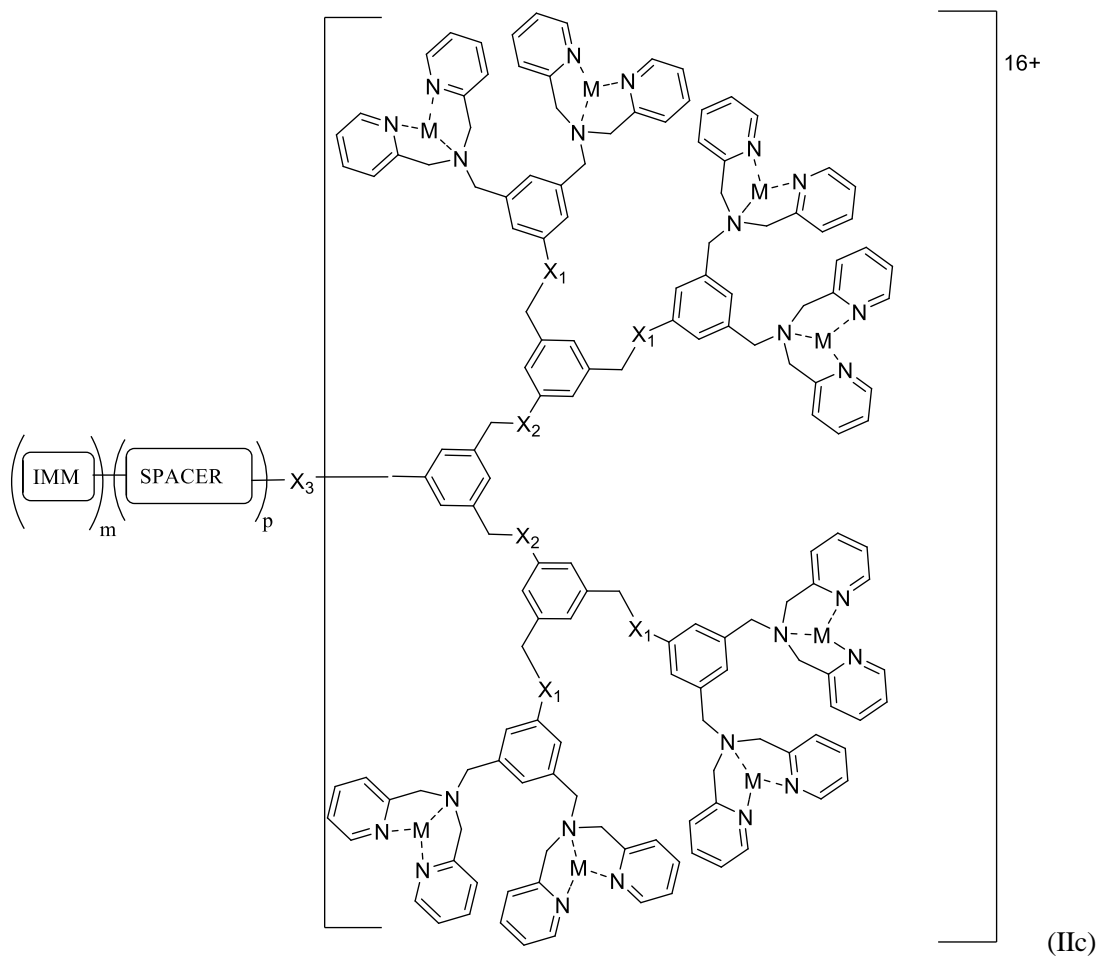
- C₂-C₂₀ saturated or unsaturated hydrocarbon chains optionally substituted, and optionally having an heteroatom such as O, NH and S on at least one of its ends ; polyamide chains comprising from 2 to 20 monomers ; polyester chains comprising from 2 to 10 monomers and polyether chains, such as polyethylene, comprising from 2 to 20 monomers and combinations thereof.
- [IMM] comprises, or consists of, a moiety selected from the group consisting of an amino group, preferably -NH₂, OH, -COOH, an activated carboxylic acid, -SH, iodoacetyl group, a carbonyl, a hydrazide group, an azido, and a strained alkyne and
- [CORE] is a chemical moiety made of at least one 3,5-di(hydroxymethyl) phenol.

7. The molecule of claim 5, which is selected from compounds of formula (IIa), (IIb) and (IIc):





- and



Wherein

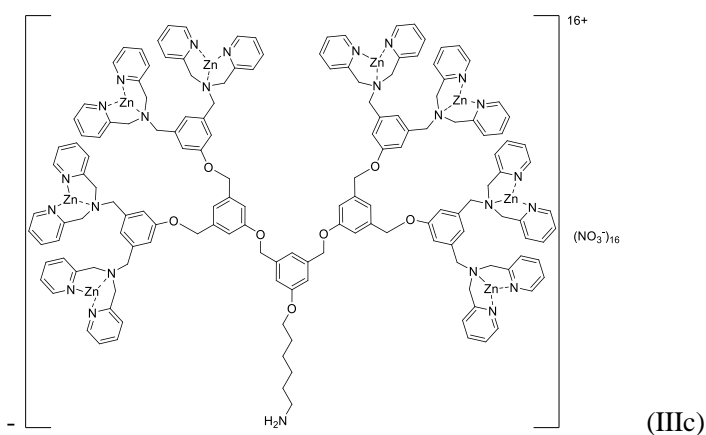
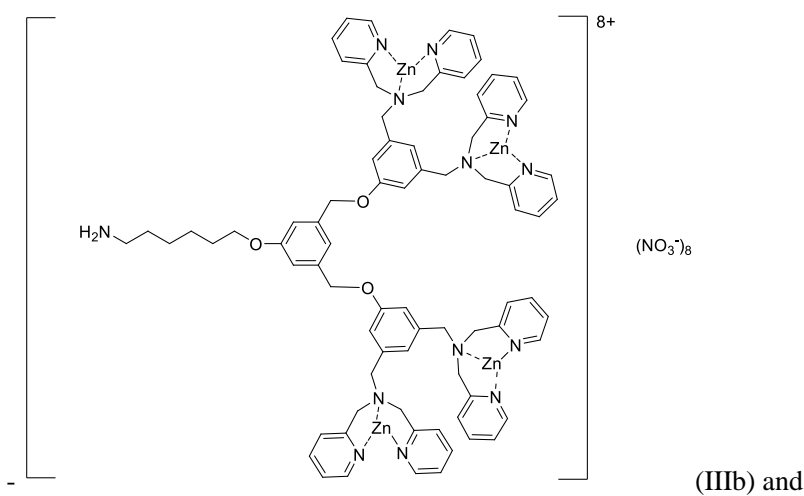
- M, m, p, [IMM] and [SPACER] are as defined above for formula (II),
- each X_1 and X_2 , when present, are selected from the group consisting of O, NH, and S, XXXX.
- X_3 is selected from -O-, C(=O)-OC(O)-, -C(O)O-, -OC(O)O-, -S-, -SS-, -SC(O)-, -OC(S)-, NR_1 -, $-NR_1C(O)$ -, $-C(O)NR_1$ -, $NR_1C(S)$ -, $C(S)NR_1$ -, $-OC(O)S$ -, $-OC(S)O$ -, $-SC(O)O$ -, $-OC(S)S$ -, $-SC(O)S$ -, $-SC(S)O$ -, $-SC(S)S$ -, $OC(O)NR_1$ -, $-OC(S)NR_1$ -, $-NR_1C(S)O$ -, $-NR_1C(O)S$ -, $NR_1C(O)NR_2$ -, $-NR_1C(S)NR_2$ -, $-SC(O)S$ -, $-SC(S)O$ -, $-S(O)$ -, $-S(O)_2$ -, $-P(O)(R_1)$ -, $-P(O)(OR_1)$ -, $P(O)(R_1)O$ -, $OP(O)(OR_1)$ -, $OP(O)(R_1)O$ -, $NR_1P(O)(R_2)$ -, $-NR_1P(O)(OR_2)$ -, $NR_1P(O)(R_2)O$ -, $OP(O)(OR_1)$ -, and $OP(O)(R_1)O$ - wherein R_1 and R_2 are independently H or CH_3 .

8. The molecule of claim 7, wherein:

- m and p are 1,
- M is Zn^{2+} , Co^{2+} , Cu^{2+} or Fe^{2+} , preferably Zn^{2+} .

- X_1 and X_2 , when present, are O,
- X_3 is O, NH, NHCO, CONH, O(C=O), (O=C)O, O(C=O)O, or NHCONH,
- [IMM]-[SPACER] is $\text{NH}_2\text{-(CH}_2\text{)}_r\text{-}$ with r an integer from 2 to 10, and
- Said molecule comprises one or several counter-anions selected from the group consisting of perchlorate, tosylate, nitrate, sulphate, sulphonate, thiosulfate, halide, hexafluorophosphate, tetraphenylborate, carbonate, and tetrafluoroborate.

9. The molecule of claim 1 which is selected from compounds of formula (IIIb) and (IIIc):



10. A support for capturing microvesicles, which comprises a molecule as defined in any one of claims 1-9 on its surface.

11. An *in vitro* method for capturing microvesicles from a sample, which comprises contacting the sample with a ligand as defined in any one of claims 1-9, or with a support as defined in claim 10.

12. The *in vitro* method of claim 11 which further comprises at least one step selecting from:

- a step of providing a sample susceptible to contain the microvesicles of interest from a body fluid of a subject, and/or
- a step of washing the support after the step of contacting the support with the sample, and/or
- a step of detecting the formation of the complex between the microvesicles of interest and said support or molecule of the invention and/or
- a step of recovering the complex formed between the microvesicles and the molecules of the invention, and/or
- a step of quantification of said microvesicles of interest, and/or
- a step of characterization of the captured microvesicles, e.g. by detecting and/or quantifying a biomarker present on the surface or within the microvesicles, and/or
- a step of releasing the microvesicles from the complex, and/or
- a step of recovering the microvesicles of interest.

13. An *in vitro* method for the diagnosis, the differential diagnosis, the prognosis, the assessment of the risk of, and/or the monitoring a disorder in a subject which comprises:

- (b) providing a support as defined in claim 10 or a molecule as defined in any one of claims 1-9,
- (c) contacting said support or said molecule with a sample obtained from the subject, in conditions suitable for the formation of a complex between the molecules of the invention and the microvesicles possibly present in the sample, and
- (d) detecting, quantifying and/or characterizing the microvesicles captured in step (b) by complexation.

14. The *in vitro* method of claim 13 wherein:

- the disorder is selected from the group consisting of diabetes and related disorders such as diabetic nephropathy, diabetic neuropathy, diabetic retinopathy, and diabetic foot syndrome, multiple sclerosis, cancer, Alzheimer's disease, Parkinson's disease, aneurysm, cerebral vasospasm, stroke, and coronary artery disease, and/or
- the sample is, or derives from, blood, blood plasma and urine.

15. Use of a ligand as defined in any one of claims 1-9, or a support as defined in claim 10 as means for capturing microvesicles from a sample of a subject, preferably for the diagnosis, the prognostic or the monitoring of a disease in a subject such cancers, parasitic diseases, as diabetes and related disorders including diabetic nephropathy, diabetic neuropathy, diabetic retinopathy, and diabetic foot syndrome, multiple sclerosis, cancer, Alzheimer's disease, Parkinson's disease, aneurysm, cerebral vasospasm, stroke, and coronary artery disease.

Ligands for capturing microvesicles and Uses thereof

The Invention relates to ligands able to bind to microvesicles, comprising a plurality of metal(II)-dipicolylamine moieties and their use in the diagnosis or prognostic of disorders in a subject.

Chapter 3: Dendron-Functionalized Surface: Efficient Strategy for Enhancing the Capture of Microvesicles (research paper in iScience)

Jian-Qiao Jiang¹²³, Christel Chanseau¹²³, Isabel D. Alves¹²³, Sylvain Nlate^{123*} s.nlate@iecb.u-bordeaux.fr, Marie-Christine Durrieu^{1234**} marie-christine.durrieu@inserm.fr

¹ Université de Bordeaux, Chimie et Biologie des Membranes et Nano-Objets (UMR5248 CBMN), Allée Geoffroy Saint Hilaire - Bât 14, Pessac 33600, France

² CNRS, CBMN UMR5248, Allée Geoffroy Saint Hilaire - Bât 14, Pessac 33600, France

³ Bordeaux INP, CBMN UMR5248, Allée Geoffroy Saint Hilaire - Bât 14, Pessac 33600, France

* *Corresponding author*

** *Corresponding author*

⁴ Lead Contact

Published in iScience, Volume 21, 22 November 2019, Pages 110-123

<https://doi.org/10.1016/j.isci.2019.10.014>

SUMMARY

Microvesicles (MVs) are used by a variety types of cells in human body for intercellular communication, making them biomarkers of great potential for the early and non-evasive diagnosis of a spectrum of diseases. An integrated analysis including morphological, quantitative and compositional studies is most desirable for the clinical application of MV detection; however such integration is limited by the currently available analysis techniques. In this context, exploiting the phosphatidylserine (PS) exposure of microvesicles, we synthesized a series of dendritic molecules with PS binding sites at the periphery. Whereas PS-dendron binding was studied at molecular level using NMR approaches, the PS containing membrane-dendron interaction was investigated in an aqueous environment using plasmon waveguide resonance spectroscopy. As a proof of concept, polyethylene terephthalate (PET) surface was functionalized with the synthetic dendrons, forming devices that can capture MVs in order to facilitate their subsequent analyses.

dendron, microvesicle, microvesicle capture, phosphatidylserine, surface functionalization, phosphatidylserine -dendron interaction, membrane-dendron interaction

INTRODUCTION

In human body, microvesicles (MVs) like other kinds of extracellular vesicles play a pivotal role in both intercellular (adjacent or distant) communication and extracellular environment adaption.[3, 32, 99, 203-205] The biogenesis of MVs is recognized as the budding of cytoplasmic membrane of eukaryotic cells upon activation.[2] Widely adopted as carriers of biomolecules (proteins, mRNA, mi RNA, lipids, etc.) from parent cells to even transkingdom recipients, they are omnipresent in all kinds of bodily fluids.[18, 89, 206-211] In light of such knowledge, for novel diagnostic methods such as liquid biopsy, there are good reasons for MVs to become attractive subjects of study: 1) MV release happens under cellular stress, precluding other

symptoms of a same disease, therefore MVs of certain composition could act as an early biomarker.[87, 212] 2) MV emission happens to a huge variety of cells from stem cells to parasites, making MV analysis useful for a spectrum of disease detection such as cancer, diabetes, virus infection, cardio/cerebrovascular diseases;[4, 99, 206, 213-216] 3) MV membrane composition is dependent on the cytoplasmic membrane composition of its parent cell, making them easier to be traced to the origin even when samples are collected at a distance to the malfunctioning tissue, allowing non-evasive sampling while improving the accuracy of the diagnosis.[87, 214]

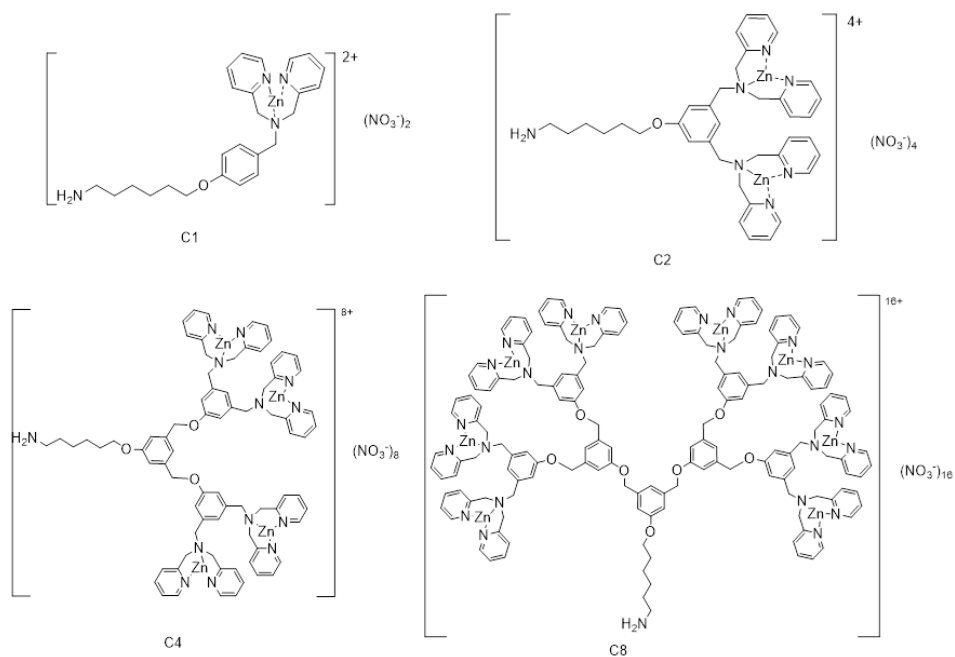
For the application of MV detection in disease diagnosis, the quantity, size distribution and the composition (lipid composition, proteins, RNAs, etc.) of the MVs in a certain sample are desired. Unfortunately, none of the currently available approaches are able to achieve both criteria: Flow cytometry failed to detect 99%-99.9% of the vesicle population due to its optical limitations, while atomic force microscopy and electron microscopy cannot provide any compositional information.[217, 218] Western blotting and qPCR on the other hand are able to give information on protein and RNA composition respectively; however both methods fail to quantify the MVs within a sample.[18, 203, 207, 208, 219]

A proper characterization method for MVs is therefore a combination of the above mentioned methods, where MVs in a sample are prepared in such a manner that electron microscopy, qPCR and western blotting can all be performed easily. For this purpose, we herein propose a device that allows MVs be captured to a device surface, allowing the future analysis.

Phosphatidylserine (PS) is the most abundant negatively charged phospholipid in human cellular membranes.[82] Despite being synthesized intracellularly, its distribution in healthy human cells is mostly limited to the plasma membrane, particularly the inner leaflet by the function of flippases.[78, 81] Its exposure to the extracellular leaflet is often considered as an early sign of programmed cell death, and its presence in MV outer membranes are also well documented.[36, 78, 206, 220, 221] MV capture devices using annexin V have been published since 1997 and have been improved over the years.[217, 222] However this MV capture process depends on Ca^{2+} in the sample milieu by the concentration of millimoles.[221] Such high concentration of Ca^{2+} would become problematic when MV capture is required before removal of

cells within the sample: Ca^{2+} influx is a well-known stimulant for MV generation for a variety of cell types, causing the contamination of MV specimen captured onto the devices.[12, 15] An alternative approach for PS capture is the application of chemosensors, *i.e.* dipicolylamine- Zn^{2+} (DPA-Zn) complexes. First published as a sensor for phosphorylated peptides, DPA-Zn rapidly expanded into a family of chemosensors for the detection of negatively charged phospholipids.[107, 108, 122, 167] The synthetic chemosensors compared against annexin V have the obvious advantages like all chemosensors such as the ease of preparation in large quantity, relatively flexible transportation and storage conditions. Most importantly, the binding of guest molecule to PS no longer requires the Ca^{2+} rich environment. For applications in MV capture, DPA-Zn molecules should be able to covalently conjugate with a supporting material. A strong interaction between DPA-Zn and PS is of course expected for the molecule to bind to MVs.

Herein, we wish to report a series of four dendron-functionalized surfaces with increasing dendricity and their use for the capture of MVs. To build these nanomaterials, and in order to evaluate the dendritic effects on the capture of MVs, we have designed four complexes with one, two, four and eight peripheral DPA-Zn units (scheme 1). For this purpose, our synthetic strategy is based on the dendron core connected to an alkyl spacer with a primary amine for surface functionalization. Multivalent binding of peripheral dendrons to PS containing MVs can be achieved to maximize the binding strength. Besides, it is suggested that spatially close DPA-Zn units have synergetic effect during PS binding.[107, 108] Phenoxy repeating units will provide a structure where DPA-Zn moieties can be kept closer to each other spatially, hopefully achieving such synergy.



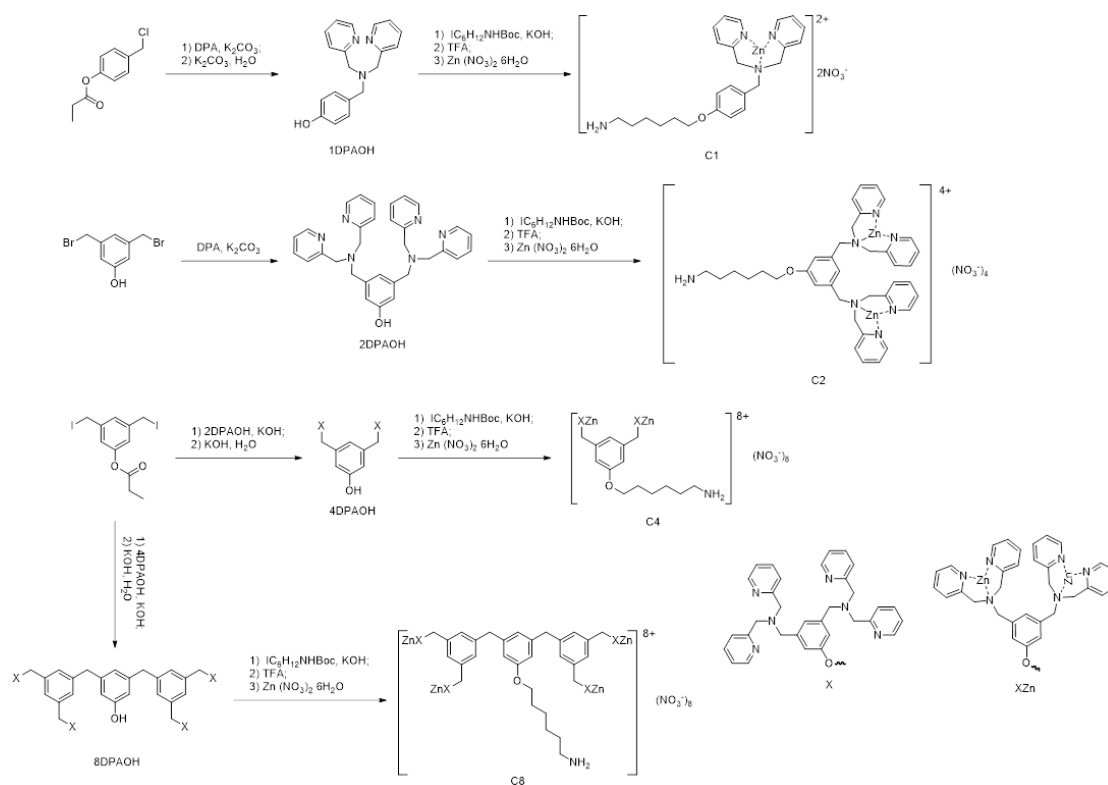
Scheme 1. DPA-Zn molecules with increased dendricity

RESULTS and DISCUSSION

Dendron synthesis

As illustrated in Scheme 2, 1DPAOH and 2DPAOH were synthesized by nucleophilic substitutions of dipicolylamine (DPA) with corresponding benzyl halide (chloride and bromide for 1DPAOH and 2DPAOH respectively) alcohol. These reactions were relatively easy to proceed in the presence of K_2CO_3 . 4DPAOH and 8DPAOH on the other hand, were synthesized using more strict reaction conditions: benzyl iodide was required for its higher reactivity during substitution reactions, while KOH was added to generate phenoxide before the addition of benzyl iodide. To facilitate higher yield in the synthesis of dendritic molecules, reactions were performed at low temperature (around $-20\text{ }^\circ\text{C}$), reducing the possible generation of side products. The convergent synthesis strategy facilitates the separation of starting material and the target compound, since the polarity of molecules increased significantly with the increase of the dendritic structure. This explained the high purity of complex 4. However, the convergent synthesis of **8DPAOH** from the phenol dendron **4DPAOH**, lead to modest yield, probably due to the much steric hindrance during

the reaction, and the high polarity of both compounds that render difficult the separation of compounds **4DPAOH** and **8DPAOH** by column chromatography. The steric hindrance can also be observed during the addition of the hexylamine spacers: for **1DPAOH** and **2DPAOH**, Boc protected spacer can be easily attached with high yields, and removed using trifluoroacetic acid also with high yields. In the case of **4DPAOH** however, Boc protection can't be removed. Thus, Teoc protection had to be used instead because its deprotection only required fluoride ion, a significantly smaller reagent which can easily find its way into the desired reaction site. For **8DPAOH**, the attachment of spacer is much more difficult because of the deeply buried phenol group within the dendritic structure, causing another significant drop in the final yield of C8 synthesis. Full characterization of all new compounds and experimental procedures are given in Supporting Information.



Scheme 2. Synthetic Routes of C1, C2, C4, and C8

For detailed synthesis protocols, please refer to “Transparent Methods in Supplemental Information, where corresponding NMR and mass spectra (Figures S4–S46) are also provided.

NMR investigation of DPA-Zn complex-PS interaction

After acquiring the DPA-Zn complexes of increased dendricity, the zinc complex-PS interactions were first studied in solution. Though proposed in many literatures that PS interacts with DPA-Zn through electrostatic affinity of phosphate anion and Zn^{2+} of the complexes, and published X-ray crystallography structures of DPA-Zn and phosphate complexes always show bondings between Zn^{2+} and phosphate, surprisingly there is no experimental proof for this assumption yet.[118, 122, 126, 223, 224] To address this issue as well as to preliminarily evaluate the binding ability of the complexes to PS, we adopted NMR investigation so that the peak shapes and chemical shifts can be used as evaluation criteria.[223]

^{31}P NMR spectroscopy was used to examine the interaction between complexes and PS in solution, since the chemical environment of phosphorous atom in 1-palmitoyl-2-oleoyl-sn-glycero-3-phospho-L-serine (POPS) will be the most affected should the complexes bind to the phosphate of POPS. Considering the similarity of the binding events (DPA-Zn to POPS), the changes in chemical shift can also roughly represent the strength of such interactions (it is assumed that the observed chemical shift is the mole fraction weighted average of the shifts of the free and DPA-Zn bound POPS).[182] As shown in Figure 1 (A), when 1 equivalent of different complexes is added into 1 equivalent of POPS in solution, the changes of the ^{31}P NMR chemical shifts varies significantly. C1, C2 and C4 make the signal shift to high field while C8 make the signal go to low field. From C1 to C4, with the increase of molecular dendricity, the change in chemical shift also increases, indicating a stronger binding ability with more binding sites. This can be easily interpreted as the result of the increase in DPA-Zn concentration in solution. For instance, even though the molarities of the complexes are the same, C4 brings 4 times the amount of DPA-Zn into the solution compared with C1, pushing the reaction equilibrium further to the formation of (DPA-Zn)-POPS complex. However the difference between different DPA-Zn molecules are not only limited to the increase of DPA-Zn moiety numbers. With the increase in DPA-Zn numbers, one obvious difference is the dendritic scaffolds to which the DPA-Zns are attached. To investigate the effect of the molecular scaffolds, another experiment was performed where the molar ratio of DPA-Zn units to POPS was fixed at 1 to 1. The ^{31}P NMR spectra of the corresponding mixtures are summarized in Figure 1 (B). Again a similar trend in chemical shift

can be observed: the changes in chemical shift increase with the increasing of the number of DPA-Zn units within complexes, in the order of C1, C2 and C4. Whereas the differences in chemical shifts between C1 and C2 complexes bearing a single phenyl ring as a molecular scaffold is less significant C4 on the other hand possessing a dendritic structure shows more significant changes in the ^{31}P NMR chemical shift of POPS. Regardless of molar ratios, C8 behaves quite differently than the other molecules. It's most likely due to the so called negative dendritic effect, in which the dendritic structure acts as a shield of steric hindrance, reducing the binding ability of DPA-Zn. In all cases, the changes are in good agreement with the assumption that DPA-Zn complexes bind to the phosphate groups on POPS, while C4 has the strongest ability to bind to POPS.

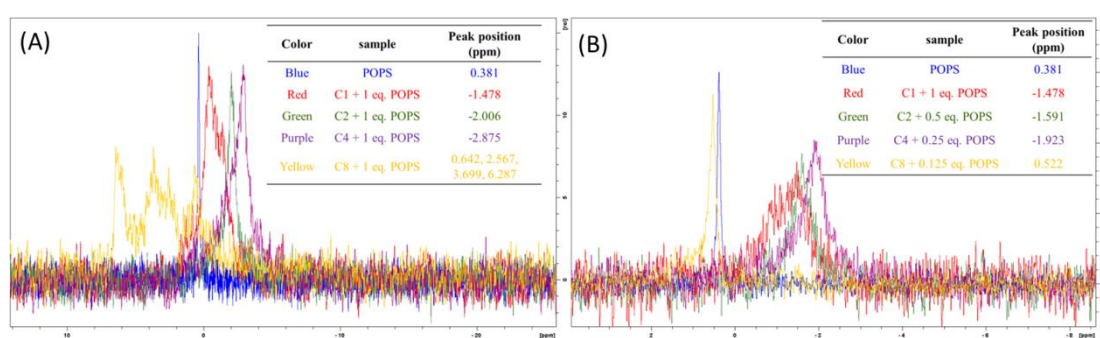


Figure 1. ^{31}P Spectra of Complex-POPS Mixture.

(A): The mixture of complexes and POPS in 1:1 stoichiometry.; (B): The mixture of complexes and POPS with stoichiometry of 1 DPA-Zn unit to 1POPS. Inset tables: mixture compositions.

Although the ^{31}P NMR can provide preliminary information about DPA-Zn complex-POPS interactions such as the interaction site on POPS and the interaction strength, the involvement of other atoms during complex-POPS binding is yet to be determined. For this purpose, ^1H NMR is another useful technique. With the involvement of heteroatoms, nearby protons will experience change in the chemical environment, causing the shift of ^1H NMR signals. However the ^1H NMR of synthesized complexes has too many overlapping regions with POPS, causing the difficulty of spectra interpretation. HSQC on the other hand is able to distinguish different proton signals of similar chemical shifts according to the carbon backbone. It was therefore used to investigate the interaction from the perspectives of both POPS and complexes.

To investigate DPA-Zn binding site on POPS, 1 equivalent of different complexes were added into POPS solution and the HSQC spectra of corresponding mixtures were recorded. Figure 2 shows the part of POPS HSQC NMR spectrum interpretation related to the head group. Looking at the glycerol moiety of the molecule (protons at positions a, c and d), there is an obvious trend that the change in chemical shifts as well as the broadenings also increase with dendricity (in the cases of C1, C2 and C4) for the proton signals. For C8-POPS mixture, there are also shifts in glycerol signals, however these shifts are less prominent compared to C4, again highlighting the negative dendritic effect. Unsurprisingly this is in good agreement with ^{31}P NMR spectra. Both ^{31}P and HSQC indicate the strongest (DPA-Zn)-POPS interaction is achieved with C4. Unfortunately signals of the serine moiety (signals b and e) can't be observed clearly after the complexation; therefore involvement of the serine moiety is still unclear. Considering the change in ^{31}P signal and the change in glycerol signals, the involvement of the phosphate group during complexation can now be confirmed.

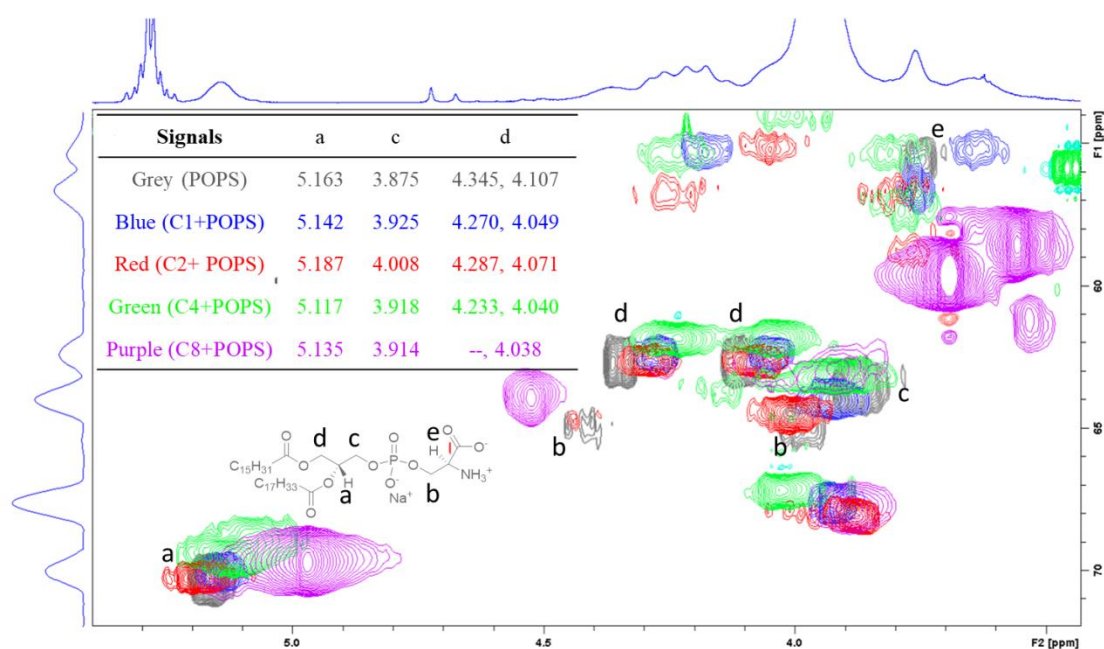


Figure 2. HSQC Spectrum of POPS Head Group.

Pure POPS, gray; C1+POPS, blue; C2+POPS, red; C4+POPS, green; and C4+POPS, purple. Inset table: the chemical shifts of the glycerol proton signals.

In order to understand the difference in DPA-Zn-POPS interaction among the synthesized molecules, study of the complexes before and after POPS binding is also performed. Since only synthesized complexes contain aromatic groups, ^1H NMR can be used directly for investigating the effect of POPS binding to the complexes without the interference of POPS signals. To compare the effect of PS binding on individual DPA-Zn moieties, 1, 0.5, 0.25 and 0.125 equivalents of C1, C2, C4 and C8 was added to POPS solution respectively to acquire corresponding ^1H NMR spectra. For C1, C2 and C4, the pyridine proton signals (Figure 3, peaks a, b, c and d in each spectrum) become broader and the spectrum details are also lost after the binding to POPS. In the 3 complexes, the change in chemical shifts are most prominent for the α protons, which locate closest to the Zn^{2+} ions. This result confirms that the synthesized molecules interact with POPS through the complexed Zn^{2+} ions. Most interestingly, the proton signals of the aromatic of benzyl ether backbone in each molecule (Figure 3, peaks e, f and g) also change significantly after binding to POPS. Considering their electron neutrality, the benzyl ether backbones are unlikely to interact directly with POPS. The chemical shift changes could come from either the change of the electron environment of the backbone after DPA-Zn of each molecule binding to POPS or the conformational change of the entire molecule after POPS binding. Although the mechanism is not clear, the indirect involvement of the benzyl ether backbones in POPS binding is confirmed. The differences of the ^{31}P NMR spectra in Figure 1(B) for C1, C2 and C4 could be explained by the involvement of benzyl ether backbones in POPS binding, while C4 with the dendritic structure has the strongest positive influence on the change of POPS ^{31}P chemical shift. Unlike the positive dendritic effect shown with C4, C8 with even higher dendricity showed little spectral change after the addition of POPS, again indicating a negative dendritic effect during POPS binding.

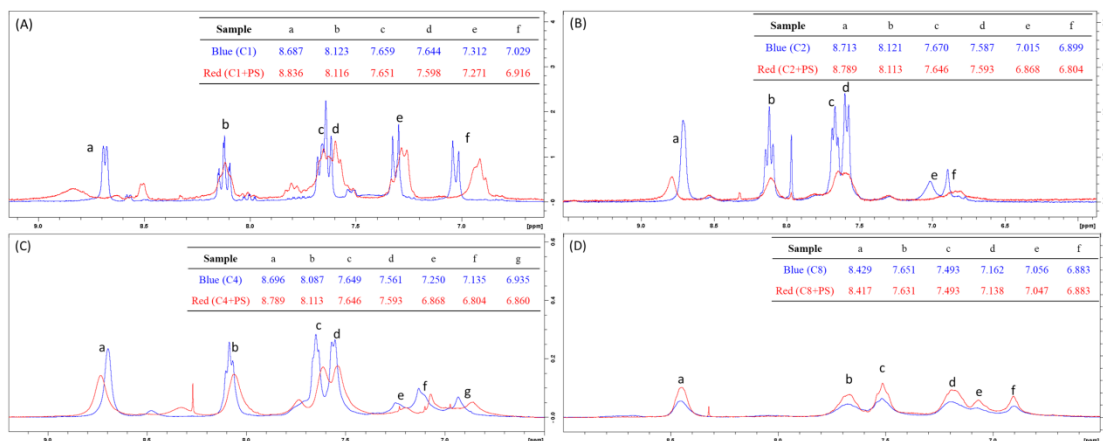


Figure 3. ^1H Spectra of Complex Aromatic Groups.

(A–D) C1 (A), C2 (B), C4 (C), and C8 (D). Inset table: the chemical shifts of proton signals.

Plasmon waveguide resonance study of DPA-Zn complex-model membrane interaction

While solution NMR provides information on the molecular interactions between POPS and zinc complexes, PS in biological systems are not solubilized and can only be found on lipid membranes. The goal of the complex design is therefore the improved interaction strength of synthesized molecules to PS containing biological membranes. To evaluate the interaction strength between POPS containing membranes and synthesized DPA-Zn complexes, a homemade plasmon waveguide resonance (PWR) spectrometer was adopted. The detailed setup of PWR and lipid bilayer constitution used herein is described elsewhere.[225, 226] A PWR spectrometer has the setup quite similar to that of a SPR spectrometer with one important difference: the plasmon generating metallic thin film (~50 nm silver) is coated with another dielectric layer (~460 nm silica) as waveguide.[183, 186] The metallic layer itself is only able to generate plasmon resonance upon the excitation of linearly polarized light that has the oscillation direction perpendicular to the metallic surface (p-polarized light), whereas the waveguide layer can generate waveguide resonance with light of both perpendicular and parallel (s-polarized light)

polarizations.[183, 227] Once adhered to the silica surface, the optical properties of lipid membrane can be probed at both perpendicular and parallel directions using p- and s- polarized light respectively. When DPA-Zn complex is interacting with such lipid membrane, the changes in s- and p-polarization signals are able to yield information on the change of membrane mass as well as anisotropy.[189, 227] Using a titration experiment, the peak positions of s- and p-polarized light can be fitted to acquire K_d values of such interactions.[188] After the formation of POPC(1-palmitoyl-2-oleoyl-sn-glycero-3-phosphocholine):POPS = 5:1 (w/w) bilayer on the prism surface, a titration experiment is performed for each complex. Briefly, each complex was dissolved in HEPES buffer, and then titrated into the Teflon sample chamber. As equilibrium was reached in each addition, the complex concentration, the spectral shifts of s-polarized light (parallel to the membrane surface) , and the spectral shifts of p-polarized light (perpendicular to the membrane surface) were recorded. The titration stopped when addition of complex solution didn't induce further change in spectral positions. The complex concentration was then plotted against the resonance angle, and the plot was fitted using GraphPad Prism 5 (Figure 4). The acquired K_d values were recorded in Table 1.

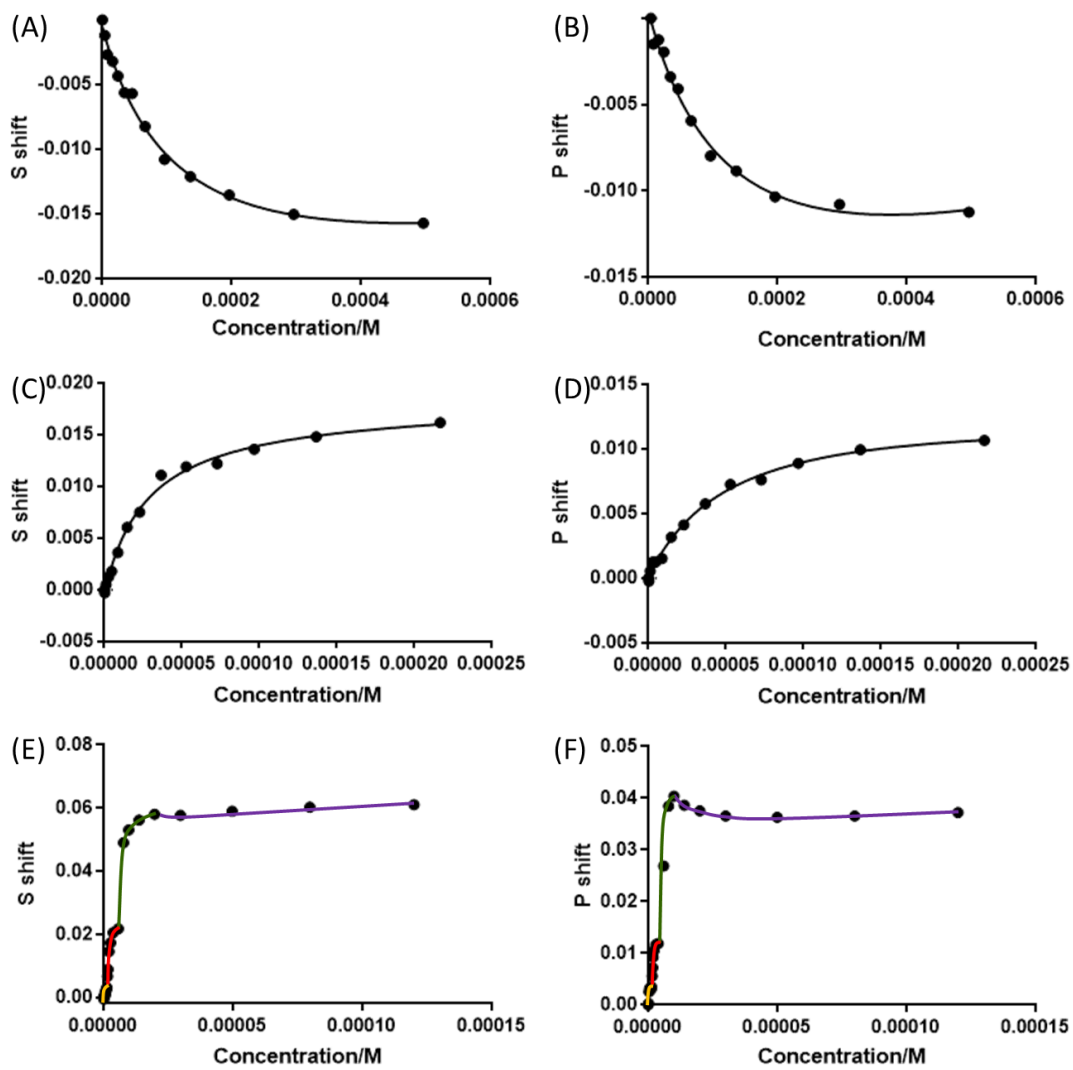


Figure 4. Fittings of Complex-PSPC Membrane Titrations.

(A–F) (A and B) Fitting of C1-PSPC membrane titration in s- and p-polarizations, respectively; (C and D) fitting of C2-PSPC membrane titration in s- and p-polarizations, respectively; (E and F) fitting of C4-PSPC membrane titration in s- and p-polarizations, respectively.

Table 1. Complex-Membrane Interaction Dissociation Constants (Kds) Acquired Using PWR

Complex	C1	C2	C4	
K _d (M)	s	1.25×10 ⁻⁴ ±3.163×10 ⁻⁵	2.092×10 ⁻⁵ ±9.509×10 ⁻⁶	1.771×10 ⁻⁷ ±9.617×10 ⁻⁸
				8.622×10 ⁻⁷ ±1.496×10 ⁻⁷
				9.346×10 ⁻⁶ ±2.565×10 ⁻⁶
	p	1.498×10 ⁻⁴ ±5.054×10 ⁻⁵	7.232×10 ⁻⁶ ±2.178×10 ⁻⁶	1.217×10 ⁻⁶ ±3.904×10 ⁻⁷
				1.42×10 ⁻⁷ ±2.811×10 ⁻⁸
				2.282×10 ⁻⁷ ±2.811×10 ⁻⁸
			3.489×10 ⁻⁶ ±1.849×10 ⁻⁷	
			6.056×10 ⁻⁶ ±1.208×10 ⁻⁶	

s, K_d values acquired using s-polarized light; p, K_d values acquired using p-polarized light.

In the PWR titration experiment, binding events can be monitored by following the changes in both p- and s- spectra for each incremental addition of the complex. As explained by Salamon and Tollin, the resonance angle change in either polarization linearly correlates to the mass density (mass per unit area) changes on the adsorbed lipid membrane.[227] Two different scenarios can generally occur: 1) complex binding to the membrane leads to an hyperbolic increase in the resonance shift upon complex addition; 2) complex binding results in a shift decrease. The first case scenario is the most common for molecules that bind and accumulate in the membrane surface without much change in the membrane organization. Therefore, increasing accumulation of the molecule at the membrane level leads to a hyperbolic response with saturation being reached. The data can be fitted to obtain a binding affinity. The second scenario can also be observed and reflects an impact of the interacting molecule in the lipid membrane organization. Indeed, such decrease in the resonance shifts can only be explained by mass removal from the system as a result of a “detergent” type effect of the molecule on the membrane. A binding affinity

can also be obtained in this case. To note that it is an apparent binding affinity that reflects both the binding of the molecule investigate and accompanying lipid reorganization. The complexes show very different binding behaviors between each other. The resonance angles of both p- and s-polarized light experienced continuous decreases upon the addition of C1, and the decreases stabilized at about 11 mdeg and 15 mdeg respectively for p- and s- polarization. The final equilibrium was only reached when the concentration of C1 in the chamber reached submillimolar level, and the interaction K_d s determined by the fitting of the titration curves were at 10^{-4} M for both polarizations. When C2 was titrated to a membrane of same constitution until equilibrium, increasing spectral shifts of same scale happened for both polarizations. The K_d values were determined to be around 10^{-5} M, indicating a stronger complex-membrane interaction. In the case of C4, the titration curves indicated a 4-stage reaction with the increase of complex concentration. The first 3 stages showed consecutive increases, with two K_d values as low as 10^{-7} M and the 3rd at 10^{-6} M. The last stage showed decreasing resonance angles of both polarities with K_d values also at 10^{-6} M level. The p- and s-polarized resonance stabilized at 60 and 37 mdeg respectively, a shift more significant than either C1 or C2.

Fabrication and characterization of the MV capture devices

The MV capture devices were then prepared by functionalizing polyethylene terephthalate (PET) sheets using the synthesized DPA-Zn complexes. The purchased PET sheets were chemically treated using similar procedures reported previously with minor adaptations as shown in Figure 5.[190, 191] Briefly, the PET sheets were hydrolyzed and then oxidized to produce abundant carboxyl groups onto the surfaces. The carboxyl groups were activated using EDC (N-(3-Dimethylaminopropyl)-N'-ethylcarbodiimide hydrochloride)/NHS (N-Hydroxysuccinimide) thereafter to assist the amide bond formation so that the complexes with amine ending spacers can be attached to the PET surfaces covalently. For each step of the surface functionalization, the carboxyl group surface density was monitored with Toluidine Blue O (TBO) test while the atomic percentage of the material surface was followed by X-ray photoelectron spectroscopy (XPS).

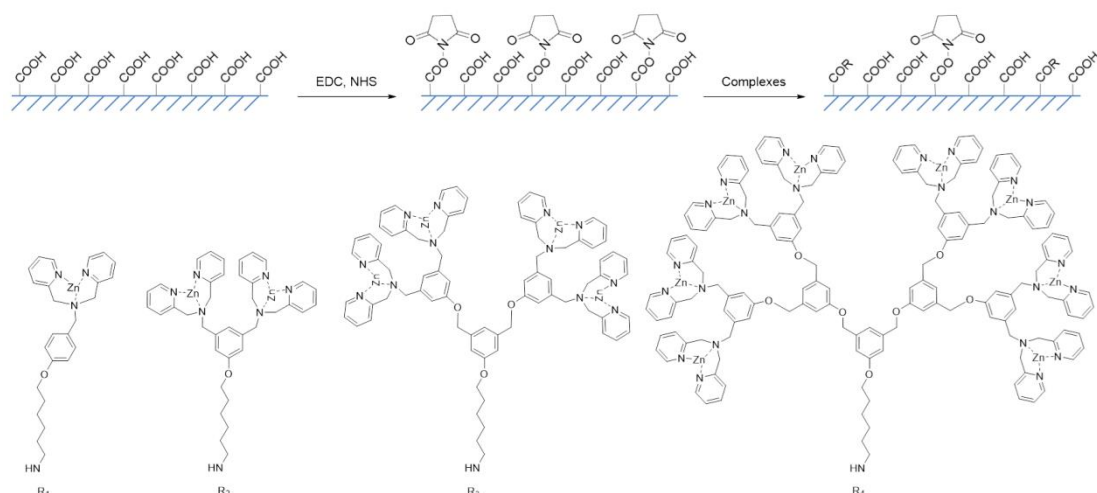


Figure 5. Surface Functionalization of PET Sheets Using Synthesized Complexes

As shown in Figure 6, the oxidized surface has the highest carboxyl group density. After the activation step, there is a drop of 43.06 pmol/mm^2 in COOH density, resulting from the substitution of hydrogen in COOH by NHS. A further drop in the COOH density can be observed after the grafting of the complexes onto the surface. This drop can result from 2 events: firstly, there is a reaction of amine and COOH in the presence of complexes, further eliminating the carboxyl groups on PET surface; secondly, when grafted on to PET surface, positively charged complexes repel the TBO^+ ions, preventing them from adsorbing onto PET.

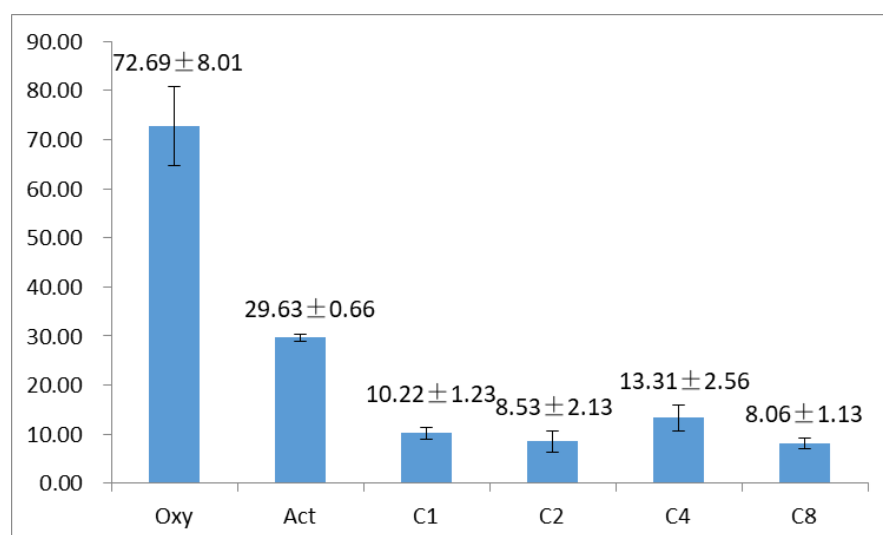


Figure 6. Carboxyl Group Density on Treated PET Surfaces

Oxy., oxidized PET; Act., NHS-activated PET; C1, C1 functionalized PET; C2, C2 functionalized PET; C4, C4 functionalized PET; C8, C8functionalized PET. Unit, pmol/mm². See also *Figure S1* and *Table S1*.

The peak areas after fittings of the high resolution XPS spectra were summarized in Table 2. The XPS results well correspond to each treatment of PET surface: After hydrolysis and oxidation steps, the ester bonds were hydrolyzed and then oxidized into carboxyl groups; therefore the highest value of COO signal among all the samples is observed. In the activation step, NHS molecules substituted the hydrogen of carboxyl groups. In the process, number of surface carboxyl groups remains the same, while the NHS brings nitrogen onto the surface, leading to significant increases in the N1s and N-C=O signals without change in the -COO signal intensity. After the functionalization with complexes, multiple changes in the XPS spectra can be observed. 1st, the emergence of Zn indicates the successful attachment of complexes onto material surface. 2nd, the significant increase in (C1s N-C=O)/(C1s COO) and (N1s 399.9)/(O1s O=C) can be interpreted as the successful replacement of NHS by complexes, further confirming the covalent attachment of the complexes to PET surface. 3rd, as shown in Table 3, molecular percentage(MP) of the complexes (which is calculated by dividing the atomic percentage of an atom by the number of the same atom within a single molecule) calculated according to Zn2p3 and N1s all indicate an increasing difficulty for larger molecules attaching to the PET surface. The MP calculated with N1s is always higher than that calculated with Zn2p3, which could come from two facts: one is that there is NHS residue left on the surface because of incomplete substitution by the complexes; the other is that during the intensive washing process, water behaved as a complexing agent and washed away the Zn(II) ion from the complex, while the ligands being covalently attached and insoluble in water, remained on the PET surface. This effect can become more prominent with the increase of dendricity, as shown in MP_{Zn}/MP_N in Table 3. Zn(II) cations are forced closer to each other in space with the increase of dendricity, experiencing more repelling force from each other, hence easier to come off.

Table 2. XPS-Determined Atomic Percentages of PET Surfaces

Name	Oxy.	Act.	C1	C2	C4	C8
Si2p	0.33	0.38	0.53	0.39	0.49	0.63
S2p	0.33	0.33	0.27	0.23	0.23	0.29

Cl2p	0.15	0.11	0	0	0	0
C-C	32.20	26.62	34.18	28.02	31.97	28.25
C-CO	12.36	14.64	15.46	18.06	15.08	23.28
C-O	12.39	14.44	13.73	13.55	14.15	13.69
N-C=O	0.24	1.55	2.29	2.19	1.38	2.85
COO	12.09	11.65	7.33	9.40	8.38	5.32
291.6	1.77	1.34	0.80	0.96	1.31	1.02
N1s 398.0	0	0.27	0.13	0.09	0.23	0.01
N1s 399.9	0	1.77	3.05	2.85	3.42	5.30
N1s 401.9	0	1.05	0.28	0.29	0.28	0.40
O1s 530.7	0	0	1.32	0.33	1.22	0.75
O1s O=C	13.41	14.02	11.63	11.81	11.32	10.37
O1s O-C	14.72	11.84	8.49	11.32	10.06	7.56
Zn2p3	0	0	0.51	0.50	0.50	0.27

Oxy., oxidized PET; Act., NHS-activated PET; C1, C1 functionalized PET; C2, C2 functionalized PET; C4, C4 functionalized PET; C8, C8 functionalized PET.

Table 3. XPS-Determined Molecular Percentages

surfaces	C1	C2	C4	C8
MP _{Zn}	0.51	0.25	0.13	0.034
MP _N	0.92	0.47	0.32	0.216
MP _{Zn} /MP _N	0.55	0.53	0.40	0.16

MP = AP/n, where MP is molecular percentage, AP is atomic percentage, and n is the theoretical number of the corresponding atom per molecule.

C1, C1 functionalized PET; C2, C2 functionalized PET; C4, C4 functionalized PET; C8, C8 functionalized PET.

Unfortunately exact molecular densities of all the complexes grafted to PET surface are yet to be determined. To the best of our knowledge, there is no technique available for such measurement. We tried to come up with an approximate value using the combination of the TBO measurement as a qualitative approach and the XPS as a semi-quantitative approach. TBO test indicated the carboxyl group densities. For the activation step, it was able to quantify the NHS groups fixed onto PET surface through the decrease of carboxyl group density, however it failed to quantify the substitution of NHS by the complexes in the next substitution step. The further decreases in carboxyl group densities were suggestive for the substitution reaction, but it no longer serve as a quantitative measurement for the reaction. The MP of a grafted complex calculated

from the XPS results is quantitative, however as it measures the total amount of atoms with a penetration about 10 nm into the bulk material, such percentage is still unable to transfer directly into molecular density at the surface of the material. Despite the above mentioned disadvantages, TBO was able to suggest that all the synthesized complexes exhibit similar degree of carboxyl group “blocking” ability, while the XPS MPs of all complexes grafted onto PET surface suggest different complexes bind to PET surface with a same order of magnitude.

For impurities appeared in the XPS spectra, Si is most likely coming from the glass containers in which we processed all the PET sheets; S is from the manufacturing of the material as its concentration is relatively stable throughout the grafting procedures; lastly, Cl in oxidized and activated surface comes from the hydrochloric acid used in the surface washing of PET.

The performances of the MV capture devices

The crucial parameters for vesicles being adsorbed on material surface in solution are the chemical composition of the substrate, temperature, and the osmotic pressure difference between the inside and the outside of the vesicles.[198, 200, 226] In our case, to compare the complexes functionalized surfaces for their MV capture abilities, the most important parameter is the surface chemical environment. Since the surface densities of complexes fixed onto PET are of the same magnitude for all 4 complexes, the MV capture abilities of functionalized surfaces can therefore be compared using the above mentioned PET sheets. Cryo-SEM and fluorescence (FL) micrograph of each surface after incubation with mesenchymal stem cell generated MVs were used to visualize the comparison (For the FL imaging of MVs, CellMask™ Deep Red was used to stain the MVs beforehand).

Figure 7 (A and B) shows how the MVs responded to the C1 grafted surface. In FL micrograph, only a small amount of donut shaped red fluorescent spots can be observed. These structures were of sizes around 1 μm , much larger than the diameter of MVs. Considering the size distribution of the MVs acquired by nanoparticle tracking analysis (supplemental information figure 2), such phenomenon can only result from the aggregation of MVs. On the cryo-SEM

image, the PET surface was blank and of a smooth morphology. No vesicle structure can be observed. MV capture using C2 functionalized PET is shown in Figure 7 (C and D). The whole material surface was covered with membrane structures, though inhomogeneity was observed throughout the surface. In FL micrograph, while large areas of the surface were covered with fluorescent membranes, there were also bright dots of MV size in the less fluorescent regions. Very bright membrane aggregations with size over 1 μm and of irregular shapes can also be observed. Observation using cryo-SEM also reveal that the majority of the PET surface was covered by coalesced membrane structures, while at the boundaries of such aggregations, holes in the membrane and a small amount of vesicles attached to PET surface can be observed as well. As shown in Figure 7. (E and F), both FL micrograph and cryo-SEM show the MVs uniformly cover the whole surface functionalized with C4. MVs were found individually attached to the material surface, there are indeed some aggregations of MVs, however such aggregation does not cause the fusion of MVs, leaving intact vesicles/vesicle aggregations captured onto the PET surface. FL micrograph and cryo-SEM in Figure 7 (G and H) both show particles uniformly cover the whole surface functionalized with C8. On the zoomed cryo-SEM image (h), the particles were found to be of the same size as MVs, however these structures resemble to rough membrane flakes rather than smooth vesicles.

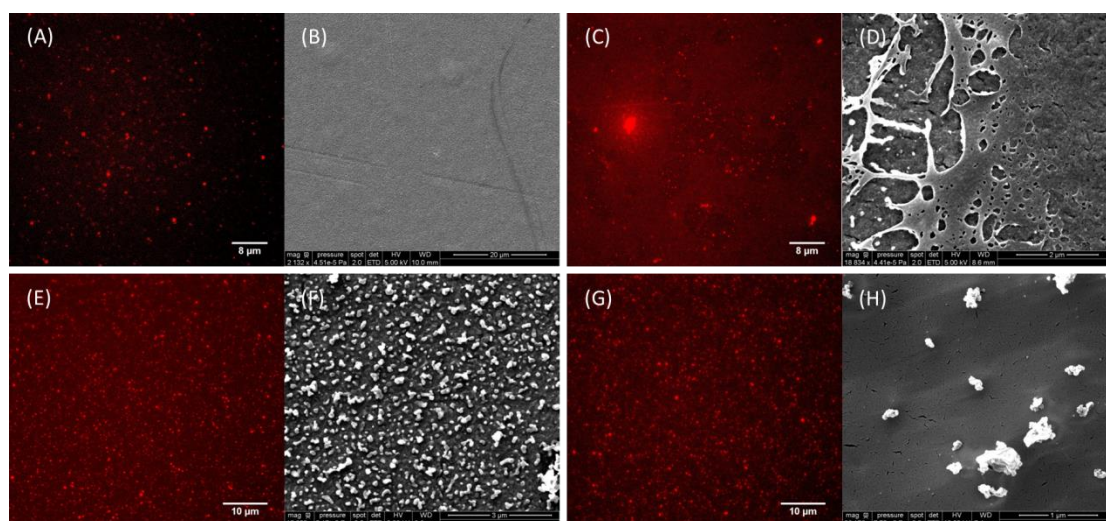


Figure 7. Micrographs of Functionalized Surfaces after 15 min of MV Incubation

(A) Fluorescence micrograph of C1 functionalized surface incubated with CellMask Deep Red-stained microvesicles; scale bar, 8 μm .

(B) Cryo-SEM image of C1 functionalized surface incubated with microvesicles; scale bar, 20 μm .

(C) Fluorescence micrograph of C2 functionalized surface incubated with CellMask Deep Red-stained microvesicles; scale bar, 8 μm .

(D) Cryo-SEM image of C2 functionalized surface incubated with microvesicles; scale bar, 2 μm .

(E) Fluorescence micrograph of C4 functionalized surface incubated with CellMask Deep Red-stained microvesicles; scale bar, 10 μm .

(F) Cryo-SEM image of C4 functionalized surface incubated with microvesicles; scale bar, 3 μm .

(G) Fluorescence micrograph of C8 functionalized surface incubated with CellMask Deep Red-stained microvesicles; scale bar, 10 μm .

(H) Cryo-SEM image of C8 functionalized surface incubated with microvesicles; scale bar, 1 μm .

See also *Figure S2* and *S3*.

Micrographs indicate the PET surfaces functionalized with C1 have very limited ability to capture MVs. This result correlates well with the PWR and NMR experiment results indicating that C1 has less ability to bind to PS. In comparison, C2, C4 and C8 functionalized surfaces were able to capture MVs due to the higher PS binding abilities, though MVs behave differently when in contact with the 3 surfaces. When captured by C2 functionalized surface, vesicles are prone to rupture and then fuse with each other into membranes. Because of the destructed morphology of the MVs, their contents were suspected to be lost during the capture process, making C2 surfaces less favorable for the future applications for the examination of the vesicle contents. A similar conclusion can be drawn for C8 functionalized surface as it also caused the rupture of MVs. So far, C4 functionalized surface seems to be the best candidate for MV capture since vesicle morphology and their contents are well preserved. A possible explanation for such differences can be attributed to the dendritic backbones of the three molecules: The morphology of the membrane on C2 functionalized surface is highly reminiscent of so called "supported lipid bilayers", where the vesicles (synthetic or naturally existing in biological systems) adhere to a hydrophilic substrate (such as silicon, glass or silica) and form a bilayer via vesicle fusion.[198, 200] Such fusion is

considered to be a process related to the chemical properties and most importantly the hydrophilicity of the surface in contact.[199] C2 being the simplest of the three, its DPA-Zn moiety has the largest exposure to the aqueous environment with the highest density on PET surface yet with limited molecular flexibility. After C2 functionalization of PET, C2-PS interaction invites the vesicle adhesion to the PET surface, while the hydrophilic nature of C2 and the stiffness of PET substrate induce the vesicle to rupture, lie flat onto the surface and fuse with each other into a larger membrane. Compared with C2, C4 is a relatively flexible molecule: As shown in Figure 3 C, when binding to PS, the aromatic signals of the benzyl ether backbone also experience significant chemical shift, indicating the conformational change of C4 when binding to PS. Besides, C4 is a less hydrophilic molecule than C2, thus vesicle rupture is less likely to happen on the C4 functionalized surface. High generation cationic dendrimers such as poly(amidoamine) (PAMAM) is known to cause membrane destruction. Mecke et al. found that PAMAM of generation 3 (G3) doesn't induce 1,2-dimyristoyl-sn-glycero-3-phosphocholine (DMPC) membrane destruction, while G5 and G7 PAMAMs are able to destroy lipid bilayer by removing lipid from membrane.[171, 172] Through computer simulation, Wang et al. discovered that PAMAMs of lower generations have more flexible structures.[174] When in contact with DMPC membranes, the smaller PAMAMs are able to adjust its conformation and cause little disruption of DMPC bilayer. In contrast, the higher generation dendrimers' conformations are limited by their interbranch steric hindrance, thus at the dendrimer-lipid bilayer interface, DMPC membranes are forced to adopt the curvature of individual dendrimer molecules, causing possible membrane destruction. Similarly among our DPA-Zn complexes, C8 is the dendron of highest generation and thus the highest conformation rigidity. When in contact with C8 functionalized surface, MVs are prone to destruction.

In conclusion, we have synthesized a series of multivalent DPA-Zn complexes with increasing dendricity. In ^{31}P NMR studies of complex-POPS interactions, dendritic C4 showed strongest POPS binding ability. This result is in good agreement with the fittings of PWR titrations where the complex-membrane (POPS containing) interaction K_d values were determined. C1 being the complex with only 1 DPA-Zn unit, has the K_d values of 10^{-4} M, C2 of similar molecular scaffold but with 2 DPA-Zn units showed K_d values of 10^{-5} M. C4 on the other hand, with 4 DPA-Zn units attached to a dendritic scaffold, showed a 4-stage binding process in the titration experiment, with K_d values as low as 10^{-7} M. Such improvement in binding strength is

beyond the simple multivalent binding effect. To understand the exponential increase of complex-membrane interaction with the increase of DPA-Zn units, we performed HSQC and ^1H NMR experiments to investigate the interaction at molecular level. The HSQC experiments indicated the complexes bind to the phosphate group of POPS, while the ^1H NMR spectra reveals the DPA-Zn involvement in the POPS binding process as hypothesized in many literatures. The ^1H chemical shifts of the benzyl ether scaffold where DPA-Zn units attached also showed significant changes after POPS binding, indicating the scaffolds are also involved in the binding processes. In the case of C2, the two DPA-Zn units showed synergetic binding to the POPS molecules, and C4 with a dendritic structure further enhanced such effect by conformational change upon PS binding. Unfortunately the enhancement effect cannot be applied to molecules of higher dendricity of the same repeating units. C8 of 8 DPA-Zn units is proven difficult to synthesize, while its PS binding performance is no better than any smaller DPA-Zn complexes according to ^{31}P NMR. All the synthesized DPA-Zn complexes were able to be attached to the model PET surface covalently with an amino hexane spacer to form a device for MV capture, while the binding molecular densities on PET surfaces were semi-quantitatively determined with TBO and XPS experiments. The molecular percentages were found to be at the same order of magnitude for all complexes, though a decreasing trend can be found with the increase in dendricity. The MV capture performance for each device were then evaluated with FL microscopy and cryo-SEM. Dendron C4 functionalized surface appear to be the best candidate for MV capture, as they not only successfully captured MVs onto the surface, but has maintained the morphology of the MVs as well. Such surface could be useful for future diagnostic applications since the device can capture biochemical information of both MV membrane as well as the inner content for analysis purpose. This interfacial engineering technique should be substrate-independent, a high added value allowing that a same reactive platform can be applied across a spectrum of substrate materials used in medical analytical and testing laboratories.

Limitation of study

The dendron enhancement of MV capture onto material surface is discussed in this article as a proof of concept. Besides molecule dendricity, other parameters such as material substrate,

spacer length and dendron scaffolds other than the poly benzyl ethers we proposed herein may also affect the performance of the capture devices.

Acknowledgements

We thank Estelle Morvan for her help in NMR experiments; thank Christine Labrugere for her help in XPS experiments, and we thank Bruno Payre for his help in cryo-SEM imaging. Jian-Qiao Jiang acknowledges financial support from China Scholarship Council. Marie-Christine Durrieu acknowledges financial support from Association France-Parkinson.

Author contributions

Marie-Christine Durrieu and Sylvain Nlate contributed equally by designing the capture device and dendrons used therein; Jian-Qiao Jiang conducted all the experiments and analysed all the data acquired; Christel Chanseau and Isabel Alves helped to establish the methodology used in material characterization. All the authors participated in the manuscript preparation.

Declaration of interest

Marie-Christine Durrieu, Sylvain Nlate, Jian-Qiao Jiang and Christel Chanseau have published 1 patent in July 2019 entitled “Ligands for capturing microvesicles and Uses thereof”.

List of acronyms used in this article:

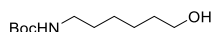
MV: microvesicle, PS: phosphatidylserine; PET: polyethylene terephthalate; DPA-Zn: dipicolylamine-Zn²⁺; DPA: dipicolylamine; POPS: 1-palmitoyl-2-oleoyl-sn-glycero-3-phospho-L-serine (sodium salt); POPC: 1-palmitoyl-2-oleoyl-sn-glycero-3-phosphocholine; PWR: plasmon waveguide resonance; EDC: N-(3-Dimethylaminopropyl)-N'-ethylcarbodiimide hydrochloride; NHS: N-Hydroxysuccinimide; TBO: toluidine blue-o; XPS: X-ray photoelectron spectroscopy; MP: molecular percentage; FL: fluorescence; PAMAM: poly(amidoamine); DMPC: 1,2-dimyristoyl-sn-glycero-3-phosphocholine.

Supplemental Information

Transparent methods

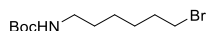
Synthesis

1) Tert-butyl (6-hydroxyhexyl)carbamate



The product is synthesized following the reported procedure.[228] 3.72 g of Di-tert-butyl-dicarbonate was added into a solution of 2 g 6-amino-1-hexanol in 40 mL tetrahydrofuran at 0 °C under stirring. The reacting mixture was allowed to slowly warm up to room temperature. After 24 h, the solvent was evaporated. The residue was dissolved in dichloromethane 50 mL and was washed with 50 mL of water for 3 times. The organic phase was gathered and dried over sodium sulfate, and then the solvent was removed with a rotary evaporator. The product is colorless oil, and the yield was 91 %. ¹H NMR (CDCl₃, 300 MHz, 25 °C): δ(ppm) 3.60 (t, 2H), 3.08 (t, 2H), 1.59-1.28 (m, 17H);

2) Tert-butyl (6-bromohexyl)carbamate



The product is synthesized following the reported procedure.[229] To a solution of 1 g tert-butyl (6-hydroxyhexyl)carbamate and 2.1 g triphenylphosphine in 12 mL tetrahydrofuran, a solution of 2.7 g tetrabromomethane in 8 mL tetrahydrofuran was added dropwise at 0 °C under stirring. The reacting mixture was allowed to slowly warm up to room temperature. After 24 h of reaction, the solvent was removed. The residue was added into a solvent mixture of 50 mL petroleum ether and 10 mL ethyl acetate. Precipitation formed instantly and then was filtered off while the filtrate was collected and evaporated to leave colorless oil behind. The oil went through

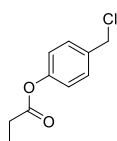
a flash column of silica using an eluent of petroleum ether: ethyl acetate= 10:1. The solvent was removed with a rotary evaporator. The product is colorless oil, and the yield was 93 %. ^1H NMR (CDCl_3 , 300 MHz, 25 °C): δ (ppm) 3.44 (t, 2H), 3.14 (t, 2H), 1.91-1.86 (m, 2H), 1.52-1.33 (m, 15H);

3) Tert-butyl (6-iodohexyl)carbamate



1.5 g tert-butyl (6-bromohexyl)carbamate was dissolved in 15 mL acetonitrile. 4.02 g of sodium iodide was added into the solution. The mixture was stirred under room temperature and kept in darkness for 48 h. The solvent was removed under vacuum, and the residue was extracted between 50 mL of dichloromethane and 50 mL water. The organic phase was washed with a saturated solution of sodium thiosulfate and then dried over sodium sulfate. The solvent was removed with rotary evaporator. The product is colorless oil, and the yield was 96 %. ^1H NMR (CDCl_3 , 300 MHz, 25 °C): δ (ppm) 3.21 (t, 2H), 1.90-1.80(m, 2H), 1.56-1.30 (m, 15H);

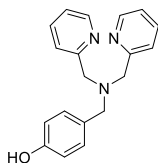
4) 4-(chloromethyl)phenyl propionate



The product is synthesized following the reported procedure.[230] Under stirring, 30 mL propionyl chloride was cooled to 0 °C. 5.1 g 4-(hydroxymethyl)phenol was added slowly into the flask so as to control the generation of hydrogen chloride at a moderate rate. After the addition, the mixture was allowed to slowly warm up to room temperature. After 12h, the mixture was poured into 500 mL ice-cold water, and then neutralized with sodium bicarbonate. The mixture was then extracted with 50 mL diethyl ether for 3 times. The organic phase was combined and

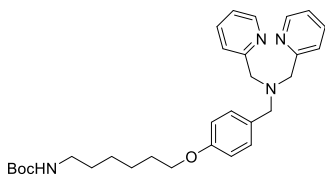
washed with 30 mL water for 3 times. The solution was then dried over sodium sulfate, and the solvent was removed using a rotary evaporator. The product is pale yellow oil, and the yield was 97%. ^1H NMR (CDCl_3 , 300 MHz, 25 °C): δ (ppm) 7.42 (d, 2H), 7.12 (d, 2H), 4.60 (s, 2H), 2.62 (q, 2H), 1.30 (t, 3H);

5) 1DPAOH



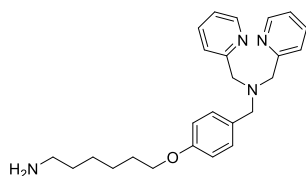
199 mg 4-(chloromethyl)phenyl propionate and 199 mg di-(2-picolyl)amine was dissolved in 10 mL dimethyl sulfoxide under stirring. After adding 414.6 mg potassium carbonate, the mixture was then heated to 60 °C. 24 h later, the reaction was cooled to room temperature, and then a solution of 0.6 g potassium carbonate in 3 mL water was then added under room temperature. Another 24 h later, the reaction mixture was dissolved in 30 mL dichloromethane, then washed with water (30 mL, 3 times), dried over sodium sulfate. The solvent was removed using a rotary evaporator to give the product as white crystals. The yield was 74%. ^1H NMR (DMSO, 300 MHz, 25 °C): δ (ppm) 9.31 (s, 1H), 8.51-8.49 (m, 2H), 7.83-7.77 (m, 2H), 7.58 (d, 2H), 7.28-7.24 (m, 2H), 7.20 (d, 2H), 6.73 (d, 2H), 3.68 (s, 4H), 3.51 (s, 2H); ^{13}C NMR (DMSO, 75MHz, 25°C): δ (ppm) 159.80, 156.87, 149.26, 137.08, 130.38, 128.98, 122.87, 122.59, 115.48, 59.33, 57.35;

6) Ligand 1-Boc



305 mg ligand 1-OH was dissolved in 4 mL dimethylformamide under stirring. 112 mg potassium hydroxide was added to the solution at room temperature. 1 h later, the mixture was cooled to -20 °C, then 392 mg tert-butyl (6-iodohexyl)carbamate was added into the mixture. The reaction was allowed to slowly warm up to room temperature. 3 h later, the reaction was quenched with water. The mixture was extracted with 20 mL dichloromethane for three times, then the combined organic phase was washed with 20 mL brine twice, and dried with sodium sulfate. The solvent was removed with rotary evaporator to afford brown oil. The crude product was then purified by silica column chromatography with an eluent of ethyl acetate: acetonitrile= 5:1. The product is pale yellow solid. The yield was 75%. ¹H NMR (MeOD, 300 MHz, 25 °C): δ(ppm) 8.43 (m, 2H), 7.86-7.71 (m, 2H), 7.70 (d, 2H), 7.32-7.28 (m, 4H), 6.89 (d, 2H), 3.99 (t, 2H), 3.77 (s, 4H), 3.61 (s, 2H), 3.06 (t, 2H), 1.81-1.76 (m, 2H), 1.54-1.44 (m, 15H); ¹³C NMR (MeOD, 75MHz, 25°C): δ(ppm) 159.34, 154.18, 147.94, 137.34, 129.86, 123.88, 123.32, 122.39, 113.99, 67.45, 66.43, 59.12, 57.81, 28.94, 27.39, 25.48;

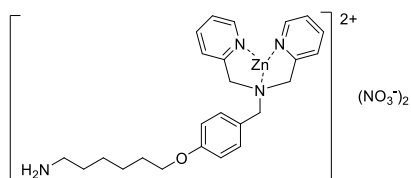
7) Ligand 1-NH₂



802.2 mg ligand 1-Boc was dissolved in 15 mL tetrahydrofuran. Trifluoroacetic acid was then added into the solution slowly at room temperature. 5 min after the addition of trifluoroacetic acid, the solution was heated to 60 °C. 30 h later, the solution was cooled to room temperature and then poured into an ice-cold sodium bicarbonate solution. The product was extracted with dichloromethane (30 mL, 3 times). The organic phase was then dried over sodium sulfate and the solvent was removed using rotary evaporator. The yield was 85%. ¹H NMR (MeOD, 300 MHz, 25 °C): δ(ppm) 8.54 (d, 2H), 7.71-7.66 (m, 2H), 7.60 (d, 2H), 7.19-7.14 (m, 2H), 6.87 (d, 2H), 3.96 (t, 2H), 3.82 (s, 4H), 3.64 (s, 2H), 2.73 (t, 2H), 1.83-1.77 (m, 2H), 1.53-1.41 (m, 6H); ¹³C NMR

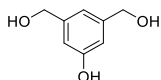
(MeOD, 75MHz, 25°C): δ (ppm) 159.94, 158.25, 148.96, 136.44, 130.69, 130.06, 122.81, 121.94, 114.31, 67.86, 59.84, 57.88, 41.88, 33.24, 29.27, 26.66, 25.94;

8) C1



108 mg ligand 1-NH₂ was dissolved in 10 mL methanol at room temperature under stirring. 79.4 mg zinc nitrate hexahydrate was dissolved in 5 mL methanol and was added in to the solution of ligand dropwise. 12 h later, the solvent in the mixture was removed under vacuum to give the final product as pale yellow powder (yield 100%). ¹H NMR (DMSO, 300 MHz, 25 °C): δ (ppm) 8.69 (d, 2H), 8.12 (t, 2H), 7.66 (m, 4H), 7.30 (d, 2H), 7.02 (d, 2H), 4.25 (d, 2H), 4.02 (t, 2H), 3.71 (t, 4H), 2.80 (t, 2H), 1.78-1.73 (m, 2H), 1.60-1.56 (m, 2H), 1.48-1.39 (m, 6H); ¹³C NMR (MeOD, 75MHz, 25°C): δ (ppm) 159.34, 154.81, 148.40, 141.26, 133.32, 125.33, 125.19, 123.98, 114.90, 67.88, 56.40, 55.68, 29.22, 29.01, 28.09, 26.10;

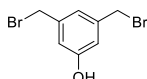
9) (5-hydroxy-1,3-phenylene)dimethanol



The product is synthesized following the reported procedure.[231, 232] To a dispersion of 1.3g lithium aluminum hydride in 40 mL anhydrous tetrahydrofuran at 0 °C, a solution of 3 g dimethyl 5-hydroxyisophthalate in 60 mL anhydrous tetrahydrofuran was added dropwise. The reaction was allowed to warm up to room temperature during 3 hours. After 12 h, the mixture was cooled to 0 °C again and quenched with 10% hydrochloric acid. The solvent was removed under reduced pressure. The residue was diluted in 50 mL brine and ethyl acetate was used to extract the

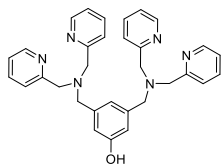
product from the aqueous solution (50 mL each time, 6 times in total). The organic layers were combined, dried over sodium sulfate and the solvent was removed using a rotary evaporator. The product is white crystal and the yield was 94%. $^1\text{H NMR}$ (CDCl_3 , 300 MHz, 25 $^\circ\text{C}$): δ (ppm) 6.69 (s, 1H), 6.61 (s, 2H), 4.41 (s, 4H);

10) 3,5-bis(bromomethyl)phenol



The product is synthesized following the reported procedure. 8.2 mL of 33% hydrogen bromide solution was added dropwise at 0 $^\circ\text{C}$ to a solution of 2 g of (5-hydroxy-1,3-phenylene)dimethanol in 20 mL acetic acid. The mixture was stirred 24 h at room temperature. 80 mL of distilled water was then added for an additional 10 min. The mixture was extracted with 70 mL dichloromethane for three times. The combined organic phases were washed with 100 mL water twice, then 100 mL saturated sodium bicarbonate solution twice and again 100 mL water. The organic phase was dried with sodium sulfate, filtered and concentrated. The crude product was purified with a flash column (silica, petroleum ether: ethyl acetate= 9:1) to afford white crystals (yield 90%). $^1\text{H NMR}$ (CDCl_3 , 300 MHz, 25 $^\circ\text{C}$): δ (ppm) 3.21 (t, 2H), 1.90-1.80(m, 2H), 1.56-1.30 (m, 15H);

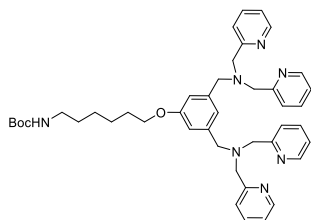
11) 2DPAOH



672 mg 3,5-bis(bromomethyl)phenol, 1196 mg N,N-dipicolylamine and 398 mg potassium carbonate was added into 10 mL dimethylformamide under nitrogen protection. The mixture was stirred under room temperature. After 3 hours, 50 mL water was added into the

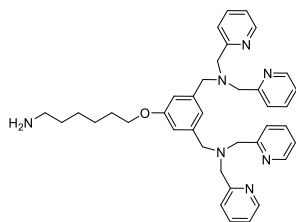
mixture, and was extracted with 50 mL dichloromethane twice. The organic layers were combined and washed with 50 mL water twice, dried over sodium sulfate, filtered and the solvent was evaporated using rotary evaporator. The remainder was purified using silica column chromatography to give the final product as white crystals (yield 80%). ¹H NMR (CDCl₃, 300 MHz, 25 °C): δ(ppm) 8.48-8.46 (m, 4H), 7.60-7.58 (m, 8H), 7.11 (q, 4H), 6.96 (s, 1H), 6.86 (s, 2H), 3.79 (s, 8H), 3.57 (s, 4H);

12) Ligand 2-Boc



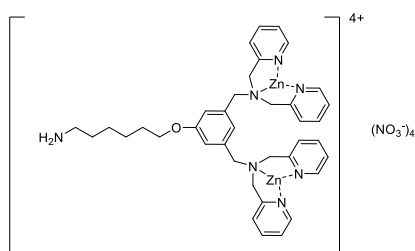
520 mg ligand 2-OH was dissolved in 4 mL dimethylformamide under stirring. 120 mg potassium hydroxide was added to the solution at room temperature. 1 h later, the mixture was cooled to -20 °C, then 400 mg tert-butyl (6-iodohexyl)carbamate was added into the mixture. The reaction was allowed to slowly warmup to room temperature. 3 h later, the reaction was quenched with water. The mixture was extracted with 20 mL dichloromethane for three times, then the combined organic phase was washed with 20 mL brine twice, and dried with sodium sulfate. The solvent was removed with rotary evaporator to afford brown oil. The crude product was then purified by silica column chromatography with an eluent of ethyl acetate: acetonitrile= 5:1. The product is pale yellow solid. The yield was 75%. ¹H NMR (DMSO, 300 MHz, 25 °C): δ(ppm) 8.43 (d, 4H), 7.79 (ddd, 4H), 7.28 (tt, 4H), 7.04 (s, 1H), 3.97 (t, 2H), 3.80 (s, 8H), 3.65 (s, 4H), 3.07 (t, 2H), 1.79 (t, 2H), 1.58-1.48 (m, 15H);

13) Ligand 2-NH₂



1350 mg ligand 2-Boc was dissolved in 15 mL tetrahydrofuran. 7.2 mL trifluoroacetic acid was then added into the solution slowly at room temperature. 5 min after the addition of trifluoroacetic acid, the solution was heated to 60 °C. 30 h later, the solution was cooled to room temperature and then poured into an ice-cold sodium bicarbonate solution. The product was extracted with dichloromethane (30 mL, 3 times). The organic phase was then dried over sodium sulfate and the solvent was removed using rotary evaporator. The yield was 85%. ^1H NMR (DMSO, 300 MHz, 25 °C): δ (ppm) 8.49 (d, 4H), 7.74 (ddd, 4H), 7.57 (d, 4H), 7.25 (dd, 4H), 7.07 (s, 1H), 6.82 (s, 2H), 3.93 (t, 2H), 3.71 (s, 8H), 3.60 (s, 4H), 3.32 (b, 4H), 1.69 (t, 2H), 1.42-1.34 (m, 6H); ^{13}C NMR (MeOD, 75MHz, 25°C): δ (ppm) 159.79, 159.20, 148.97, 140.49, 136.42, 122.76, 121.95, 121.48, 113.56, 67.85, 60.09, 58.63, 41.31, 29.07, 26.81, 26.58, 26.13.

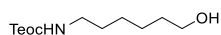
14) C2



1110 mg ligand 2-NH₂ was dissolved in 10 mL methanol at room temperature under stirring. 1072 mg zinc nitrate hexahydrate was dissolved in 5 mL methanol and was added in to the solution of ligand dropwise. 12 h later, the solvent in the mixture was removed under vacuum to give the final product as pale yellow powder (yield 100%). ^1H NMR (DMSO, 300 MHz, 25 °C): δ (ppm) 8.71 (b, 4H), 8.11 (t, 4H), 7.67 (t, 4H), 7.60 (d, 4H), 7.01 (b, 2H), 6.89 (s, 1H), 4.35 (d, 2H), 4.07 (b, 2H), 3.81 (d, 8H), 2.84 (t, 2H), 1.79 (b, 2H), 1.65-1.46 (m, 6H); ^{13}C NMR (MeOD,

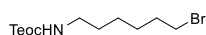
75MHz, 25°C): δ (ppm) 162.85, 159.27, 155.04, 148.50, 141.37, 134.32, 127.12, 125.32, 117.96, 68.03, 57.51, 56.15, 39.86, 36.26, 31.24, 29.05, 27.79, 26.11, 25.62.

15) 2-(trimethylsilyl)ethyl (6-hydroxyhexyl)carbamate



352 mg of 6-amino-1-hexanol was dissolved in 5 mL dichloromethane. 0.9 mL triethylamine was added into the solution and then 850 mg of 4-Nitrophenyl 2-(trimethylsilyl)ethyl carbonate in 1.4 mL dichloromethane was also added into the mixture at room temperature under stirring. After 24 h, the solvent was evaporated. The residue was dissolved in dichloromethane 50 mL and was washed with 50 mL of saturated NaHCO_3 solution for 3 times and then 50 mL of 2 M NaOH solution for 3 times. The organic phase was gathered and dried over sodium sulfate, and then the solvent was removed with a rotary evaporator. The product is colorless oil, and the yield was 98 %. ^1H NMR (CDCl_3 , 300 MHz, 25 °C): δ (ppm) 4.64 (b, 1H), 4.17 (t, 2H), 3.67 (t, 2H), 3.20 (q, 2H), 1.68-1.34 (m, 8H), 1.00 (t, 2H), 0.07 (s, 9H);

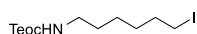
16) 2-(trimethylsilyl)ethyl (6-bromohexyl)carbamate



To a solution of 748 mg 2-(trimethylsilyl)ethyl (6-hydroxyhexyl)carbamate and 1311 mg triphenylphosphine in 12 mL tetrahydrofuran, a solution of 1.66 g tetrabromomethane in 8 mL tetrahydrofuran was added dropwise at 0 °C under stirring. The reacting mixture was allowed to slowly warm up to room temperature. After 24 h of reaction, the solvent was removed. The residue was added into a solvent mixture of 50 mL petroleum ether and 10 mL ethyl acetate. Precipitation formed instantly and then was filtered off while the filtrate was collected and evaporated to leave colorless oil behind. The oil went through a flash column of silica using an eluent of petroleum ether: ethyl acetate= 10:1. The solvent was removed with a rotary evaporator.

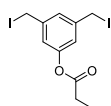
The product is colorless oil, and the yield was 84 %. ¹H NMR (CDCl₃, 300 MHz, 25 °C): δ(ppm) 4.61 (b, 1H), 4.18 (t, 2H), 3.43 (t, 2H), 3.19 (q, 2H), 1.94-1.84 (m, 2H), 1.62-1.34 (m, 6H), 1.00 (t, 2H), 0.07 (s, 9H);

17) 2-(trimethylsilyl)ethyl (6-iodohexyl)carbamate



846 mg 2-(trimethylsilyl)ethyl (6-bromohexyl)carbamate was dissolved in 15 mL acetonitrile. 2 g sodium iodide was added into the solution. The mixture was stirred under room temperature and kept in darkness for 48 h. The solvent was removed under vacuum, and the residue was extracted between 50 mL of dichloromethane and 50 mL water. The organic phase was washed with a saturated solution of sodium thiosulfate and then dried over sodium sulfate. The solvent was removed with rotary evaporator. The product is colorless oil, and the yield was 96 %. ¹H NMR (CDCl₃, 300 MHz, 25 °C): δ(ppm) 4.61 (b, 1H), 4.18 (t, 2H), 3.24-3.16 (m, 4H), 1.89-1.80 (m, 2H), 1.58-1.33 (m, 6H), 1.00 (t, 2H), 0.07 (s, 9H);

18) 3,5-bis(iodomethyl)phenyl propionate

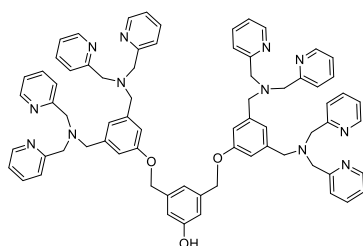


1.15 mL propionyl chloride was dissolved in 30 mL of dichloromethane. At 0°C, 2.8 g 3,5-bis(bromomethyl)phenol dissolved in 10 mL dichloromethane was added into the solution under stirring. 5 min later, 3 mL triethylamine in 10 mL dichloromethane was also added into the solution and the cold bath was removed. 2h after the addition of triethylamine, the reaction was quenched with 10 mL water. The mixture was extracted with 50 mL dichloromethane twice, and the organic phase was combined and washed first with 15 mL saturated sodium bicarbonate

solution, then with 15 mL brine. The organic phase was dried with sodium sulfate before the solvent was removed under vacuum.

The product of the above reaction was dissolved in 15 mL acetonitrile. 7.5 g sodium iodide was added into the solution. The mixture was stirred under room temperature and kept in darkness for 48 h. The solvent was removed under vacuum, and the residue was extracted between 50 mL of dichloromethane and 50 mL water. The organic phase was washed with a saturated solution of sodium thiosulfate before the organic phase was collected and dried over sodium sulfate. The solvent was removed with a rotary evaporator. The product is colorless crystal, and the yield was 96 %. ^1H NMR (CDCl_3 , 300 MHz, 25 °C): δ (ppm) 7.27 (t, 1H), 7.04 (d, 2H), 4.41 (s, 4H), 2.62 (q, 2H), 1.30 (t, 3H);

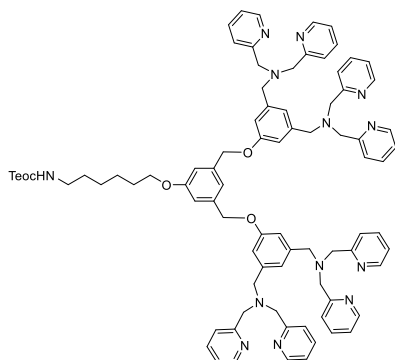
19) 4DPAOH



1284 mg ligand 2-OH was dissolved in 4 mL dimethylformamide under stirring. 126 mg potassium hydroxide was added to the solution at room temperature. 1 h later, the mixture was cooled to -20 °C, then 520 mg 3,5-bis(iodomethyl)phenyl propionate was added into the mixture. The reaction was allowed to slowly warm up to room temperature. 3 h later, the reaction was quenched with water. The mixture was extracted with 20 mL dichloromethane for three times, then the combined organic phase was washed with 20 mL brine twice, and dried with sodium sulfate. The solvent was removed with rotary evaporator to afford brown oil. The crude product was then purified by silica column chromatography with an eluent of ethyl acetate: acetonitrile= 5:1. The product is pale yellow solid. The yield was 75%. ^1H NMR (DMSO, 300 MHz, 25 °C): δ (ppm) 8.47 (tt, 8H), 7.71 (ddd, 8H), 7.54-7.51 (m, 8H), 7.20 (qq, 8H), 7.06 (s, 2H), 6.96 (s, 1H), 6.90 (s, 4H), 6.83 (s, 2H), 5.01(s, 4H), 3.70 (s, 16H), 3.57 (s, 8H); ^{13}C NMR (CDCl_3 , 75MHz,

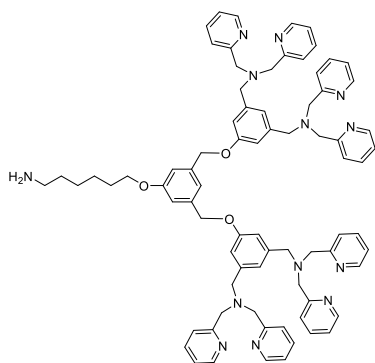
25°C): δ (ppm) 159.68, 158.63, 157.79, 148.87, 140.61, 139.88, 138.99, 136.64, 122.84, 122.49, 122.05, 117.89, 114.94, 115.18, 69.96, 59.87, 58.33.

20) Ligand 4-Teoc



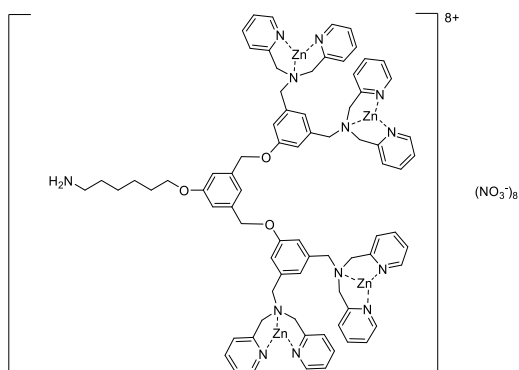
930 mg ligand 4-OH was dissolved in 10 mL dimethylformamide under stirring. 90.5 mg potassium hydroxide was added to the solution at room temperature. 1 h later, the mixture was cooled to $-20\text{ }^{\circ}\text{C}$, then 360 mg 2-(trimethylsilyl)ethyl (6-iodohexyl)carbamate was added into the mixture. The reaction was allowed to slowly warm up to room temperature. 3 h later, the reaction was quenched with water. The mixture was extracted with 20 mL dichloromethane for three times, then the combined organic phase was washed with 20 mL brine twice, and dried with sodium sulfate. The solvent was removed with rotary evaporator to afford brown oil. The crude product was then purified by silica column chromatography with an eluent of ethyl acetate: acetonitrile= 5:1. The product is pale yellow solid. The yield was 75%. ^1H NMR (CDCl_3 , 300 MHz, $25\text{ }^{\circ}\text{C}$): δ (ppm) 8.54-8.51 (m, 8H), 7.65-7.55 (m, 16H), 7.16-7.11 (m, 11H), 7.00-6.98 (m, 6H), 5.05 (s, 4H), 4.17 (t, 2H), 3.97 (t, 2H), 3.82 (s, 16H), 3.68(s, 8H), 3.18 (q, 2H), 1.83-1.72 (m, 2H), 1.54-1.34 (m, 6H), 0.99 (t, 2H), 0.06 (s, 9H); ^{13}C NMR (CDCl_3 , 75MHz, 25°C): δ (ppm) 162.55, 159.75, 159.67, 159.02, 148.99, 140.73, 139.09, 136.42, 122.73, 121.96, 121.88, 118.52, 113.82, 113.11, 69.91, 67.92, 60.10, 58.57, 40.86, 36.49, 30.94, 30.05, 29.19, 26.54, 25.79, 17.80, -1.44;

21) Ligand 4-NH₂



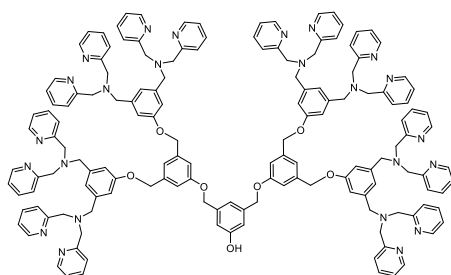
900 mg ligand 4-Teoc was dissolved in 10 mL tetrahydrofuran under stirring. 6.5 mL of 1 M tetrabutylammonium fluoride solution was then added at room temperature. The reaction mixture was then kept at 60 °C overnight. After cooled to room temperature, the solvent was removed in vacuo. The residue was dissolved in dichloromethane, and then washed with 50 mL 0.5 M NaOH solution once and 50 mL saturated NaHCO₃ solution twice. The organic phase was dried with sodium sulfate. The solvent was removed with rotary evaporator to afford brown solid. The yield was 90%. ¹H NMR (DMSO, 300 MHz, 25 °C): δ(ppm) 8.48-8.45 (t, 8H), 7.70 (ddd, 8H), 7.51 (d, 8H), 7.22 (ddd, 8H), 7.11 (s, 1H), 7.06 (s, 2H), 6.97 (s, 2H), 6.92 (s, 4H), 5.07 (s, 4H), 3.89 (t, 2H), 3.69 (s, 16H), 3.57 (s, 8H), 1.61 (t, 2H), 1.37-1.19 (m, 6H); ¹³C NMR (DMSO, 75MHz, 25°C): δ(ppm) 159.61, 159.29, 158.79, 149.79, 149.26, 140.72, 139.49, 136.95, 122.81, 122.57, 121.69, 114.10, 113.30, 69.48, 59.66, 57.94, 55.39, 41.52, 32.60, 29.05, 26.48, 25.80; ESI-MS: m/z: 1250.68 [M-H⁺] (calcd 1250.68).

22) C4



125 mg ligand 4-NH₂ was dissolved in 10 mL methanol at room temperature under stirring. 119 mg zinc nitrate hexahydrate was dissolved in 5 mL methanol and was added in to the solution of ligand dropwise. 12 h later, the solvent in the mixture was removed under vacuum to give the final product as brown powder (yield 100%). ¹H NMR (DMSO, 300 MHz, 25 °C): δ(ppm) 8.70 (d, 8H), 8.10 (t, 8H), 7.67 (t, 8H), 7.58 (d, 8H), 7.27 (s, 1H), 7.17 (s, 4H), 7.06 (s, 1H), 6.96 (s, 2H), 5.27 (s, 4H), 4.38 (d, 8H), 4.10 (q, 2H), 3.83 (t, 16H), 2.81 (t, 2H), 2.22 (t, 2H), 1.55 (t, 2H), 1.44-1.32 (m, 4H); ¹³C NMR (DMSO, 75MHz, 25°C): δ(ppm) 159.44, 159.08, 154.85, 148.45, 141.27, 139.20, 134.29, 127.73, 125.32, 125.13, 118.35, 114.09, 69.86, 68.05, 57.42, 56.14, 49.09, 29.27, 26.05, 25.55, 20.34, 19.72;

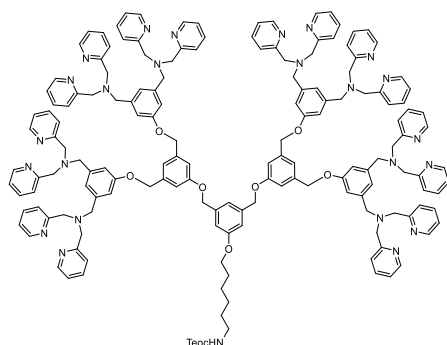
23) 8DPAOH



1151 mg (1 mmol) ligand 4-OH was dissolved in 4 mL dimethylformamide under stirring. 126 mg (2.25 mmol) potassium hydroxide was added to the solution at room temperature. 1 h later, the mixture was cooled to -20 °C, then 220 mg (0.51 mmol) 3,5-bis(iodomethyl)phenyl propionate was added into the mixture. The reaction was allowed to slowly warm up to room temperature. 3 h later, the reaction was quenched with water. The mixture was extracted with 20 mL dichloromethane for three times, then the combined organic phase was washed with 20 mL brine twice, and dried with sodium sulfate. The solvent was removed with rotary evaporator to afford brown oil. The crude product was then purified by silica column chromatography with an eluent of ethyl acetate: acetonitrile= 5:1. The product is pale yellow solid. The yield was 75%. ¹H NMR (DMSO, 300 MHz, 25 °C): δ(ppm) 8.48-8.44 (m, 16H), 7.74-7.64 (m, 16H), 7.54-7.51 (m, 16H), 7.22-7.14 (m, 16H), 7.07 (d, 6H), 6.96 (s, 1H), 6.90 (d, 8H), 6.83 (s, 2H), 6.79 (s, 1H), 6.75 (s, 1H), 6.71 (s, 1H), 6.66 (s, 1H), 5.05-4.97(m, 12H), 3.69 (d, 32H), 3.57 (d, 16H); ¹³C NMR

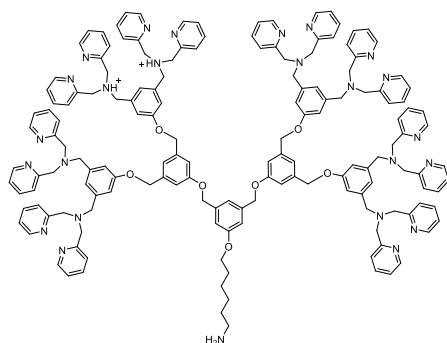
(CDCl₃, 75MHz, 25°C): δ(ppm) 159.68, 158.63, 157.79, 148.87, 140.61, 139.88, 138.99, 136.64, 122.84, 122.49, 122.05, 117.89, 114.94, 115.18, 69.96, 59.87, 58.33.

24) Ligand 8-Teoc



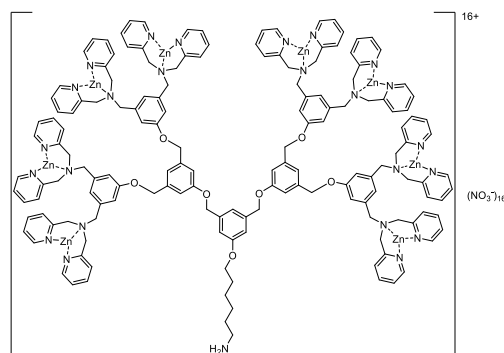
605 mg (0.25 mmol) ligand 8-OH was dissolved in 10 mL dimethylformamide under stirring. 30 mg (0.54 mmol) potassium hydroxide was added to the solution at room temperature. 1 h later, the mixture was cooled to -20 °C, then 95 mg (0.256 mmol) 2-(trimethylsilyl)ethyl (6-iodohexyl)carbamate was added into the mixture. The reaction was allowed to slowly warm up to room temperature. 3 h later, the reaction was quenched with water. The mixture was extracted with 20 mL dichloromethane for three times, then the combined organic phase was washed with 20 mL brine twice, and dried with sodium sulfate. The solvent was removed with rotary evaporator to afford brown oil. The crude product was then purified by silica column chromatography with an eluent of ethyl acetate: acetonitrile= 5:1. The product is pale yellow solid. The yield was 73%. ¹H NMR (DMSO, 300 MHz, 25 °C): δ(ppm) 8.47-8.43 (m, 16H), 7.72-7.63 (m, 16H), 7.53-7.47 (m, 16H), 7.23-7.13 (m, 16H), 7.00 (b, 2H), 6.93-6.88 (m, 9H), 6.81 (s, 1H), 6.78 (s, 1H), 5.13-4.99 (m, 12H), 4.05-3.98 (m, 2H), 3.67 (d, 32H), 3.55 (d, 16H), 1.71-1.58 (m, 2H), 1.43-1.20 (m, 8H), 0.94-0.84 (m, 2H), 0.00(s, 9H); ¹³C NMR (CDCl₃, 75MHz, 25°C): δ(ppm) 162.55, 159.75, 159.67, 159.02, 148.99, 140.73, 139.09, 136.42, 122.73, 121.96, 121.88, 118.52, 113.82, 113.11, 69.91, 67.92, 60.10, 58.57, 40.86, 36.49, 30.94, 30.05, 29.19, 26.54, 25.79, 17.80, -1.44;

25) Ligand 8-NH₂



400 mg (0.15 mmol) ligand 8-Teoc was dissolved in 10 mL tetrahydrofuran under stirring. 1.5 mL of 1 M tetrabutylammonium fluoride solution was then added at room temperature. The reaction mixture was then kept at 60 °C overnight. After cooled to room temperature, the solvent was removed in vacuo. The residue was dissolved in dichloromethane, and then washed with 50 mL 0.5 M NaOH solution once and 50 mL saturated NaHCO₃ solution twice. The organic phase was dried with sodium sulfate. The solvent was removed with rotary evaporator to afford brown solid. The yield was 90%. ¹H NMR (DMSO, 300 MHz, 25 °C): δ(ppm) 8.45-8.43 (m, 16H), 7.73-7.58 (m, 16H), 7.56-7.45 (m, 16H), 7.24-7.11 (m, 18H), 7.10-6.97 (m, 10H), 6.93-6.88 (m, 9H), 5.05-4.99 (m, 12H), 3.91-3.84 (m, 2H), 3.67 (b, 32H), 3.55 (b, 16H), 1.64-1.56 (m, 2H), 1.37-1.23 (m, 8H); ¹³C NMR (DMSO, 75MHz, 25°C): δ(ppm) 159.61, 159.29, 158.79, 149.79, 149.26, 140.72, 139.49, 136.95, 122.81, 122.57, 121.69, 114.10, 113.30, 69.48, 59.66, 57.94, 55.39, 41.52, 32.60, 29.05, 26.48, 25.80; ESI-MS: m/z: 2520.30 [M-H⁺] (calcd 2520.30), 1260.66 [M-2H⁺] (calcd 1260.65).

26) Complex 8-NH₂



250 mg (0.1 mmol) ligand 8-NH₂ was dissolved in 10 mL methanol at room temperature under stirring. 30 mg (1 mmol) zinc nitrate hexahydrate was dissolved in 5 mL methanol and was added in to the solution of ligand dropwise. 12 h later, the solvent in the mixture was removed under vacuum to give the final product as brown powder (yield 100%). ¹H NMR (DMSO, 300 MHz, 25 °C): δ(ppm) 8.45 (b, 16H), 7.67 (b, 16H), 7.51 (b, 16H), 7.20 (b, 18H), 7.07 (b, 9H), 6.90 (b, 10H), 5.05 (b, 12H), 3.90 (b, 2H), 3.67 (b, 32H), 3.56 (b, 16H), 1.58 (b, 2H), 1.25 (b, 8H); ¹³C NMR (DMSO, 75MHz, 25°C): δ(ppm) 159.44, 159.08, 154.85, 148.45, 141.27, 139.20, 134.29, 127.73, 125.32, 125.13, 118.35, 114.09, 69.86, 68.05, 57.42, 56.14, 49.09, 29.27, 26.05, 25.55, 20.34, 19.72;

The functionalization of PET films with complexes:

10 cm² PET films were first cleaned with ethanol, and then immersed in a hydrolysis solution (20 mL water, 20 mL acetonitrile and 0.2 g NaOH). The hydrolysis was kept at 60 °C for 18 h. The films were cleaned with water, and then immersed in an oxidation solution (38.4 ml fresh milliQ water, 1.6 ml H₂SO₄, 2 g KMnO₄). The oxidation was kept at 60 °C for 1 h. The oxidized film was washed first with 50% HCl once and then water 3 times. The oxidized films were immersed in the activation solution (MES hydrate 390.5 mg/2 mmol, ethylcarbodiimide hydrochloride(EDC) 766.8 mg/4 mmol, N-hydroxysuccinimide(NHS) 230.18 mg/2 mmol), then kept at room temperature for 1h. The films were washed with water. The activated films were subsequently immersed in 20 mL 1 mM solution of complexes in DMSO under room temperature. 24 h later, the films were removed from the solution and washed intensively with water.

The TBO characterization:

First, a linear correlation between TBO concentration in 50% AcOH and the solution's absorbance @ 633nm (200 μ L solution in each well of a transparent 96 well plate) was established using a series of TBO solutions shown in Table S1. In future TBO tests, 5 mL 50% acetic acid would be used to remove the TBO dye adsorbed on 1 cm² squares, and 200 μ L of each solution would also be added into each individual well of a transparent 96 well plate for absorbance test. Thus TBO concentrations in Table S1 can then be further converted into molecule density on PET surface. The plot was then linearly fitted, as shown in Figure S1.

Table S1. TBO solutions used in absorbance calibration, Related to Figure 6.

Desired TBO concentration (mM)	TBO solution used for dilution	50% (V/V) acetic acid (μ L)	Total amount
0.5	100 μ L of TBO 5mM	900	1mL
0.1	200 μ L of TBO 5mM	800	1mL
0.05	100 μ L of TBO 0.5mM	900	1mL
0.01	200 μ L of TBO 0.5mM	800	1mL
0.005	100 μ L of TBO 0.05mM	900	1mL
0.001	200 μ L of TBO 0.05mM	800	1mL
0.0005	100 μ L of TBO 0.005mM	900	1mL

0.0001	200 μ L of TBO 0.005mM	800	1mL
0.00005	100 μ L of TBO 0.0005mM	900	1mL
0.00001	200 μ L of TBO 0.0005mM	800	1mL

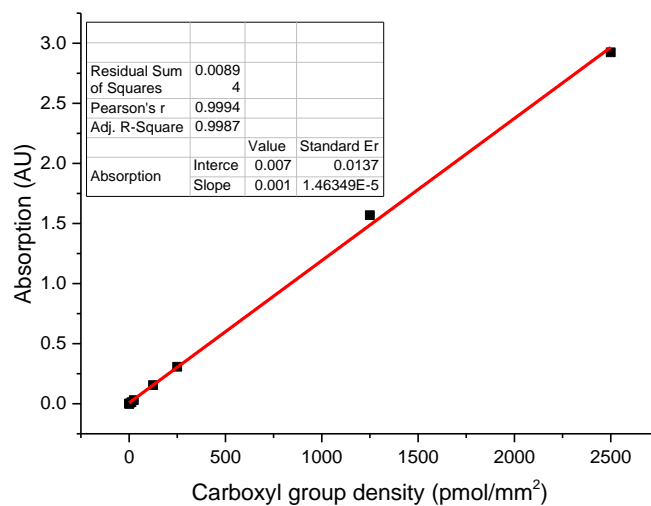


Figure S1. Calibration curve of carboxyl group density plotted against absorbance @ 633 nm, Related to Figure 6.

After acquiring the calibration curve, the TBO test was performed: A 5×10^{-4} M solution of toluidine blue-o solution was prepared by first dissolving NaOH into milli-Q water until pH 10, then dissolving toluidine blue-o to reach desired concentration. 1 cm by 1 cm PET squares were immersed in 10 mL of the TBO solution and then were kept under shaking in darkness at room temperature. 6 hours later, the supernatant was removed from tube and the stained PET surface was washed with 10 mL NaOH solution (pH 10) once and 10 mL pure water twice. The stained films were then immersed in 5 mL 50% acetic acid to remove the adsorbed TBO dye during 10

min. 200 μL of the washed solution from each sample was loaded into 96 well plate and the absorption at 633 nm is measured with a 96 well plate reader. The absorbance was then translated to the surface density of carboxyl groups and summarized in Figure 6 using the calibration curve shown in Figure S1.

X-ray photoelectron spectroscopy (XPS)

A VG Scientific ESCALAB photoelectron spectrometer was used for the surface analysis with a non-monochromatized MgK 1253.6 eV source of 100 W. The area of the analytical X-ray spot on the sample surface is about 250 microns. We used a 45 degree insert angle that corresponds to 3-5 nm of analyzed depth. A flood gun was used for charge compensation. Acquisition of high resolution spectra was done at constant pass energy of 20 eV. Fitting was then realized with software provided by VG Scientific, each spectrum being referenced to carbon pollution at 284.8 eV. Binding energies values are given with a precision of ± 0.2 eV.

Microvesicle preparation

Microvesicles were collected from mesenchymal stem cells. After 6 passages, TNF α was introduced into the incubation medium at a concentration of 100 ng/ml. After 36 h, the supernatant was collected, and then purified in 3 steps: 1) Removal of cellular debris: Centrifuge the incubation supernatant at 4 °C 1500 g for 15 min, take the supernatant and centrifuge at 4 °C 13000 g for another 2 min. 2) Concentrating microvesicles: Take the supernatant again, centrifuge at 4 °C 20000 g for 90 min and then take the pellet. 3) Wash the microvesicles: Re-disperse the pellet in 500 μ L 1x PBS of 4 °C, centrifuge at 4 °C 20000 g for 90 min. Remove 400 μ L of the supernatant without disturbing the pellet, then add another 400 μ L fresh 1x PBS of 4 °C, re-disperse again, and centrifuge at 4 °C 20000 g for 90 min. Remove 450 μ L of the supernatant without disturbing the pellet, then add 50 μ L 1x PBS of 4 °C to redisperse the pellet. When not being used, the microvesicles were stored at – 80 °C.

Microvesicle staining

Stock of microvesicles was allowed to warm up to room temperature, and then 950 μL 1x PBS was used to dilute the suspension. 1 μL CellMask™ Deep Red Plasma membrane Stain was added into the diluted suspension to stain the microvesicles under room temperature. 15 min later, the stained suspension was centrifuged at 4 °C 20000 g for 90 min. 950 μL of the supernatant was then removed without disturbing the pellet, and another 950 μL of fresh PBS was added to redisperse the pellet. The centrifugation-redispersion step was repeated twice so as to remove the free CellMask™ Deep Red molecules from the PBS buffer.

Microvesicle characterization using fluorescence microscope:

Stained microvesicles were visible under fluorescence microscope (Leica microsystem DM5500B, microscope with a motorized, programmable stage using a CoolSnap HQ camera controlled by Metamorph 7.6).

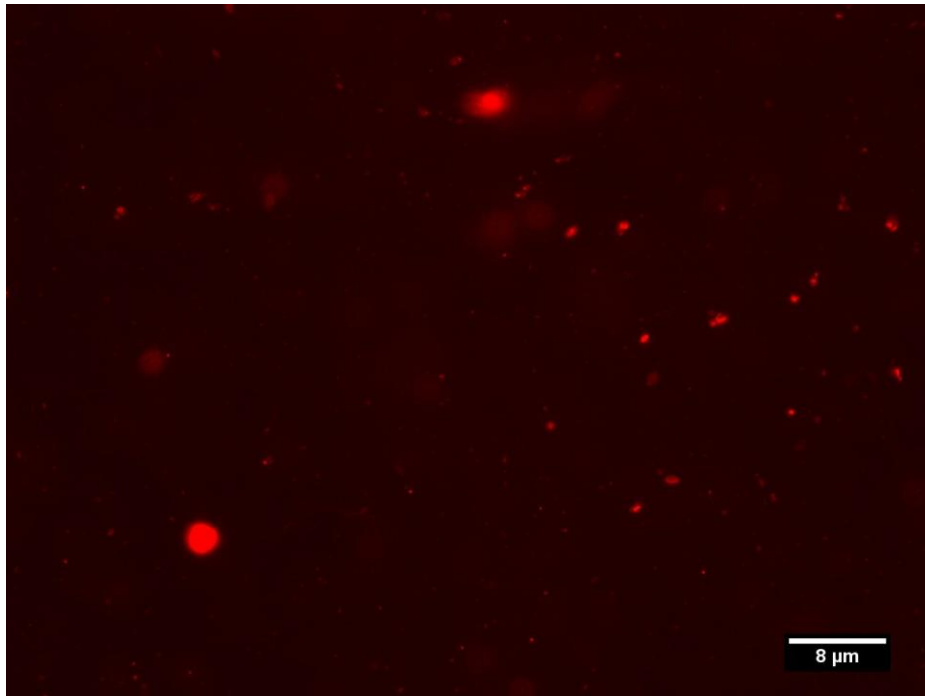


Figure S2: fluorescence micrograph of CellMask™ Deep Red stained microvesicle suspension, Related to Figure 7.

Microvesicle characterization using nanoparticle tracking analysis (NTA):

NTA experiment of prepared microvesicles was performed using NanoSight NS300 instrument. The analysis was performed under 22 °C, using 532nm laser beam as light source. The instrument was calibrated using the standard nanoparticle dispersions provided by the manufacturer before test.

For the test, stock of microvesicles was allowed to warm up to room temperature, and then 1x PBS was used to dilute the suspension to 1 mL. The suspension was then vortexed to reach an even distribution of microvesicles inside the dilution.

The NTA experiment was performed by 5 video recordings of 30s of the microvesicle dispersion flowing through the sample chamber at the syringe pump speed of 70 (AU).

The videos were simultaneously analyzed by software NTA 3.2 Dev Build 3.2.16, where the microvesicle concentration and size distribution per frame of picture were recorded.

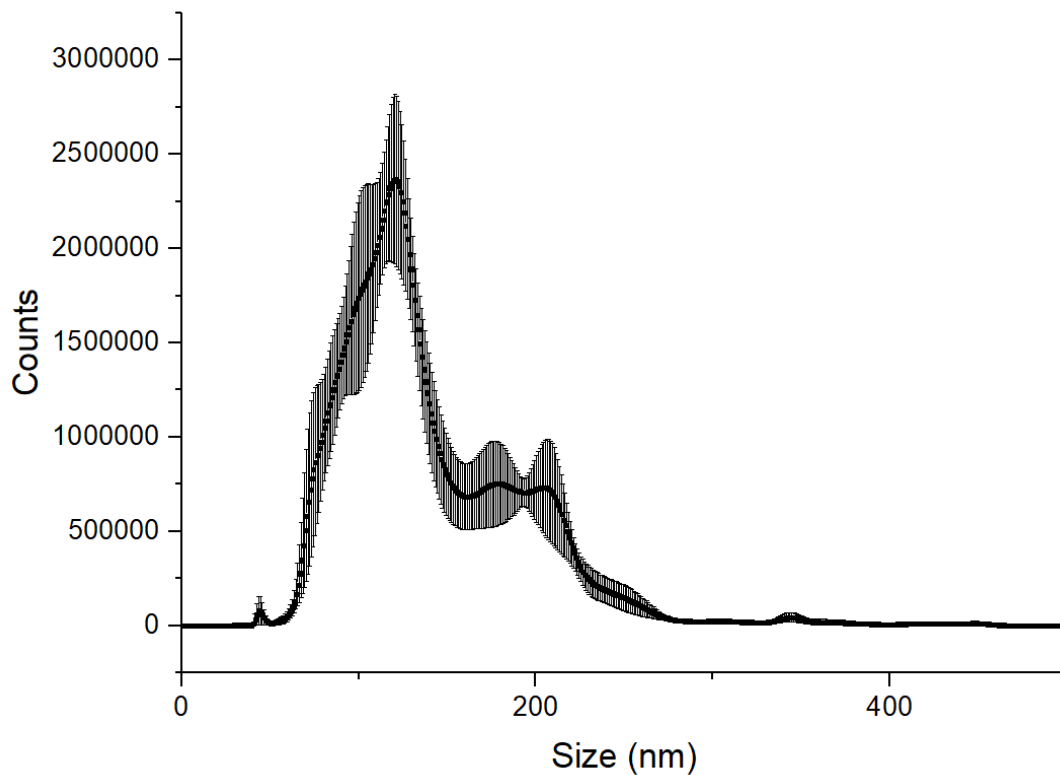


Figure S3. microvesicle size distribution according to NTA analysis, Related to Figure 7.

Microvesicle capture

For all materials, the same procedure was used to capture the microvesicles: The stock microvesicle (stained with CellMask™ Deep Red for FL microscopy and nonstained for Cryo-scanning electron microscopy) dispersion was diluted to 2 mL with 1× PBS. 250µL of the dispersion was added onto a functionalized 1 cm² PET square and was incubated under room temperature for 15 min. The PET squares were then washed with milli-Q water to remove any free vesicles adhered to the surface.

Observation of captured microvesicles using FL microscope

After the capturing process, fluorescence microscopy (Leica microsystem DM5500B, microscope with a motorized, programmable stage using a CoolSnap HQ camera controlled by Metamorph 7.6) of PET sheets was used to evaluate the capture ability of PET functionalized with different complexes.

Observation of captured microvesicles using Cryo-scanning electron microscopy (Cryo-SEM)

After the capturing process, PET sheets were mounted on freezing stub for the preparation chamber Quorum PP3000T specimen shuttle. The whole was plunged in slush nitrogen paste for cryo-fixation. After quick transfer under vacuum in the preparation chamber the samples were sublimed at -95 °C during 30 min and then coated by platinum sputtering. They were at last transferred in the cryo-SEM Quanta 250 FEG chamber and kept at -140 °C for observation at an accelerating voltage of 10kV.

NMR & MS spectra of synthesized compounds:

BocHNC6OH 1st

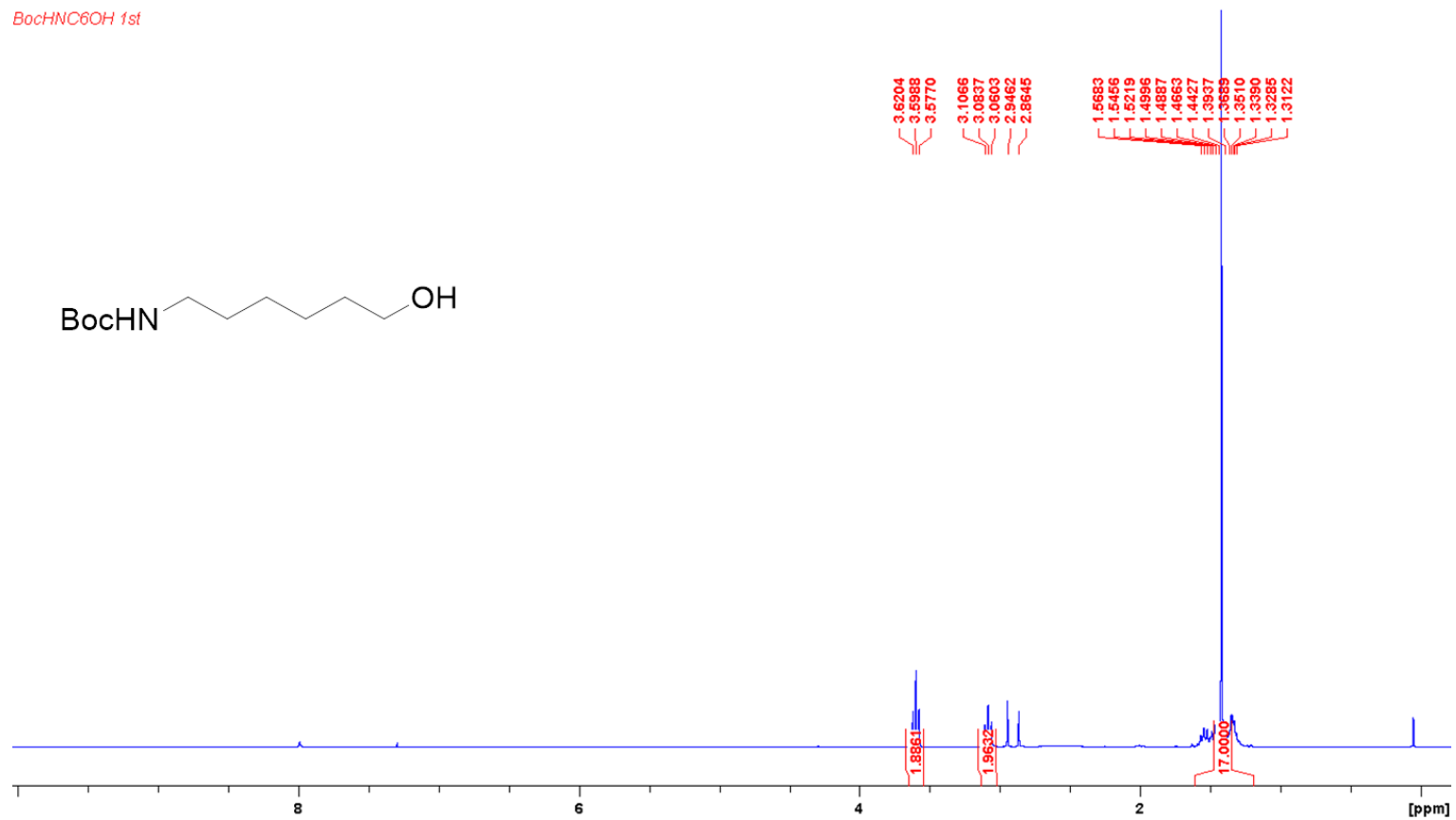


Figure S4. ¹H NMR spectrum of Tert-butyl (6-hydroxyhexyl)carbamate. Related to Scheme 2.

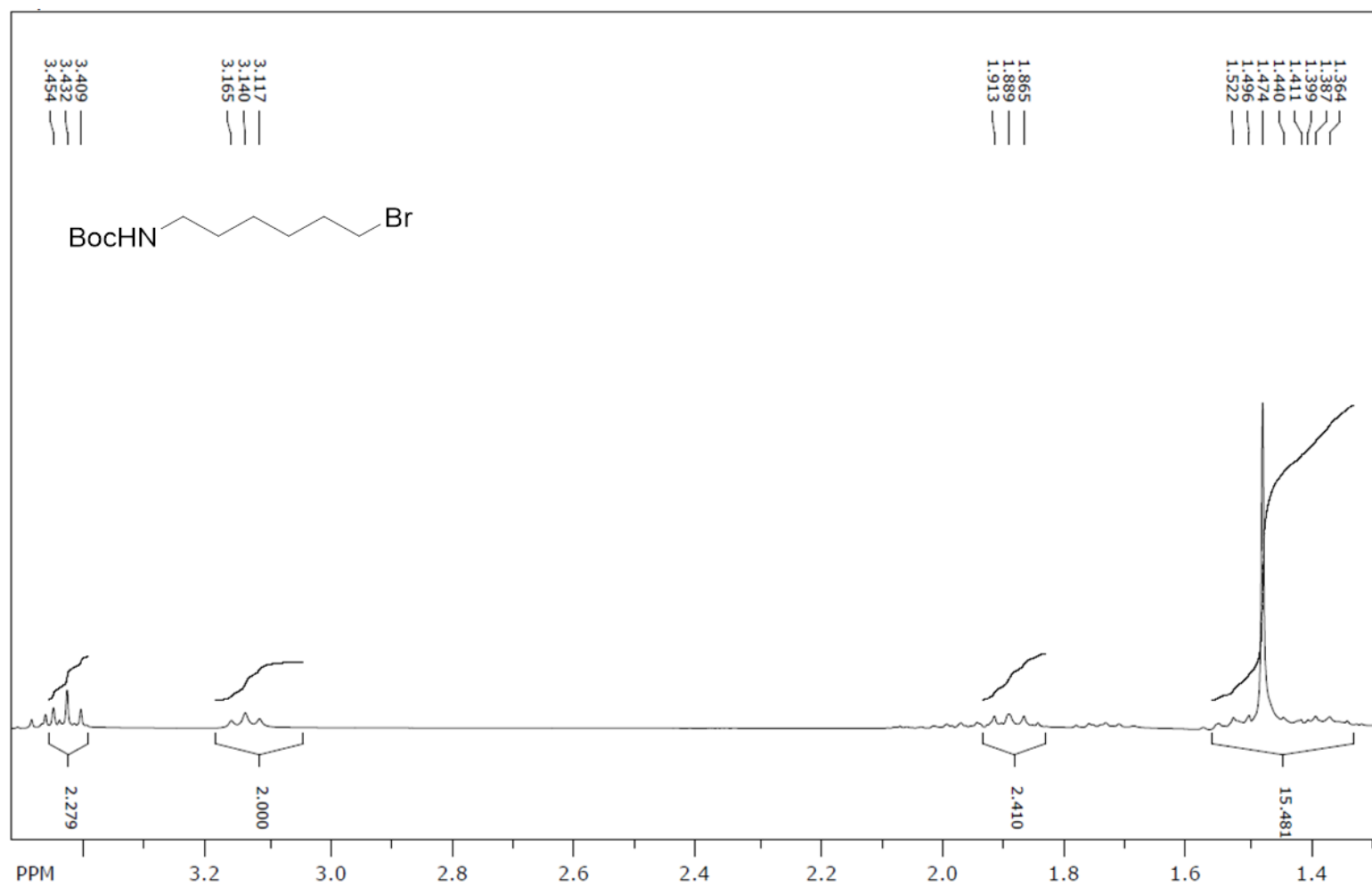


Figure S5. ¹H NMR spectrum of Tert-butyl (6-bromohexyl)carbamate, Related to Scheme 2.

BocNHC6I 3

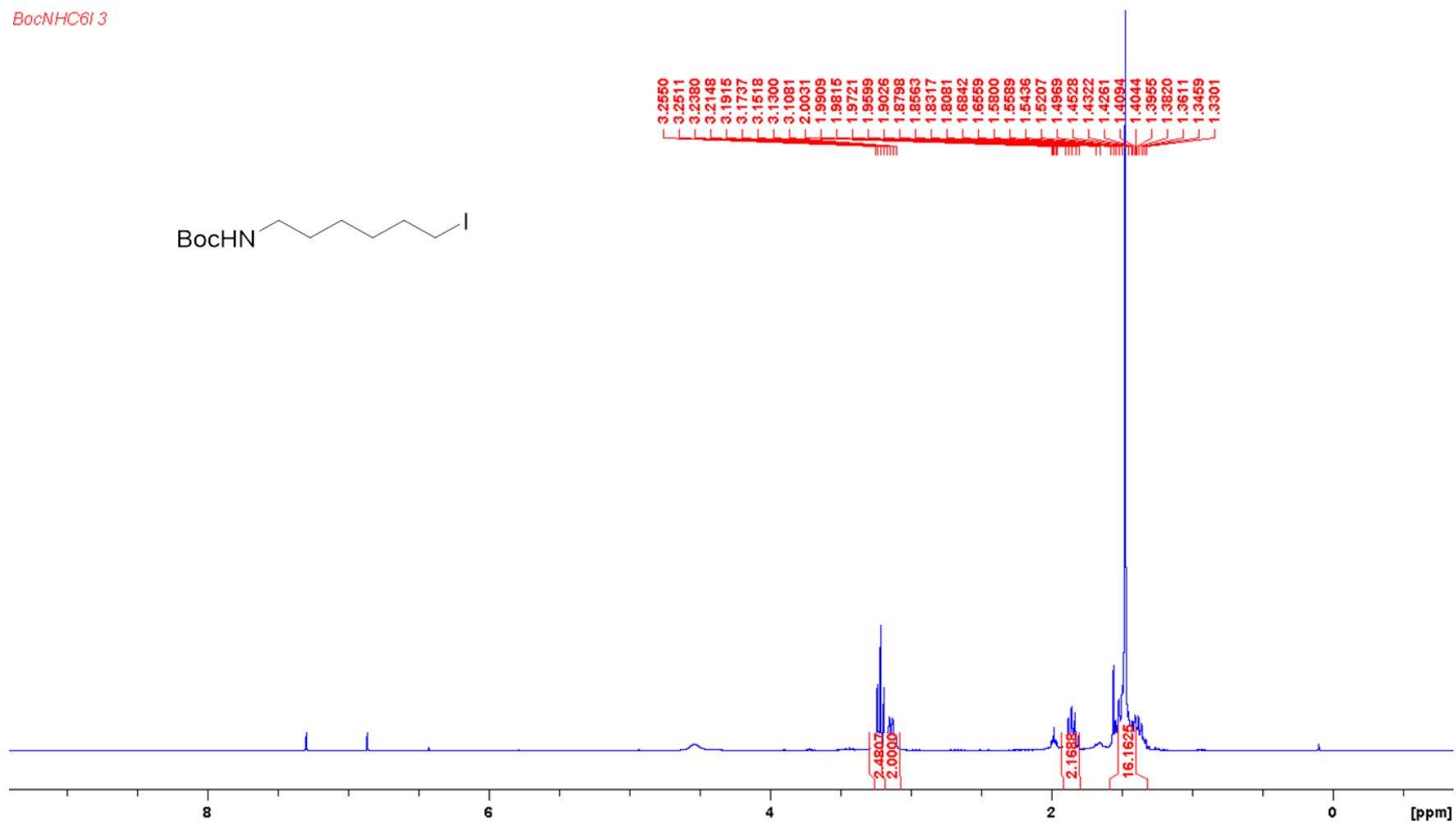
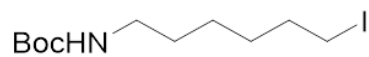


Figure S6. ¹H NMR spectrum of tert-butyl (6-iodohexyl)carbamate, Related to Scheme 2.

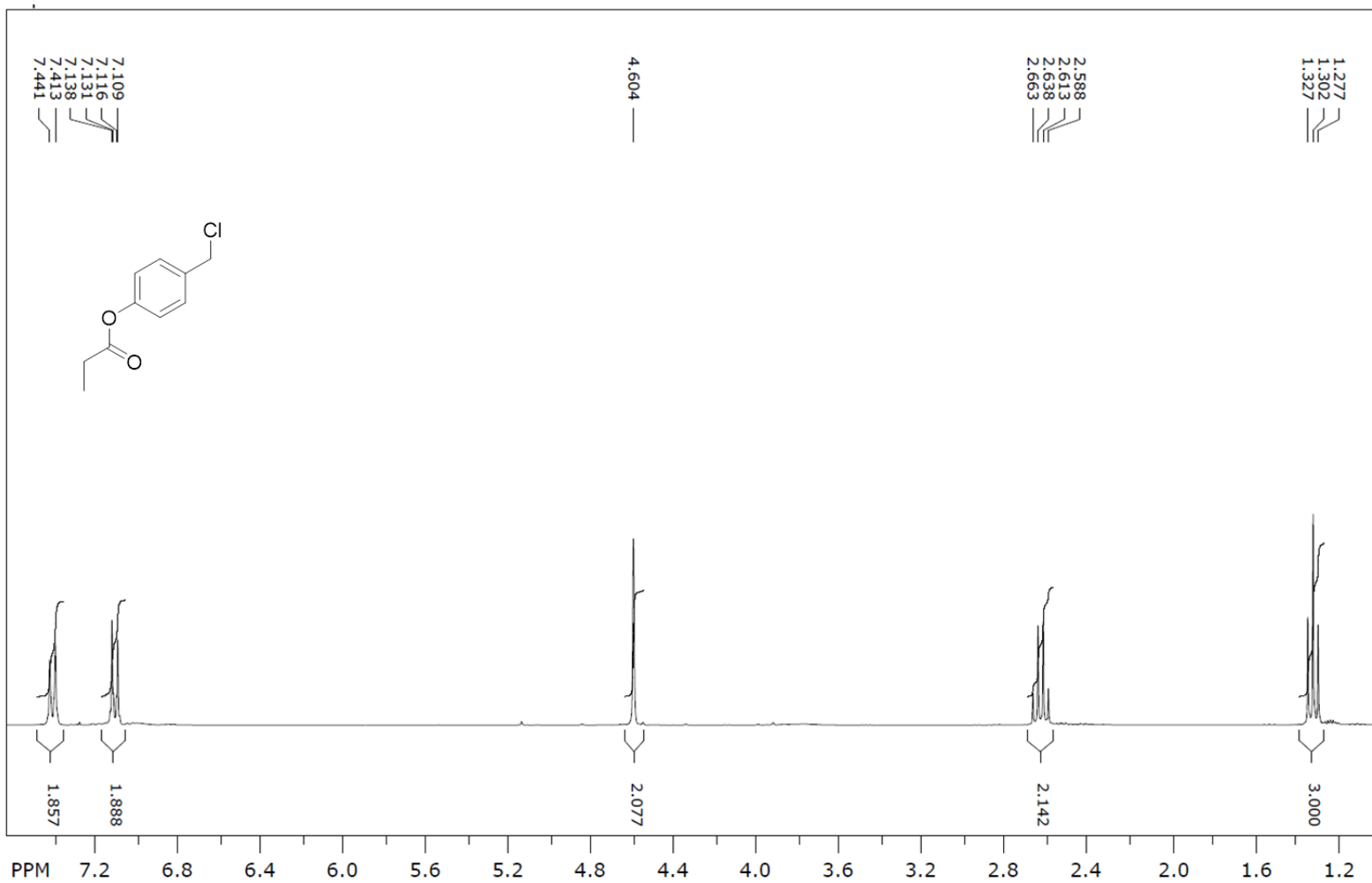


Figure S7. ¹H NMR spectrum of 4-(chloromethyl)phenyl propionate, Related to Scheme 2.

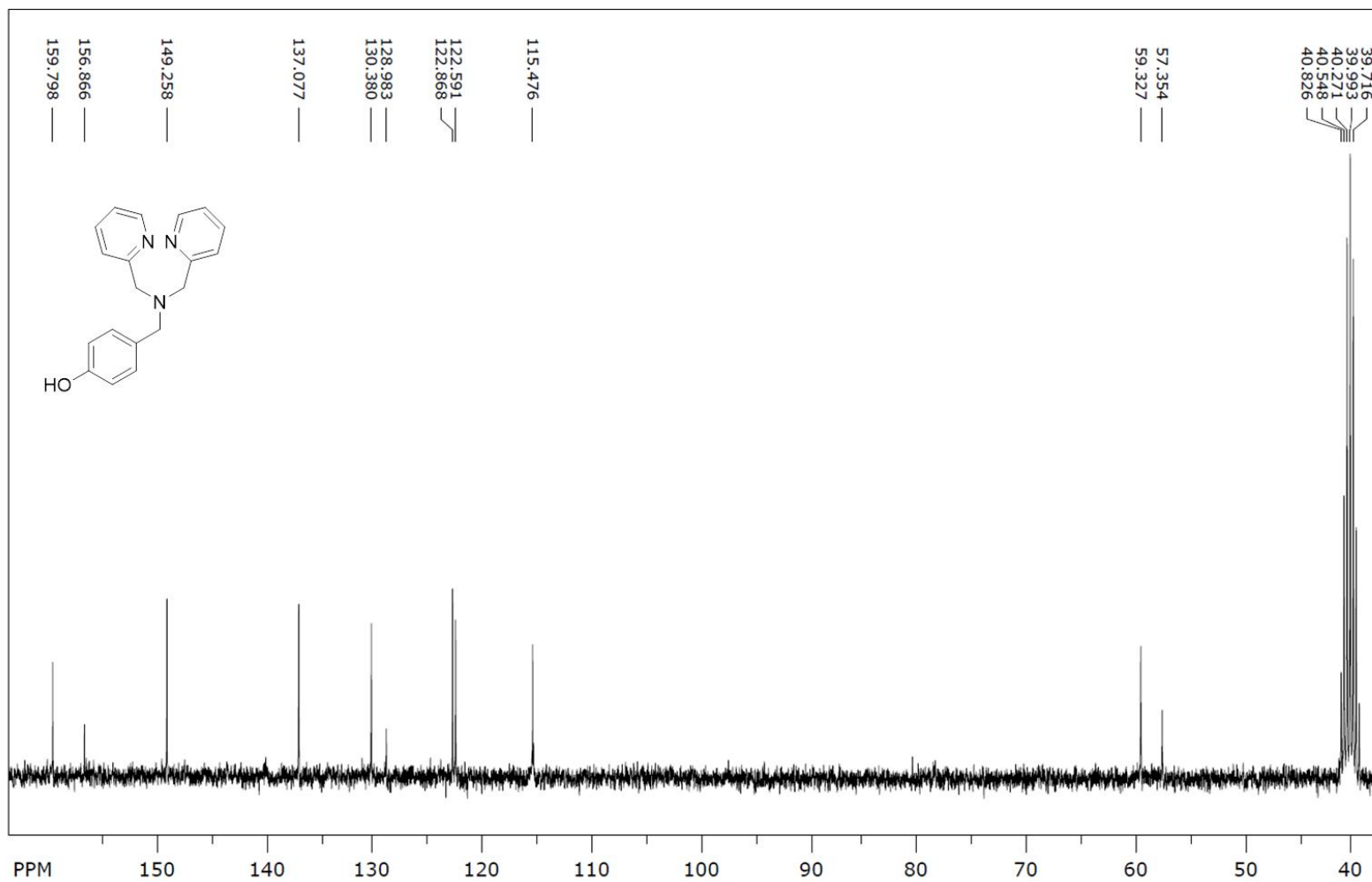


Figure S9. ¹³C NMR spectrum of 1DPAOH, Related to Scheme 2.

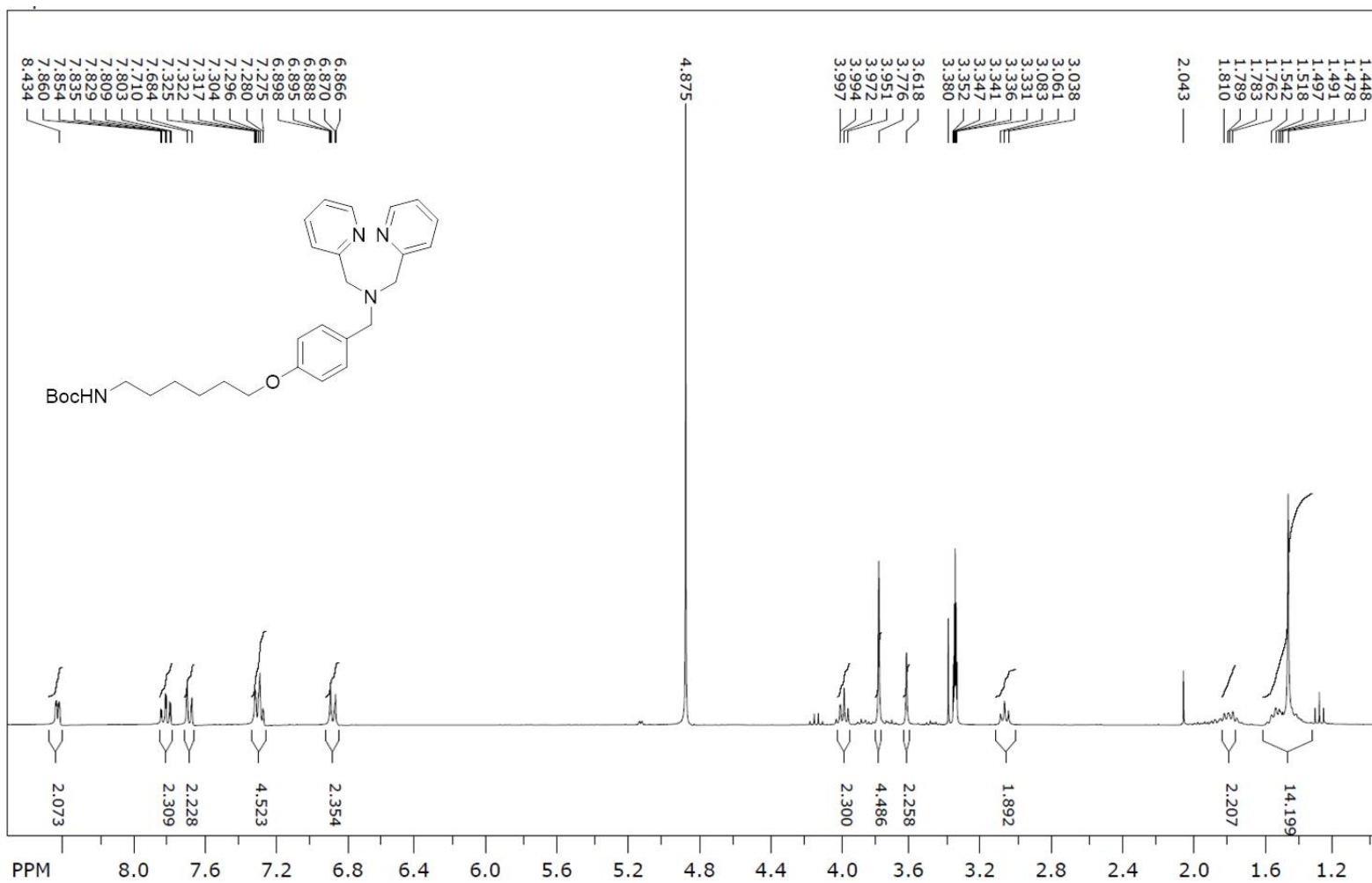


Figure S10. ¹H NMR spectrum of Ligand 1-Boc, Related to Scheme 2.

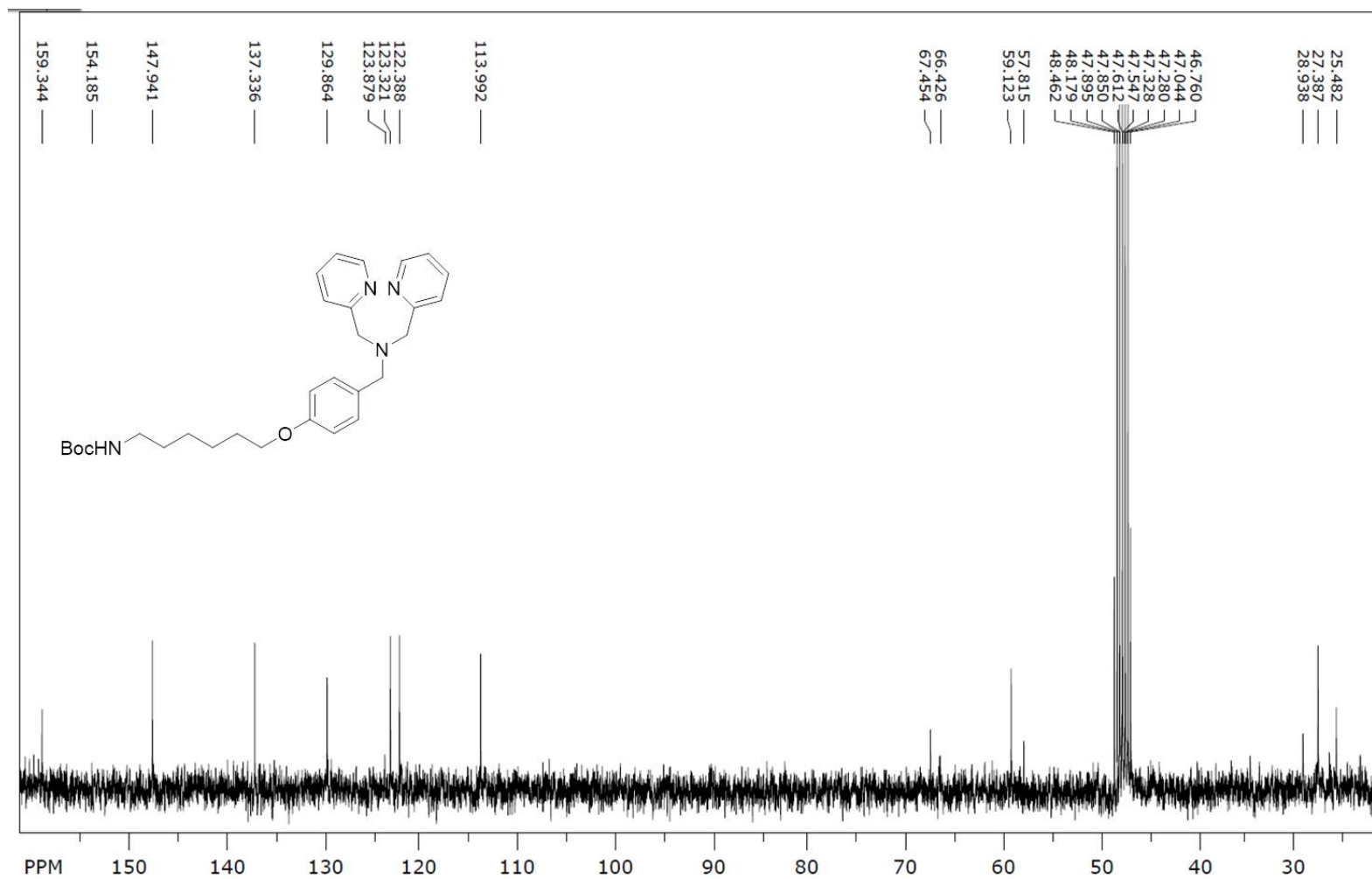


Figure S11. ^{13}C NMR spectrum of Ligand 1-Boc, Related to Scheme 2.

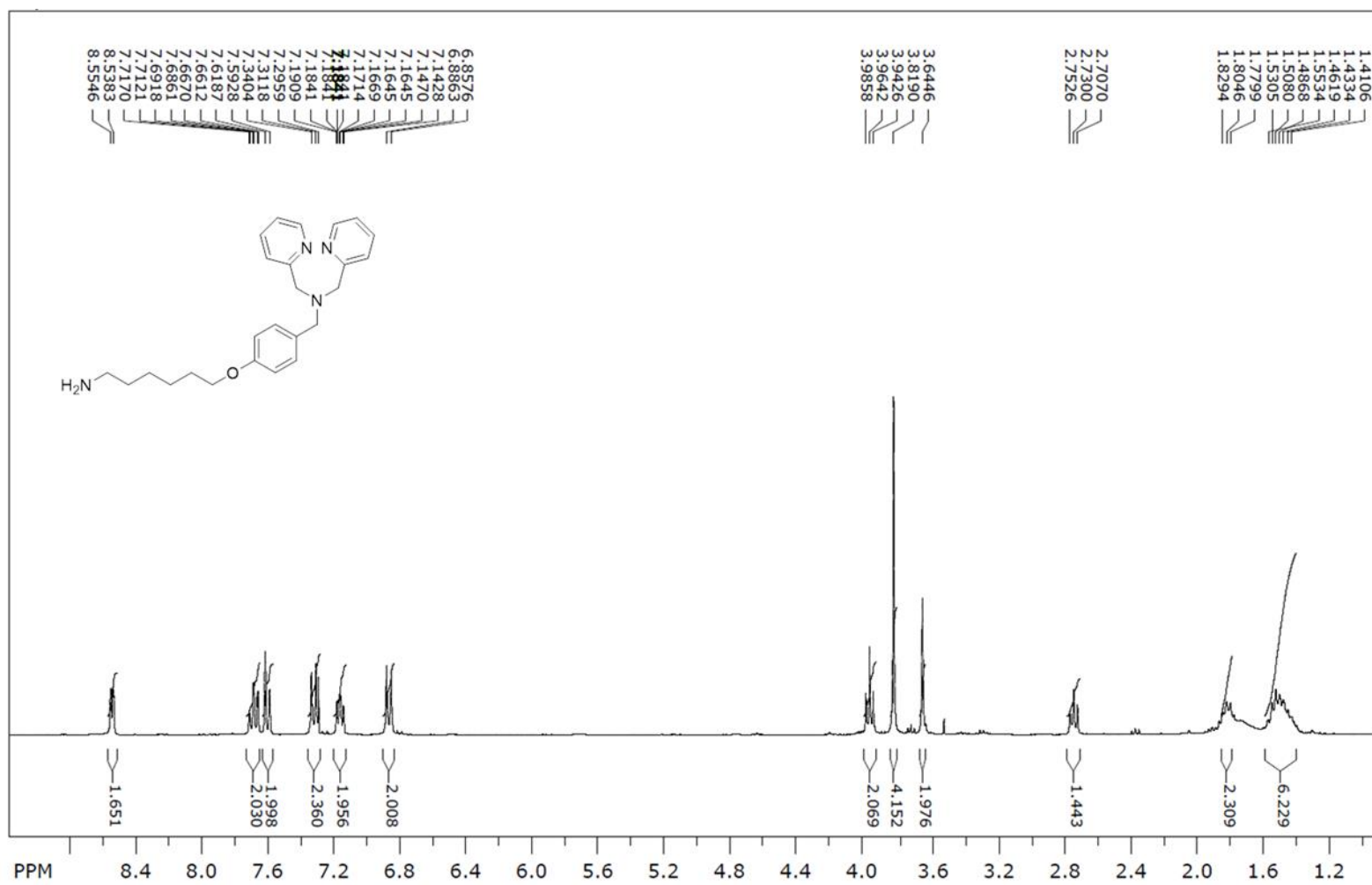


Figure S12. ¹H NMR spectrum of Ligand 1-NH₂, Related to Scheme 2.

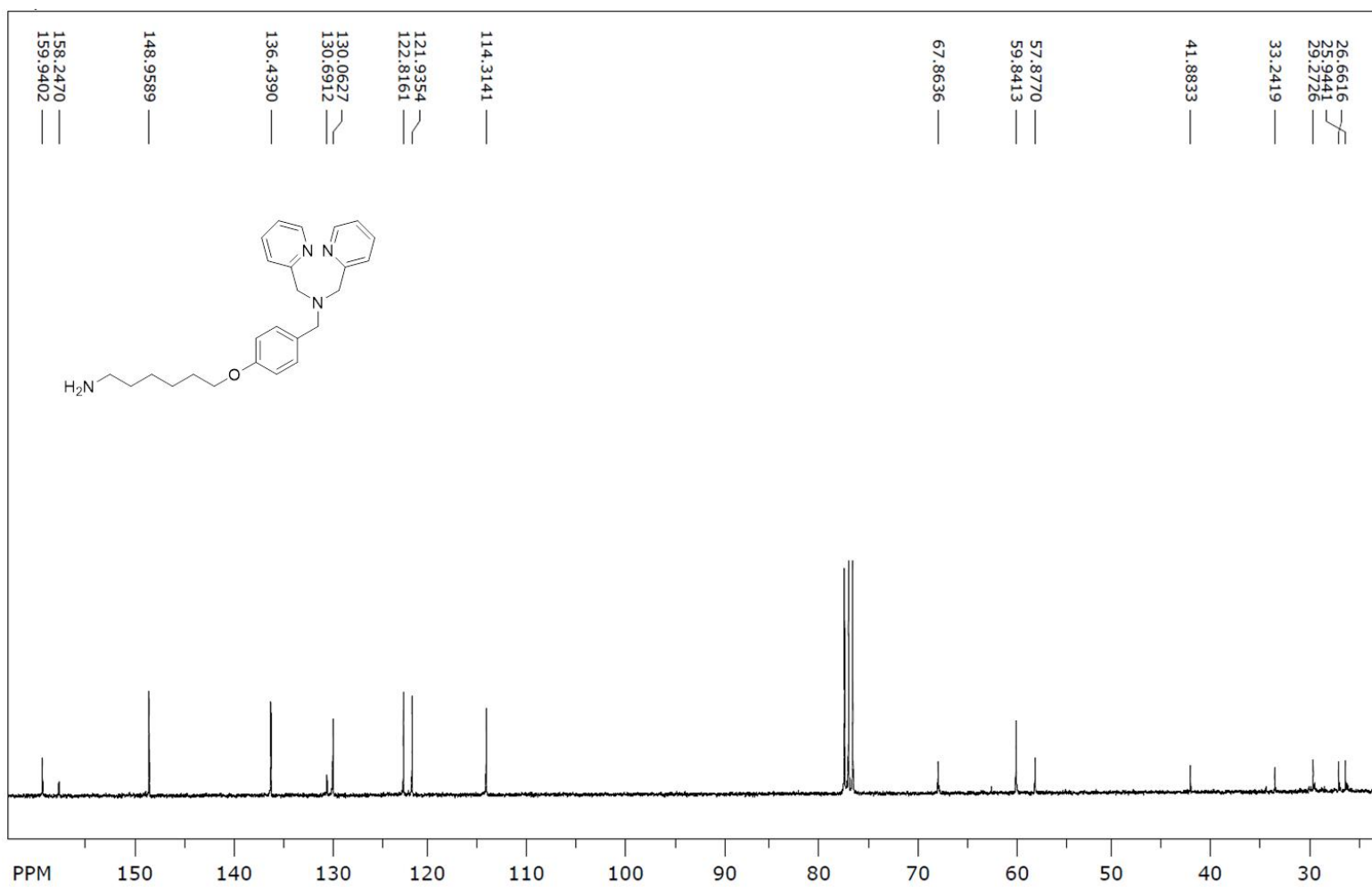


Figure S13. ¹³C NMR spectrum of Ligand 1-NH₂, Related to Scheme 2.

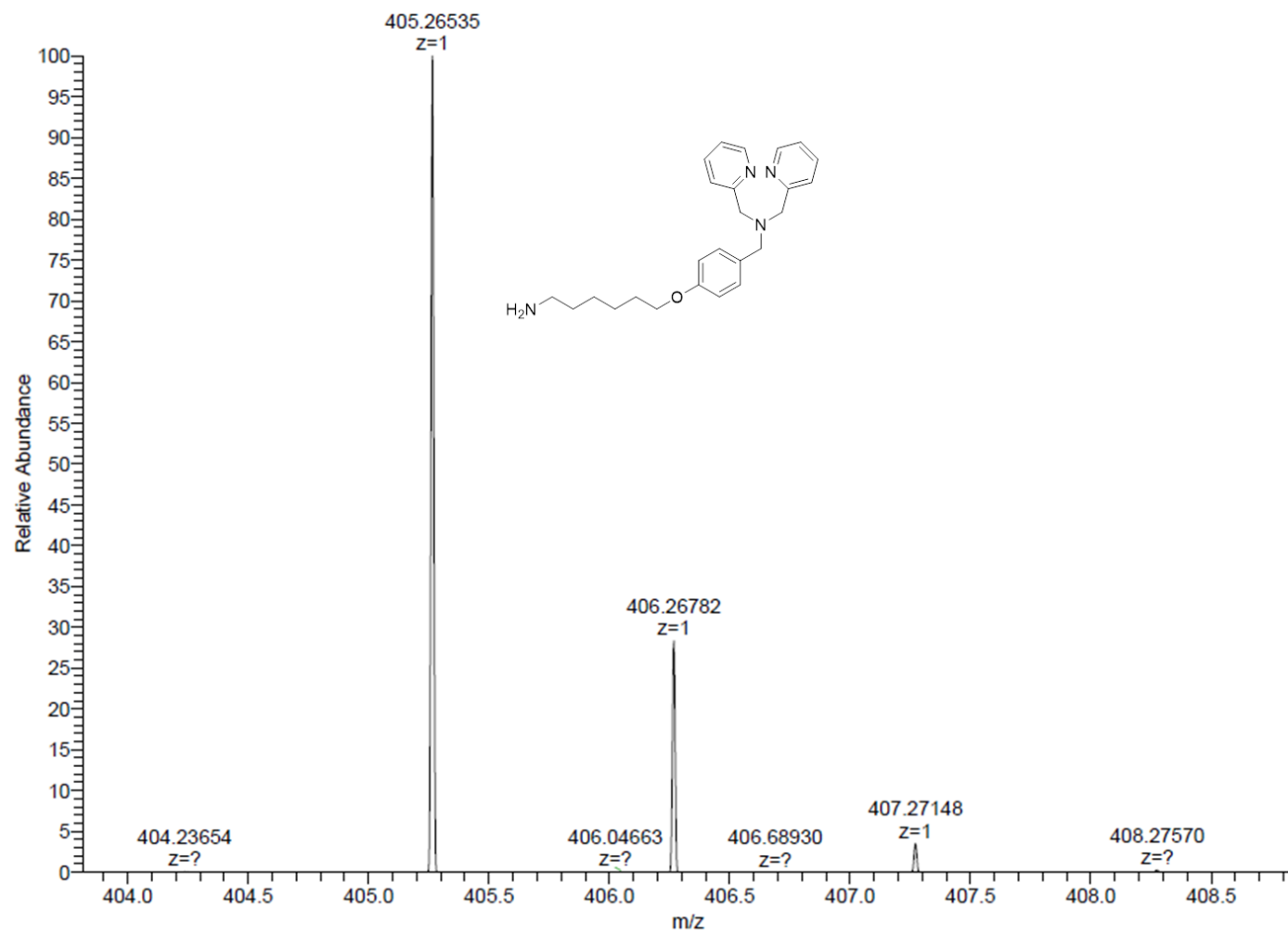


Figure S14. ESI-MS spectrum of Ligand 1-NH₂, Related to Scheme 2.

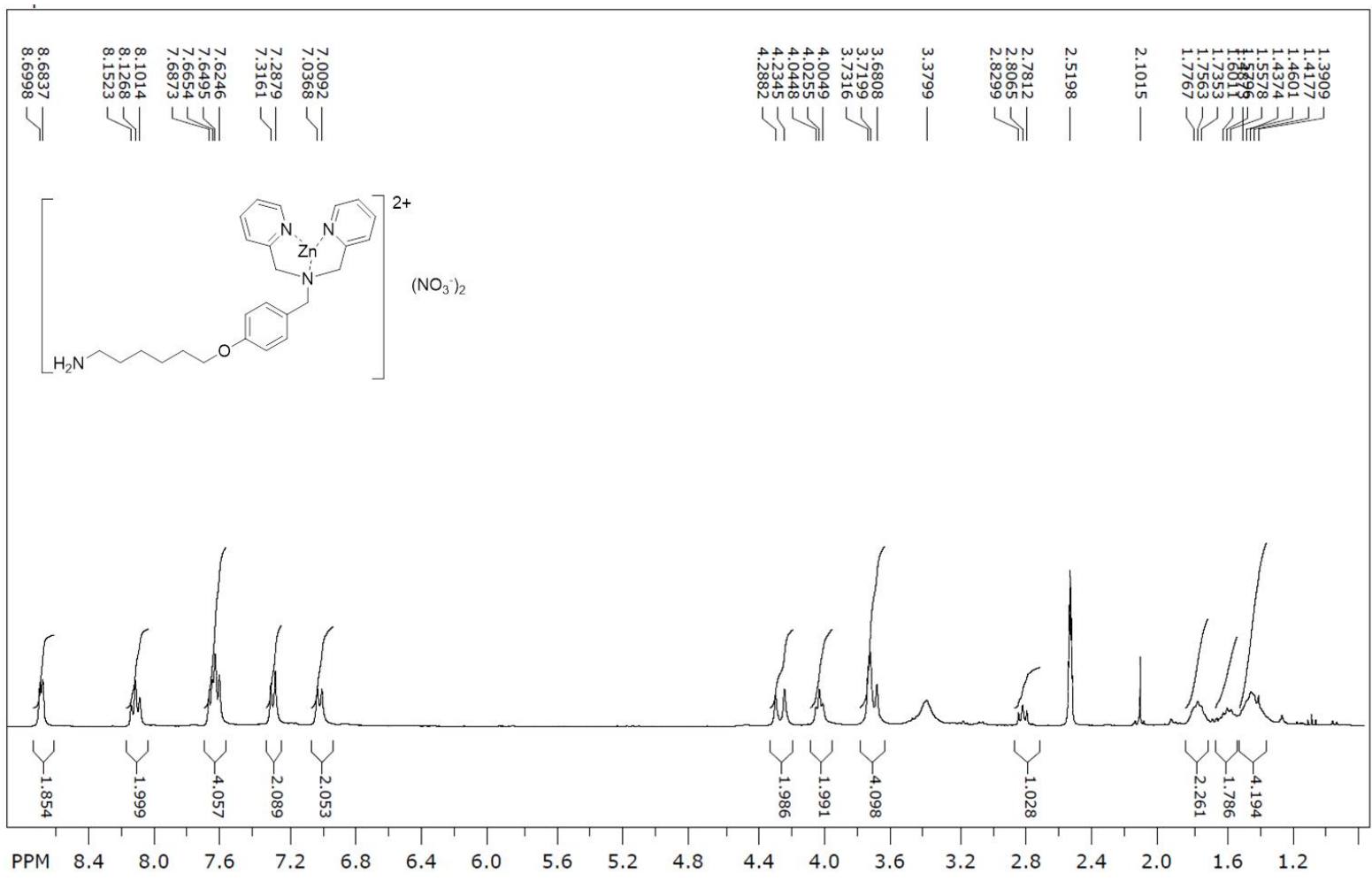


Figure S15. 1H NMR spectrum of C1, Related to Scheme 2.

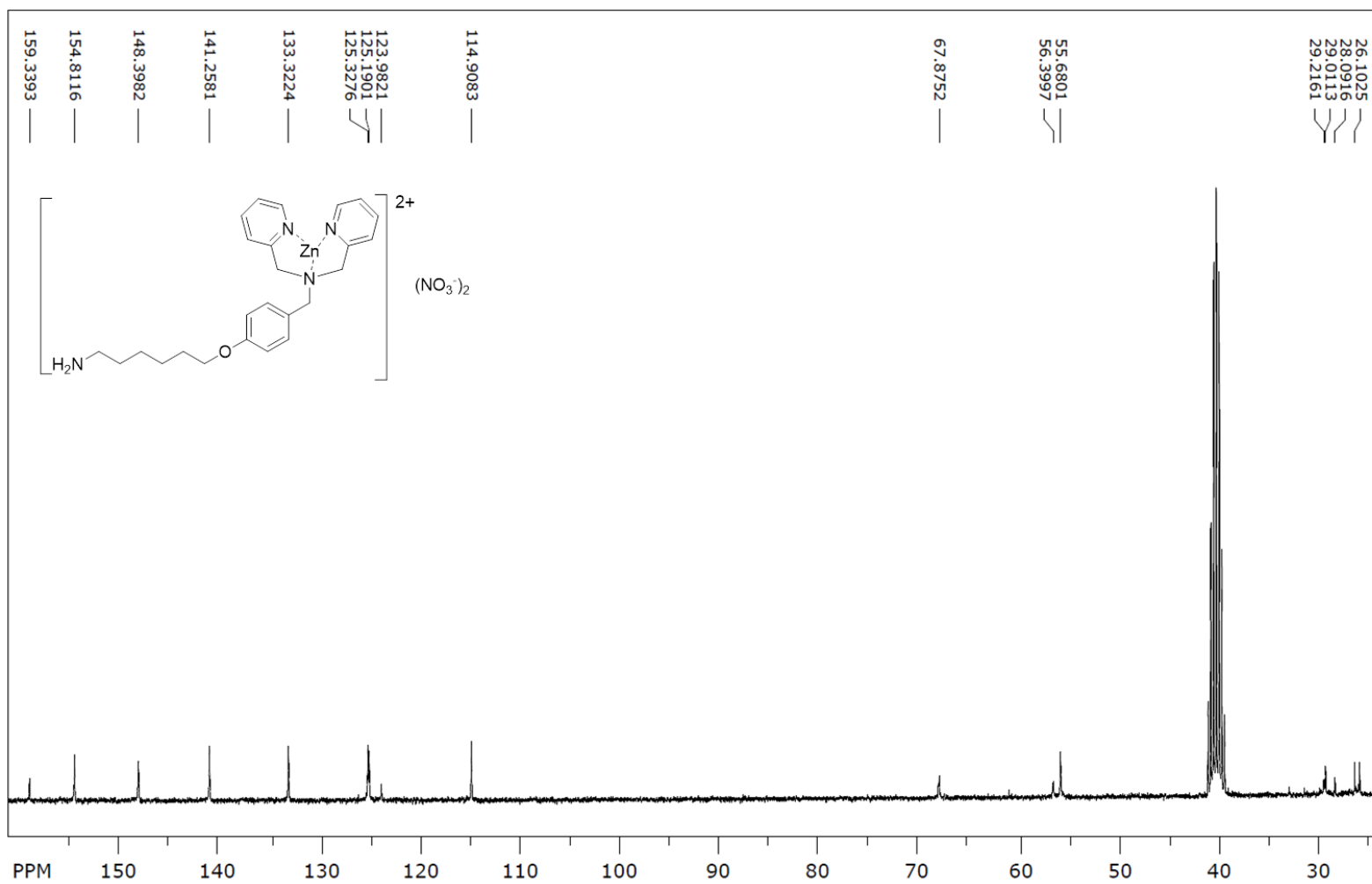


Figure S16. ^{13}C NMR spectrum of C1, Related to Scheme 2.

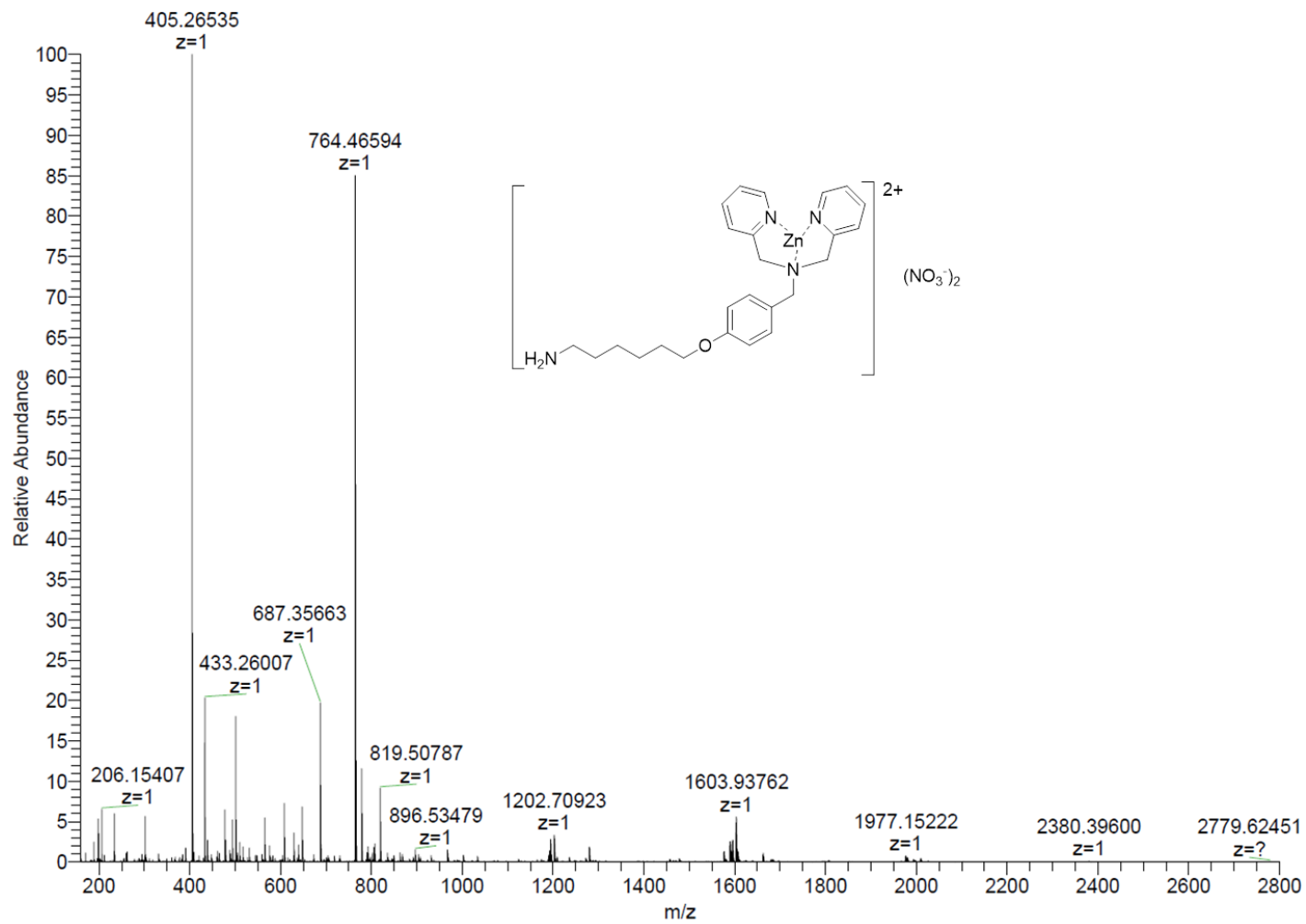


Figure S17. ESI-MS spectrum of C1, Related to Scheme 2.

181030-Exac-6255-Ro-JQJ-C1 #1-28 RT: 0.03-0.44 AV: 28 NL: 4.20E6
T: FTMS + p ESI Full ms [100.00-2000.00]

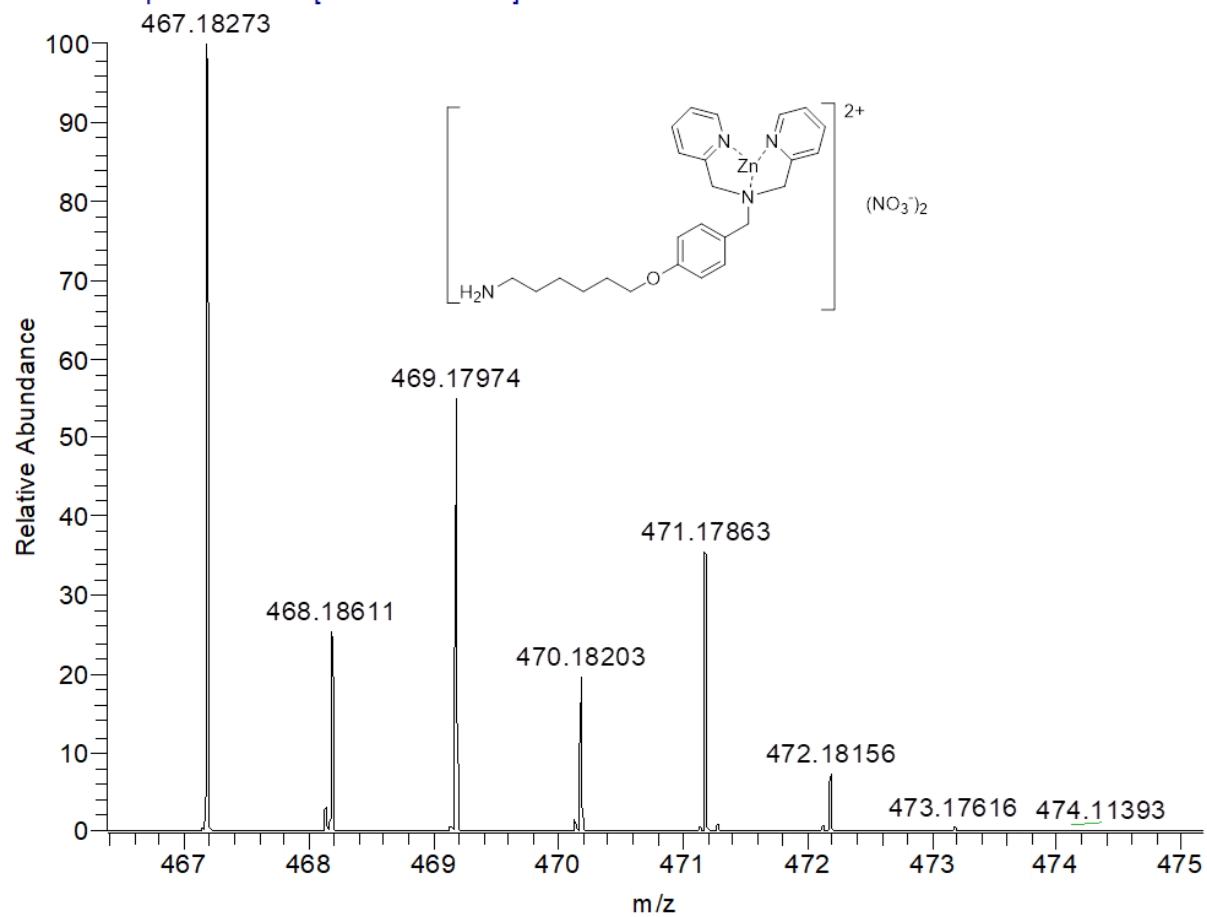


Figure S18. ESI-MS spectrum of C1, Related to Scheme 2.

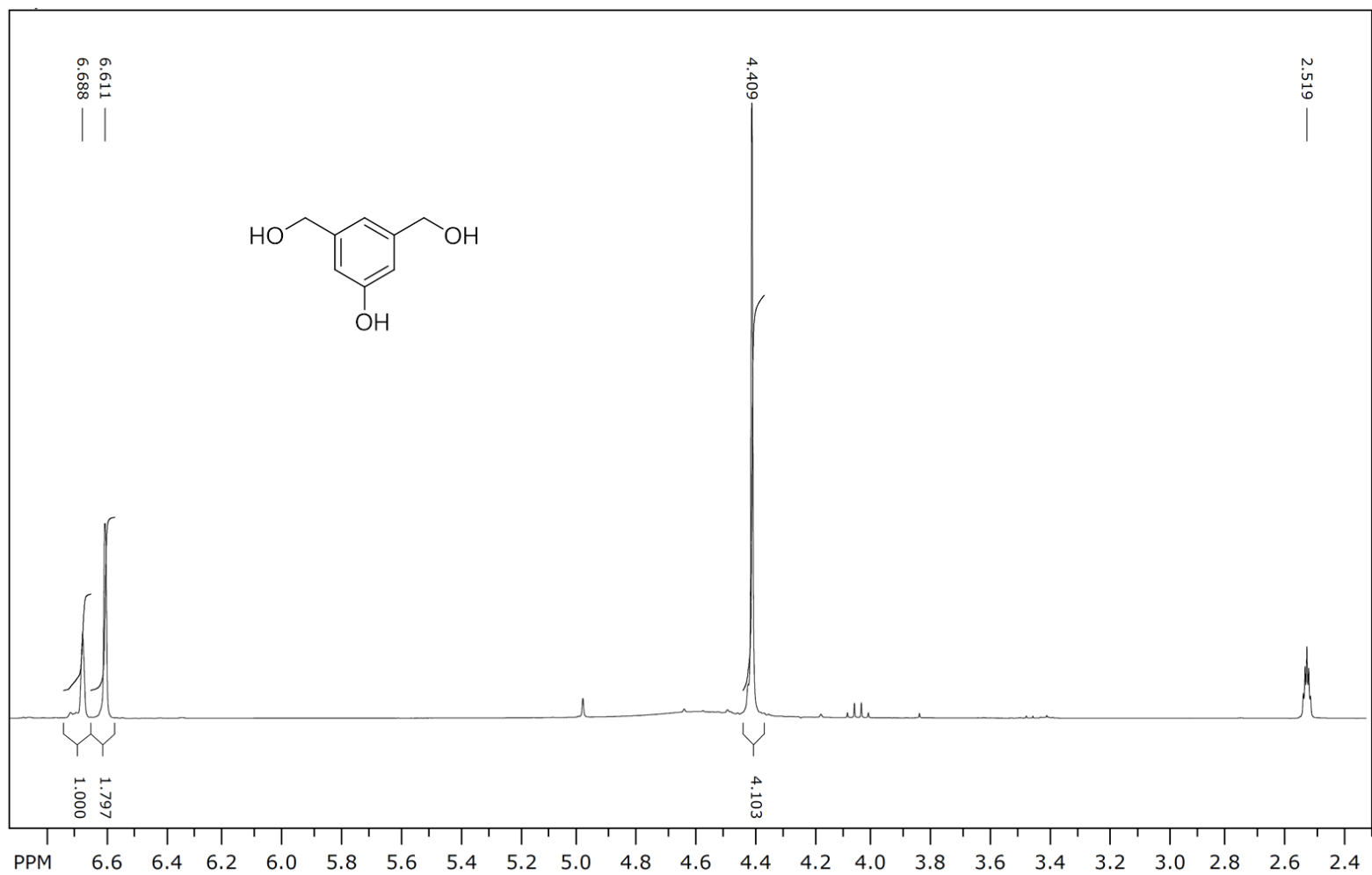


Figure S19. ¹H NMR spectrum of (5-hydroxy-1,3-phenylene)dimethanol, Related to Scheme 2.

BrMe2PhOH 12th

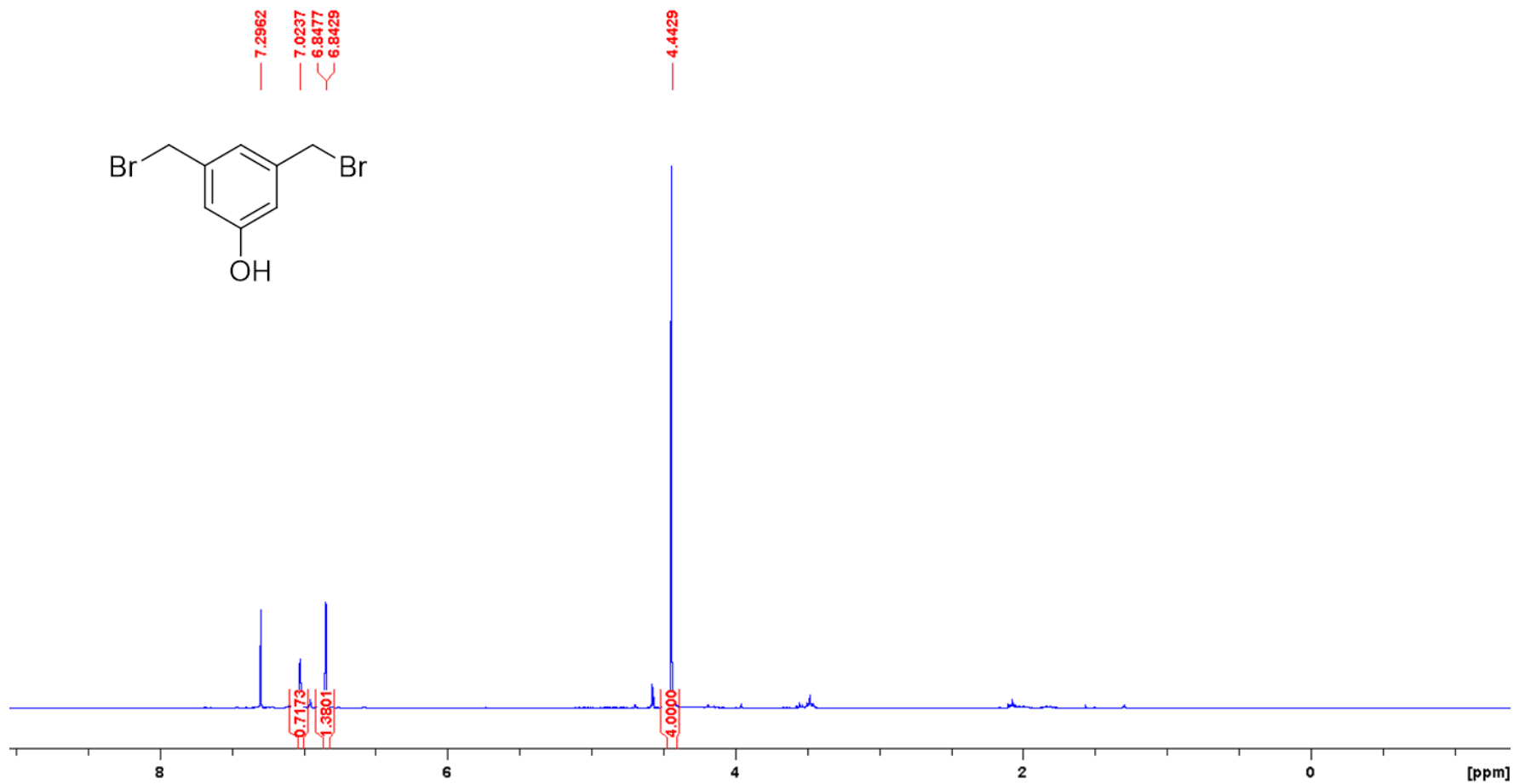


Figure S20. ¹H NMR spectrum of 3,5-bis(bromomethyl)phenol, Related to Scheme 2.

2DPA-Ph-OH 6

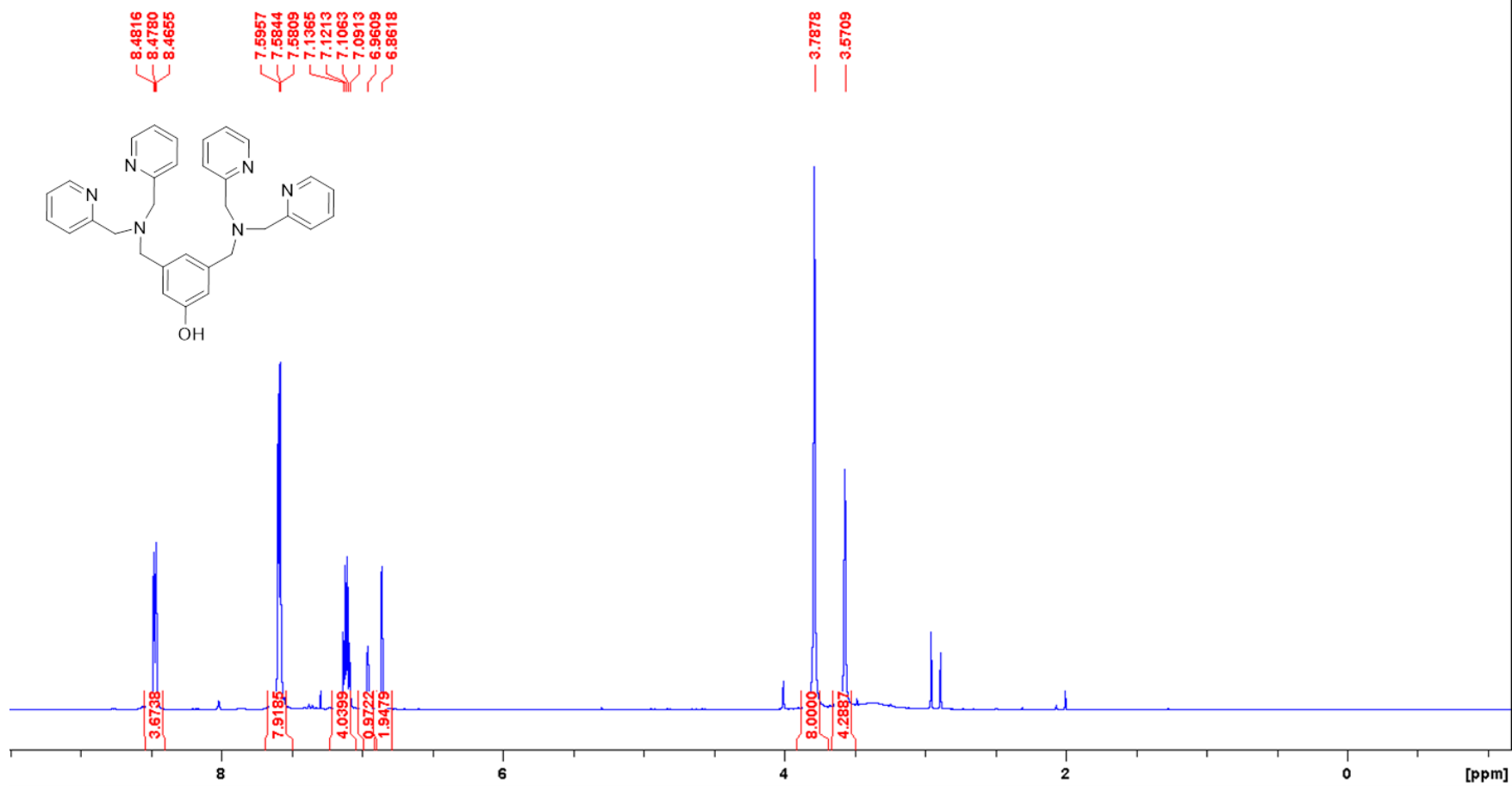


Figure S21. ¹H NMR spectrum of 2DPAOH, Related to Scheme 2.

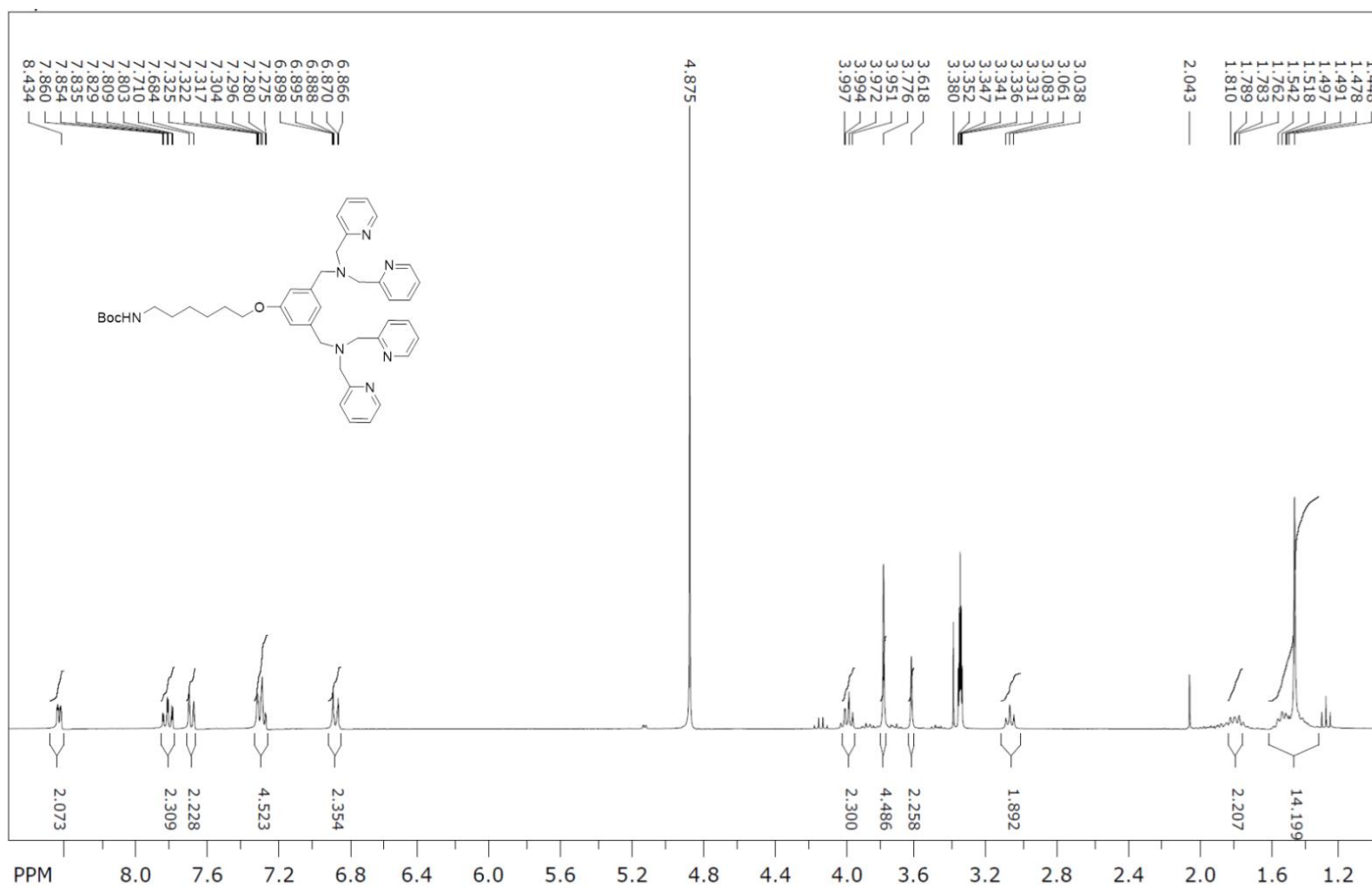


Figure S22. ¹H NMR spectrum of Ligand 2-Boc, Related to Scheme 2.

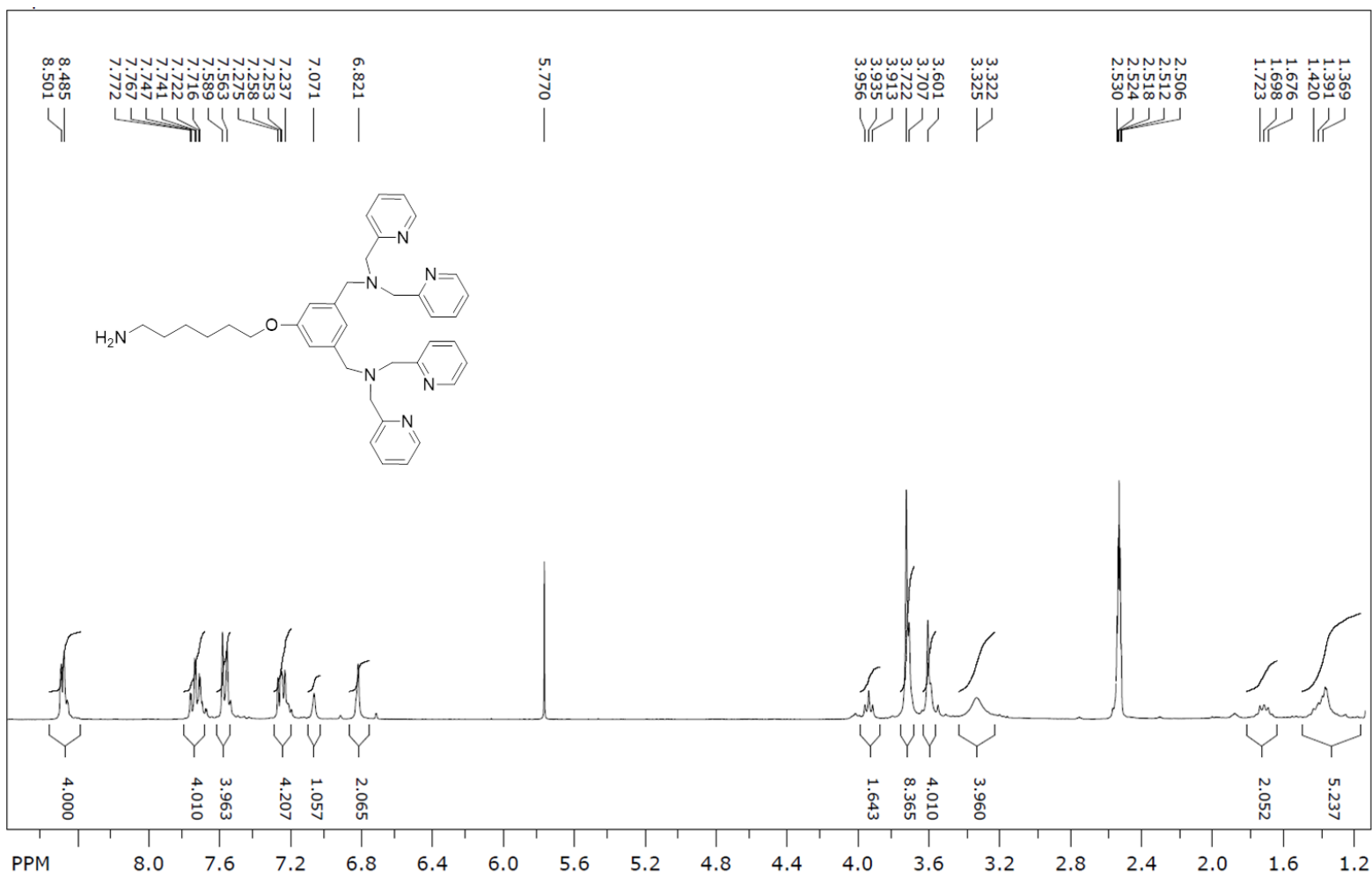


Figure S23. ¹H NMR spectrum of Ligand 2-NH₂, Related to Scheme 2.

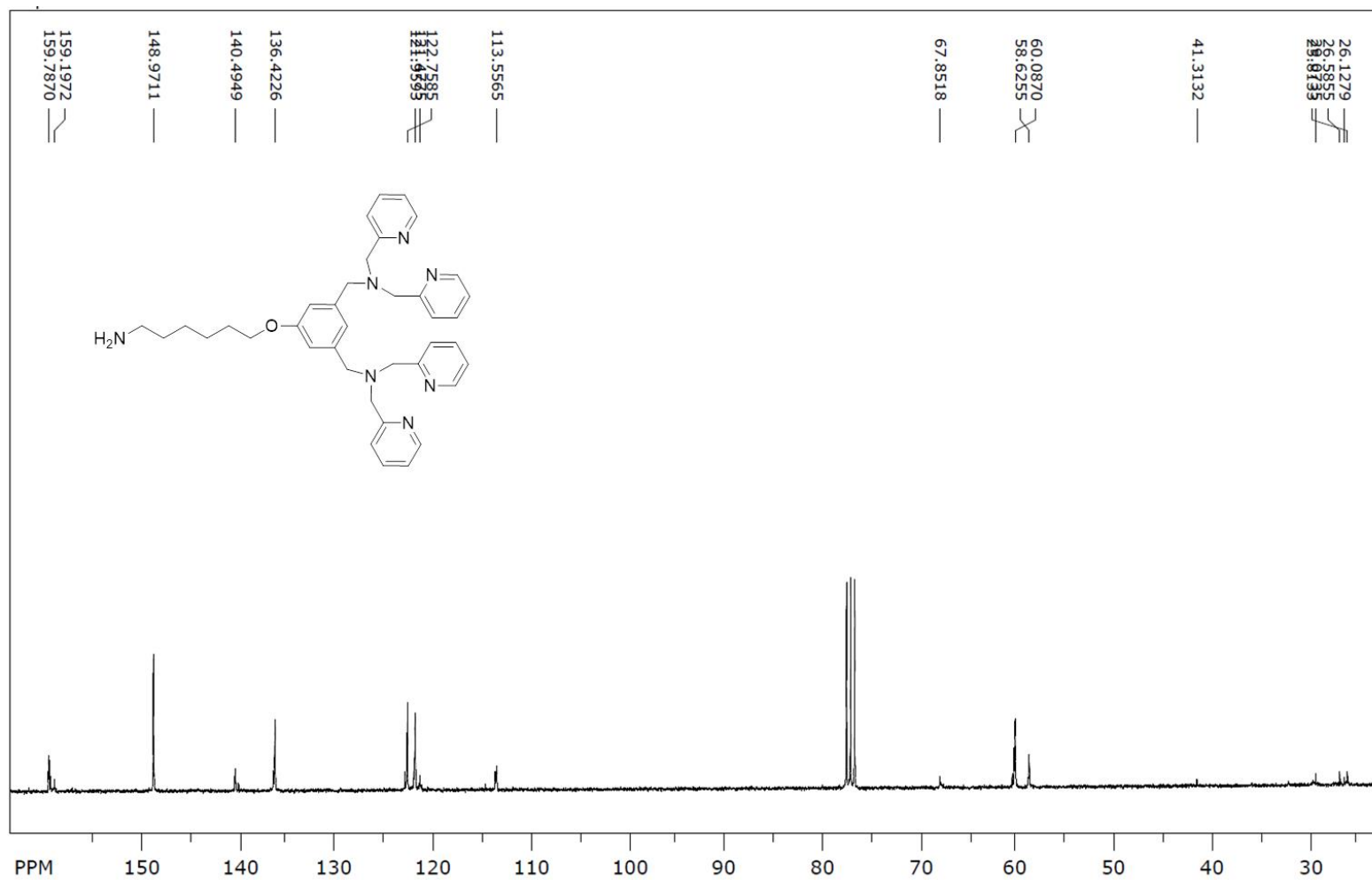


Figure S24. ¹³C NMR spectrum of Ligand 2-NH₂, Related to Scheme 2.

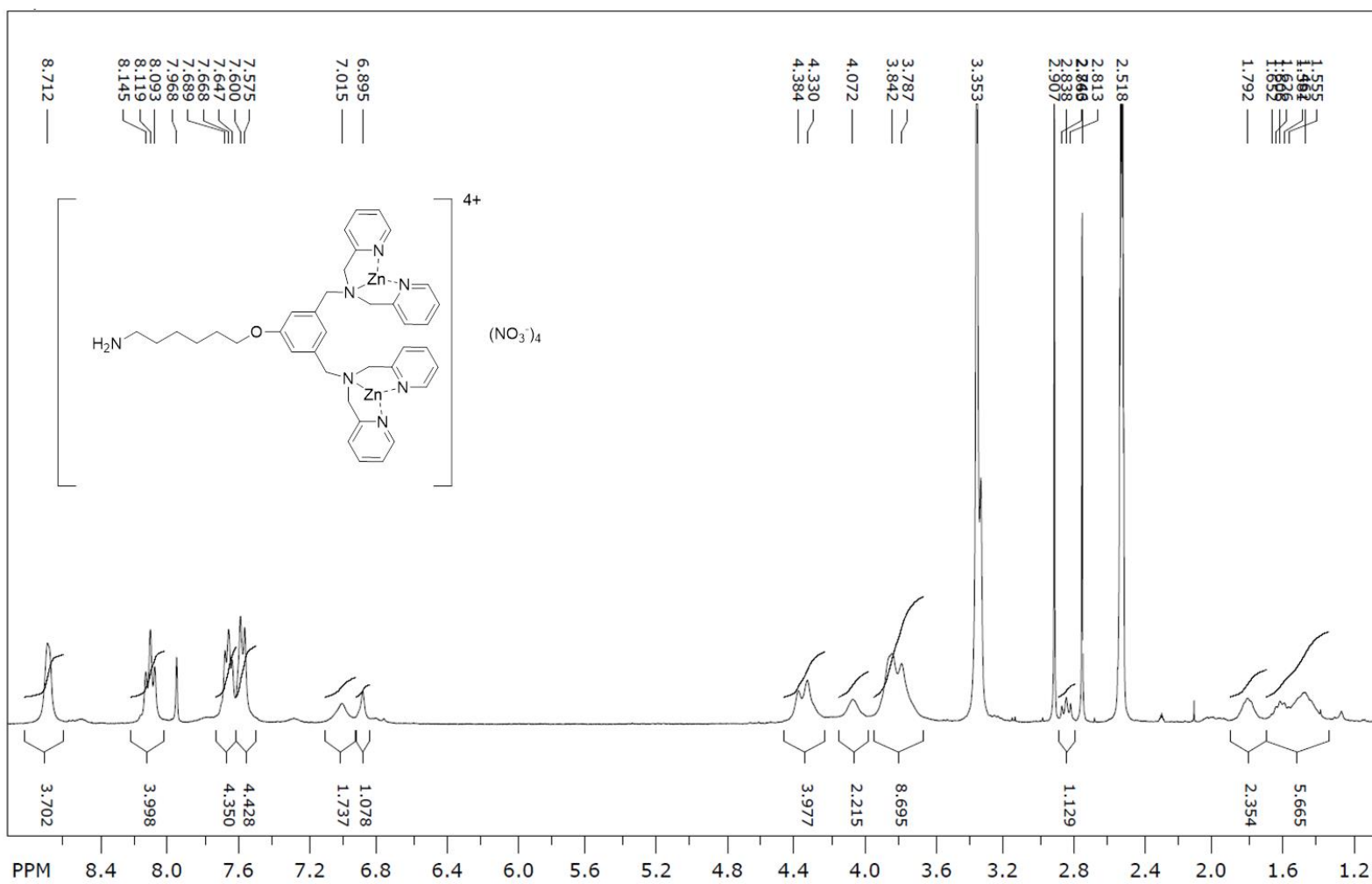


Figure S25. ¹H NMR spectrum of C2, Related to Scheme 2.

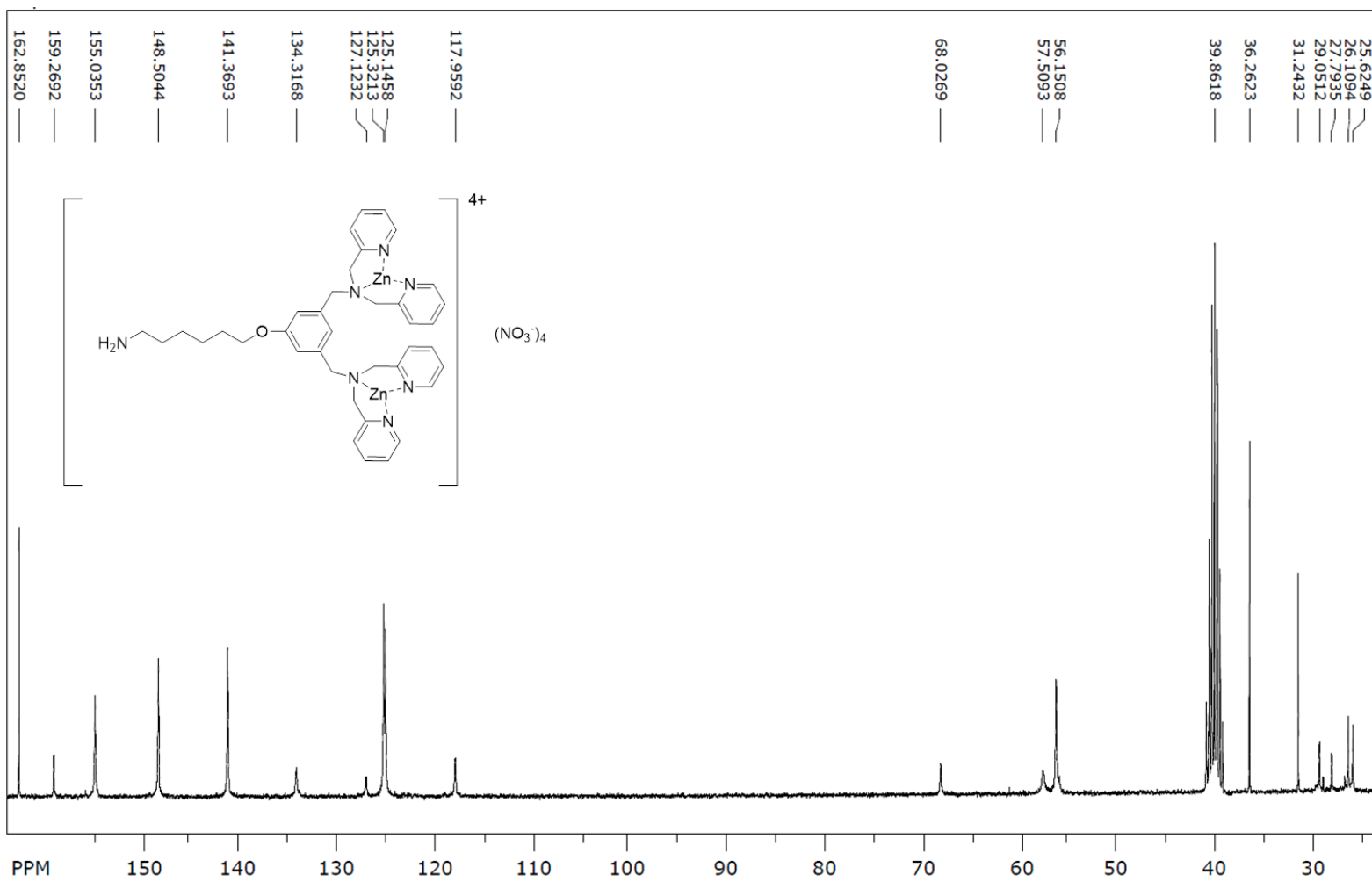


Figure S26. ^{13}C NMR spectrum of C2, Related to Scheme 2.

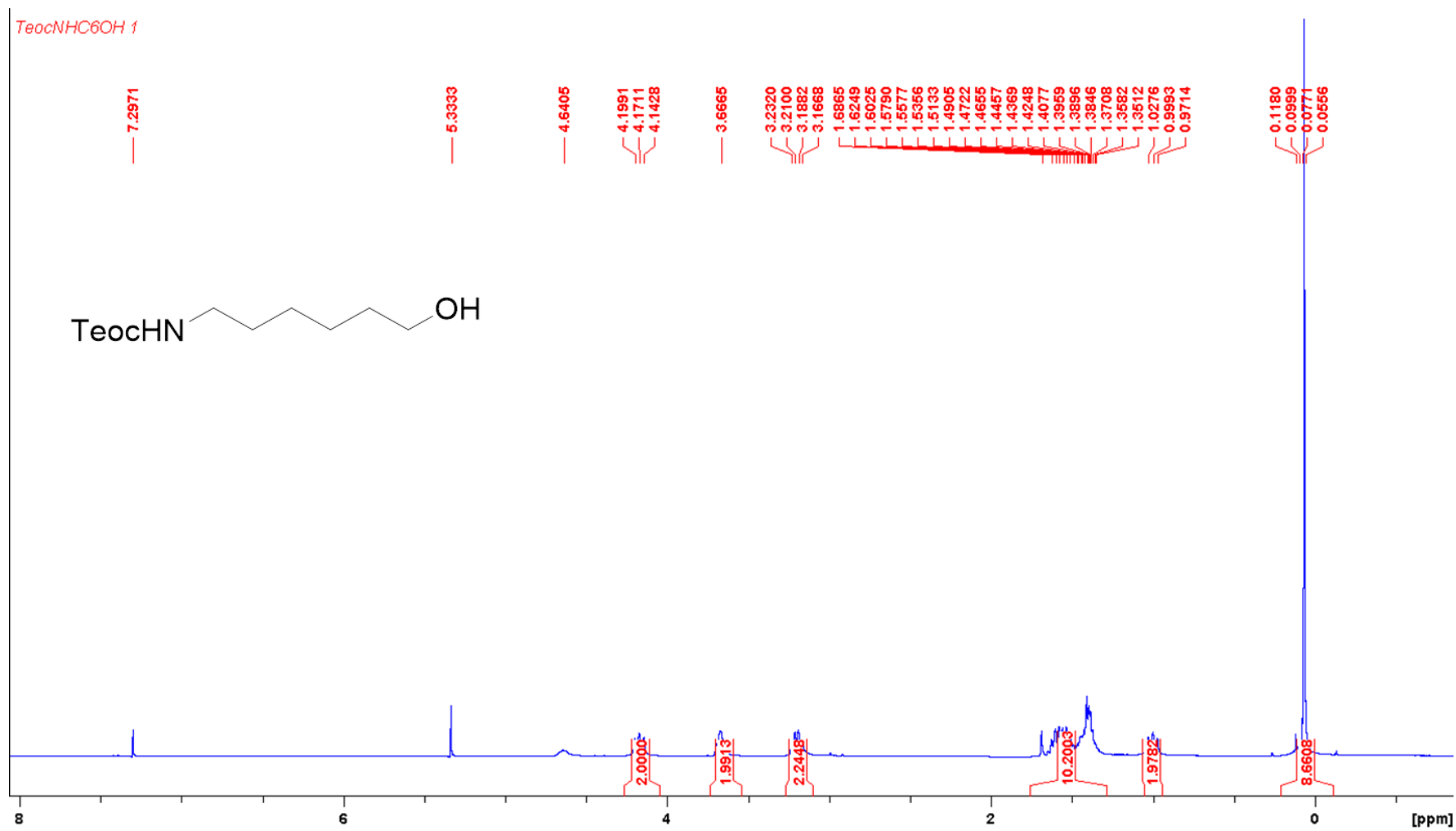


Figure S27. ^1H NMR spectrum of 2-(trimethylsilyl)ethyl (6-hydroxyhexyl)carbamate, Related to Scheme 2.

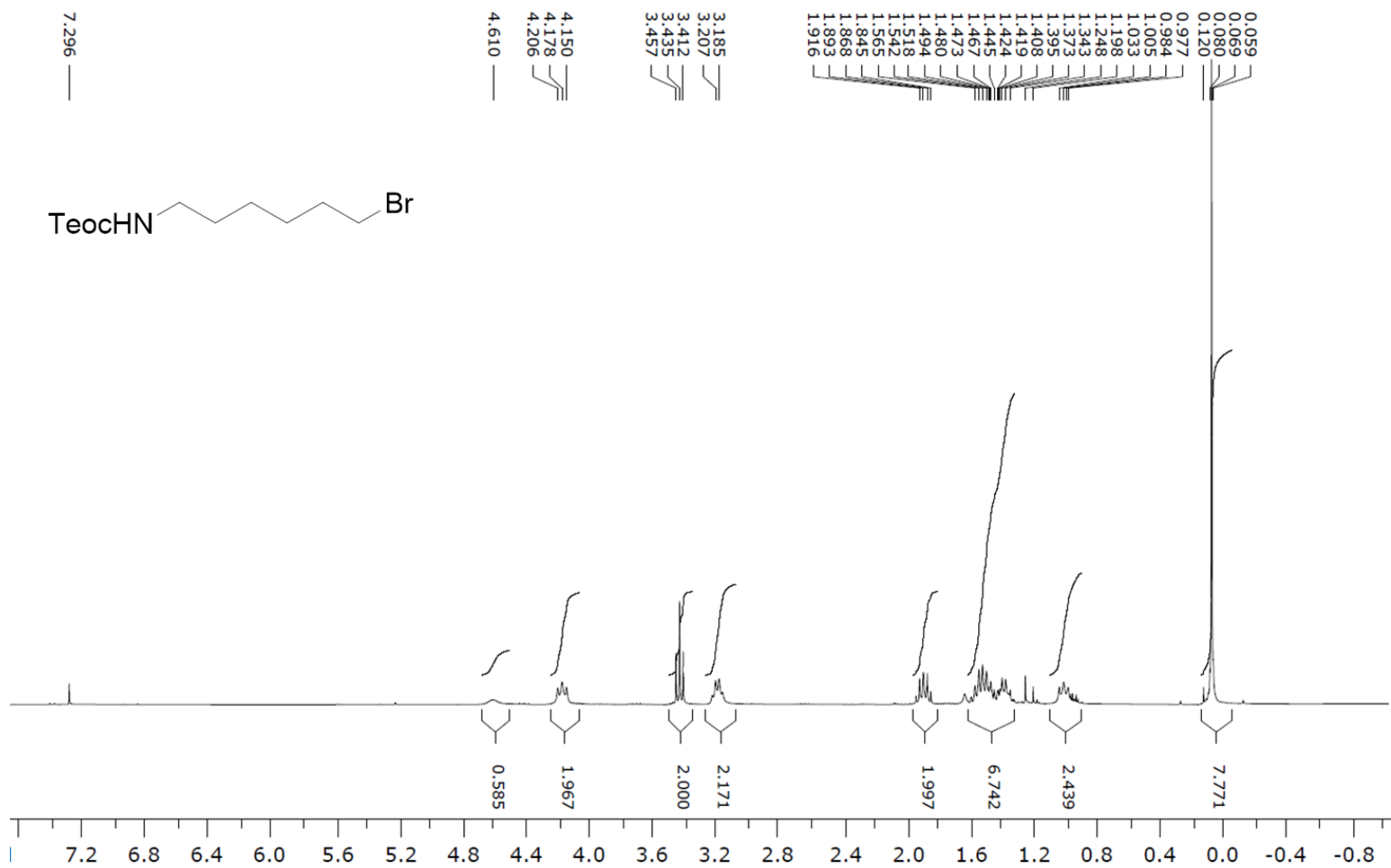


Figure S28. ^1H NMR spectrum of 2-(trimethylsilyl)ethyl (6-bromoxyhexyl)carbamate Related to Scheme 2.

TeocNHC6l 1

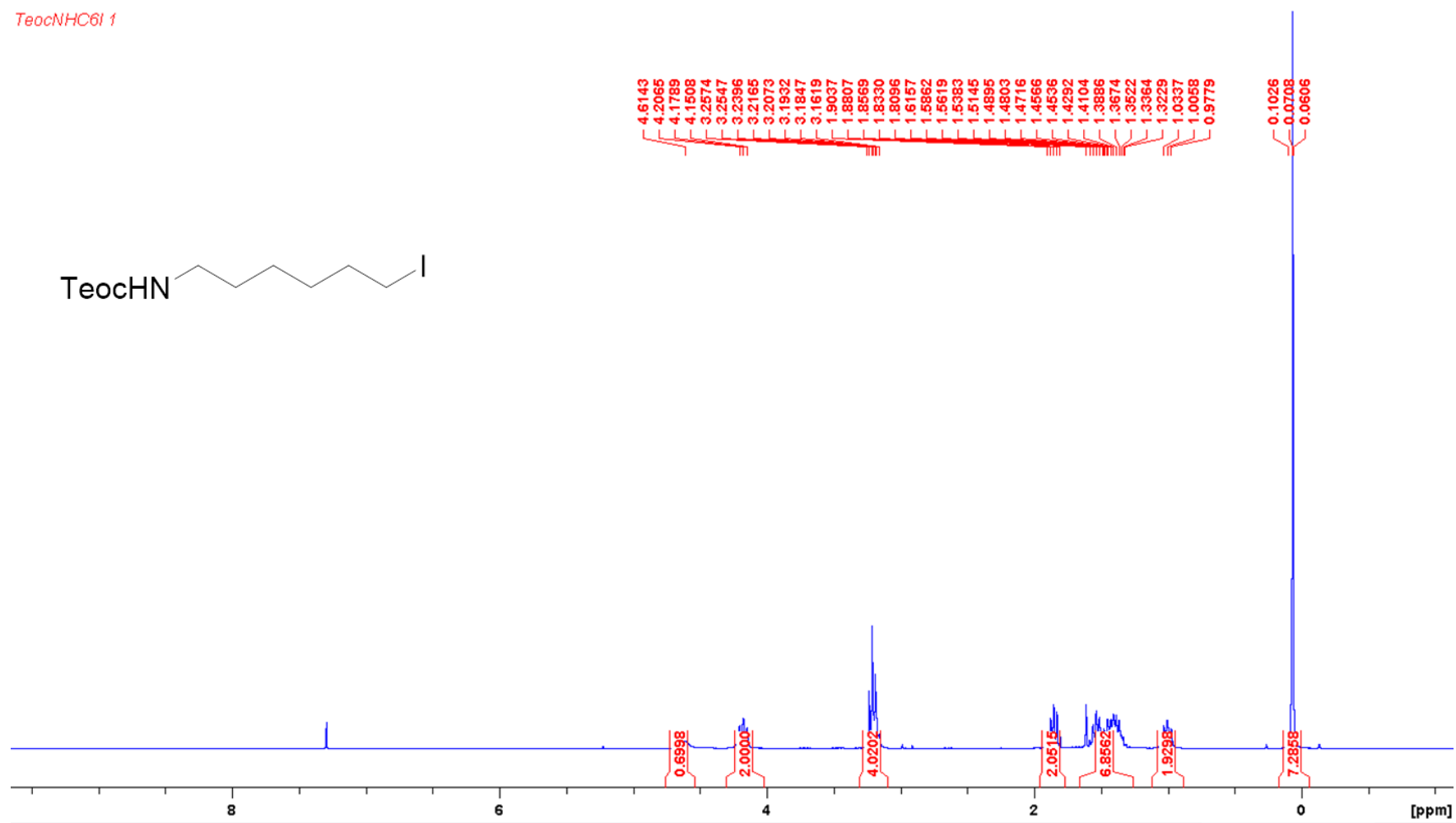


Figure S29. ¹H NMR spectrum of 2-(trimethylsilyl)ethyl (6-iodohexyl)carbamate Related to Scheme 2.

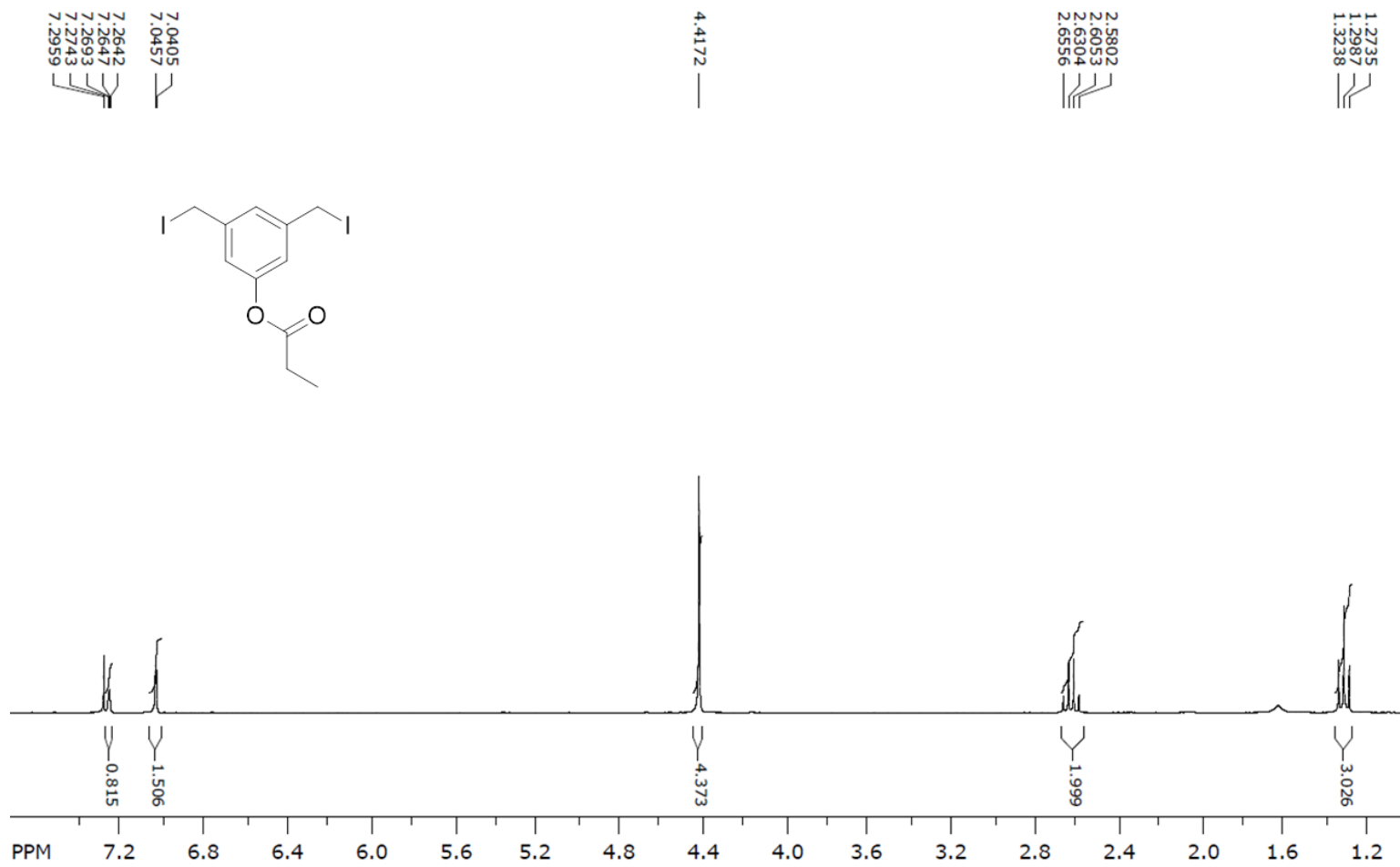


Figure S30. ¹H NMR spectrum of 3,5-bis(iodomethyl)phenyl propionate Related to Scheme 2.

4DPA-OH 5

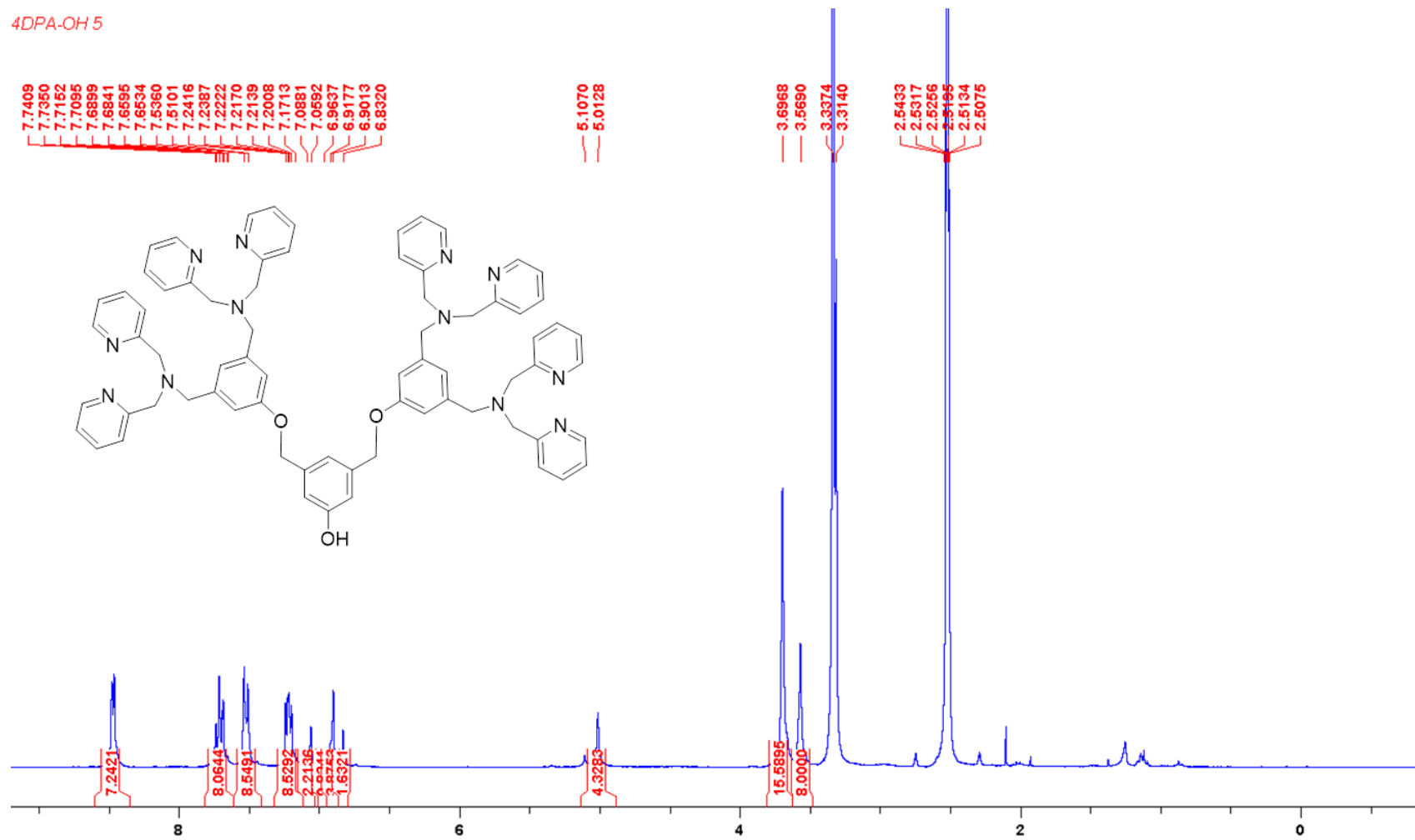


Figure S31. ¹H NMR spectrum of 4DPAOH Related to Scheme 2.

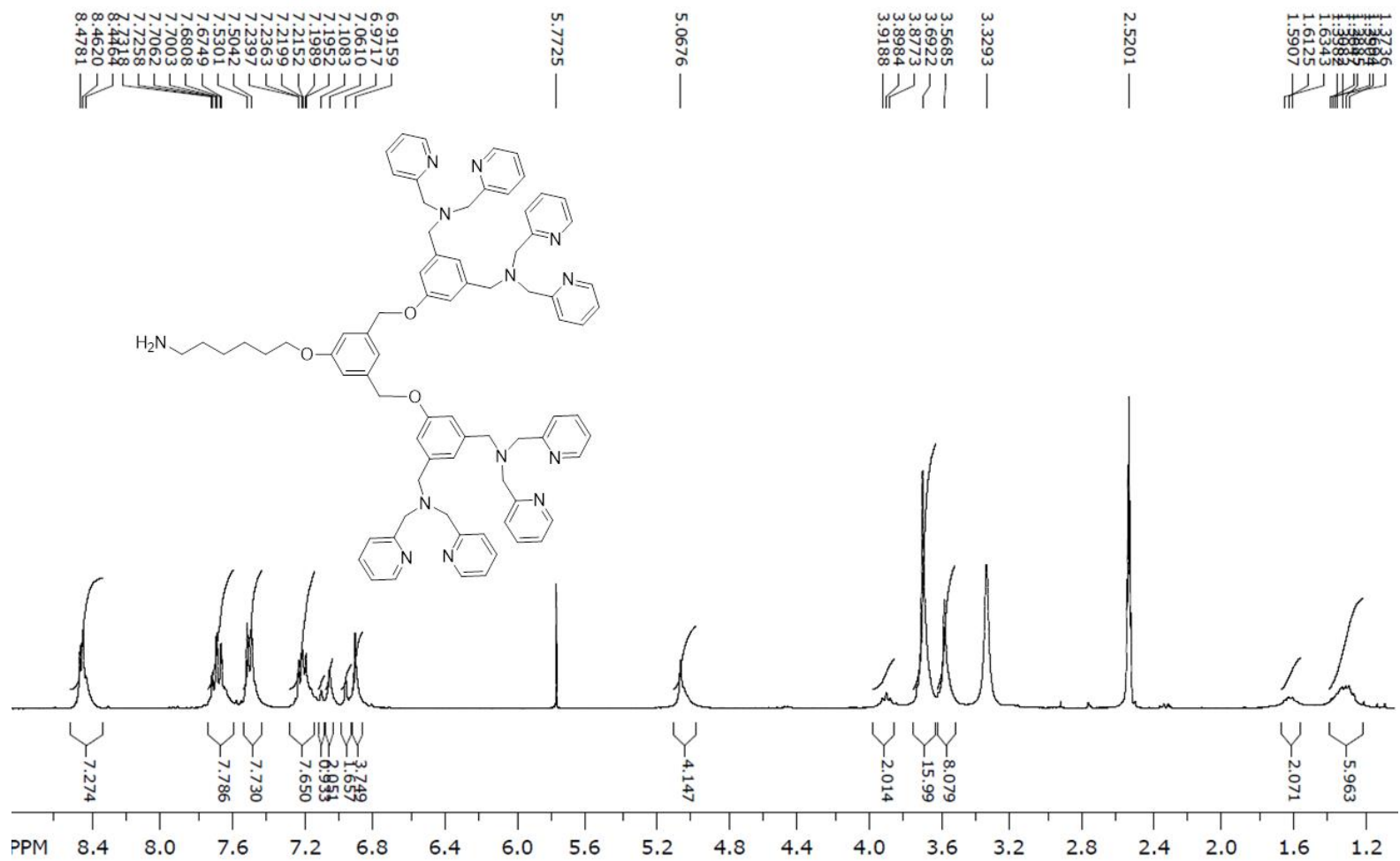


Figure S34. ¹H NMR spectrum of Ligand 4-NH₂, Related to Scheme 2.

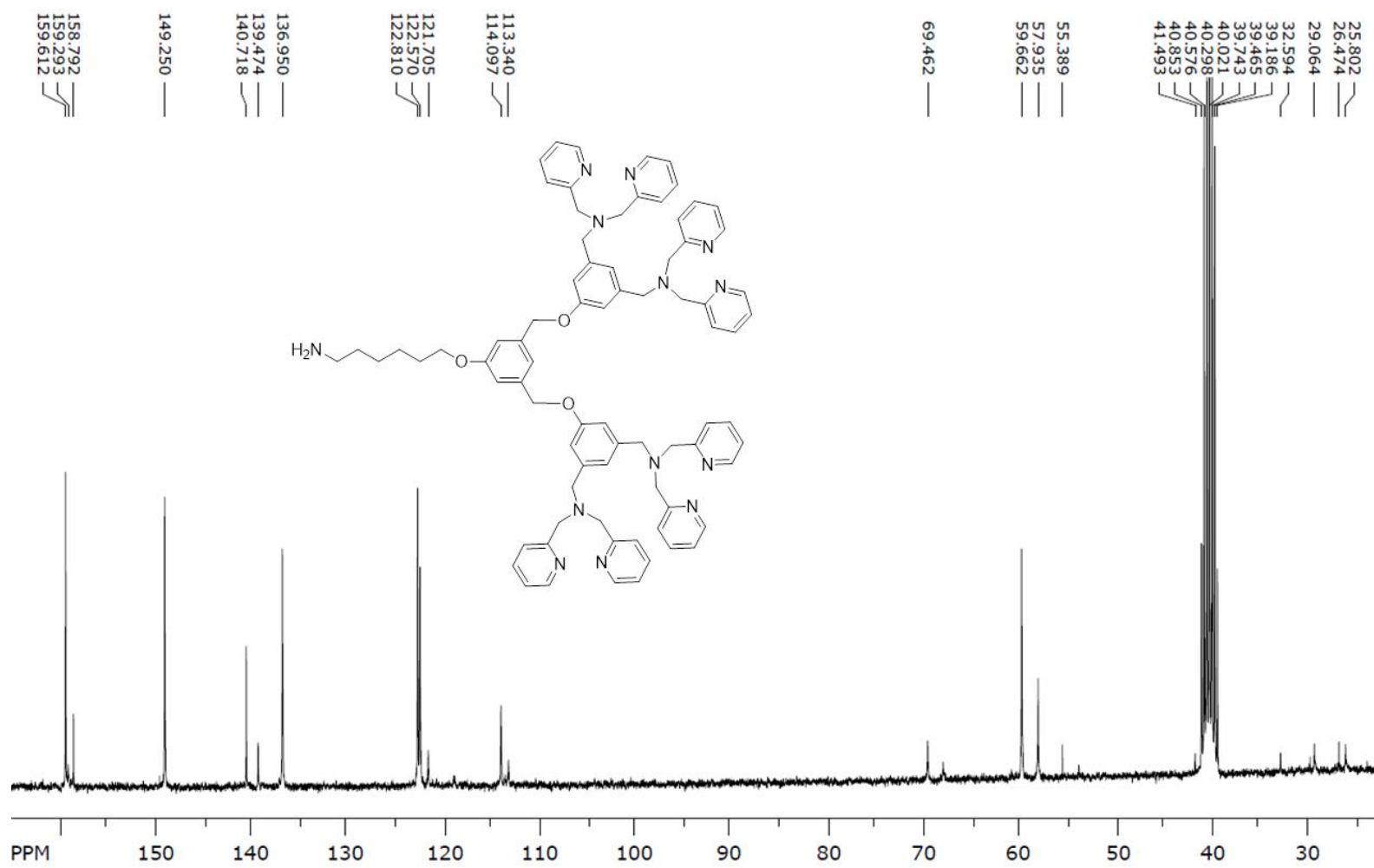


Figure S35. ¹³C NMR spectrum of Ligand 4-NH₂, Related to Scheme 2.

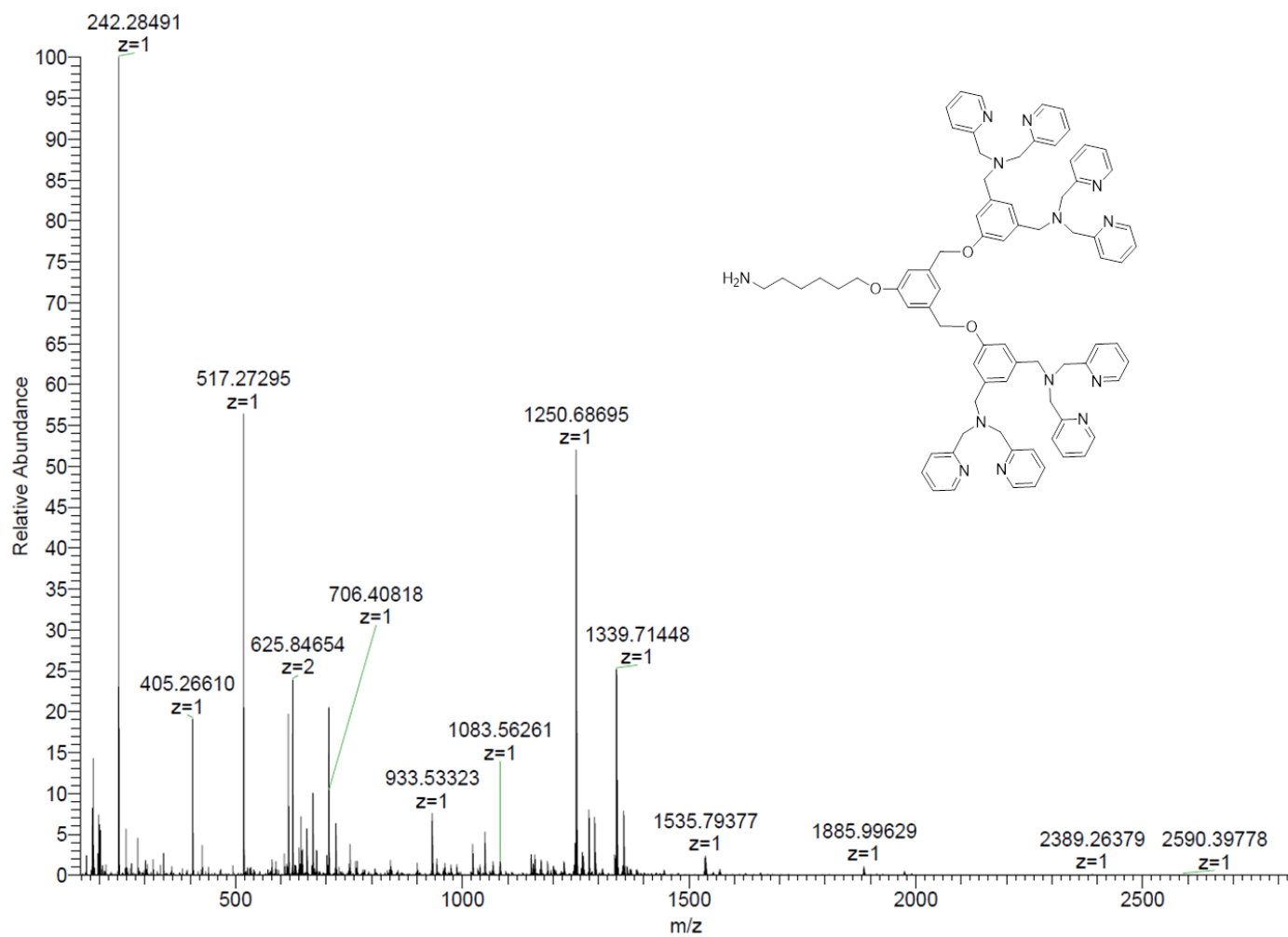


Figure S36. ESI-MS spectrum of Ligand 4-NH₂, Related to Scheme 2.

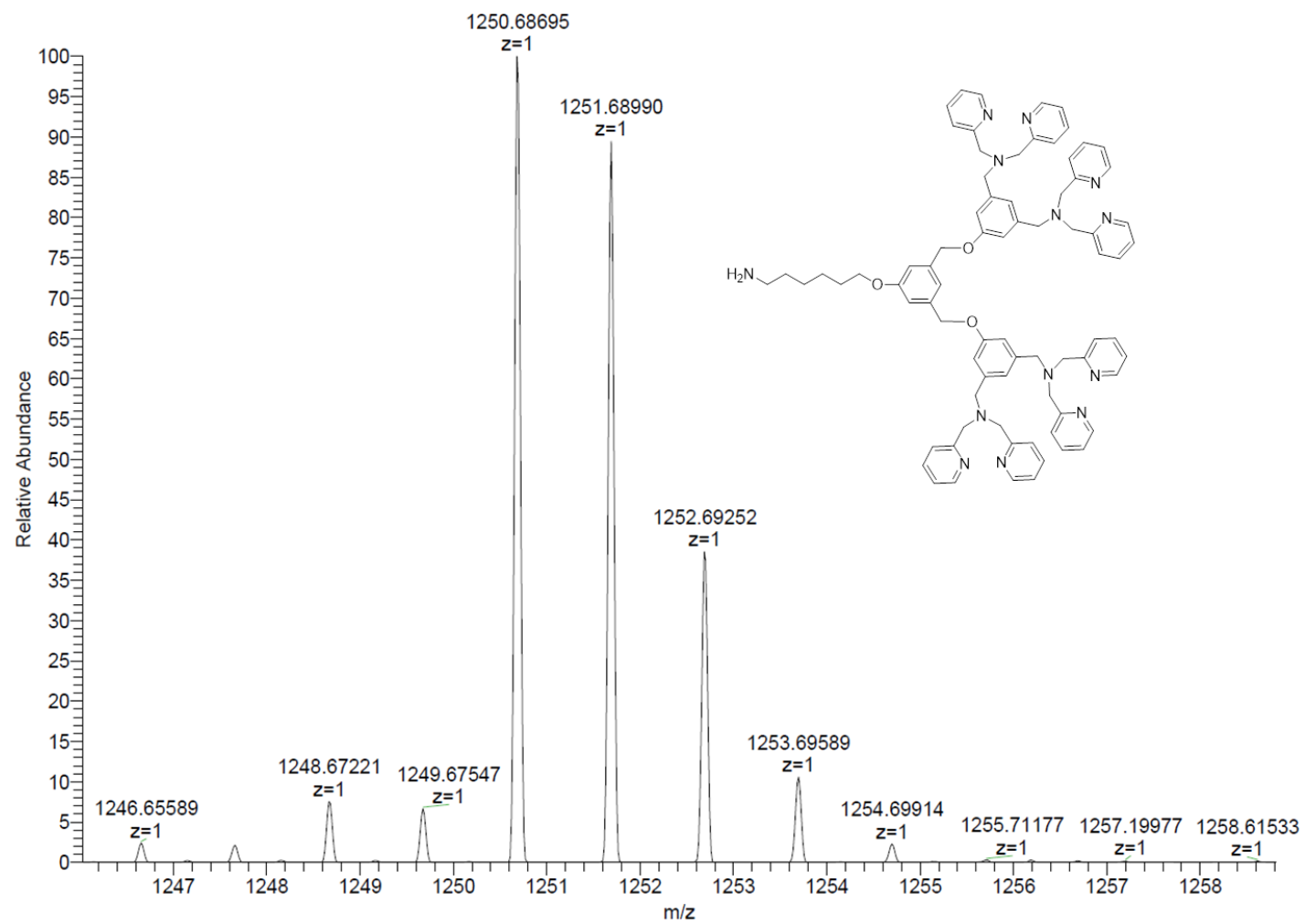


Figure S37. ESI-MS spectrum of Ligand 4-NH₂, Related to Scheme 2.

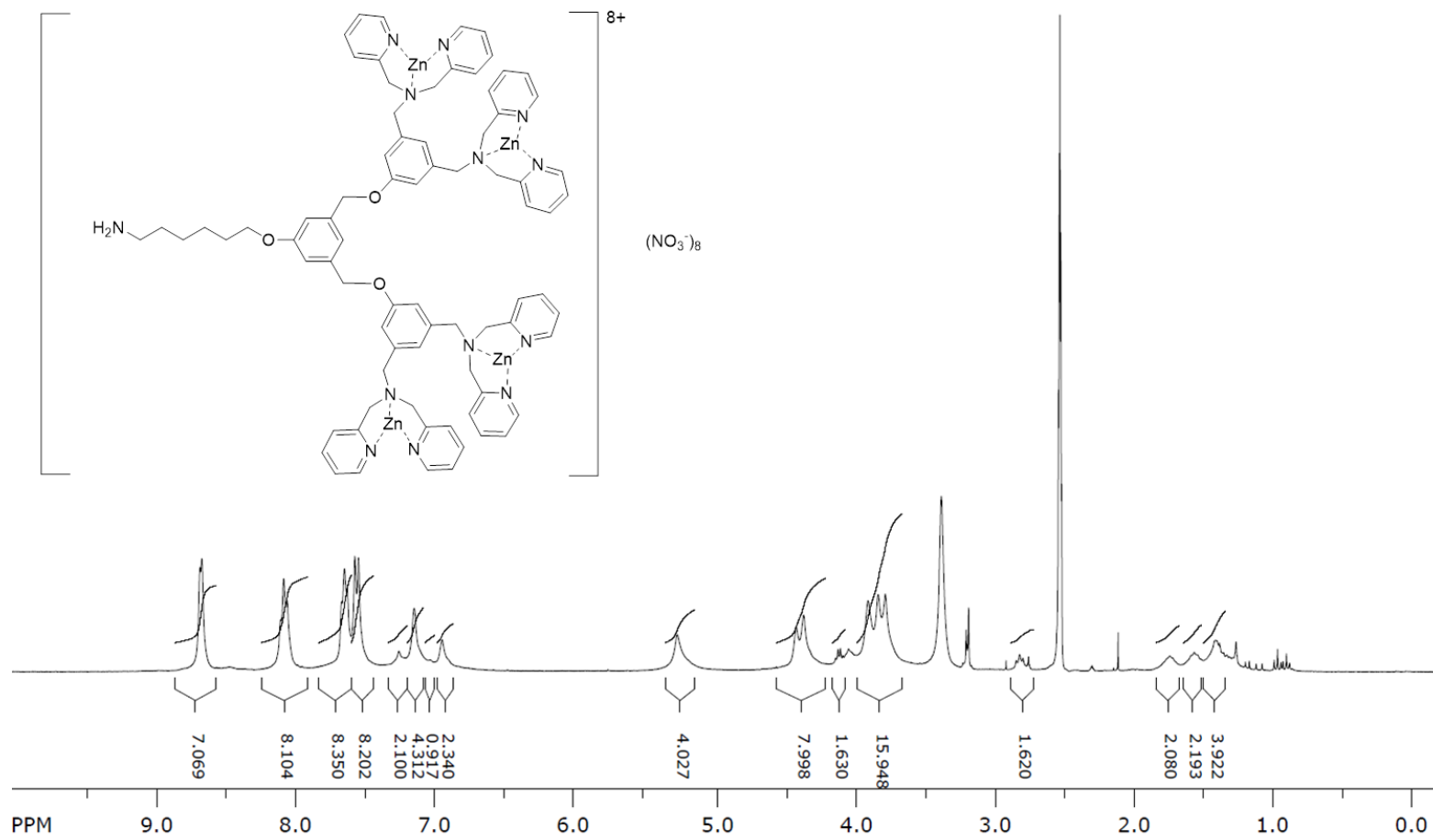


Figure S38. ¹H NMR spectrum of C4, Related to Scheme 2.

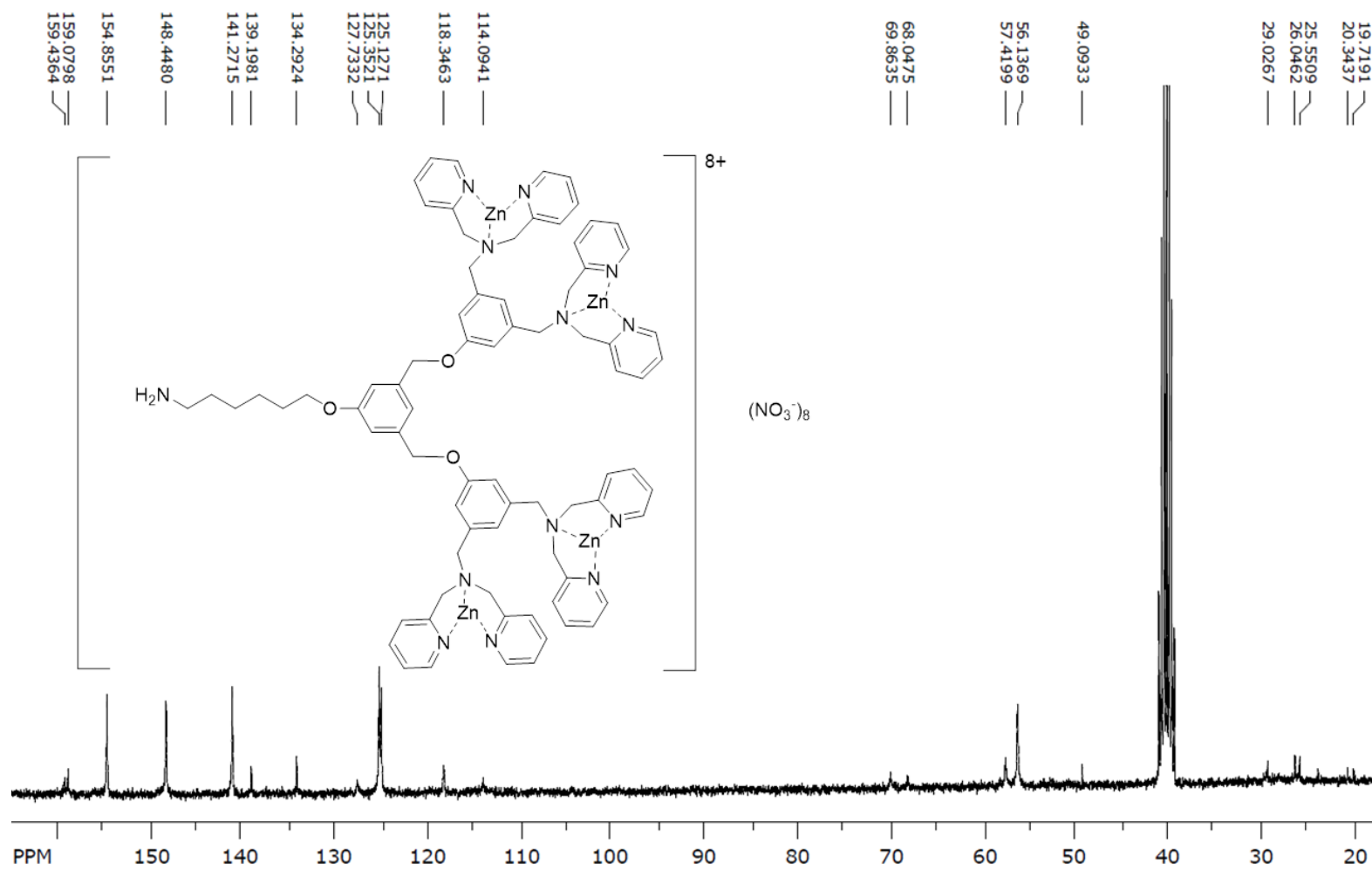


Figure S39. ^{13}C NMR spectrum of C4, Related to Scheme 2.

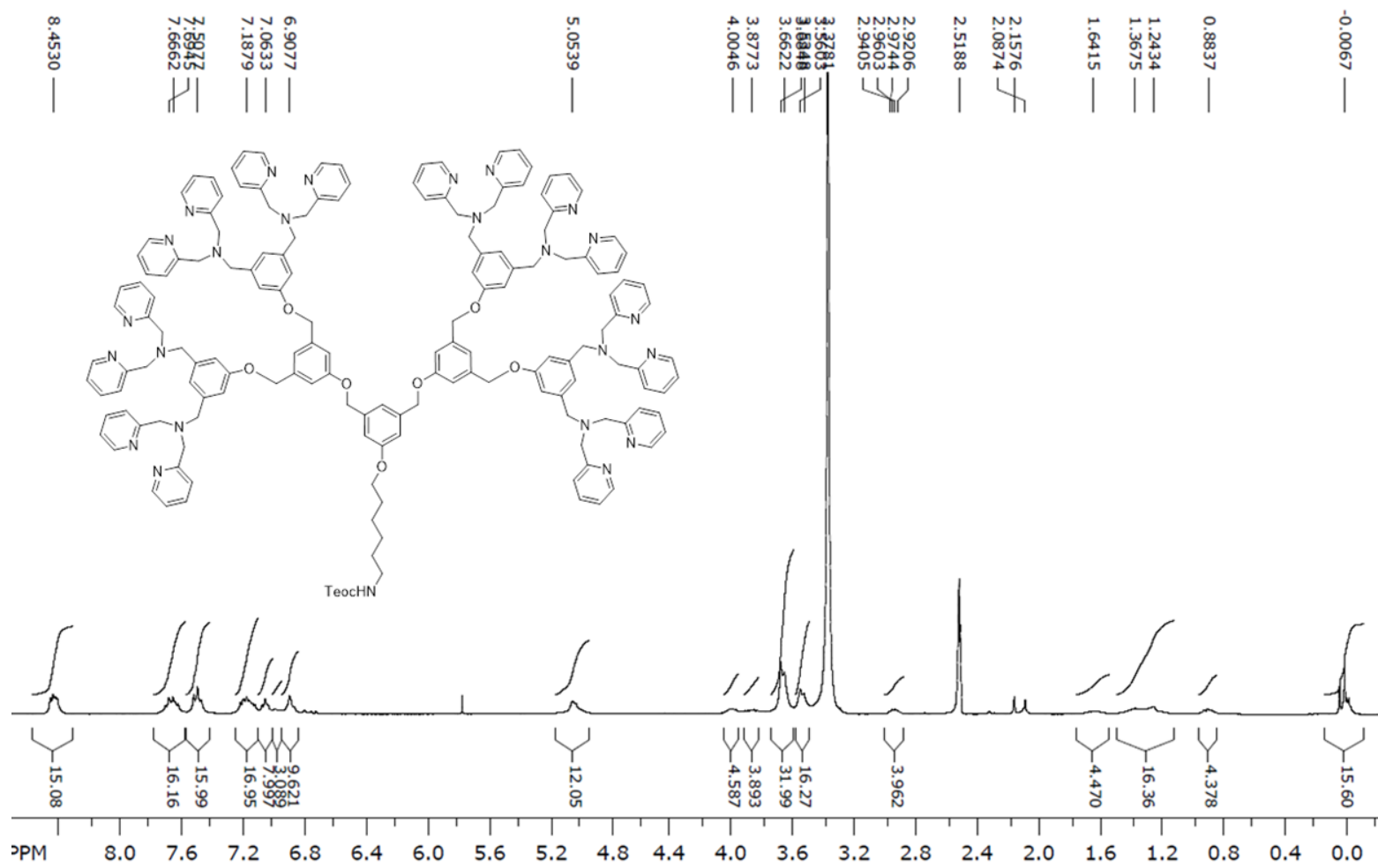


Figure S41. ¹H NMR spectrum of Ligand 8-Teoc, Related to Scheme 2.

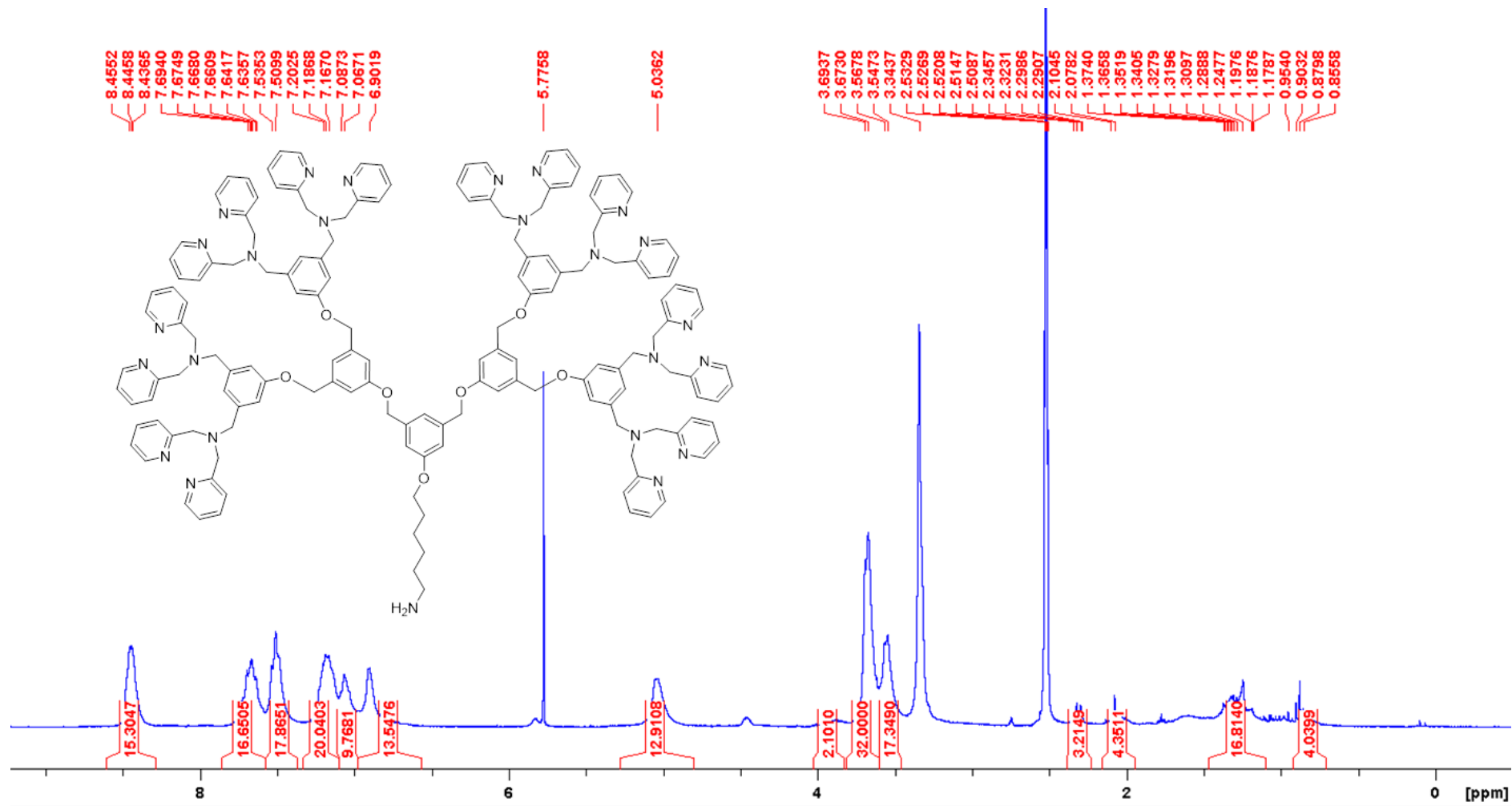


Figure S42. ¹H NMR spectrum of Ligand 8-NH₂, Related to Scheme 2.

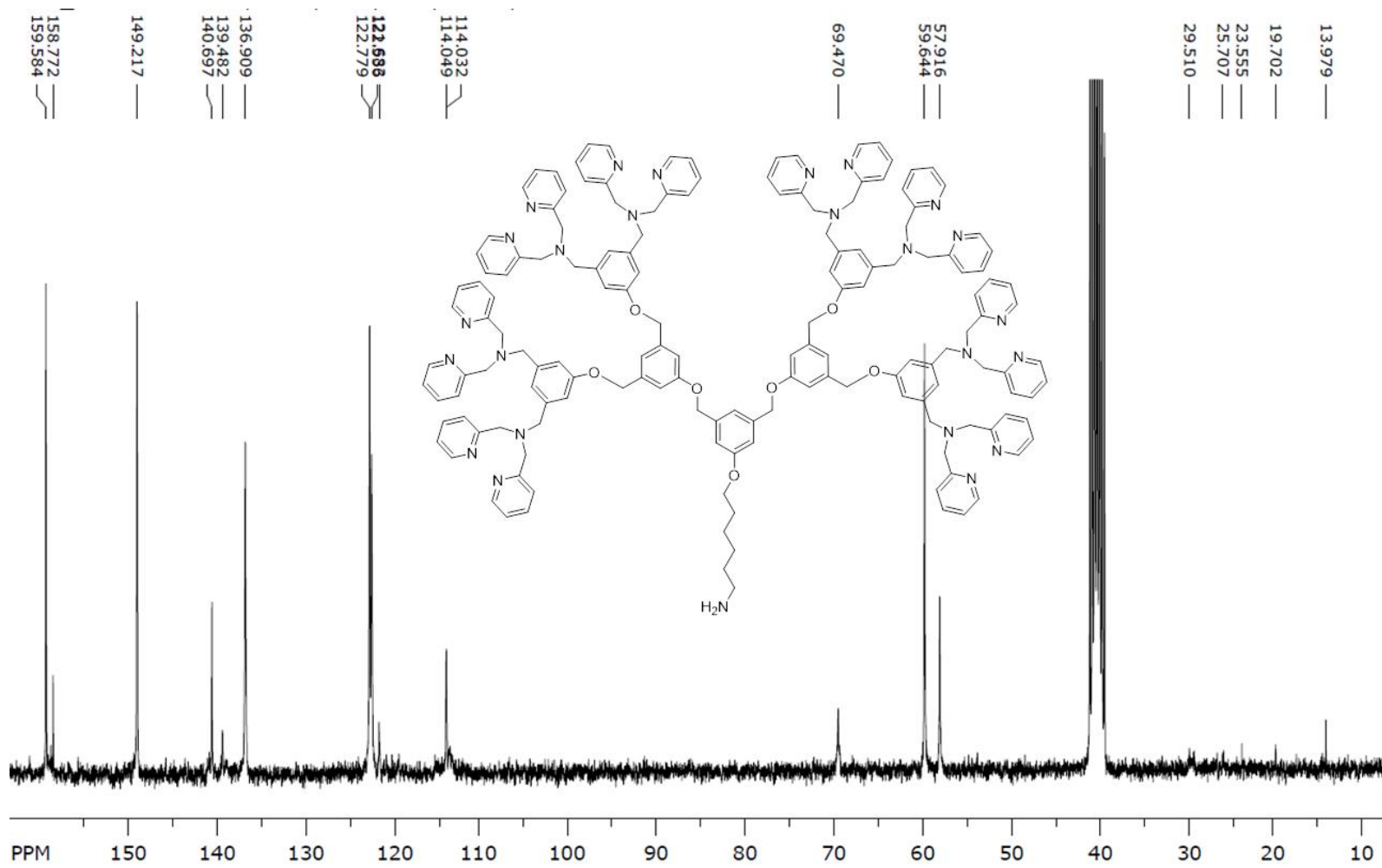


Figure S43. ¹³C NMR spectrum of Ligand 8-NH₂, Related to Scheme 2.

190306-Exac-6477-RO-L8 #2-65 RT: 0.05-1.06 AV: 64 NL: 2.50E5
T: FTMS + p ESI Full ms [160.00-2800.00]

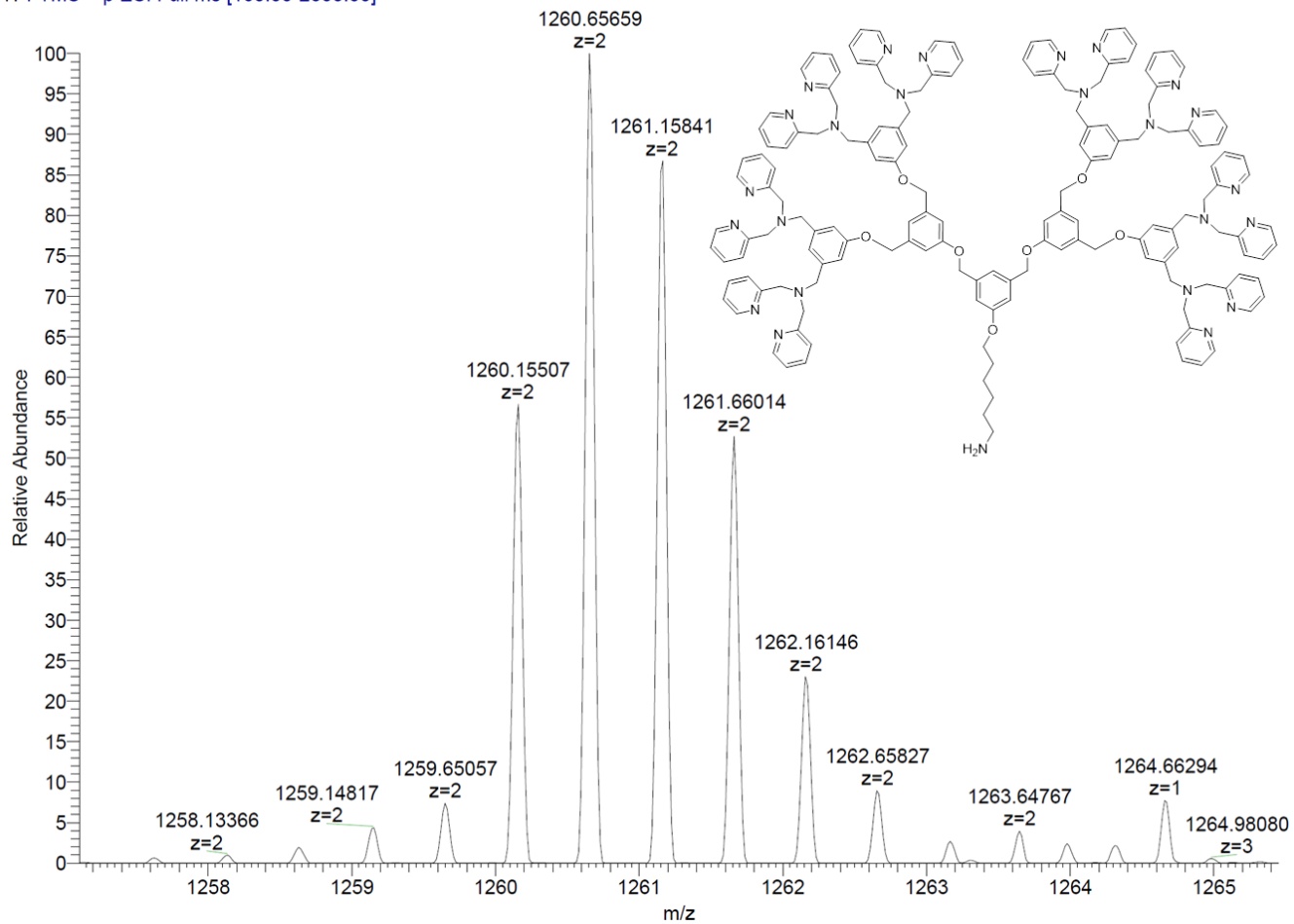


Figure S44. ESI-MS spectrum of Ligand 8- NH₂, Related to Scheme 2.

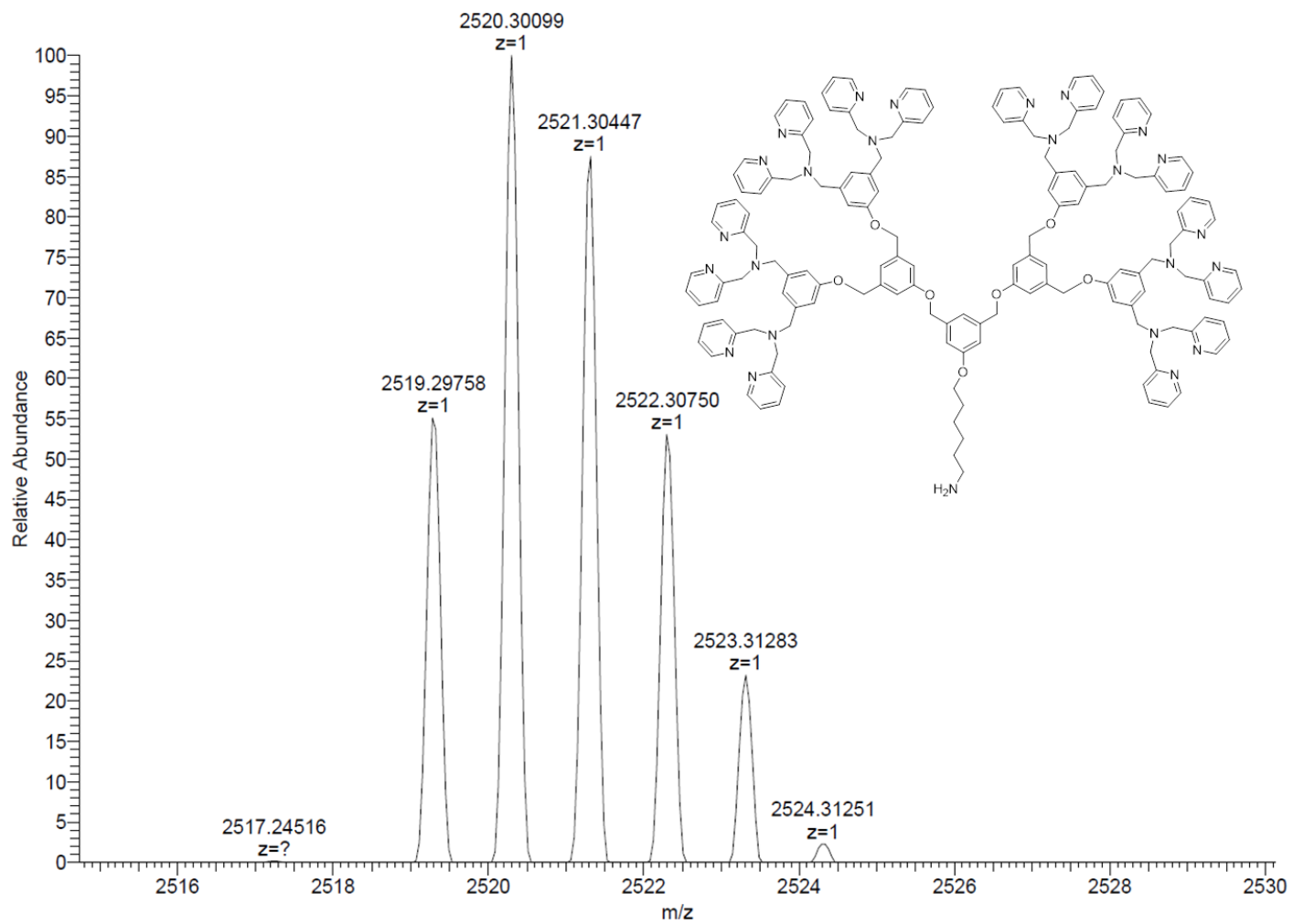


Figure S45. ESI-MS spectrum of Ligand 8- NH₂, Related to Scheme 2.

3DPAZn-NH2 1

ecb_proton DMSO /disk2/ODA/data/JIANG/nmr ODA 9

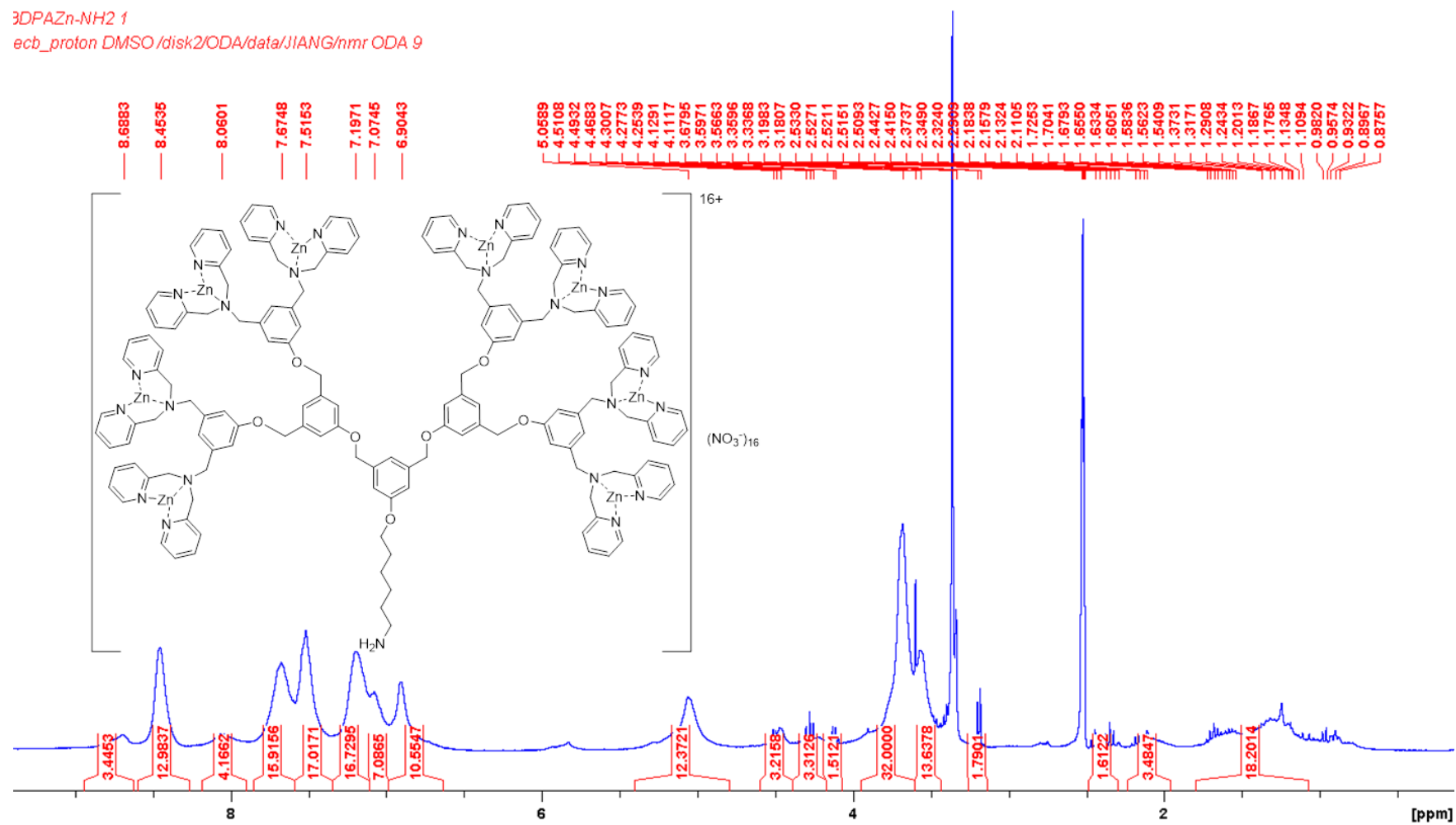


Figure S46.C8, ^1H NMR spectrum of Related to Scheme 2.

Conclusions and perspectives

The MV capture device discussed in the thesis is constructed in several steps, and the conclusions and perspectives of the thesis are therefore presented in the following sections:

Molecule design and synthesis:

In general, dendritic structures are useful in achieving high local concentration of binding sites, allowing faster binding kinetics. On the other hand, high generation cationic dendrimers are also reported to be able to destruct lipid membrane due to their high conformational rigidity. In the case of DPAZn complexes binding to PS, spatially adjacent DPAZn units are able to act synergistically when binding with phosphate groups, thus the dendritic structure may also introduce higher binding affinity. Taking all these factors into consideration, to fine-tune the binding of DPAZn to microvesicle, we have designed and successfully synthesized DPAZn complexes of 1, 2, 4 and 8 complexing units (C1, C2, C4, and C8, respectively), while C4 and C8 are based on the scaffold of a poly(benzyl ether) dendron. Whereas C2 is synthesized following the reported procedures, C1, C3 and C4 are prepared using new protocols we have developed.

Most of these molecules are constructed from Phenol- and amine-based derivatives, essentially by nucleophilic substitutions. Increasing the dendron generations, increased the steric hindrance around the active site and thus the difficulty to prepare perfect high generations of dendron, as usually observed in the syntheses of dendrimers. In this context, C8 is the more difficult complex to synthesize due to the high steric hindrance around the active sites. This compound is also difficult to purify, as the polarity and solubility of 4DPAOH and 8DPAOH are almost similar in the common column chromatography eluents, and the strong amine/pyridine-silica interaction prevent the elution process.

From the feedback of complex-PS interaction strength and MV capture performance, C4 with 4 DPAZn units is the best candidate for future applications as it not only binds to the MVs with sufficient strength but also able to keep the morphology of MVs intact on the capture device. From the aspect of binding strength, C2, C4, and C8 are all qualified. However, according to our results and other literatures, local rigidity at MV-device interface seems to be another important factor to take into consideration. Smaller molecules are more likely to conduct the rigidity of material substrate to the MV membranes, causing possible rupture and fusion of MV membranes on rigid surfaces, limiting the application of such molecules on rigid substrates. In contrast, molecules with multiple DPAZn units are capable of insulate the MVs from the rigidity of material substrate, yet the high molecule conformational rigidity also causes membrane destruction. Only molecules with flexible binding sites and sufficient rigidity insulation are able to achieve MV capture without membrane destruction.

Indeed, in future applications of such molecules, other parameters such as solubility, reactivity to the substrate surface, toxicity, etc. must also be taken into account. As indicated in Chapter 3, all these parameters can be adjusted by changing the complexing metals, dendritic scaffolds or the spacer for fixing the material.

Complex-PS interaction and complex-membrane interaction studies

The complexation of PS molecules on Zinc complexes has been studied by NMR. It turned out that these are interactions between the phosphate groups of the PS and the Metal cation Zn^{2+} of the corresponding complexes. In terms of binding forces, NMR titration is unfortunately not sensitive enough to give quantitative results such as K_d values. Nevertheless, the semi-quantitative results presented as changes in chemical shifts indicated that C4 is the molecule with the highest binding capacity with PS. The binding of these complexes to model membranes containing PS were studied by PWR spectroscopy. Linked forces are quantified as K_d values. As with NMR experiments, compound C4 has the highest membrane binding strength compared to compounds C1 and C2. As explained in Chapter 2, changes in the positions of PWR peaks when complexes are titrated on membranes are representative of changes in mass and changes in membrane anisotropy occurring on the adsorbed lipid bilayer. C1 and C2 both have one-step coordination, while C4 binds to the PS-containing membrane in 4 steps. In addition, if C8 is truly destructive to the lipid bilayer, as assumed in Chapter 2, PWR titration would show a significant shift towards a smaller resonance angle. Unfortunately, due to the low solubility of C8 in water, its characterization of membrane binding was not possible with PWRs.

Surface functionalization and its characterization

As a proof of concept, PET was chosen as the model material used in the construction of capture devices. The surface modification of PET was done using the protocol developed in our lab with some modifications. The synthesized complexes has better solubility in organic solvents, therefore the functionalization was done in DMSO instead of water. All the complexes are able to be grafted onto PET surface with different molecular densities. Unsurprisingly, with the increase of molecular dendricity, the complexes are increasingly more difficult to be grafted.

The characterization of such surfaces as discussed in chapters 1 and 2, should be the quantification of molecules similar to that used in TBO test. Unfortunately, at this date no technique is capable of such quantification. So we adopted the combination of TBO and XPS. Both techniques are highly sensitive to the chemistry of the outmost layer of material, thus semi-quantitative characterization is achieved.

A possible truly quantitative determination method for the grafted complexes would be a technique similar to TBO test, as shown in Figure 1. As reviewed in ref. [118, 224], DPAZn dendrons are able to specifically bind to pyrophosphate containing molecules with high affinity. For this reason, a pyrophosphate molecule binding to a chromophore/fluorophore can be synthesized and this molecule should be able to dissolve in a same medium as Dendron containing DPAZn. The binding stoichiometry between dendrons and pyrophosphate can then be determined in solution using job plot.[233] If we assume this stoichiometry won't change when DPAZn dendrons are attached to PET surface, similar to TBO test, the functionalized PET can be immersed in pyrophosphate solution to allow saturated binding. The bound pyrophosphate can then be washed with an acid and its concentration can be determined using UV-Vis or

fluorescence spectrometer, which could result in a quantity of surface complex. Similar labeling strategies can also be employed, as discussed by Ivanov et al. for fluorescence labeling of surface carboxyl groups.[193] However, such test requires molecular design, synthesis, evaluation and so on. Given the time limit and deviation from our main purpose of MV capture device construction, such experiments are not included in the duration of this thesis.

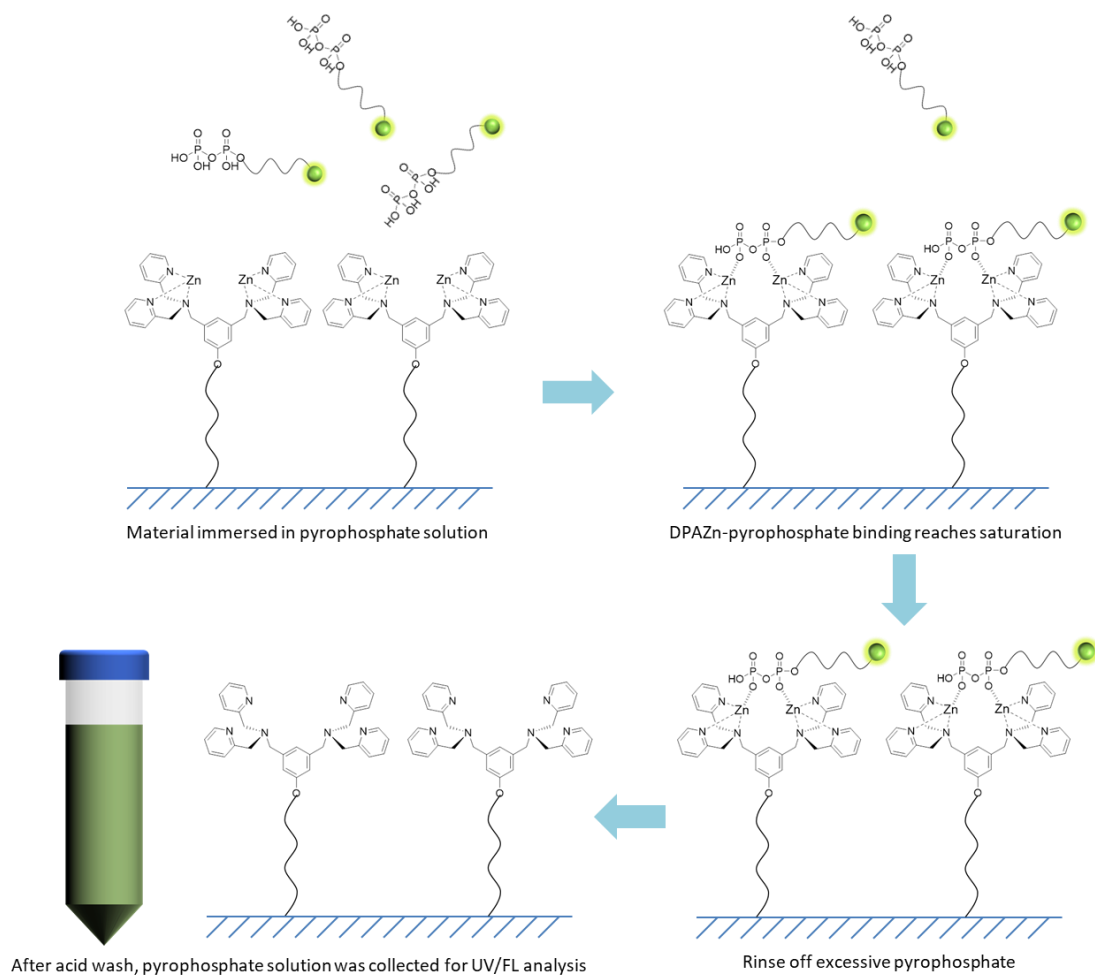


Figure 1. A hypothetical surface DPAZn complex quantification method.

MV capture device

The capture of MVs was examined using fluorescence microscope and cryo-SEM. C4 functionalized PET was found to be the only device capable of capturing MVs while maintaining their morphology.

As discussed in chapter 1, MV capture is a potentially useful method for efficient MV purification. The next application oriented research on this dendron-functionalized system would be the purification performance test, although MV and exosomes remain indistinguishable from each other. It is therefore,

more precisely, the purification of EVs. To date, the isolation of EVs from fluidic samples still face many problems including: loss of time, high cost, poor sample purity, and so on. Based on our preliminary test, these difficulties seem to be solved using Dendron-based capture devices: Incubation with capture device only takes 15 min, much shorter compared to a centrifugation of several hours the dendron functionalized PET are much cheaper than centrifuges or flow cytometers; and only PS containing particles can be captured onto the device, guaranteeing the sample purity.

However, for such applications, additional experiments must be conducted: for instance to confirm the exclusion of non-vesicular contaminants after capture, the proteomics of the sample fluid and vesicles should be compared on the capture device; to study the need for pre-capture purification to exclude cellular debris capture devices should be incubated with samples with and without purification before capture.

In some cases, the purified MVs are desirable in the form of suspension, for instance, when they are to be used for therapeutics rather than diagnosis.[1, 90, 234, 235] On the capture devices, MVs are bound to the material, which is undesirable for such applications. One possible solution this problem would be to wash the capture device with buffer containing EDTA. EDTA is a molecule that binds to Zn^{2+} with K_d as low as 10^{-16} M; it could therefore could replace the PS from the Zn^{2+} ions.[236] This hypothetical MV the EDTA also damage the MVs.

References:

1. S. El Andaloussi, et al. (2013). *Nature Reviews Drug Discovery*. *12*, 347.
2. C. Tricarico, et al. (2017). *Small GTPases*. *8*, 220.
3. R.C. Paolicelli, et al. (2018). *Neuroscience*.
4. D.G. Meckes, Jr., et al. (2011). *J Virol*. *85*, 12844.
5. C.T. Roberts, Jr., et al. (2013). *Cancer Res*. *73*, 3200.
6. D.S. Choi, et al. (2015). *Mass Spectrom Rev*. *34*, 474.
7. E.R. Abels, et al. (2016). *Cell Mol Neurobiol*. *36*, 301.
8. K.M. Kim, et al. (2017). *Wiley Interdiscip Rev RNA*. *8*,
9. C. Verderio, et al. (2018). *J Lipid Res*. *59*, 1325.
10. A.Y. Wu, et al. (2019). *Proteomics*. *19*, e1800162.
11. E. Boilard (2018). *J Lipid Res*. *59*, 2037.
12. B. Hugel, et al. (2005). *Physiology (Bethesda)*. *20*, 22.
13. S. Azouzi, et al. (2018). *Am J Hematol*. *93*, E110.
14. A.B. García-Arribas, et al. (2016). *Chem Phys Lipids*. *199*, 26.
15. J. Taylor, et al. (2019). *Proteomics*. *19*, e1800165.
16. K. Al-Nedawi, et al. (2008). *Nat Cell Biol*. *10*, 619.
17. M.J. Kean, et al. (2009). *J Cell Sci*. *122*, 4089.
18. J.W. Clancy, et al. (2015). *Nat Commun*. *6*, 6919.
19. M. Chen, et al. (2019). *PLoS One*. *14*, e0210003.
20. M.F. Bolukbasi, et al. (2012). *Mol Ther Nucleic Acids*. *1*, e10.
21. E. Cocucci, et al. (2015). *Trends Cell Biol*. *25*, 364.
22. O. Schmidt, et al. (2012). *Curr Biol*. *22*, R116.
23. V. Muralidharan-Chari, et al. (2009). *Curr Biol*. *19*, 1875.
24. A. Sobieszek, et al. (1993). *Biochem J*. *295 (Pt 2)*, 405.
25. N.S. Barteneva, et al. (2013). *Front Cell Infect Microbiol*. *3*, 49.

26. Q. Liang, et al. (2019). *Nat Biomed Eng.*
27. H. Kalra, et al. (2012). *PLoS Biol.* *10*, e1001450.
28. M. Pathan, et al. (2019). *Nucleic Acids Res.* *47*, D516.
29. E. Wang, et al. (2019). *Thromb Res.* *178*, 26.
30. X. Sun, et al. (2019). *Stem Cell Res Ther.* *10*, 8.
31. S. Suzuki, et al. (2019). *Sci Rep.* *9*, 3825.
32. Q. Wang, et al. (2017). *Nature Communications.* *8*, 709.
33. L. Balaj, et al. (2011). *Nat Commun.* *2*, 180.
34. X. Bian, et al. (2019). *Mol Cancer.* *18*, 50.
35. M.A. Rahman, et al. (2019). *J Neuroimmune Pharmacol.*
36. T. Iba, et al. (2018). *J Intensive Care.* *6*, 68.
37. S. Lin, et al. (2019). *Hum Cell.* *32*, 64.
38. M. Dziechciowski, et al. (2018). *Ginekol Pol.* *89*, 682.
39. L. Zhong, et al. (2019). *Exp Biol Med (Maywood).* 1535370218819726.
40. S. Paone, et al. (2019). *Cell Mol Life Sci.* *76*, 1093.
41. C.A. Elia, et al. (2019). *Bioessays.* *41*, e1800199.
42. L.K. Winberg, et al. (2019). *APMIS.*
43. S.K. Urban, et al. (2019). *Semin Liver Dis.* *39*, 70.
44. C. Xie, et al. (2019). *Mol Cancer.* *18*, 83.
45. B. Ebert, et al. (2019). *Methods Mol Biol.* *1885*, 287.
46. A.W. Brenner, et al. (2019). *Methods Mol Biol.* *1882*, 229.
47. A. Finkielstein, et al. (2018). *J Vis Exp.*
48. S. Kagota, et al. (2019). *Int J Mol Sci.* *20*,
49. D. Sproviero, et al. (2019). *Front Neurosci.* *13*, 344.
50. A. Gezzi, et al. (2019). *Exp Mol Med.* *51*, 33.
51. M. Pathan, et al. (2017). *J Extracell Vesicles.* *6*, 1321455.
52. M. Pathan, et al. (2015). *Proteomics.* *15*, 2597.

53. P. Zhang, et al. (2019). *SLAS Technol.* 2472630319846877.
54. F. Momen-Heravi, *Isolation of Extracellular Vesicles by Ultracentrifugation*, in *Extracellular Vesicles: Methods and Protocols*, W.P. Kuo and S. Jia, Editors. 2017, Springer New York: New York, NY. p. 25.
55. C. Thery, et al. (2018). *J Extracell Vesicles.* 7, 1535750.
56. E. Pariset, et al. (2017). *Advanced Biosystems.* 1, 1700040.
57. G. Vazirabadi, et al. (2003). *J Gen Virol.* 84, 1997.
58. K. Menck, et al. (2017). *J Vis Exp.*
59. J. Caradec, et al. (2014). *Clin Biochem.* 47, 1286.
60. X. Li, et al. (2008). *Methods Mol Biol.* 440, 97.
61. R. Cantin, et al. (2008). *J Immunol Methods.* 338, 21.
62. S. Chutipongtanate, et al. (2018). *Sci Rep.* 8, 15039.
63. I.P. Sauter, et al. (2019). *JCI Insight.* 4,
64. T. Visnovitz, et al. (2019). *J Extracell Vesicles.* 8, 1565263.
65. D.D. Taylor, et al., *Exosome Isolation for Proteomic Analyses and RNA Profiling*, in *Serum/Plasma Proteomics: Methods and Protocols*, R.J. Simpson and D.W. Greening, Editors. 2011, Humana Press: Totowa, NJ. p. 235.
66. J.Z. Nordin, et al. (2015). *Nanomedicine.* 11, 879.
67. E.A. Mol, et al. (2017). *Nanomedicine.* 13, 2061.
68. A.N. Boing, et al. (2014). *J Extracell Vesicles.* 3,
69. N. Karimi, et al. (2018). *Cellular and Molecular Life Sciences.* 75, 2873.
70. B. Roda, et al. (2009). *Anal Chim Acta.* 635, 132.
71. J.Z. Nordin, et al. (2019). *Methods Mol Biol.* 1953, 287.
72. O.P.B. Wiklander, et al. (2018). *Front Immunol.* 9, 1326.
73. P. Spitzer, et al. (2019). *Sci Rep.* 9, 7089.
74. S. Cointe, et al. (2017). *J Thromb Haemost.* 15, 187.
75. M. Takao, et al. (2018). *Genes Cells.* 23, 963.
76. D.G. Nguyen, et al. (2003). *J Biol Chem.* 278, 52347.
77. ; Available from: https://en.wikipedia.org/wiki/Flow_cytometry#Cell_sorting_by_flow_cytometry.

78. K. Segawa, et al. (2015). *Trends Cell Biol.* 25, 639.
79. A.M. deCathelineau, et al. (2003). *Essays Biochem.* 39, 105.
80. T. Skotland, et al. (2019). *J Lipid Res.* 60, 9.
81. H.M. Hankins, et al. (2015). *Traffic.* 16, 35.
82. P.A. Leventis, et al. (2010). *Annu Rev Biophys.* 39, 407.
83. H. Pollet, et al. (2018). *Biomolecules.* 8,
84. C. Subra, et al. (2007). *Biochimie.* 89, 205.
85. J. Kowal, et al. (2016). *Proc Natl Acad Sci U S A.* 113, E968.
86. D.W. Greening, et al. (2017). *Expert Rev Proteomics.* 14, 69.
87. M. Jayachandran, et al. (2008). *Am J Physiol Heart Circ Physiol.* 295, H931.
88. H. Julich, et al. (2014). *Front Immunol.* 5, 413.
89. Y.R. Nievas, et al. (2018). *Cell Mol Life Sci.* 75, 2211.
90. I. Panfoli, et al. (2018). *Expert Rev Proteomics.* 15, 801.
91. A. Iwasaki, et al. (1987). *J Biochem.* 102, 1261.
92. C.P. Reutelingsperger, et al. (1985). *Eur J Biochem.* 151, 625.
93. J.F. Tait, et al. (1989). *Journal of Biological Chemistry.* 264, 7944.
94. H.A. Andree, et al. (1990). *Journal of Biological Chemistry.* 265, 4923.
95. I. Vermes, et al. (1995). *Journal of Immunological Methods.* 184, 39.
96. G. Koopman, et al. (1994). *Blood.* 84, 1415.
97. N. Arraud, et al. (2015). *J Thromb Haemost.* 13, 237.
98. L. Ayers, et al. (2011). *Thromb Res.* 127, 370.
99. K. Aupeix, et al. (1997). *J Clin Invest.* 99, 1546.
100. M. Miyanishi, et al. (2007). *Nature.* 450, 435.
101. W. Nakai, et al. (2016). *Sci Rep.* 6, 33935.
102. T. Yeung, et al. (2008). *Science.* 319, 210.
103. G.K. Patel, et al. (2019). *Sci Rep.* 9, 5335.
104. P.A. Cuypers, et al. (1983). *Journal of Biological Chemistry.* 258, 2426.

105. M. Brini, et al. (2013). *Met Ions Life Sci.* *13*, 81.
106. A. Melcrova, et al. (2016). *Sci Rep.* *6*, 38035.
107. A. Ojida, et al. (2002). *J Am Chem Soc.* *124*, 6256.
108. A.V. Koulov, et al. (2003). *Cell Death Differ.* *10*, 1357.
109. A.V. Koulov, et al. (2005). *Israel Journal of Chemistry.* *45*, 373.
110. A. Ojida, et al. (2004). *J Am Chem Soc.* *126*, 2454.
111. B.A. Smith, et al. (2013). *Mol Pharm.* *10*, 3296.
112. W.M. Leevy, et al. (2006). *J Am Chem Soc.* *128*, 16476.
113. R.G. Hanshaw, et al. (2005). *Chembiochem.* *6*, 2214.
114. A.G. White, et al. (2012). *Bioorg Med Chem Lett.* *22*, 2833.
115. D.R. Rice, et al. (2015). *Photochem Photobiol Sci.* *14*, 1271.
116. Y.W. Liu, et al. (2017). *Bioconjug Chem.* *28*, 1878.
117. J.J. Lee, et al. (2014). *Nano Lett.* *14*, 1.
118. H.T. Ngo, et al. (2012). *Chem Soc Rev.* *41*, 4928.
119. C. Pigault, et al. (1994). *J Mol Biol.* *236*, 199.
120. J.H. Walker, et al. (1992). *Biochemical Society Transactions.* *20*, 828.
121. A. Zweifach (2000). *Biochem J.* *349*, 255.
122. V.E. Zwicker, et al. (2019). *Angew Chem Int Ed Engl.* *58*, 3087.
123. P. Meers, et al. (1991). *Biochemistry.* *30*, 2903.
124. R.A. Blackwood, et al. (1990). *Biochem J.* *266*, 195.
125. R.A. Haraszti, et al. (2016). *J Extracell Vesicles.* *5*, 32570.
126. A.J. Plaunt, et al. (2014). *Bioconjug Chem.* *25*, 724.
127. A.J. Plaunt, et al. (2012). *Chem Commun (Camb).* *48*, 8123.
128. C. Belle, et al., *Grafted dinuclear metal complexes, and use thereof as cellular microparticle sensors.* 2012.
129. A.W. Bosman, et al. (1999). *Chem Rev.* *99*, 1665.
130. S.M. Grayson, et al. (2001). *Chem Rev.* *101*, 3819.

131. D.A. Tomalia, et al. (1985). *Polymer Journal*. *17*, 117.
132. P.G. de Gennes, et al. (1983). *Journal de Physique Lettres*. *44*, 351.
133. G.R. Newkome, et al. (1999). *Chem Rev*. *99*, 1689.
134. C.H. Huang, et al. (2012). *ACS Nano*. *6*, 9416.
135. A.M. Caminade, et al. (2015). *Chem Soc Rev*. *44*, 3890.
136. R.S. Kalhapure, et al. (2015). *Pharm Dev Technol*. *20*, 22.
137. C.J. Hawker, et al. (1990). *J Am Chem Soc*. *112*, 7638.
138. M.-L. Lartigue, et al. (1997). *Macromolecules*. *30*, 7335.
139. D.A. Tomalia, et al. (1990). *Angewandte Chemie International Edition in English*. *29*, 138.
140. Y. Zheng, et al. (2015). *Chem Soc Rev*. *44*, 4091.
141. C.J. Hawker, et al. (1997). *J Am Chem Soc*. *119*, 9903.
142. P. Welch, et al. (1998). *Macromolecules*. *31*, 5892.
143. C.J. Hawker, et al. (1993). *J. Chem. Soc., Perkin Trans. 1*. 1287.
144. M. Liu, et al. (2000). *Journal of Controlled Release*. *65*, 121.
145. G. Chen, et al. (2017). *Biomacromolecules*. *18*, 2205.
146. A.M. Brinkman, et al. (2016). *Biomaterials*. *101*, 20.
147. U. Gupta, et al. (2006). *Biomacromolecules*. *7*, 649.
148. K.R. Gopidas, et al. (1991). *J Am Chem Soc*. *113*, 7335.
149. A.S. Chauhan (2018). *Molecules*. *23*,
150. K. Mizuno, et al. (1992). *Life Sciences*. *51*, PL183.
151. A.S. Erturk, et al. (2017). *Pharm Dev Technol*. *22*, 111.
152. J. Li, et al. (2014). *Cell Metab*. *19*, 373.
153. L. Zhao, et al. (2017). *J Control Release*. *247*, 153.
154. T.P. Thomas, et al. (2004). *Biomacromolecules*. *5*, 2269.
155. K. Kono, et al. (1999). *Bioconjug Chem*. *10*, 1115.
156. T.P. Thomas, et al. (2005). *J Med Chem*. *48*, 3729.
157. T.D. McCarthy, et al. (2005). *Mol Pharm*. *2*, 312.

158. P.R. Ashton, et al. (1997). *Chemistry - A European Journal*. **3**, 974.
159. H.B. Agashe, et al. (2006). *J Pharm Pharmacol*. **58**, 1491.
160. U. Boas, et al. (2007). **28**.
161. A. Agarwal, et al. (2008). *Int J Pharm*. **350**, 3.
162. S. Galeazzi, et al. (2010). *Biomacromolecules*. **11**, 182.
163. M. Mammen, et al. (1998). *Angewandte Chemie International Edition*. **37**, 2754.
164. J.J. Lundquist, et al. (2002). *Chem Rev*. **102**, 555.
165. N. Nagahori, et al. (2002). *Chembiochem*. **3**, 836.
166. L.A. de Jong, et al. (2005). *J Chromatogr B Analyt Technol Biomed Life Sci*. **829**, 1.
167. D.R. Rice, et al. (2016). *Chem Commun (Camb)*. **52**, 8787.
168. N.K. Jain, et al. (2008). *Expert Opin Drug Metab Toxicol*. **4**, 1035.
169. V.K. Yellepeddi, et al. (2009). *Expert Opin Drug Deliv*. **6**, 835.
170. S. Parimi, et al. (2008). *Langmuir*. **24**, 13532.
171. A. Mecke, et al. (2005). *Langmuir*. **21**, 10348.
172. A. Mecke, et al. (2004). *Chem Phys Lipids*. **132**, 3.
173. N. Martinho, et al. (2014). *Molecules*. **19**, 20424.
174. Y.L. Wang, et al. (2012). *Phys Chem Chem Phys*. **14**, 8348.
175. H. Lee, et al. (2008). *J Phys Chem B*. **112**, 7778.
176. S. Berenyi, et al. (2014). *Colloids Surf B Biointerfaces*. **118**, 164.
177. B. Klajnert, et al. (2005). *Int J Pharm*. **305**, 154.
178. C.A. Schalley, et al. (2006). *Journal of Physical Organic Chemistry*. **19**, 479.
179. A.-M. Caminade (2011). **35**.
180. T. Felder, et al. (2005). *Chemistry*. **11**, 5625.
181. P.J. Berkeley, et al. (1963). *The Journal of Physical Chemistry*. **67**, 846.
182. L. Fielding (2000). *Tetrahedron*. **56**, 6151.
183. Z. Salamon, et al. (1997). *Biophysical Journal*. **73**, 2791.
184. A.V. Zayats, et al. (2005). *Physics Reports*. **408**, 131.

185. Z. Salamon, et al. (1999). *Trends in Biochemical Sciences*. *24*, 213.
186. Z. Salamon, et al. (1997). *Biochimica et Biophysica Acta (BBA) - Reviews on Biomembranes*. *1331*, 117.
187. K.A. Willets, et al. (2007). *Annu Rev Phys Chem*. *58*, 267.
188. E. Harte, et al. (2014). *Chem Commun (Camb)*. *50*, 4168.
189. I.D. Alves, et al. (2019). *Acc Chem Res*. *52*, 1059.
190. C. Chollet, et al. (2007). *Biomol Eng*. *24*, 477.
191. C. Chollet, et al. (2009). *Biomaterials*. *30*, 711.
192. E. Uchida, et al. (1993). *Langmuir*. *9*, 1121.
193. V.B. Ivanov, et al. (1996). *Surface and Interface Analysis*. *24*, 257.
194. J. Brison, et al. (2010). *J Phys Chem C Nanomater Interfaces*. *114*, 5565.
195. I.A. Mudunkotuwa, et al. (2014). *Analyst*. *139*, 870.
196. X. Jin, et al. (2016). *Colloids Surf B Biointerfaces*. *145*, 275.
197. P. Luan, et al. (2019). *Langmuir*. *35*, 4270.
198. T. Isono, et al. (2007). *e-Journal of Surface Science and Nanotechnology*. *5*, 99.
199. J. van Weerd, et al. (2015). *Adv Healthc Mater*. *4*, 2743.
200. N. Granqvist, et al. (2014). *Langmuir*. *30*, 2799.
201. S. Ohno, et al. (2012). *196*.
202. J. Nijssse, et al. (1999). *Scanning*. *21*, 372.
203. J.S. Henao Agudelo, et al. (2017). *Front Immunol*. *8*, 881.
204. M.P. Wyllie, et al. (2017). *Pathog Dis*. *75*,
205. V. Jeney (2018). *Exp Suppl*. *108*, 211.
206. A.P. Owens, 3rd, et al. (2011). *Circ Res*. *108*, 1284.
207. M. Bruschi, et al. (2019). *Clin J Am Soc Nephrol*. *14*, 834.
208. Y. Sun, et al. (2018). *J Proteome Res*. *17*, 1101.
209. T. Takahashi, et al. (2017). *J Allergy Clin Immunol*. *140*, 720.
210. N.G. Sampaio, et al. (2017). *Malar J*. *16*, 245.
211. A.S.O. Chavez, et al. (2019). *J Cell Sci*. *132*,

212. V. La Marca, et al. (2017). *Int J Mol Sci.* *18*,
213. V. Muralidharan-Chari, et al. (2010). *J Cell Sci.* *123*, 1603.
214. A.M. Andrews, et al. (2016). *Front Cell Neurosci.* *10*, 43.
215. K. Bergen, et al. (2018). *Thromb Res.* *172*, 158.
216. L.S. Holliday, et al. (2019). *Orthod Craniofac Res.* *22 Suppl 1*, 101.
217. S. Obeid, et al. (2017). *Biosens Bioelectron.* *93*, 250.
218. P.E. Rautou, et al. (2013). *Expert Rev Hematol.* *6*, 91.
219. F.C. Svedman, et al. (2018). *PLoS One.* *13*, e0206942.
220. S. Nagata, et al. (2016). *Cell Death Differ.* *23*, 952.
221. M. van Engeland, et al. (1998). *Cytometry.* *31*, 1.
222. K. Gajos, et al. (2017). *Anal Bioanal Chem.* *409*, 1109.
223. K. Selmeczi, et al. (2007). *Chemistry.* *13*, 9093.
224. E.J. O'Neil, et al. (2006). *Coordination Chemistry Reviews.* *250*, 3068.
225. P. Calmet, et al. (2016). *Sci Rep.* *6*, 36181.
226. E. Reimhult, et al. (2003). *Langmuir.* *19*, 1681.
227. Z. Salamon, et al. (2004). *Biophysical Journal.* *86*, 2508.
228. Y. Xiang, et al. (2015). *Langmuir.* *31*, 7738.
229. M.C. Segretti, et al. (2015). *ACS Med Chem Lett.* *6*, 1156.
230. A. Johansson, et al. (2003). *Inorg Chem.* *42*, 7502.
231. S. Turkyilmaz, et al. (2014). *Org Biomol Chem.* *12*, 5645.
232. A.K. Jain, et al. (2009). *Biochemistry.* *48*, 10693.
233. J.-Q. Jiang, et al. (2015). *Sensors and Actuators B: Chemical.* *220*, 659.
234. A. Stoddart (2014). *Nature Materials.* *14*, 13.
235. L.-M. Shen, et al. (2018). *ACS Applied Nano Materials.*
236. J.K. Nyborg, et al. (2004). *Biochem J.* *381*, e3.